Doctoral Thesis

Exploring HIV-1 lipid-interacting partners by chemical-based approaches

Aroa Arboleya Agudo

April 2022

Supervisor

Maier Lorizate Nogales

eman ta zabal zazu

Universidad del País Vasco
Euskal Herriko Unibertsitatea

Dedicada a Mamá, Papá y Zuri.

Acknowledgments

Contributions

Journal publications

- Morana, O., Nieto-Garai, J. A., Björkholm, P., Bernardino de la Serna, J., Terrones, O., <u>Arboleya, A.</u>, Ciceri, D., Rojo-Bartolomé, I., Blouin, C. M., Lamaze, C., Lorizate, M., & Contreras, F. X. (2022). Identification of a New Cholesterol-Binding Site within the IFN-γ Receptor that is Required for Signal Transduction. Advanced science (Weinheim, Baden-Wurttemberg, Germany), e2105170. Advance online publication. https://doi.org/10.1002/advs.202105170

- Nieto-Garai, J. A., Contreras, F. X., <u>Arboleya, A.</u>, & Lorizate, M. (2022). Role of Protein-Lipid Interactions in Viral Entry. Advanced biology, e2101264. Advance online publication. https://doi.org/10.1002/adbi.202101264

- Lorizate, M., Terrones, O., Nieto-Garai, J. A., Rojo-Bartolomé, I., Ciceri, D., Morana, O., Olazar-Intxausti, J., <u>Arboleya, A.</u>, Martin, A., Szynkiewicz, M., Calleja-Felipe, M., Bernardino de la Serna, J., & Contreras, F. X. (2021). Super-Resolution Microscopy Using a Bioorthogonal-Based Cholesterol Probe Provides Unprecedented Capabilities for Imaging Nanoscale Lipid Heterogeneity in Living Cells. Small methods, 5(9), e2100430. https://doi.org/10.1002/smtd.202100430

- Nieto-Garai, J. A., <u>Arboleya, A.</u>, Otaegi, S., Chojnacki, J., Casas, J., Fabriàs, G., Contreras, F. X., Kräusslich, H. G., & Lorizate, M. (2020). Cholesterol in the Viral Membrane is a Molecular Switch Governing HIV-1 Env Clustering. Advanced science (Weinheim, Baden-Wurttemberg, Germany), 8(3), 2003468. https://doi.org/10.1002/advs.202003468

Congress contributions

- <u>Arboleya, A.</u>, Nieto-Garai, J. A., Contreras, F. X., Lorizate, M. (Barcelona, Spain, 20-23/07/2021). A chemical tool to unravel HIV-1 palmitoylome. 43 Congreso de la Sociedad Española de Bioquímica y Biología Molecular (SEBBM).

- Nieto-Garai, J. A., <u>Arboleya, A.</u>, Otaegi, S., Chojnacki, J., Casas, J., Fabriás, G., Contreras, F. X., Kräusslich, H. G., Lorizate, M. (Barcelona, Spain, 20-23/07/2021). HIV-1 Env clustering is driven by its interaction with viral membrane cholesterol. 43 Congreso de la Sociedad Española de Bioquímica y Biología Molecular (SEBBM).

- <u>Arboleya, A.</u>, Nieto-Garai, J. A., Contreras, F. X., Lorizate, M. (Santander, Spain, 10-13/09/2018). The role of HIV-1 Env CT in cellular lipid interaction and the relationship with the recruitment of Env into virions. 41 Congreso de la Sociedad Española de Bioquímica y Biología Molecular (SEBBM).

- Nieto-Garai, J. A., <u>Arboleya, A.</u>, Lopez, S., Contreras, F. X., Lorizate, M. (Santander, Spain, 10-13/09/2018). HIV envelope protein-cholesterol interaction in the viral membrane: a promising requirement for cell entry. 41 Congreso de la Sociedad Española de Bioquímica y Biología Molecular (SEBBM).

Resumen

El Virus de la Inmunodeficiencia Humana tipo 1 (VIH-1), es el agente causante del síndrome de la inmunodeficiencia adquirida (SIDA), el cual es responsable de más de 35 millones de muertes desde que comenzó el brote hace treinta años. Por lo tanto, la infección por el VIH-1 es, sin duda alguna, una de las principales preocupaciones a nivel mundial.

El VIH-1 es un retrovirus de ARN monocatenario perteneciente al género Lentivirus, cuyos viriones empaquetan todos los componentes necesarios para su infectividad. La poliproteína Gag está a cargo de la morfogénesis del VIH-1, promoviendo el proceso de gemación el cual incrusta la proteína de envuelta (Env) en la membrana viral. Después de ser escindida por la proteasa (PR), Gag se descompone en sus cuatro constituyentes: cápside (CA), matrix (MA), nucleocápside (NC) y p6 (Ilustración I). Env es una glicoproteína compuesta por dos subunidades, gp120 o proteína de superficie y gp41 o proteína transmembrana. Las dos subunidades están unidas de forma no covalente formando un heterodímero, tres de los cuales se asocian para generar un homotrímero de heterodímeros. En el virión maduro, los trímeros de Env se asocian en una sola espícula o clúster (Ilustración I), el cual se ha descrito como necesario en el reconocimiento eficaz del receptor y correceptor de la célula huésped y la posterior entrada del virus en la célula.
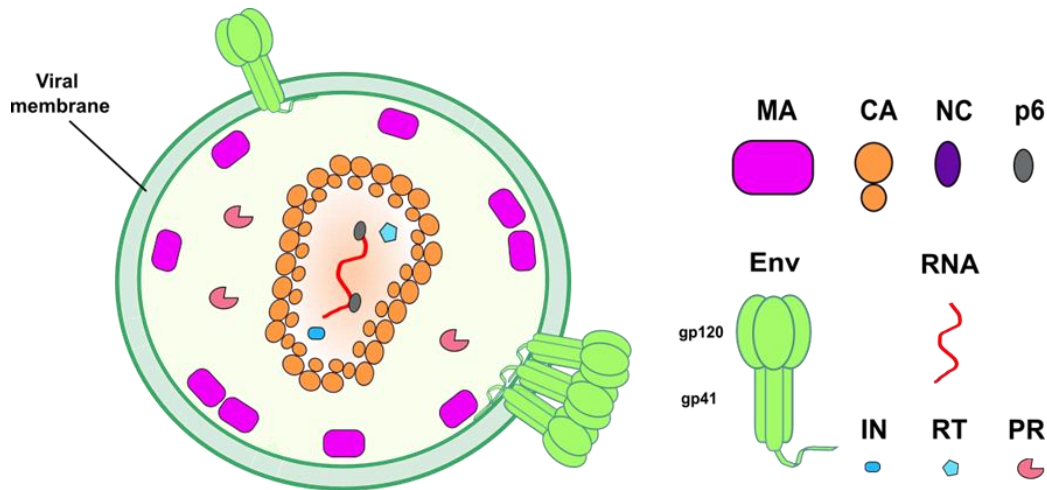
Ilustración I. Estructura esquemática de un virión maduro del VIH-1. El VIH-1 está delimitado por una membrana lipídica, en la que las proteínas de envuelta están embebidas y sobresalen hacia el exterior. MA permanece asociada a la membrana viral, y CA genera una cápsula en forma de cono que rodea al ARN viral, el cual se empaqueta gracias a NC. Las enzimas virales RT, IN y PR también están empaquetadas dentro del virus.

La composición de la membrana viral del VIH-1 se conoce tanto de forma cuantitativa como cualitativa y difiere de la composición de la membrana celular de la cual el VIH-1 nace. Se sabe que esta membrana viral es rica en colesterol, esfingomielina fosfatidilserina y en especies saturadas de fosfatidilcolina. Estos mismos lípidos también se encuentran enriquecidos en los nanodominios *ratfs* de la membrana celular. Además, la membrana viral presenta una estructura similar a la adoptada por los lípidos en la fase líquida ordenada, como también ocurre en estos nanodominios.

Se sabe que la subunidad gp41 de Env está palmitoilada en Cys-764 y Cys-837, las cuales se encuentran en los *Lentiviral Lytic Peptides* (LLPs) de la cola citoplasmática (CT) de gp41. Los grupos de palmitato unidos covalentemente a estas cisteínas se insertan en la bicapa lipídica, interactuando con diferentes proteínas de la membrana durante la gemación y el ensamblaje del VIH-1, y anclan a gp41 a la membrana celular. Se sabe que las proteínas palmitoiladas se dirigen preferentemente a las balsas lipídicas, las cuales constituyen dominios menores en la mayoría de las membranas, por lo que se cree que estos dominios aglutinan las proteínas palmitoiladas (virales o celulares) con otros componentes virales, lo que facilita las interacciones proteína-proteína y la gemación del VIH-1. El conjunto completo de las proteínas palmitoiladas presentes en el virión maduro constituye el palmitoiloma del VIH-1. Estas proteínas provienen del

propio virión, como Env, pero la gran mayoría son proteínas derivadas del huésped incorporadas durante la gemación del virus a partir presumiblemente de estos nanodominios de tipo *raft*. Aunque el proteoma del VIH-1 es conocido, el palmitoiloma detallado aún sigue siendo un enigma hoy en día.

MA es el dominio amino-terminal de Gag, y se encarga de anclar esta proteína a la membrana celular y, aunque no se comprende completamente, también recluta a la glicoproteína Env a los sitios de gemación. Más concretamente, la localización final de Gag en sitios determinados de la membrana celular está impulsada por interacciones específicas entre MA y fosfatidilinositol-4,5-bisfosfato [PI(4,5)P_2]. El hecho de que Gag pueda formar por sí sola partículas similares a virus completos, junto con que el VIH-1 carece de enzimas propias para la síntesis lipídica y que la membrana viral presenta una diferente composición en comparación con la membrana celular, abren la posibilidad de la existencia de otros lípidos como PI(4,5)P_2 que podrían estar interviniendo durante la morfogénesis. Uno de estos candidatos podría ser el colesterol, ya que constituye aproximadamente el 50% del total de moléculas lipídicas en esta membrana viral, y se ha demostrado que este lípido juega un papel clave en diferentes pasos del ciclo de replicación del VIH-1. Se ha postulado que las proteínas MA y Env, las dos proteínas virales unidas a la membrana viral, están asociadas con el colesterol según estudios en membranas resistentes a detergentes. Además, descubrimientos recientes en nuestro grupo de investigación han demostrado que la subunidad gp41 de la glicoproteína Env del VIH-1 interactúa directamente con el colesterol tanto en la membrana celular como en la membrana viral, de manera dependiente de su cola citoplasmática. Todo lo anterior en conjunto, lleva a plantear la hipótesis de que podría estar ocurriendo una interacción entre Gag/MA y el colesterol durante la morfogénesis del VIH-1.

Objetivos

Esta Tesis Doctoral se centra principalmente en el uso de sondas lipídicas bifuncionales y sondas lipídicas basadas en la química click para el estudio de interacciones proteína-lípido y proteína-proteína relevantes en diferentes eventos que

tienen lugar en la membrana celular durante la morfogénesis del VIH-1. Los principales objetivos de este trabajo son:

1. Estudiar la interacción entre las proteínas Gag/MA del VIH-1 y el colesterol en las membranas celular y viral durante la morfogénesis, utilizando un análogo del colesterol que es fotoactivable y está rmarcado radiactivamente, el [³H]-photo-cholesterol ([³H]-photo-chol).

2. Testar un análogo "clickable" del ácido pálmitico, que está modificado con un grupo alquín, para desarrollar un protocolo para la extracción de proteínas palmitoiladas del VIH-1.

3. Intentar descifrar el palmitoiloma del VIH-1 aplicando el protocolo indicado anteriormente.

Interacción de Gag/MA con el colesterol

La posible interacción entre Gag/MA y el colesterol durante la morfogénesis y maduración del VIH-1 se pudo estudiar gracias al uso de un análogo del colesterol, [³H]-photo-cholesterol (Ilustración II), que es capaz de unirse covalentemente a cualquier molécula que esté a 3 Å de distancia.
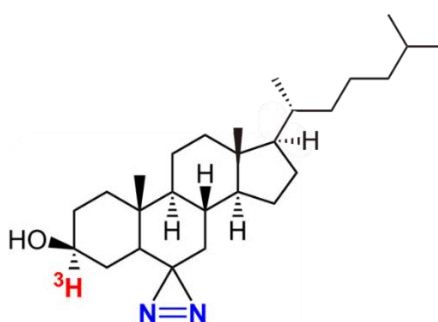

Ilustración II. Colesterol fotoactivable marcado radiactivamente. Estructura del análogo del colesterol, el cual es fotoactivable y está tritiado. El anillo de diazirina está coloreado en azul y el marcaje con tritio en rojo.

Los diferentes estudios de interacción proteína-lípido realizados en esta Tesis con esta sonda bifuncional han demostrado que ni Gag ni MA parecen interactuar

directamente con el colesterol tanto en la membrana celular como en la viral. Sin embargo, después de experimentos de inmunoprecipitación conjunto con ensayos de interacción lípido-proteína, se pudo detectar una banda delgada en la autorradiografía del Western blot alrededor de ~55 kDa de peso molecular correspondiente al tamaño de Gag (Ilustración III A), incluso cuando la proteína que se inmunoprecipitó fue la glicoproteína Env (Ilustración III B). Esto significa que potencialmente Gag podría estar interactuando con Env, por lo que ambos co-inmunoprecipitan y la señal radiactiva que está presente en la autorradiografía correspondería a Env interactuando con el colesterol al mismo tiempo que interactúa con Gag.
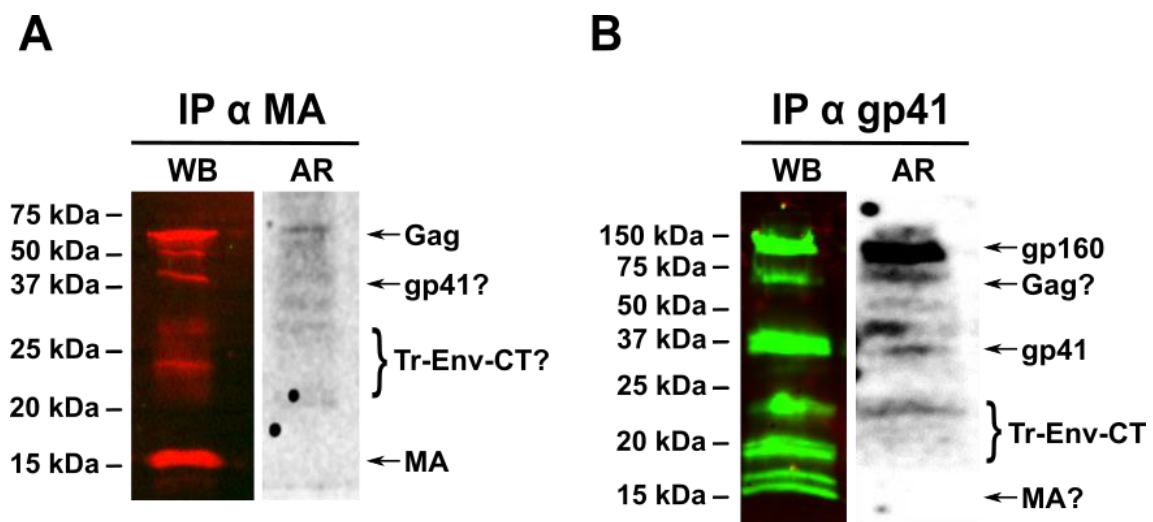

Ilustración III. Relación entre la co-inmunoprecipitación de Env y MA/Gag y la interacción [³H]-photo-chol. A) Inmunoprecipitación (IP) de MA en partículas virales purificadas y detectada mediante Western blot (WB) y autorradiografía de la misma membrana. Se ha usado como anticuerpo primario α-MA de conejo y como anticuerpo secundario α-conejo IRDye680 (rojo) para detectar Gag/MA. **B)** El 10% del sobrenadante (SN) de la IP anterior de MA en A se ha utilizado para inmunoprecipitar (IP) gp41 y se ha visualizado mediante Western blot usando Chessie-8 α-gp41 como anticuerpo primario y como anticuerpo secundario α-ratón IRDye800 (verde) para detectar gp41. T-Env-CT = Dominio truncado de la cola citoplasmática de Env.

Se sugieren tres posibles situaciones que podrían estar ocurriendo durante la interacción de Gag/MA con el colesterol, por los cuales se podrían explicar la ausencia de señal en los estudios previos con el colesterol bifuncional. Estas situaciones podrían ser las siguientes: 1) la no interacción directa entre Gag/MA y el colesterol podría ser real; 2) la interacción no pudo evaluarse con el análogo del colesterol porque la distancia

está más allá de 3 Å; y 3) podría haber una interacción indirecta entre Gag/MA y el colesterol a través de la glicoproteína Env, lo cual lleva a enunciar la teoría del "modelo sándwich" (Ilustración IV). Este modelo propone lo siguiente. Gag y el colesterol podrían impulsar la formación de nanodominios de membrana enriquecidos en colesterol que pueden alojar determinadas proteínas, como Env, y reducen su movilidad en la membrana. Ahí, Env interactúa directamente con este lípido y con Gag/MA, pudiendo quedar atrapado formando un sándwich durante la morfogénesis, donde no habría una interacción directa entre Gag/MA y el colesterol, pero podría existir una interacción indirecta a través de Env, debido al hecho de que se sabe que Gag juega un papel importante en la redistribución, orientación e incorporación de Env durante la maduración viral.

El trabajo desarrollado durante esta Tesis apoya la más plausible de las hipótesis antes mencionadas, que es la última situación, el modelo de sándwich donde Gag/MA no interactúa directamente con el colesterol durante la morfogénesis del VIH-1 y, sin embargo, ambos mantienen una relación esencial y fuerte durante el ensamblaje del VIH-1 necesaria para el desarrollo de nuevas partículas virales.
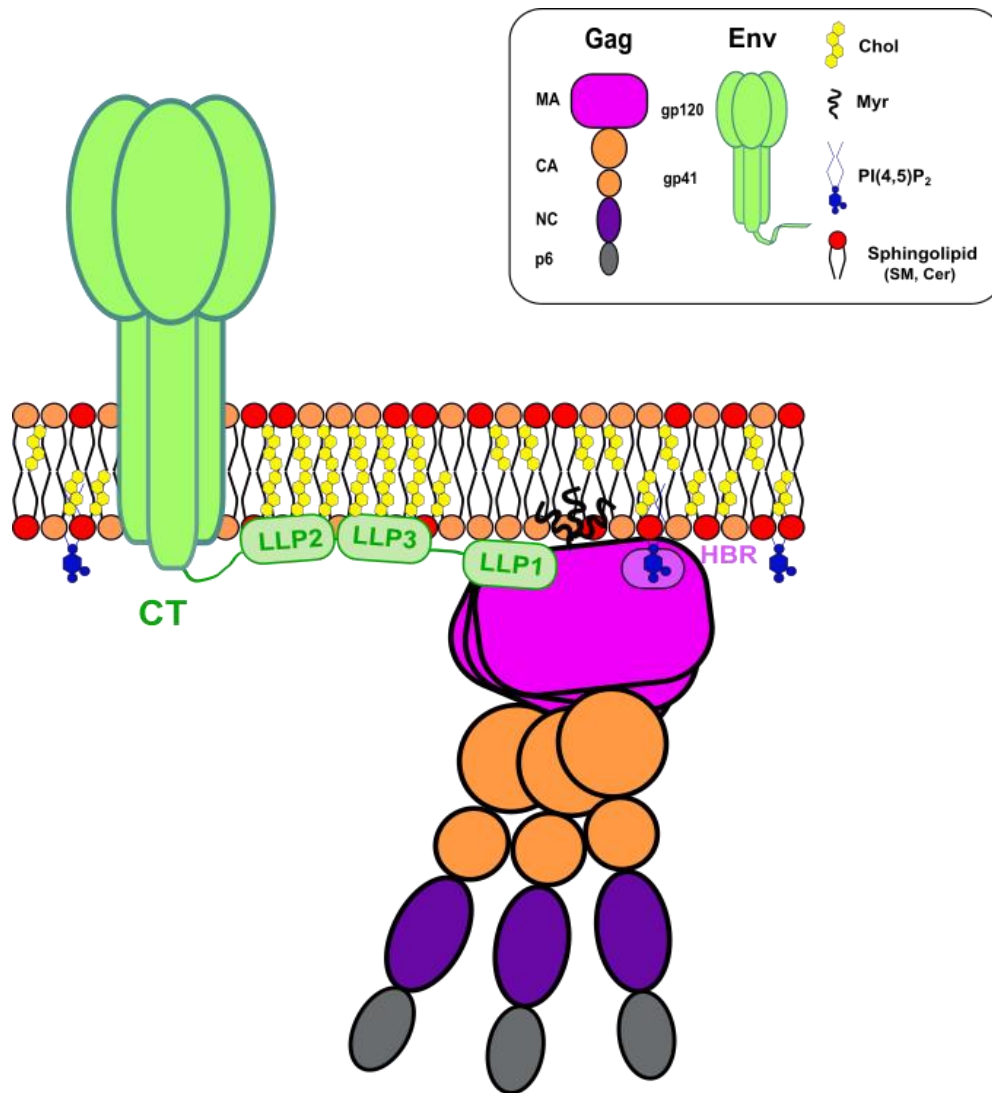
Ilustración IV. Interacción indirecta entre Gag/MA y el colesterol según el "modelo sándwich".
Gag está anclado a la membrana plasmática gracias a la interacción entre MA (dominios Myr más HBR) y PI(4,5)P$_2$. La presencia de Gag y colesterol en la membrana podría impulsar la formación de nanodominios enriquecidos en colesterol que podrían retener algunas proteínas seleccionadas por el huésped como Env y reducir su movilidad. Como se sabe que Env podría interactuar con el colesterol a través de su CT, precisamente a través de LLP2 y LLP3, y también podría interactuar con MA a través de este mismo dominio, este modelo plantea la hipótesis de una interacción entre MA y el LLP1 de gp41, mientras que al mismo tiempo Env podría ser interactuando con el colesterol a través de los otros dos LLP. Por lo tanto, Env estaría atrapado entre Gag y el colesterol formando un sándwich durante la morfogénesis, donde hay una interacción indirecta entre Gag/MA y el colesterol a través de la glicoproteína Env.

El análogo modificado del palmitoilo actúa como el palmitoilo natural.

El análogo del palmitoilo modificado con el grupo alquín utilizado en esta Tesis se desarrolló con el fin de imitar los restos de palmitoilo agregados a las proteínas durante el proceso de palmitoilación, actuando como sustrato para las

palmitoiltransferasas. Esta sonda en la que se puede hacer química clic tiene un grupo alquín unido a su región terminal (Ilustración V), la cual es accesible a sufrir la reacción de cicloadición de azida-alquín catalizada por cobre (I) (CuAAC) así poder ser detectado mediante fluorescencia y/o utilizarse para el enriquecimiento por afinidad y el posterior análisis proteómico.
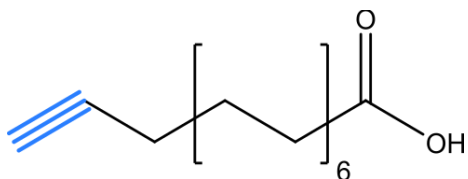

Ilustración V. Análogo del palmitoilo modificado con alquín. Estructura del análogo del palmitoilo modificado con alquín, ácido 15-octadecinoico. El grupo alquín está coloreado en azul.

El análogo del palmitoilo se añadió al cultivo celular durante el crecimiento, por lo que las proteínas diana después de 24 h de incubación se marcan con un resto del palmitoilo que contiene el grupo alquín al final de la cadena. El correcto funcionamiento de esta sonda "clickable" se pudo verificar con éxito mediante una prueba de palmitoilación desarrollada en base a la reacción de CuAAC junto con la inmunoprecipitación de gp41 mediante Chessie-8 acoplado a perlas de Sepharosa con Proteína G (Ilustración VI). Se puede observar claramente una banda correspondiente a gp41 en ~41-50 kDa en ambos canales en las partículas virales tratadas con el análogo y no está presente en el canal verde en el caso de los virus control, lo cual significa la correcta palmitoilación de gp41 por el análogo clickable. Por lo tanto, este análogo del palmitoilo puede palmitoilar las cisteínas de gp41 del VIH-1 como su equivalente natural después de su incubación en células HEK 293T.
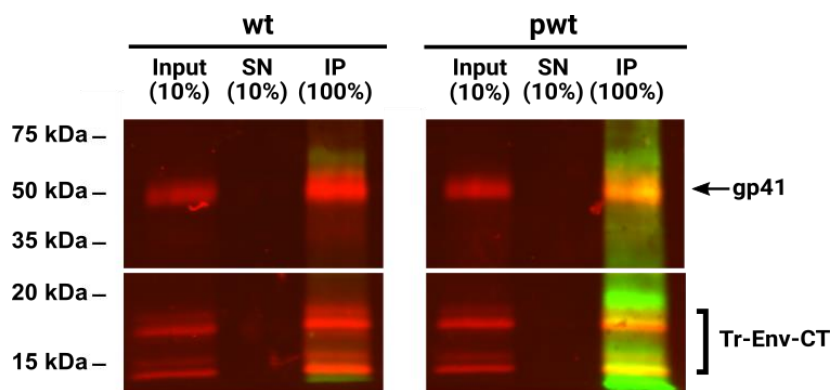
Ilustración VI. gp41 palmitoilado en partículas virales tratadas con el análogo del palmitoilo modificado. Resultados del Western blot de la muestra inicial (input), el sobrenadante (SN) y el inmunoprecipitado (IP) para la proteína Env gp41 en VLP de tipo salvaje (wt) y VLP tratadas con el análogo modificado del palmitoilo (pwt). El Western blot se desarrolló con el anticuerpo primario Chessie-8 α-gp41 y el anticuerpo α-ratón IRDye680 como anticuerpo secundario (rojo). Se aplicó química clic en el análogo modificado con el palmitoilo usando IRDye 800CWAzide Infrared Dye (verde).

Se desarrolló un protocolo para la extracción de proteínas palmitoiladas del VIH-1

Después de múltiples ensayos y pruebas para controlar todas las variables, factores y condiciones de unión específicas que afectan al proceso de inmunoprecipitación, se desarrolló un protocolo definitivo para la extracción de las proteínas palmitoiladas del VIH-1. Este protocolo puede consultarse en el Apartado 4.2.3.2 de esta Tesis. El protocolo final se basa en la reacción de CuAAC, el análogo modificado del palmitoilo y la fuerte unión que existe entre la biotina y la avidina.

La Ilustración VII muestra una transferencia de Western blot y una tinción de plata representativas después de aplicar el protocolo de extracción final a partículas virales de tipo salvaje (wt) y partículas virales tratadas con el análogo del palmitoilo (pwt). La existencia de señal correspondiente al tamaño de gp41 del VIH-1 en el eluido resultante de las partículas virales tratadas con el análogo indica que el protocolo ha sido efectivo para la extracción de proteínas palmitoiladas (Ilustración VII A). Como era de esperar, no hay señal en la muestra eluida para las partículas control. En la tinción de plata de la Ilustración VII B, se pudo apreciar una gran diferencia en el patrón proteico entre los pellets eluidos del control y del tratado, lo que significa que existe un enriquecimiento en proteínas palmitoiladas en la muestra tratada. Por lo tanto, este

protocolo podría usarse para extraer proteínas palmitoiladas de VIH-1 y su siguiente análisis proteómico por espectrometría de masas.
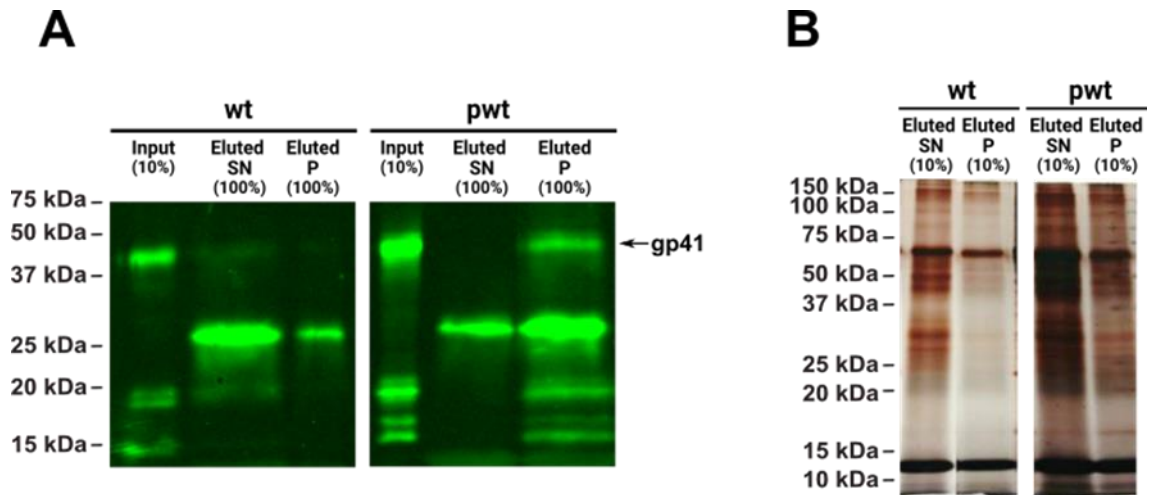

Ilustración VII. Resultados representativos del protocolo optimizado para la extracción de proteínas palmitoiladas. Western blot (A) y tinción de plata (B) de ambas partículas virales eluidas, control (wt) y tratadas con el análogo de palmitoilo (pwt), después del último protocolo de extracción modificado. P y SN son el pellet y el sobrenadante resultantes del protocolo de extracción de etanol/cloroformo, respectivamente. El Western blot se desarrolló con el anticuerpo primario Chessie-8 α-gp41 y el anticuerpo secundario α-ratón IRDye800.

Después de estudios proteómicos, se detectaron 153 proteínas potencialmente palmitoiladas exclusivamente en partículas virales tratadas con el análogo modificado del palmitoilo. El 76,47% de las proteínas palmitoiladas potenciales se describen como palmitoiladas de acuerdo con la base de datos SwissPalm. La gran mayoría de estas proteínas se localizaron formando parte principalmente del espliceosoma y el proteasoma. Tras analizar sus funciones biológicas y moleculares, se podría sugerir que las proteínas palmitoiladas detectadas estarían implicadas en el control y regulación de la maquinaria de transcripción y secreción durante la morfogénesis del VIH-1.

Summary

Human Immunodeficiency Virus type 1 (HIV-1), the causative agent of acquired immunodeficiency syndrome (AIDS), is blamed for over 35 million deaths since the outbreak begun thirty years ago. Thus, HIV-1 infection is, without a shred of a doubt, one of the main concerns around all the four corners of the globe.

The HIV-1 is single strand positive-sense retrovirus from the *Lentivirus* genera, whose virions package all of the components needed for infectivity (Illustration I). Gag polyprotein is charge of HIV-1 morphogenesis promoting budding process that embedded viral fusion envelope protein (Env) within the viral membrane. After protease (PR) cleavage, Gag generates the viral capsid (CA), matrix (MA), nucleocapsid (NC) and p6 (Illustration I). Env is a glycoprotein composed of two subunits, gp120 or surface protein, and gp41 or transmembrane protein. The two subunits are non-covalently bound forming a heterodimer, three of which associate to generate a homotrimer of heterodimers. In the mature virion, Env trimers associate into a single spike or cluster (Illustration I), which has been described to be necessary for efficient recognition of the host cell receptor and co-receptor and posterior viral entry.

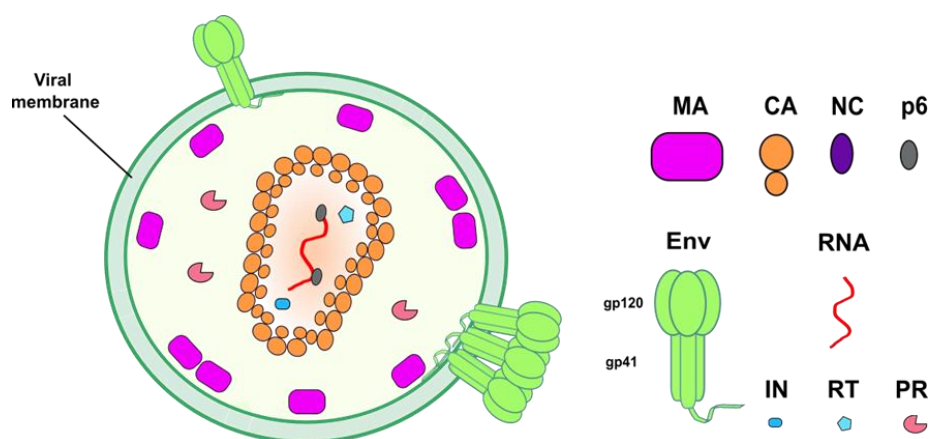**Illustration I. Schematic structure of a mature HIV-1 virion.** HIV-1 is delimited by a lipidic membrane, in which the Env proteins are embedded and protrude to the outside. Underneath the viral membrane MA remains associated with it, and CA generates a cone shaped capsid that surrounds the viral RNA, which is packed thanks to NC. The viral enzymes RT, IN and PR are also packed inside the virus.

The composition of the HIV-1 viral membrane is known both quantitatively and qualitatively and differs from the composition of the cell membrane from which HIV-1 buds. This viral membrane is known to be enriched in cholesterol, sphingomyelin phosphatidylserine and saturated species of phosphatidylcholine. Those same lipids are also enriched in lipid rafts nanodomains. Moreover, the viral membrane presents a structure similar to the adopted by lipids in the liquid-ordered phase, as in raft-like nanodomains.

The gp41 subunit of Env is known to be palmitoylated in Cys-764 and Cys-837, which are located in the Lentiviral Lytic Peptides (LLPs) of the cytoplasmic tail of gp41. Palmitate groups covalently attached to these cysteines insert into the lipid bilayer, interacting with different membrane proteins during HIV-1 budding and assembly, and anchor gp41 to the cell membrane. It is known that palmitoylated proteins preferentially target lipid rafts, which constitute minor domains in most membranes, therefore, these domains are thought to agglutinate palmitoylated (viral or cellular) proteins with other viral components, facilitating protein-protein interactions and HIV-1 budding. The complete set of palmitoylated proteins present in the mature virion, constitutes the HIV-1 palmitoylome. These proteins come from the own virion, such as Env, but the vast majority are host-derived proteins incorporated during HIV-1 budding from presumably raft-like nanodomains. Even though the HIV-1 proteome has been deciphered, the detailed HIV-1 palmitoylome is still an enigma.

MA is the amino-terminal Gag domain, and it functions to bind to the cell membrane and, although not completely understood, to recruit the viral Env glycoprotein to the budding sites. Precisely, the final localization of Gag on punctate sites of the cell membrane is driven by specific interactions between MA and phosphatidylinositol-4,5-bisphosphate [PI(4,5)P$_2$]. The fact that Gag can form, by its own, virus-like particles together with the lack of enzymes for lipid biosynthesis on HIV-1 and the different composition of the viral membrane in comparison to the cell membrane, leads the possibility of the existence of other lipids like PI(4,5)P2 that could be taking part in the morphogenesis. The perfect candidate could be the cholesterol due the fact it constitutes up to the 50% of the total lipid molecules in this viral membrane, and this lipid has been shown to play a key role in different steps of HIV-1 replication

cycle. MA and Env proteins, the two viral proteins linked to the viral membrane, have been postulated to be associated with cholesterol in detergent-resistant membranes studies. Moreover, recent discoveries in our research group have demonstrated that the gp41 subunit of the HIV-1 Env glycoprotein interacts directly with cholesterol in cellular and viral membranes, in a manner dependent of its cytoplasmic tail (CT) domain. The aforesaid mentioned leads to hypothesize that a Gag/MA-cholesterol interaction could be happening during HIV-1 morphogenesis.

Objectives

This doctoral Thesis focuses primarily on the use of bifunctional lipid probes and clickable lipid probes for the study of relevant protein-lipid and protein-protein interactions in different events taking place at the cell membrane during HIV-1 morphogenesis. The main objectives of this work are:

1. To study the interaction between HIV-1 Gag/MA proteins and cholesterol in cellular and viral membranes during morphogenesis, using a photoactivatable and radiolabelled cholesterol analogue, [^{3}H]-photo-cholesterol ([^{3}H]-photo-chol).
2. To test an alkyne-modified palmitoyl analogue to develop a protocol for the extraction of HIV-1 palmitoylated proteins.
3. Try to unveil the palmitoylome of HIV-1 by applying the previous stated protocol.

Gag/MA interaction with membrane cholesterol

The possible Gag/MA-cholesterol interaction during HIV-1 morphogenesis and maturation could have been studied thanks to the use of the photoactivatable cholesterol analogue [³H]-photo-cholesterol (Illustration II), which is capable of covalently bind to any molecule closer than 3 Å.
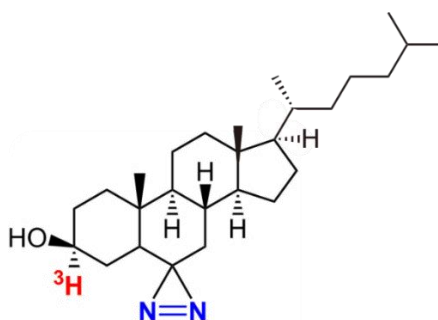
Illustration II. Radioactive photoactivatable cholesterol. Structure of tritium-labelled photoactivatable cholesterol analogue, [³H]-photo-cholesterol. The diazirine ring is coloured in blue and the tritium label in red.

The different studies of protein-lipid interaction carried out in this Thesis with this bifunctional probe have demonstrated that nor Gag neither MA seems to interact directly with cholesterol both in cellular and viral membranes. However, after immunoprecipitation experiments coupled to lipid-protein interaction assays, a thin band in Western blot autoradiography around ~55 kDa corresponding to Gag molecular weight could be detected (Illustration III A), even when the protein that was immunoprecipitated was Env glycoprotein (Illustration III B). This potentially means that Gag could be interacting with Env, so both co-immunoprecipitated, and the radioactive signal that was present in the autoradiography correspond to Env interacting with cholesterol at the same time.

Illustration III. Relationship between Env-MA/Gag co-immunoprecipitation and [³H]-photo-chol interaction. A) Immunoprecipitate (IP) ag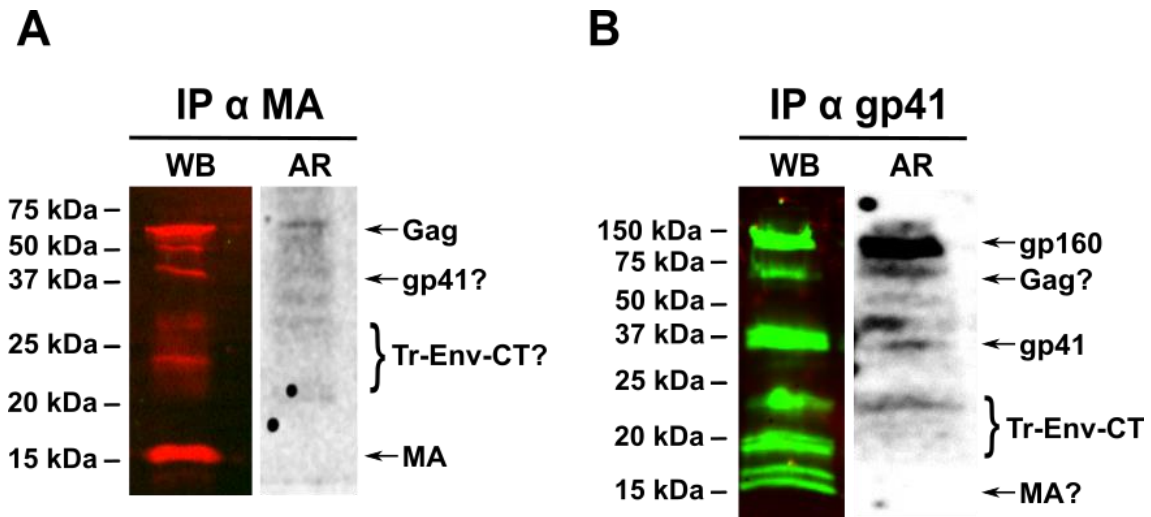ainst MA from concentrated viral particles were detected by Western blot (WB) and autoradiography developed with rabbit α-MA primary antibody and α-rabbit IRDye680 secondary antibody (red) to detect Gag/MA. **B)** 10% of the supernatant (SN) of the previous IP α MA in A and immunoprecipitate (IP) against gp41 from the SN of IP α MA in A were visualized by Western blot with Chessie-8 α-gp41 as primary antibody and α-mouse IRDye800 secondary antibody (green) to detect gp41. T-Env-CT=Truncated cytoplasmic tail domain of Env.

Three possible conditions were suggested that could be happening during Gag/MA–cholesterol interaction, which would explain the absence of signal in the previous protein-lipid studies with [³H]-photo-chol. These situations could be the following: 1) the no direct interaction between Gag/MA and cholesterol could be real; 2) the interaction could not be assessed with [³H]-photo-chol because the distance is far from 3 Å; and 3) there could be an indirect Gag/MA–cholesterol interaction via Env glycoprotein, which leads to state the theory of the sandwich model (Illustration IV). This model proposes the following. Gag and cholesterol could drive the formation of cholesterol-enriched membrane nanodomains that host-selected proteins, such as Env, and reduce their mobility in the membrane. In there, Env, which interacts directly with this lipid and Gag/MA, could be stuck forming a sandwich during morphogenesis, where there would not be a direct interaction between Gag/MA and chol, but an indirect interaction could exist via Env, due to the fact that it is known that Gag plays a role in the redistribution, targeting and incorporation of Env during viral maturation.

The work develop during this Thesis supports the most plausible of the aforementioned hypothesis, which is the last situation, the sandwich model where Gag/MA does not interact directly with cholesterol during HIV-1 morphogenesis, and, however, they maintain an essential and strong relationship during HIV-1 assembly needed for the development of new infectious viral particles.
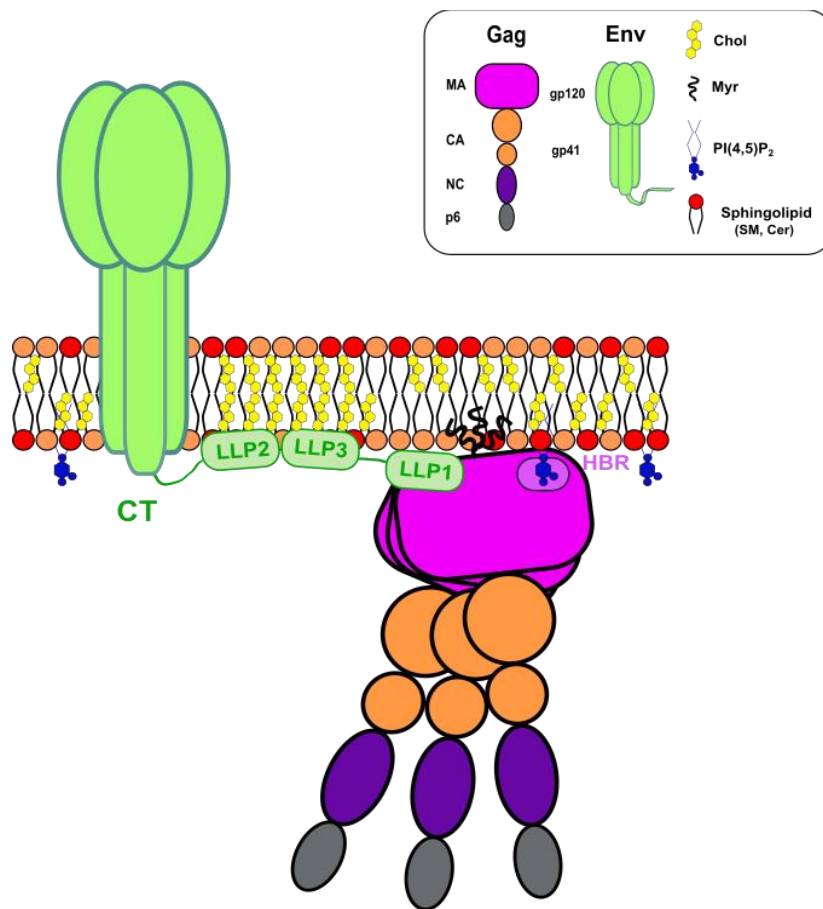
Illustration IV. Indirect Gag/MA-cholesterol interaction as "the sandwich model". Gag is anchored to the plasma membrane thanks to the interaction between MA (Myr plus HBR domains) and PI(4,5)P2. The presence of Gag and cholesterol in the membrane could drive the formation of cholesterol-enriched nanodomains that could retain some host-selected proteins as Env and reduce their mobility. As it is known that Env could interact with cholesterol through its CT, precisely through LLP2 and LLP3, and could also interact with MA through this same domain, this model hypothesises a interaction between MA and Env LLP1, while at the same time Env could be interacting with cholesterol through the other two LLPs. Thus, Env is stuck between Gag and cholesterol forming a sandwich during morphogenesis, where there is an indirect interaction between Gag/MA and cholesterol via Env glycoprotein.

The palmitoyl-modified analogue acts as its natural counterpart

The alkyne-modified palmitoyl analogue used in Thesis was developed to mimic palmitate moieties added to the proteins during palmitoylation, acting as a substrate for palmitoyltranferases. This clickable probe has an alkyne group attached to its terminal moiety (Illustration V), being accessible to suffer Copper(I)-Catalyzed Azide-Alkyne Cycloaddition (CuAAC) reaction for sensitive fluorescence detection and/or for affinity enrichment and proteomic analysis.
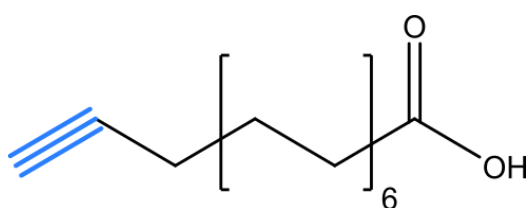
Illustration V. Alkyne-modified palmitoyl analogue. Structure of alkyne-modified palmitoyl analogue, 15-octadecynoic acid. Alkyne group is coloured in blue.

The palmitoyl analogue was added to the cell culture during growth, so the target proteins after 24 h incubation are labelled with a palmitoyl moiety containing the alkyne group at the end of the fatty acid chain. The correct function of this clickable probe could have been successfully verified by a palmitoylation test developed based in the CuAAC reaction together with the immunoprecipitation of gp41 by Chessie-8 coupled to Protein G Sepharose beads (Illustration VI). A corresponding band to gp41 at ~41-50 kDa can be clearly observed in both channels in the treated viral-like particles (VLPs) and it is not present in the green channel in the case of control VLPs, meaning the correct palmitoylation of gp41 by the clickable analogue. Thus, this palmitoyl analogue could palmitoylate HIV-1 gp41 cysteines as its natural counterpart after incubation in HEK 293T cells.

Illustration VI. Palmitoylated gp41 in viral particles treated with the alkyne-modified palmitoyl analogue. Western blot images of the input, supernatant (SN) and immunoprecipitate (IP) for Env gp41 protein in wild type VLPs (wt) and VLPs treated with the palmitoyl-modified analogue (pwt). The Western blot was developed with Chessie-8 α-gp41 primary antibody and anti-mouse IRDye680 antibody as a secondary antibody (red). The palmitoyl-modified analogue was clicked using IRDye 800CWAzide Infrared Dye (green).
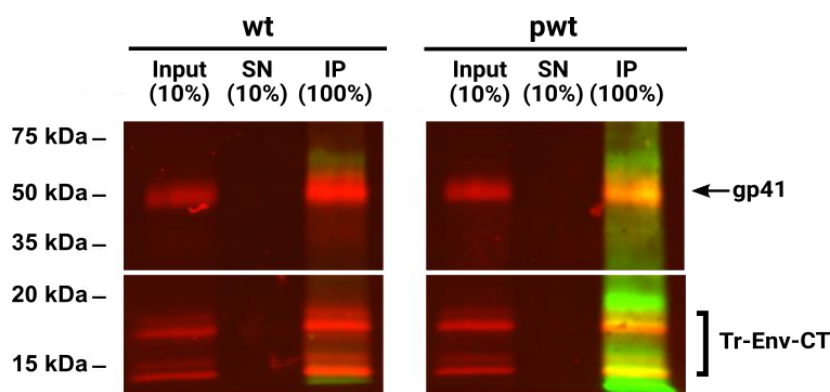
A protocol for the extraction of HIV-1 palmitoylated proteins was developed

After multiple assays and tests to control all the variables, factors and specific binding conditions that affect the immunoprecipation process, a definitive protocol for the extraction of the HIV-1 palmitoylated proteins could have been developed. This protocol could be consulted in Section 4.2.3.2 of this Thesis. The final protocol is based in based in the CuAAC reaction, the palmitoyl-modified analogue and the strong biotin-avidin binding.

The Illustration VII shows representative Western blot and silver stain after applying the final extraction protocol to wild type viral particles (wt) and viral particles treated with the palmitoyl analogue (pwt). A positive signal around the size of HIV-1 gp41 in the eluted pellet of the treated viral particles indicates that the protocol has been effective for the extraction of palmitoylated proteins (Illustration VII A). As expected, there is no signal in the eluted sample of wild type particles. In the silver stain of Illustration VII B, a huge difference in the protein pattern could be seen between the eluted pellets of wild type and treated with palmitoyl analogue, meaning an enrichment in palmitoylated proteins in the treated sample. Therefore, this protocol could be used to extract HIV-1 palmitoylated proteins to their subsequent proteomic analyses by mass spectrometry.
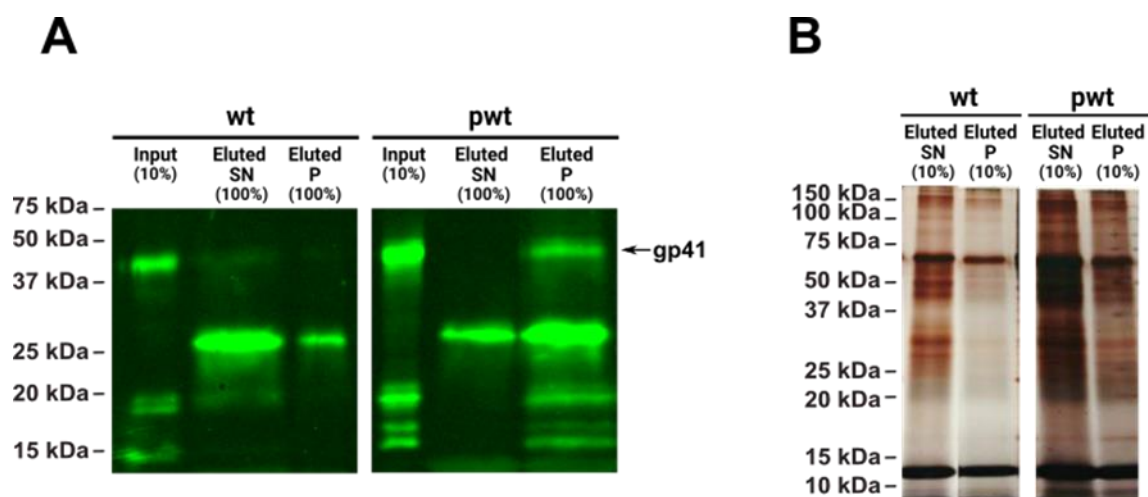
Illustration VII. Representative results of optimized protocol for extraction of palmitoylated proteins. Western blot (**A**) and silver stain (**B**) of both eluted viral particles of wild type (wt) and treated with the palmitoyl analogue (pwt) after the last modified extraction protocol. P and SN are the pellet and supernatant resulting from the ethanol/chloroform protocol, respectively. Western blot was developed with Chessie-8 α-gp41 primary antibody and α-mouse IRDye800 secondary antibody.

After proteomic studies, 153 potentially palmitoylated proteins were detected exclusively in viral particles treated with the palmitoyl-modified analogue. The 76.47% of the potential palmitoylated proteins, are described to be palmitoylated in accordance with the SwissPalm database. The vast majority of these proteins were localized to be mainly forming part of the spliceosome and the proteasome. After analysing their biological and molecular functions, it could be suggested that the detected palmitoylated proteins would be implicated in the control and regulation of the machinery of transcription and secretion during HIV-1 morphogenesis.

Contents

Abbreviations

AIDS	Acquired Immunodeficiency Syndrome
ALEM	Acidic Lipid Enriched Microdomains
AR	Autoradiography
BCA	Bicinchoninic acid assay
BSA	Bovine Serum Albumin
CA	Capsid (HIV-1 protein)
Cav-1	Caveolin-1 protein
CCR5	C-C chemokine Receptor type 5
Chol	Cholesterol
CHR	C-terminal heptad repeat (gp41 domain)
CKs	Cytokin kinases
cpm	Counts Per Minute
CRAC	Cholesterol Recognition Amino acid Consensus (gp41 region)
CRD	Cysteine Rich Domain
CT	Cytoplasmic Tail (gp41 domain)
CuAAC	Copper(I)-Catalyzed Azide-Alkyne Cycloaddition
CVP	Concentrated Viral Particles
CXCR4	C-X-C chemokine Receptor type 4
DHHC	Aspartate-histidine-histidine-cysteine motif
DMSO	Dimethyl sulfoxide
DRiPs	Defective Ribosomal Products
DNA	Deoxyribonucleic acid
DPG	Aspartate-proline-glycine motif
dpm	Disintegrations Per Minute
DRMs	Detergent Resistant Membranes
ED	Ectodomain (gp41 domain)
EDTA	Ethylenediamine tetraacetic acid
Env	Envelope glycoprotein (HIV-1 protein)

1

ER	Endoplasmic Reticulum
ESCRT	Endosomal Sorting Complexes Required for Transport
FBS	Fetal Bovine Serum
FP	Fusion peptide (gp41 domain)
Gag	Gag precursor polyprotein (HIV-1 protein)
GagPol	Gag and Pol polyproteins expressed in tandem (HIV-1 protein)
GCCs	Gag-Containing Complexes
GFP	Green Fluorescent Protein
gp120	Glycoprotein 120, surface glycoprotein (HIV-1 protein)
gp160	See "Env"
gp41	Glycoprotein 41, transmembrane glycoprotein (HIV-1 protein)
GxxxG	Helix-helix membrane dimerization motif (gp41 region)
HAART	Highly Active Antiretroviral Therapy
HBR	Highly Basic Region (MA domain)
HBS	HEPES-Buffered Saline
HDF	HIV-1 dependency factor
HEPES	4-(2-hydroxyethyl)-1-piperazineethanesulfonic acid
HIV	Human immunodeficiency virus
hnRNPs	Heterogeneous nuclear ribonucleoproteins
IN	Integrase (HIV-1 protein)
IP	Immunoprecipitation/Immunoprecipitate
IP6	Inositol hexakisphosphate
LE/MVBs	Late Endosomal/Multivesicular Bodies
LLP	Lentiviral Lytic Peptide
MA	Matrix (HIV-1 protein)
MPER	Membrane Proximal External Region (gp41 region)
Myr	Myristoyl group of MA
Myr(e)	Myr-exposed state
Myr(s)	Myr-sequestered state
NC	Nucleocapsid (HIV-1 protein)
Nef	Negative factor (HIV-1 protein)

NHR	N-terminal Heptad Repeat (gp41 domain)
P	Pellet
p6	Budding p6 protein (HIV-1 protein)
PaCCT	Palmitoyltransferase Conserved C-terminus motif
PATs	Protein palmitoyltransferases
PBS	Phosphate-Buffered Saline
PC	Phosphatidylcholine
PE	Phosphatidylethanolamine
PGSB	Protein G Sepharose Beads
pI-PE	Plasmenylethanolamine
$PI(4,5)P_2$	Phosphatidylinositol (4,5)-biphosphate
Pol	Pol precursor polyprotein (HIV-1 protein)
PR	Protease (HIV-1 protein)
PS	Phosphatidylserine
PTMs	Post-translational modifications
PVP	Purified Viral Particles
pwt	Palmitoylated HIV-1 VLPs by the palmitoyl-modified analogue
Rev	Regulator of Expression of Virion proteins (HIV-1 protein)
RER	Rough Endoplasmic Reticulum
RNA	Ribonucleic acid
rpm	Revolution Per Minute
RT	Reverse Transcriptase (HIV-1 protein) / Room Temperature
SD	Standard Desviation
SDS	Sodium Dodecyl Sulfate
SIV	Simian Immunodeficiency virus
SPL	Sphingolipids
SM	Sphingomyelin
SN	Supernatant
SP	Sphingosine
SS	Silver Stain
TAE	Tris base, acetic acid and EDTA

Tat	Trans-Activator of Transcription (HIV-1 protein)
TBS	Tris-buffered saline
TBS-T	TBS with Tween 20
TBTA	Tris[(1-benzyl-4-triazolyl)methyl]amine
TEMs	Tetraspanin-Enriched Microdomains
TfR	Transferrin Receptor
THPTA	Tris((1-hydroxy-propyl-1H-1,2,3-triazol-4-yl)methyl)amine
TLC	Thin Layer Chromatography
TM	Transmembrane domain (gp41 domain)
Tr-Env-CT	Truncated cytoplasmic tail domain of Env
TTx-E	Threonine-threonine-x-glutamate motif (x; any amino acid)
UV	Ultraviolet
VLPs	Viral-Like Particles
Vpr	Viral Protein R (HIV-1 protein)
Vpu	Viral Protein U (HIV-1 protein)
WB	Western blot
wt	HIV-1 wild type VLPs

Chapter 1.

Introduction

Chapter 1: Introduction

1.1. Cell membrane

The cell membrane is more than a thin semi-permeable barrier that surrounds the cytoplasm of a cell. Cell membranes are a hydrophobic matrix of polar lipids, intercalated proteins and carbohydrates, which could be bound to these lipids and proteins. Cell membranes are not only boundaries between two aqueous compartments, but they also act as a specific compartment that accommodates and takes part in a wide range of essential functions: communication with the external environment, molecular transport, cell shape maintenance, metabolism, cell signalling, cell adhesion, cell differentiation and cell death (Stillwell, 2016).

1.1.1. The cell membrane model

Singer and Nicolson in 1972 combined all the discoveries about the cell membrane up to date and postulated the basis of the "fluid mosaic model" (Singer & Nicolson, 1972) (Figure 1.1), which is the paradigm of the structure of the cell membrane accepted nowadays.
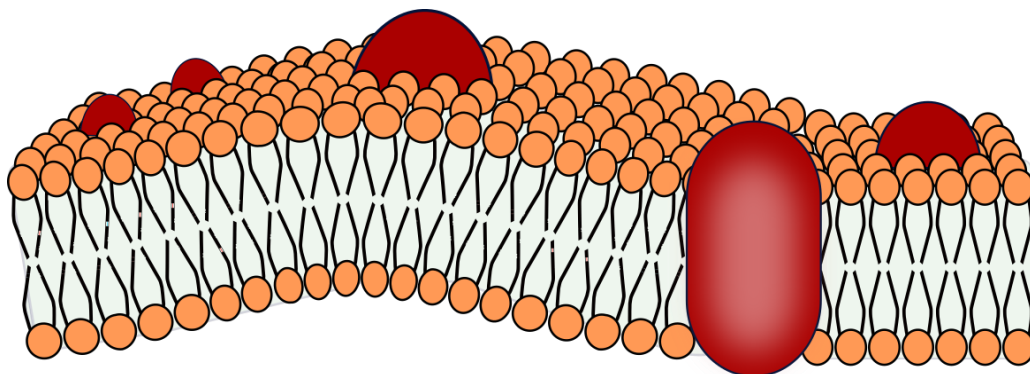
Figure 1.1. Schematic representation of the Singer–Nicholson "fluid mosaic model."

It is named as mosaic model because Singer and Nicolson proposed lipids and proteins to organize in a structure reminiscent of the Roman mosaics. The amphipathic nature of lipids induces the formation of a double layer where proteins are scattered across the bilayer and along its surface. They could interact with the lipids, either being embedded in the lipid matrix (integral proteins) or being associated with them through hydrophilic interactions (peripheral proteins) (Figure 1.1). The model was named fluid because they suggested that lipids and proteins were constantly moving in each lipid monolayer, diffusing laterally in the plane of the membrane. This dynamism facilitates interactions between lipids and proteins, important for membrane function making both sides of the bilayer different in composition and structure.

The fluid mosaic model has suffered several modifications in the last decades, which update the original model (Engelman, 2005; Goñi, 2014; Jacobson et al., 1995). In this day and age, it is widely known that membranes are full of proteins whose mobility can be limited by the cytoskeleton in eukaryotic cells, and which can also create large complexes to carry out many functions in the membrane. This high protein density will result in a strong perturbation of the lipid bilayer. Thus, the lipid bilayer is no longer seen as a static homogeneous structure.

This dynamic view of the bilayer also affects the lipids, accepting the presence of a high number of lipid phases and non-lamellar structures. The Singer and Nicolson model referred as liquid-crystalline phases as the only relevant ones in the well-organized lamellar structure, however, a number of phases as the liquid-ordered, the inverted hexagonal or the cubic ones must also be considered because the membrane can transiently adopt non-lamellar structures in small regions. Additionally, the presence of non-lamellar structures confirms that the lipid bilayer is curved. A further adjustment is related to the limited movement of the lipids across the bilayer since trans-bilayer lipid motion has been confirmed (Contreras et al., 2011).

An important contribution regarding the lateral heterogeneity of membranes was the proposal by Simons and Ikonen in 1997 based on the existence of lateral structures, which are enriched in cholesterol (chol) and sphingolipids (SPLs), that could serve as platforms for protein anchoring during signal transduction (Simons & Ikonen, 1997).

These structures, denoted as "lipid rafts" (Section 1.1.2.2.1), are believed to have profound effects on the nature of the membrane and opened the door to the now well-accepted view on the importance of membrane domains for its biological function.

1.1.2. Structure and composition

The main constituents of the cell membrane are membrane lipids (glycerolipids, SLPs and sterols) and membrane proteins (integral and peripheral membrane proteins) (Figure 1.2).

The structure adopted by the membrane is the most thermo-dynamically stable. Membrane lipids expose their hydrophilic headgroups to the aqueous environment on both sides of the bilayer, while the hydrophobic tails are trapped in a non-polar core facing each other. Integral proteins are embedded in the lipid bilayer matrix, where they are able to establish hydrophobic and hydrophilic interactions with their respective lipid counterparts. Peripheral proteins can also be transiently associated with membrane surfaces through weaker interactions. Furthermore, lipids at the outer leaflet of the membrane and extracellular domains of proteins are often glycosylated (Stillwell, 2016).
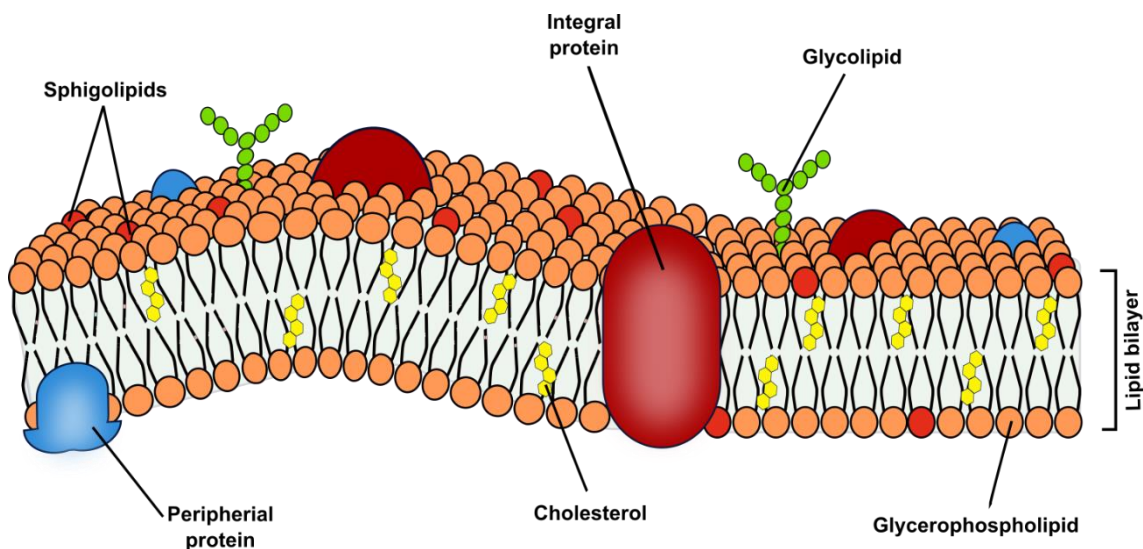
Figure 1.2. Schematic representation of the structure and composition of the cell membrane.

Understanding the relationship between lipids and proteins, and between their selves, could give further insights into the mechanisms of certain cellular events taking place in the bilayer, even though in abnormal situations such as many diseases (cancer, obesity, neurodegenerative disorders and cardiovascular pathologies). Therefore, novel pharmacological strategies based on the regulation of membrane lipids and/or proteins against these pathological conditions have gained notoriety in the last century (Escribá, 2006). The importance of the existence of different interactions at the cell membrane, including protein-lipid and protein-protein interactions, will be further discussed in Section 1.4.

1.1.2.1. Membrane proteins

It is known that the 20-30% of all genes in most genomes encode for membrane proteins (Krogh et al., 2001). The protein-to-lipid ratios in membranes is highly fluctuating, from 76% protein content in the inner mitochondrial membrane to 50% protein content in the plasma membranes of most animal cells (Dupuy & Engelman, 2008). This variability depends on their specific cellular localization and function; therefore, they can densely populate the membrane or be alternatively confined to certain areas.

The classification of membrane proteins depends on their anchorage to the lipid bilayer. Integral membrane proteins are embedded into the membrane, passing through via one or multiple transmembrane domains. Peripheral membrane proteins are attached to the exterior of the lipid bilayer by electrostatic interactions (Lodish et al., 2007) (Figure 1.2).

Most of the diverse activities exhibited by biological membranes are carried out by membrane proteins. As an example, proteins have a crucial role in the selective permeability of the membrane. While small uncharged molecules such as oxygen and carbon dioxide can freely diffuse across the membrane, the diffusion of larger molecules is restricted by the lipid bilayer. Specific transport proteins allow these molecules to cross the membrane. Some of the transport proteins just facilitate diffusion by forming

10

pores or channels, but others can actively transport molecules against their concentration gradient, thus, promoting the accumulation of solutes and the creation of solute gradients. Membrane proteins could also possess enzymatic activity, supporting cell metabolism, as well as communication across the membrane without transport of molecules (Yeagle, 2012).

1.1.2.2. Membrane lipids

Approximately, the 5% of the genome of an eukaryotic cell codify for multiple different lipids (van Meer et al., 2008). The variety of headgroups or acyl chains that can be attached to lipid backbones is the main reason why there are more than a thousand of different lipid species estimated in any eukaryotic cell, however, only hundreds of species form membranes naturally. These lipid molecules make up ~40% of cell membrane dry weight (Harrison & Lunt, 1980; Shevchenko & Simons, 2010; van Meer et al., 2008), defining the membrane biophysical properties, such as thickness, lateral diffusion, and fluidity.

Lipids are organic molecules of amphipathic nature that contain a hydrophobic tail and a hydrophilic headgroup. The hydrophobic effect makes them insoluble in polar solvents, consequently, they form the most thermodynamically stable structure that maximizes both hydrophobic and hydrophilic interactions. Therefore, they self-aggregate forming bilayers, the basic components of cell membranes. This hydrophobic effect can be affected by several parameters such as the chemical nature of the molecules, temperature, pressure, ionic strength, hydration level, size of the lipid, salinity and pH of the solution (Lombard, 2014; Stillwell, 2016).

The basic hydrophobic moieties of most membrane lipids are the fatty acids. A fatty acid is a monocarboxylic acid that could be either saturated or unsaturated. Fatty acids are classified depending on their carbon chain length, which could vary from 4 to 24 carbons: short-chain (4-6 carbons), medium-chain (8-10 carbons) and long-chain (12-24 carbons). Long-chain fatty acids are the most common in membranes, where they are relevant for the maintenance of membrane structure (Stillwell, 2016). In addition, other

lipid functions include acting as energy and heat sources due to their chemically reduced state, signalling molecules, protein recruitment platforms and substrates for translational protein-lipid modifications (Harayama & Riezman, 2018).

Membrane lipids are classified depending on their chemical composition. Their chemical structures are the responsible for their physicochemical properties, explaining their behaviour in membranes. They are divided into three main groups: glycerolipids, SPLs, and sterols (Figure 1.3).
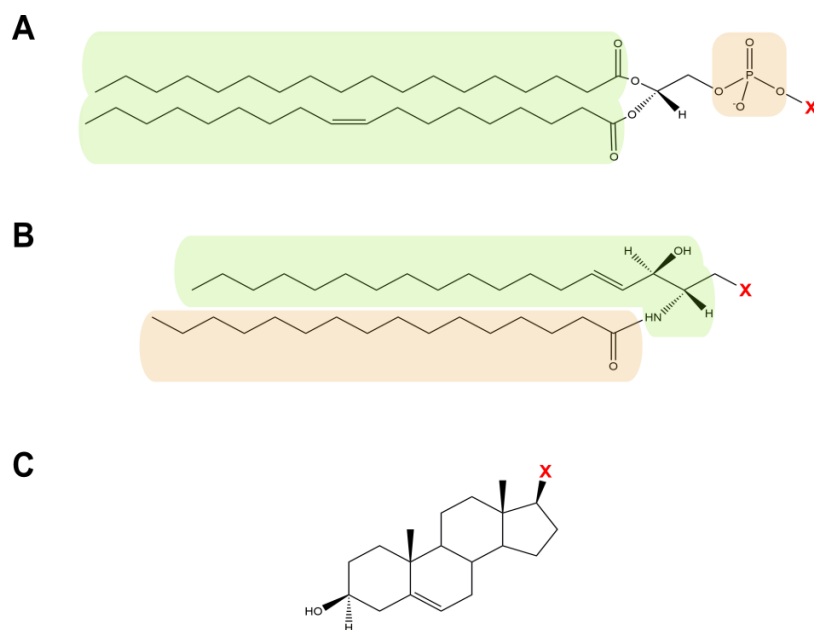
Figure 1.3. Representation of the general chemical structures of membrane lipids. A) Chemical structure of glycerophospholipids. A glycerol group (black), a saturated fatty acid in *sn*-1 and an unsaturated one in *sn*-2 (green), a phosphate group (orange) and the polar headgroup substituent (red). **B)** Chemical structure of sphingolipids. A sphingosine backbone (green), a saturated fatty acid (orange) and the polar headgroup substituent (red). **C)** Chemical structure of sterols. The hydrocarbon tail substituent is coloured in red.

The lipid distribution of the different membrane lipids in the cell membrane is quite heterogeneous. The outer leaflet of the cell membrane is highly enriched in choline-containing glycerophospholipids, mostly phosphatidylcholine (PC) and sphingomyelin (SM), while the inner cytoplasmic leaflet is rich in amine-containing glycerophospholipids, such as phosphatidylethanolamine (PE) and phosphatidylserine (PS). Other minor phospholipids, such as phosphatidic acid, phosphatidylinositol, and

phosphatidylinositol phosphates, are also enriched in the cytoplasmic face of the membrane where they take part in cell signalling (Cooper & Hausman, 2013). The maintenance of this heterogeneity is critical for the correct physiological homeostasis of the cell. A loss of asymmetry has been frequently associated with mechanisms of programmed cell death and may also contribute to the development of lipid imbalances and human pathologies such as cancer and neurological and metabolic diseases (Casares et al., 2019; Fadeel & Xue, 2009). In addition, membrane lipids show lateral asymmetry due to the formation of specialized membrane regions also called nanodomains such as lipid rafts, caveolae, coated pits and synaptosomes (Goldstein et al., 1979; Simons & Ikonen, 1997; Thomas & Smart, 2008; Whittaker et al., 1964).

1.1.2.2.1. Lipids rafts

Lipid rafts are highly dynamic microdomains in the cell membrane composed of chol and SPLs, such as SM and ceramide (Figure 1.4). Cholesterol and SPLs carrying saturated hydrocarbon chains assemble to form tightly packed subdomains corresponding to liquid-ordered phases (Brown & London, 1998; Simons & Ikonen, 1997). This lipid structure is assumed to be in cellular lipid rafts. Lipid rafts float freely in the surrounding membrane, which is more fluid. The higher fluidity is the consequence of the high surface area occupied by unsaturated phospholipids compared to the dense packing of the sphingolipid-chol and saturated phosphoglicerolipids-chol assemblies. Cholesterol also condenses monounsaturated phospholipids but leaves them in the liquid-disordered phase (Silvius, 2003; Wiśniewska et al., 2003).
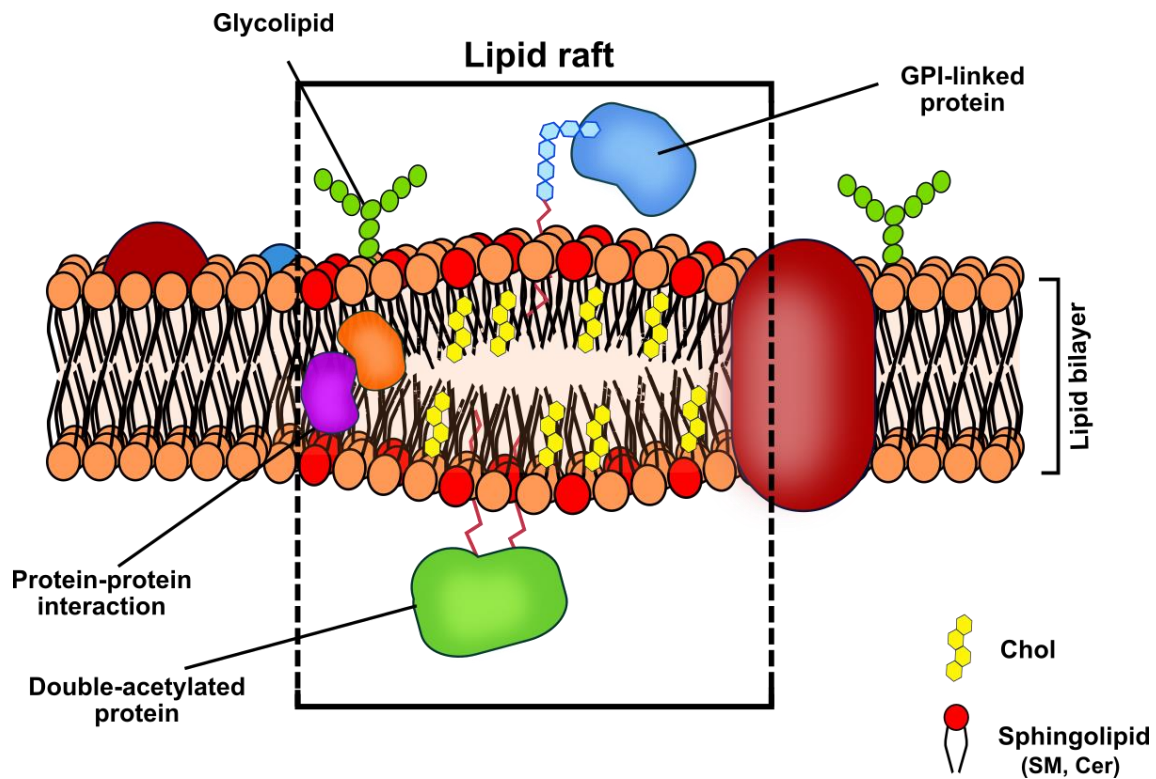
Figure 1.4. Schematic representation of a lipid raft.

Cholesterol and ceramide are synthesized in the endoplasmic reticulum (ER), but the steady-state concentration of these compounds is too low to allow formation of rafts. Sphingomyelin and glycosphingolipids are synthesized in the Golgi apparatus, and it is here where raft assembly takes place. Cholesterol and other raft lipids are excluded from retrograde traffic between the Golgi apparatus and ER, and the overall consequence is an increasing concentration of chol and SPLs from the ER to the cell membrane (Füllekrug & Simons, 2004).

Individual rafts are believed to be small and dynamic, therefore, they are difficult to detect *in vivo*. There are many types of nanodomains with different stiffness and containing different amounts of chol (Lorizate et al., 2021). Based on fibroblast measurements, only to about 10–20 protein molecules are present in these individual rafts (Füllekrug & Simons, 2004). The binding energy of raft-associated proteins provide is not sufficient to anchor a protein to a membrane. Therefore, proteins can only maintain an efficient membrane interaction when a second membrane-binding site is present. This second membrane binding site can be created by a nearby stretch of basic residues or

palmitoyl chains as in the Src family of protein kinases or the α subunits of heterotrimeric G proteins. Glycosylphosphatidylinositol (GPI)-linked proteins such as CD55, PLAP and Thy-1 are the most abundant proteins associated with the outer leaflet of the raft bilayer. Hence, for efficient interaction of different raft-associated proteins, lipid rafts need to coalesce in larger platforms (up to 500 nm) (Briggs et al., 2003; Harder et al., 1998; Lucero & Robbins, 2004).

Lipid rafts are associated with many molecular processes such as cell signalling, cell adhesion, cell differentiation and cell death. In addition, these raft-like nanodomains have been described to be able to include or exclude certain proteins from specific regions of the cell membrane (Simons & Toomre, 2000), suggesting that these structures may act as regulators of the function of certain proteins, which might need a specific localization or association with other proteins. In fact, those platforms are thought to concentrate the viral components, facilitating protein-protein interactions during viral assembly (Suomalainen, 2002; Veit, 2012). Indeed, it is known that cholesterol properties, including its raft-promoting function, contribute to HIV-1 infectivity (Campbell et al., 2002, 2004; Hawkes et al., 2015).

1.1.2.2.1.1. The relevance of cholesterol in the cell membrane

Cholesterol makes up to 30 mol% of the total lipid content, being present in even higher amounts in red blood cells and ocular lens membranes. The 80–90% is present mainly at the cell membrane whereas very little content has been associated with the ER and mitochondrial inner membranes (Sadava et al., 2009). The cholesterol composition in the membrane is altered in multiple diseases, at different cancer stages and during pathogenic infections (Kumar et al., 2016; Kuzu et al., 2016; Song et al., 2021).

The unique chemical structure of chol allows it to be inserted into the membrane and be extracted from them quite easily. In essence, it consists of a tetracyclic cyclopenta[a]phenanthrene structure with an iso-octyl sidechain at C-17, which inserts into the bilayer (Figure 1.5).
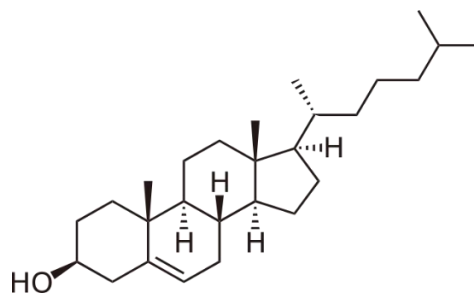
Figure 1.5. Chemical structure of natural cholesterol.

Cholesterol is unable to form bilayers by itself due to its small polar head group, a β-hydroxyl group (-OH) at C-3, which cannot effectively shield the hydrophobic part from water (Huang & Feigenson, 1999). However, it could interact with membrane lipids of large headgroups such as SM or with the transmembrane domain of a protein (Björkbom et al., 2010). Due to its asymmetric structure, chol interacts with SPLs through its planar sterane backbone and with transmembrane proteins through its aliphatic groups (methyl substituents in C-10 and C-13, and the terminal iso-octyl chain at C-17) (Fantini & Barrantes, 2013; Garmy et al., 2005).

As a result of its relatively rigid structure, chol has a substantial effect on the physicochemical properties of membranes, such as viscosity and interleaflet coupling. Thus, it is responsible for the thickness and the stiffness of the membrane by avoiding the tight packing of glycerophospholipids structures to regulate the lipid bilayer fluidity (Maxfield & van Meer, 2010; Mouritsen & Zuckermann, 2004). This lipid plays an essential role in the organization, dynamics, function and sorting of membranes, as well as, in trafficking and signalling transduction processes. Furthermore, cholesterol can regulate the lateral organization of membranes by associating with SPLs to generate lipid rafts(R. Schroeder et al., 1994; Simons & Ikonen, 1997; Xu & London, 2000).

Dysregulation of this sterol uptake and metabolism in cells is the cause of a wide range of human diseases, including lysosomal storage disorders (Tay–Sachs, Fabry, Niemann–Pick type A or B, and Sandhoff diseases), atherosclerosis, cardiovascular disorders, neurodegeneration, diabetes, COVID-19 and cancer (Kuzu et al., 2016; Maxfield & Tabas, 2005; Song et al., 2021; Vance, 2012).

1.2. The HIV virus

1.2.1. The relevance of HIV and AIDS

Human immunodeficiency virus (HIV) is the responsible of causing the acquired immunodeficiency syndrome (AIDS) pandemic infection. This virus most likely spread from non-human primates to humans throughout the 1900s in populations of Central and East Africa. Nevertheless, only in 1981 did the HIV become target of world's attention when the first case of AIDS in the United States was reported (Faria et al., 2014; Keele et al., 2006).

There are two main strains or types of HIV: HIV-1 and HIV-2. HIV-1 is more prevalent and more pathogenic than HIV-2 and is the cause for the vast majority of the global pandemic. Sequence comparisons suggest that both strains are the result of cross-species transmissions of simian immunodeficiency virus (SIV) from chimpanzees (SIV$_{cpz}$) and sooty mangabeys (SIV$_{smm}$), respectively. The reduced pathogenicity of HIV-2 in humans is thought to be the result of lower levels of virus replication, perhaps reflecting incomplete adaptation of SIV to the human host (Bell & Bedford, 2017; Sharp & Hahn, 2010). Therefore, due to its virulence, this Thesis will verse about HIV-1 even though both types of HIV could cause AIDS.

According to the data published by UNAIDS in 2021, the annual number of deaths from AIDS-related illness among people living with HIV from all ages, globally, has fallen from 1.9 million in 2004 to 680,000 in 2020. Since 2010, AIDS-related mortality has declined by 53% among women and girls and by 41% among men and boys. However, COVID-19 pandemic has widened inequalities between countries, disrupted HIV testing and led to steep drops in diagnoses and referrals to HIV treatment. Hence, reaching the 2030 milestone of ending up completely with AIDS pandemic seems hard in this context, requiring to each country to identify the gaps in their HIV responses and apply an equality lens to close those gaps and to totally implement the Global AIDS Strategy and the Political Declaration on AIDS.

In Spain, since the beginning of the outbreak until the 31st of June of 2021, a total of 88,684 cases of AIDS have been reported in accordance with the annual report of the Unity of Vigilance of HIV, STDs and Hepatitis from the Ministry of Health, Government

of Spain. After reaching its zenith in the mid-1990s, the number of reported cases has experienced a progressive decline from 1996, a year prior to the generalization of the highly active antiretroviral therapy (HAART), until today. Here, in the Basque Country, the number of new HIV infections per year is quite fluctuating. In the period 1997-2020, the highest peak of cases is reached in 1997 with 229 and the lowest in 2020 with 105 cases according to the Basque Health Agency (Osakidetza) annual report. However, new data from 2020-2021 is affected by COVID-19 pandemic. These aforesaid results could indicate that the control of new infections is still a tedious fight, even in regions such as the Basque Country where HAART is available.

AIDS and HIV-1 infection are, without a shred of a doubt, one of the main concerns around all the four corners of the globe. Therefore, unravelling the molecular mechanisms that govern HIV-1 infection is totally needed to develop new antiretroviral therapies that could complete eradicate the pandemic.

1.2.2. HIV-1

The HIV-1 is a single strand positive-sense RNA virus, whose virions package all the components needed for infectivity. This virus belongs to the *Retroviridae* family, which is characterized by the use of reverse transcriptase to convert their genomic RNA into DNA, which a virus-born integrase enzyme will subsequently help integrating into the host cell genome. This cell will assume the viral genetic material as part of its own, leading to the translation of proteins required for assembly of new viral copies. Moreover, it is included in the *Lentivirus* genera, whose members exhibit an especial long incubation period, i.e., the time it takes for immunodeficiency symptoms to appear after the initial exposure to the pathogen (Levy, 1993; Smith & Daniel, 2006; Sundquist & Kräusslich, 2012). Their genome comprises three main genes, namely:

- *pol* encodes for the viral enzymes, which are reverse transcriptase (RT), integrase (IN) and protease (PR).
- *gag* codifies for the Gag precursor polyprotein, which is responsible for virus morphogenesis. After PR cleavage, Gag generates p24 or viral capsid (CA), p17 or matrix (MA), p7 or nucleocapsid (NC) and p6 (Ross et al., 1991).

- *env* encodes for gp160 or the envelope protein precursor, which is cleaved by cellular furins into gp120 and gp41 proteins. They form spikes that allow the recognition of the cellular receptor and posterior viral entry.

In addition, there is a set of accessory genes that vary across different lentivirus, which in particular for HIV-1 are *vif*, *vpr*¸ *vpu*, *tat*, *rev*, and *nef*, and they codify for the rest of the viral proteins. Although the *gag* gene can be expressed by itself to generate the Gag polyprotein, *pol* is always expressed in tandem with *gag* as the GagPol polyprotein.

In the Figure 1.6, the typical structure of a mature HIV-1 virion is shown. HIV-1 virion is covered by a lipidic membrane with a size of 120 nm in diameter, approximately. Inside the viral membrane, there are two copies of the positive-sense RNA packaged into a furenelle cone viral capsid (~250 CA hexamers and 12 CA pentamers) (Rossi et al., 2021) and the necessary enzymes for the viral replication cycle: PR, RT, and IN. Two main proteins could be found associated to the viral membrane: MA is underneath the viral membrane, and the envelope (Env) protein is embedded in the membrane and protruding to the outside.
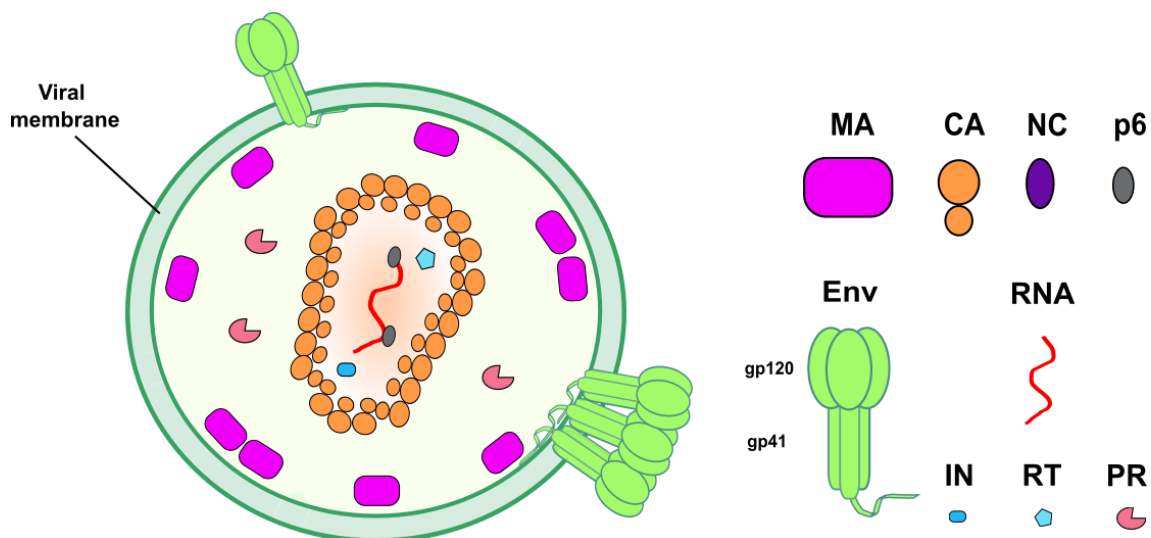
Figure 1.6. Schematic structure of a mature HIV-1 virion. HIV-1 is delimited by a lipidic membrane, in which the Env proteins are embedded and protrude to the outside. Underneath the viral membrane MA remains associated with it, and CA generates a cone shaped capsid that surrounds the viral RNA, which is packed thanks to NC. The viral enzymes RT, IN and PR are also packed inside the virus.

1.2.2.1 HIV-1 Replication cycle

A schematic representation of HIV-1 replication cycle is shown in Figure 1.7. The replication cycle begins with the fusion of HIV-1 membrane with the host cell membrane. Typically, host cells are CD4$^+$ T cells and cells of the monocyte/macrophage lineage. In the first step of the replication cycle takes place the entry process, where gp120 binds to CD4 receptor and CCR5 or CXCR4 co-receptors and gp41 catalyses the fusion between viral and cellular membranes, releasing the viral core into the cytoplasm (Checkley et al., 2011; Wilen et al., 2012). Intact viral capsids are transported to the nucleus by the help of the microtubule network and some adaptor proteins, such as FEZ1 and BICD2. Once there, they pass through nuclear pore complexes thanks to the interaction with NUP153, NUP358, TNPO3, and CPSF-6 (Malikov et al., 2015; Rossi et al., 2021; Zila et al., 2021). In the nucleus, viral capsids are uncoated near their integration site (Li et al., 2021), and viral RNA is converted into double stranded DNA by the HIV-1 RT and inserted into the host genome by IN. HIV-1 RT enzyme lacks proofreading activity, so it gives rise to the huge variability among HIV isolates existing nowadays (Roberts et al., 1988).

Integrated viral DNA could stay latent for an undefined period of time. HIV-1 latency is one of the main issues in current HAART. Antiretroviral therapy could effectively fight against spread of the virus in most of the cases and reduce viral load in the blood (viremia) of HIV-1 infected patients to undetectable levels, however, is not capable of defeating the dormant HIV-1 (Siliciano et al., 2003).

When replication is activated, DNA is transcribed into RNA, exported to the cytoplasm and translated into the viral proteins. Gag is produced as a 55 kDa polyprotein and it would be involved in the morphogenesis of the future virions. Two copies of non-translated positive-sense viral RNA in each viral particle dimerize and Gag forms low-order oligomers that bind to this RNA triggering the formation of high-ordered ribonucleoprotein complexes, which are targeted to the cell membrane and accumulated in Gag assembly sites (Bou-Nader et al., 2021; Durand et al., 2022; Jouvenet et al., 2006; Moore & Hu, 2009). At the same time Gag is being synthesized, *gag* and *pol* genes are expressed in tandem to generate the GagPol polyprotein precursor. GagPol

contains the constituents of Gag (MA, CA, NC and p6) and the constituents of Pol (PR, RT, and IN).

In the rough endoplasmic reticulum (RER), the Env protein is produced as the gp160 polyprotein precursor. When gp160 reaches the Golgi apparatus through the secretory pathway, it is proteolytically cleaved by cellular furins or furin-like proteases leading to gp41 and gp120 subunits which still be bound by weak non-covalent interactions. Env is targeted to Gag assembly sites in the cell membrane by an unknown mechanism although it is related with gp41 cytoplasmic tail (CT). Deletion mutants of CT cause gp41 to distribute randomly in the cell membrane of infected cells and, in addition, it is known gp41 CT interacts with MA trimers during morphogenesis (Hogue et al., 2012; Muranyi et al., 2013). When the recruitment of new Gag molecules happens, it induces the cell membrane budding and the release of a new viral particle with envelope proteins recruited in the nascent virion (Checkley et al., 2011).

Budding of a new viral particle is a highly energic demanding process. Due to the fact that HIV-1 genome does not codify for fission machinery, it must recruit cellular proteins so the budding process could take place. The p6 protein of the Gag polyprotein contains several highly conserved sequences, known as "late domains", which interact with the cellular Endosomal Sorting Complexes Required for Transport (ESCRT) machinery. TSG101 and ALIX proteins interact with p6 and are recruited to the budding sites where they could assemble into circular arrays in a thin connection between the viral components and the cell membrane, constricting the membrane and inducing fission and release of the viral particle (Freed, 2015; Meusser et al., 2020; Rose et al., 2020).

Coordinately with or shortly after budding, the viral PR, which still remains part of the GagPol polyprotein, dimerizes and cleaves the GagPol and Gag polyproteins to release their main constituents: MA, CA, NC, p6, RT, IN and the PR itself. This process is called maturation. MA remains attached to the viral membrane, while CA coalesces to form the cone shape viral capsid protecting the RNA molecules, packed thanks to NC (Freed, 2015). During maturation, Env trimers redistribute through the viral membrane and usually constitute a single Env cluster of approximately 20-45 molecules (~7-15 trimers) (Chertova et al., 2002; Chojnacki et al., 2012; Nieto-Garai et al., 2021). The

resulting mature free virions are able to infect new cells and to start again the replication cycle.
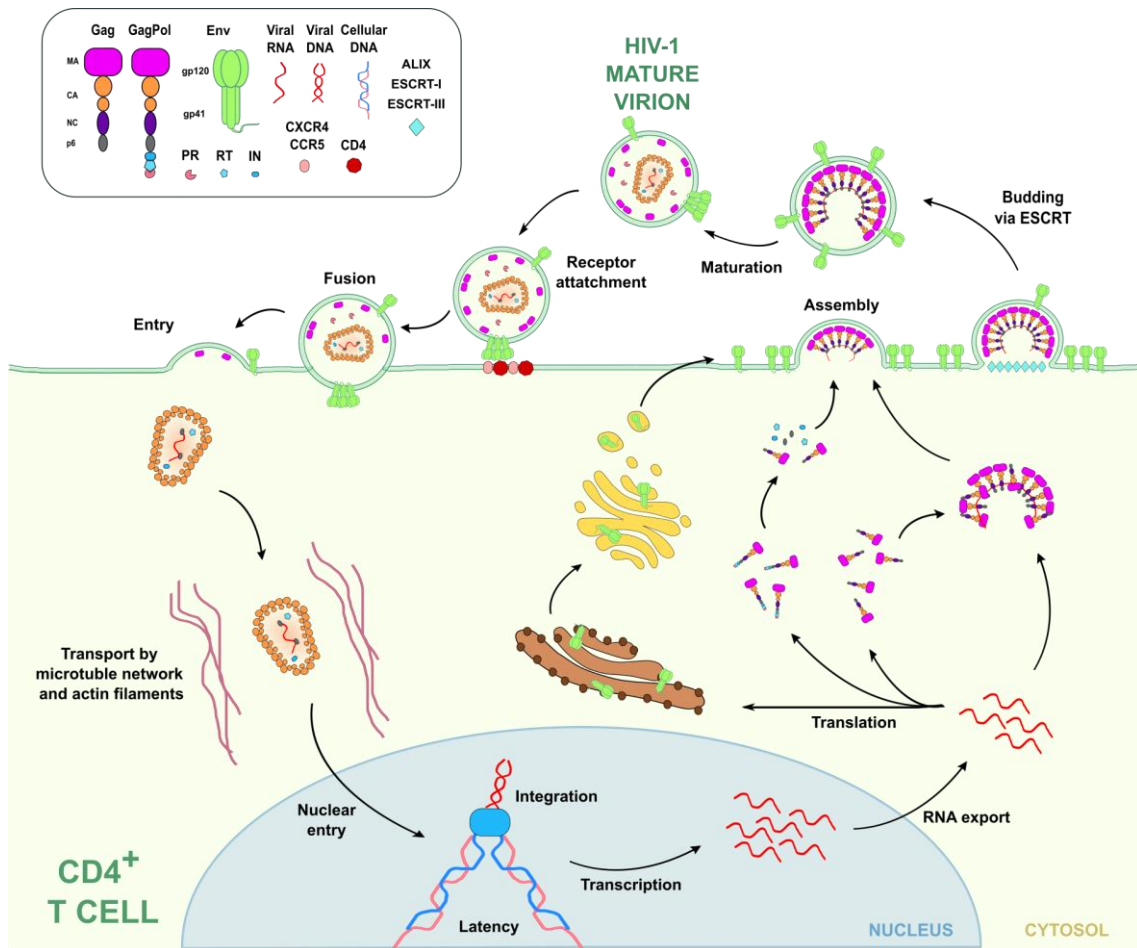
Figure 1.7. Schematic representation of the HIV-1 replication cycle. After Env mediated cell receptor and co-receptor recognition and viral and cellular membrane fusion, the HIV-1 capsid enters the host cell. The viral capsid is transported and enter the nucleus, concomitant with the retrotranscription of the HIV-1 RNA to DNA. Viral DNA is integrated in the cellular chromosomes until its transcription to new RNA molecules. The RNA molecules are in part translated into viral proteins. Gag and GagPol are synthesized in the cytosol, while Env is produced in the RER and finally targeted to the cell membrane. Two RNA molecules per virus dimerize and associate with the recently synthesized Gag and GagPol proteins, and also associate to the cell membrane, initiating the budding of a new viral particle. The viral particle is released and, concomitantly or shortly after, the PR in GagPol separates the constituents of the polyprotein in a process known as maturation.

1.2.2.1.1. Gag as promotor of viral morphogenesis

HIV-1 morphogenesis is carried out by the viral polyprotein Gag, which is capable on its own of forming virus-like particles (Gheysen et al., 1969). As it is said before, Gag is synthesized as a precursor polyprotein, which is cleaved into four major domains upon viral release (MA, CA, NC and p6) (Figure 1.8) and two spacer peptides (SP1 and SP2). The amino-terminal Gag domain is called MA, and it functions to bind to the cell membrane targeting viral assembly site and, although not completely known, to recruit the viral Env polyprotein to the budding sites. The central domain of Gag is called CA, and it mediates the protein–protein interactions required for immature virion assembly and upon maturation, creates the conical shell called the capsid. NC captures the viral genome and keeps it protected in the capsid interior. The carboxy-terminal p6 region contains the so-called late domains, which bind the ESCRT machinery in order to induce viral particle budding and release (Freed, 2015; Lorizate & Kräusslich, 2011; Sundquist & Kräusslich, 2012). Gag polyprotein considered as the master coordinator of HIV-1 assembly and maturation has nowadays emerged as one of the most outstanding drug targets (A. Dick & Cocklin, 2021).
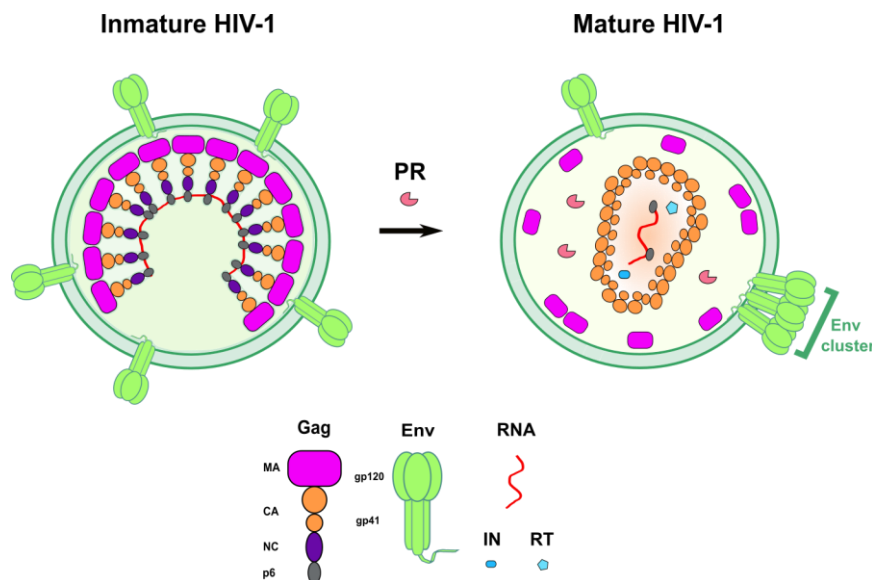
Figure 1.8. Structure and maturation of HIV-1 virions. In immature HIV-1 particles, immature Gag lattice is surrounding RNA and reducing Env mobility. Matrix (MA), capsid (CA), nucleocapsid (NC) and p6 subunits are formed after protease (PR) cleavage and Env glycoproteins are able to move around in the viral membrane, forming clusters. These mature virions are able fuse with cell membrane through Env clusters.

During synthesis of the Gag polyprotein, the N-terminal domain of the MA protein is modified by the attachment of a myristic acid , a 14-carbon fatty acid that can switch between being sequestered in the protein or anchored in the membrane. In this equilibrium, the monomeric myristoyl group of MA (Myr) is in the sequestered state [Myr(s)], whereas the trimer is in the exposed state [Myr(e)], implying that multimerization promotes the myristoyl switch (Figure 1.9). After Gag binding to the inner leaflet of the membrane by ionic interactions through the highly basic region (HBR) of MA, this myristoyl switch takes place and the hidden myristoyl group appear to stabilize the anchor of Gag to the cell membrane (Freed, 2015; Ghanam et al., 2012; Lorizate & Kräusslich, 2011; Ono et al., 2000; Ono & Freed, 1999; Paillart et al., 1999; Resh, 2004; Spearman et al., 1994, 1997; Sundquist & Kräusslich, 2012; Tanaka et al., 2016; Zhou et al., 1996). Exposure of Myr is also modulated by other factors including the pH, surface charge, protein concentration and the binding of calmodulin (A. Dick & Cocklin, 2021; Eells et al., 2017; Fledderman et al., 2010; Ghanam et al., 2010; C. Tang et al., 2003). Meanwhile the myristoyl switch is not happening, MA is interacting with RNA, concretely with the D arm of tRNA[Lys3] to avoid non-specific or premature membrane binding (Alfadhli & Barklis, 2014; Bou-Nader et al., 2021; Chen et al., 2020; Chukkapalli et al., 2010; Datta et al., 2011; Engeland et al., 2014a; Gaines et al., 2018; Inlora et al., 2014; Shkriabai et al., 2006; Socas & Ambroggio, 2018; Sumner et al., 2022; Thornhill et al., 2020; Todd et al., 2017; Tran et al., 2019).
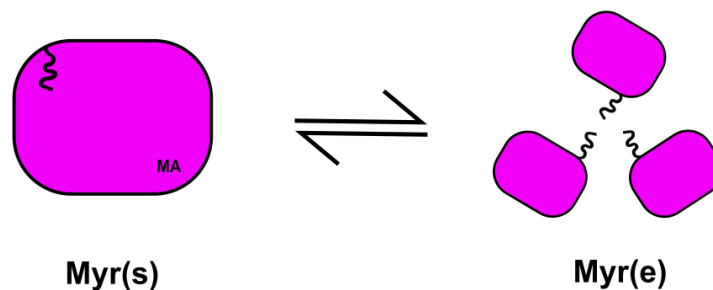
Figure 1.9. Myristoyl switch. The myristoyl group of MA (Myr) could be present in two states in equilibrium: the monomeric Myr, which is in the sequestered state [Myr(s)], and the trimer, which is the exposed state [Myr(e)] and is the responsible of Gag anchoring to the cell membrane during assembly.

Interestingly, the ionic interactions and the myristoyl anchor do not seem to be sufficient to completely anchor Gag lattices in the cell membrane. A variety of structural, *in vivo* and *in vitro* studies have shown that Gag trafficking and targeting to the cell membrane are orchestrated events that depend on different cellular proteins, such as AP-1, AP-2, and AP-3 from the endosomal pathway, soluble N-ethylmaleimide-sensitive factor attachment protein receptor (SNARE) and suppressor of cytokine signaling protein 1 (SOCS1) among others (Klingler et al., 2020); and specific membrane lipids like phosphatidylinositol (4,5)-biphosphate [PI(4,5)P$_2$], a minor lipid localized on the inner leaflet of the cell membrane but enriched in the HIV-1 viral membrane (Anraku et al., 2010; Barklis et al., 2018; S. M. Campbell et al., 2001; Shkriabai et al., 2006; Wen et al., 2020).

It is established that the final localization of Gag on punctate sites in the cell membrane is driven by specific interactions between the MA domain of Gag (HBR plus Myr) and PI(4,5)P$_2$ (Figure 1.10). In addition, it has been demonstrated that the interaction between MA and PI(4,5)P$_2$ plays a role beyond initial targeting of Gag to the plasma membrane due to the fact that depletion of this lipid results in complete loss of already assembled Gag lattices, indicating that Gag association with the membrane is a highly dynamic process dependent on specific protein-lipid interactions (Chan et al., 2008; Charlier et al., 2014; Chen et al., 2020; Chukkapalli et al., 2008, 2010; Freed & Mouland, 2006; Ghanam et al., 2012; Inlora et al., 2014; Mercredi et al., 2016; Monje-Galvan & Voth, 2020; Mücksch et al., 2017; Ono & Freed, 2004; Saad et al., 2006, 2008; Thornhill et al., 2020; Tran et al., 2019). Moreover, a recent study has shown that inositol hexakisphosphate (IP6), and PI(4,5)P$_2$ have neighbouring alternate binding sites within the same highly basic region (residues 18–33). IP6, is an abundant endogenous polyphosphorylated carbohydrate linked to Gag oligomerization, viral particle assembly and core stability. Thus, IP6 and PI(4,5)P$_2$ bindings are not mutually exclusive and may act in coordinating the membrane localization of viral particles (Ciftci et al., 2021; Datta et al., 2007; R. A. Dick et al., 2018; Dostálková et al., 2020; Sowd & Aiken, 2021).
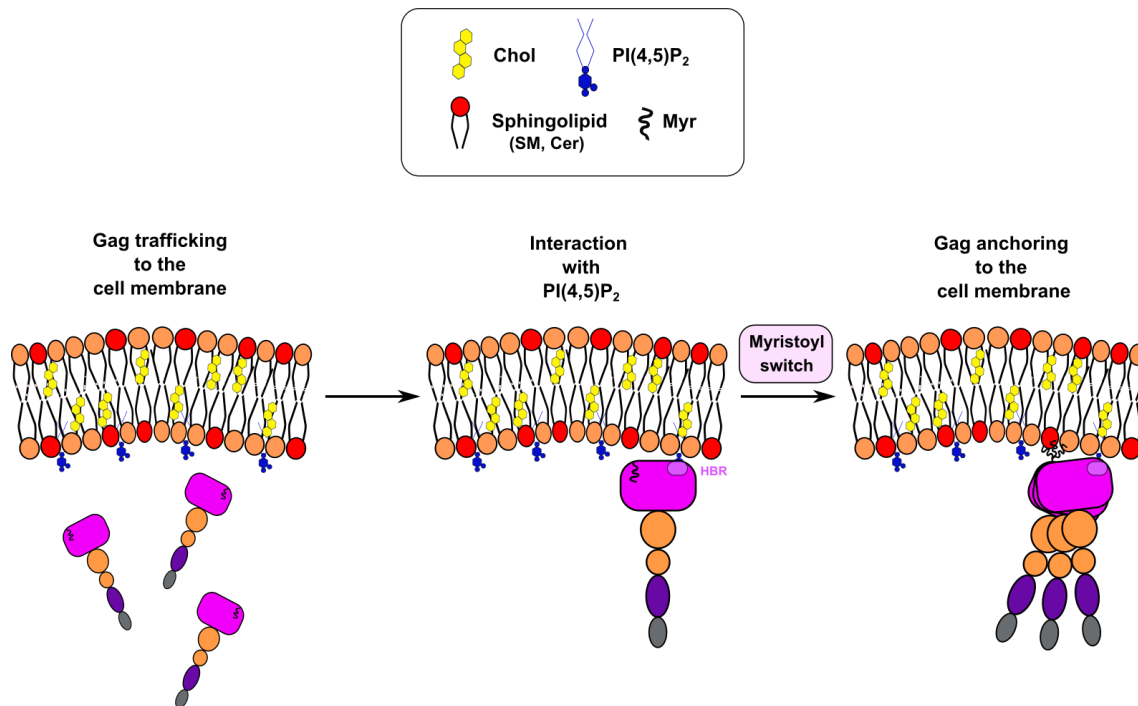
Figure 1.10. Schematic representation of Gag anchoring to the cell membrane depending on PI(4,5)P₂ and the myristoyl switch. After Gag trafficking and binding to the inner leaflet of the membrane by ionic interactions through the highly basic region (HBR) of MA with PI(4,5)P₂, the myristoyl switch happens and the hidden myristoyl group appears to anchor Gag to the cell membrane.

Gag could be the selector of the HIV-1 lipid composition due to the fact that Gag alone is able to produce viral-like particles (VLPs) and the virus lacks enzymes that codify for lipid biosynthesis (Gheysen et al., 1969; Mariani et al., 2014; Sundquist & Kräusslich, 2012). The ratio of Gag and PI(4,5)P₂ molecules involved during morphogenesis quantified in the viral membrane is 1:3 (Mücksch et al., 2019), however, the possibility of other lipids (especially, negatively charge) and/or proteins that could contribute to the process could not be completely discarded (Chan et al., 2008; Dalton et al., 2007; Lorizate et al., 2013; Lorizate & Kräusslich, 2011; Scarlata et al., 1998; Vlach & Saad, 2013; Zhou et al., 1994).

One lipid candidate that could contribute during morphogenesis could be cholesterol due to its role during the viral life cycle and its considerable quantity constituting the HIV-1 viral membrane. Moreover, Gag has been described to interact with detergent resistant membranes (DRMs) (Bhattacharya et al., 2006; Ding et al., 2003;

Halwani et al., 2003; Holm et al., 2003; Lindwasser & Resh, 2004; Nguyen & Hildreth, 2000; Ono & Freed, 2001; Patil et al., 2010), and to indirectly interact with cholesterol (Dick et al., 2012; Dick & Vogt, 2014; Doktorova et al., 2017; Favard et al., 2019; Lalonde & Sundquist, 2012; Pérez Socas & Ambroggio, 2020; Thiele et al., 2000; Yandrapalli et al., 2016), although there is no probe of the existence of a direct interaction of Gag with this lipid. Nevertheless, it opens the possibility that a Gag/MA-chol interaction could be taking place during viral morphogenesis because it is confirmed that cholesterol is required in other steps of the HIV-1 replication cycle, such as the entry process (C. Luo et al., 2008; Nieto-Garai et al., 2021; Percherancier et al., 2003).

1.2.2.1.2. Gag as Env-recruiting force during budding

Gag polyprotein has long been suggested to be implicated in Env incorporation to the budding sites based on the proposed interaction between the MA domain and the cytoplasmic domain of gp41 (Alfadhli et al., 2016, 2019; Brandano & Stevenson, 2012; Checkley et al., 2011; Davis et al., 2006; Dorfman et al., 1994; Eastep et al., 2021; Freed & Martin, 1995; Groves et al., 2020; Tedbury et al., 2013, 2015, 2016, 2019; Tedbury & Freed, 2014, 2015; Wyma et al., 2004; Yu et al., 1992). There are also evidences that the multimerization of Gag stabilizes, recruits, or reorganizes the cell membrane microdomains by attracting the envelope polyprotein (Hogue et al., 2012), in fact, a CT-dependent enrichment of Env has been seen at the periphery and surroundings of the Gag assembly sites (Buttler et al., 2018; Muranyi et al., 2013). Additionally, a crucial role of Gag in the redistribution and targeting of Env in viral maturation has also been demonstrated (Chojnacki et al., 2012, 2017; Groves et al., 2020; Shiraishi et al., 2001). Several models have been proposed to explain Env incorporation into virions with and without Gag's aid (Buttler et al., 2018; Ghanam et al., 2012; Groppelli et al., 2014; Murphy & Saad, 2020; Pezeshkian et al., 2019; Qu et al., 2021; Tedbury & Freed, 2014), however, despite the progress made in understanding the structural details of Env and its components, as well as the trafficking pathway of Env polyprotein, the mechanism by which Env is incorporated into virions is not completely understood.

Env polyprotein is composed by two subunits, the surface subunit gp120 and the transmembrane subunit gp41, both linked by disulfide bridges. Env proteins are found forming trimers in the viral membrane surface (Figure 1.10), around 12-18 trimers per viral particle. The gp41 subunit induces membrane fusion upon activation through gp120 binding to the corresponding receptors and co-receptors. HIV-1 gp41 has an N-terminal ectodomain (ED), a transmembrane domain (TM) and a C-terminal cytoplasmic tail (CT) (Figure 1.11) (Chojnacki et al., 2012; Lorizate & Kräusslich, 2011).
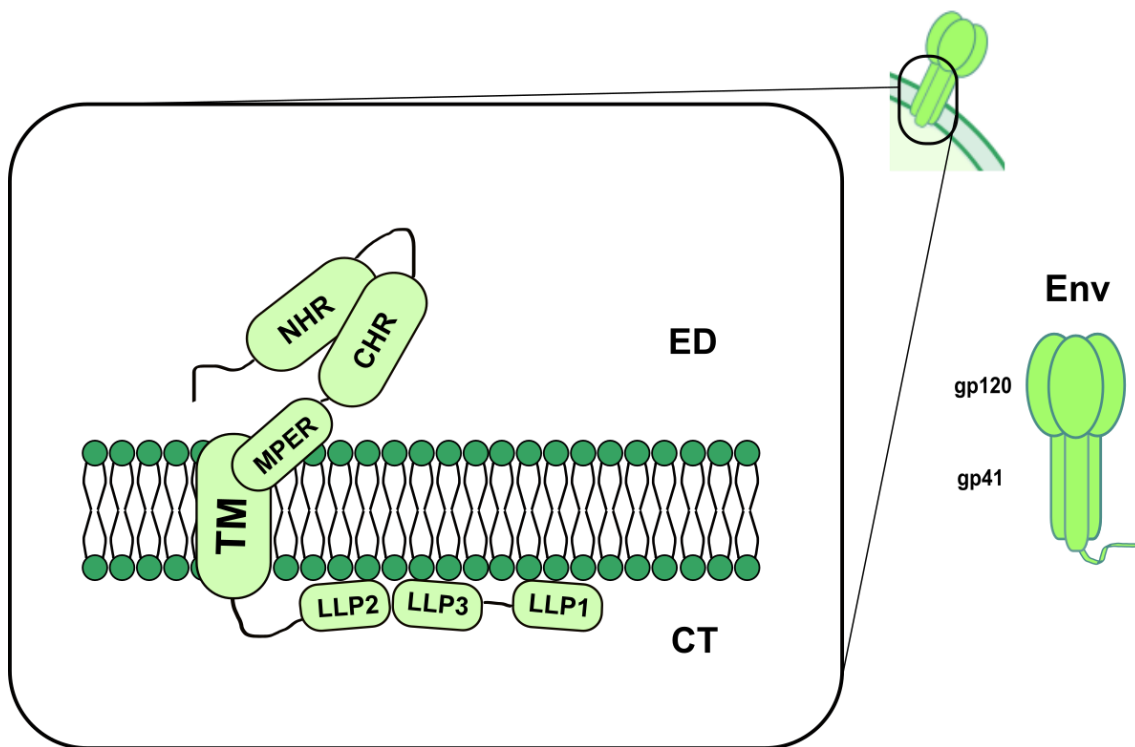
Figure 1.11. gp41 structure. Approximate disposition of the regions of gp41 in the viral membrane. Ectodomain (ED); Cytoplasmic tail (CT); N-terminal Heptad Repeat (NHR); C-terminal Heptad Repeat (CHR); Membrane Proximal External Region (MPER); Transmembrane domain (TM); Lentiviral Lytic Peptides (LLP1-3).

As mentioned before, it has been suggested that is likely that gp41 interacts with MA by the CT for Env incorporation. This is one of the described domains that interact with cholesterol. There are several regions that are proposed as lipid-interacting motifs, among others, in the membrane proximal external region (MPER) of the ectodomain exist a cholesterol recognition amino acid consensus (CRAC) motif that is proposed for interacting directly with Chol; and in the TM, a GxxxG helix-helix membrane

dimerization motif which mediates TM domain assembly, but it also could be involved in lipidic interactions. In the CT region, there are found the Lentivirus Lytic Peptide (LLP) domains, three domains (LLP1-3) whose functions are related to the expression of Env to the cell membrane, the fusogenity of the Env protein and its incorporation into viral particles. In addition, LLP1 and LLP3 appear to be associated with lipid domains such as DRMs, leading to increased permeability and decreased stability of the lipid bilayer (Aisenbrey et al., 2020; Epand, 2006; Klug et al., 2017; L. Lu et al., 2008; Murakami & Freed, 2000; Russ & Engelman, 2000; C. Schroeder, 2010; Vincent et al., 2002). Furthermore, recently it has been seen that Env interacts with cholesterol in an Env-CT dependent manner that has an implication in Env clustering into a single foci (Nieto-Garai et al., 2021).

Therefore, all the aforesaid might led to think that Gag/MA could possess other cholesterol-interacting motifs as Env, and, in addition, through this Gag/MA-cholesterol interaction, Gag could have an impact on Env incorporation into viral particles and may also induce clustering of chol or establish budding regions through chol platforms although non-direct interactions occur.

1.2.2.2. The viral membrane

HIV-1 viral membrane comes from the host cellular membrane through the budding process. As aforesaid mentioned, it is believed that Gag is the selector of the viral membrane composition due to the fact that Gag is capable on its own of forming VLPs. As every retrovirus, HIV-1 does not encode for lipid-synthesizing machinery or metabolizing enzymes, hence, the lipid composition of the viral membrane depends on the host cellular membrane from which virions bud. As a consequence, the composition of the HIV-1 viral membrane would be expected to resemble the composition of the cell membrane, however, it shows quite significant differences with the host cell membrane (Aloia et al., 1988, 1993; Brügger et al., 2006; Chan et al., 2008; Lorizate et al., 2009, 2013; Mücksch et al., 2019). These differences between both membranes suggest that a selection of a specific lipid domain or an active enrichment of certain lipids is happening during the budding of new HIV-1 virions. In fact, it is known that HIV-1 actively

remodels the assembly site in the membrane, generating its distinct protein composition through a lipid-based sorting mechanism aided by changes in the membrane curvature at the viral assembly site, producing as consequence the final composition of the bud virion (Sengupta et al., 2019; Sengupta & Lippincott-Schwartz, 2020).

The composition of the viral membrane is known both quantitatively and qualitatively. It is enriched in PS, SM, hexosylceramide, saturated species of PC (Brügger et al., 2006; Lorizate et al., 2009, 2013), and PI(4,5)P$_2$ (Chan et al., 2008; Mücksch et al., 2019) when compared to the host cell membrane (Figure 1.12). Furthermore, chol constitutes up to 50% of the total lipid molecules in the HIV-1 membrane (Brugger et al., 2006; Lorizate et al., 2009).
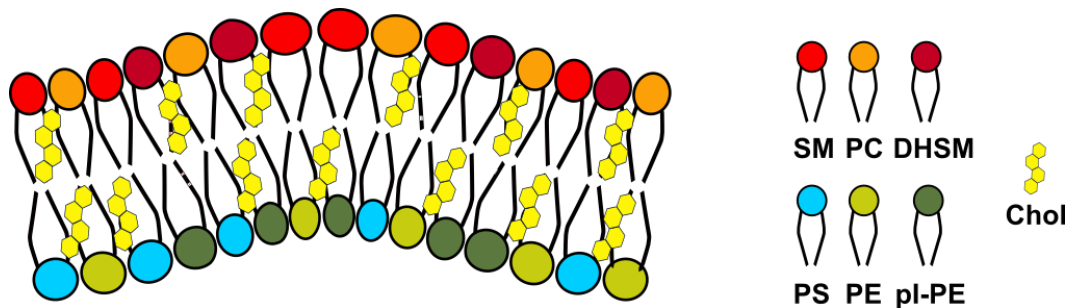
Figure 1.12. Schematic representation of the HIV-1 viral membrane composition. Sphingomyelin (SM); phosphatidylcholine (PC); dihydrosphingomyelin (DHSM); phosphatidylserine (PS); phosphatidylethanolamine (PE), 1-alkenyl,2-acylglycerophosphoethanolamine referred to as plasmalogen PE (plasmenylethanolamine, pl-PE), cholesterol (Chol).

The high amount of saturated glycerophospholipids, SM and chol in the viral membrane has led to its comparison to lipid rafts (Brügger et al., 2006) due to cell membrane rafts play a critical role in HIV-1 assembly and release (Waheed & Freed, 2009). Moreover, the similarities between the viral membrane and lipid rafts are also extended to its structure due to several studies, using the phase-sensitive stain Laurdan, where they have found that the HIV-1 viral membrane displays a liquid-ordered phase (Lorizate et al., 2009). Indeed, it has been demonstrated that HIV-1 membrane structure could be altered by using different raft-like compounds which act as entry inhibitors (Nieto-Garai et al., 2018).

1.3. S-palmitoylation

Post-translational modifications (PTMs) comprise a group of alterations that are based in covalently attach chemical groups to newly synthesised proteins to change their properties and, hence, their function. PTMs contribute to biological and pathological conditions, playing a key role in many cellular processes such as cell differentiation, protein degradation, signalling and regulatory processes, regulation of gene expression, and protein-protein interactions (Duan & Walther, 2015; Grotenbreg & Ploegh, 2007).

Lipidation is a group of lipidic PTMs that affects eukaryotic proteins and includes N-myristoylation, S-palmitoylation and prenylation. N-myristoylation describes the addition of myristic acid to a glycine residue with an exposed amine group after cleavage of the immediately adjacent methionine. Prenylation involves the attachment of farnesyl or geranyl isoprenoids to a C-terminal cysteine present within a defined consensus sequence (Crowell & Huizinga, 2009; D. D. O. Martin et al., 2011; Salaun et al., 2010).

S-palmitoylation consists in the thioesterification of palmitate to cysteine residues. S-acylation and thioacylation are more general terms used to describe this same process when fatty acids thioesterified to proteins are saturated, monounsaturated, and polyunsaturated species of different chain lengths (C14 or longer) (Smotrys & Linder, 2004).

Palmitoylation reactions occur at the cytosolic interface of the membrane catalysed by enzymes that are polytopic membrane proteins, called protein palmitoyltransferases (PATs). These proteins are mainly found in the membrane of the Golgi apparatus, and less present in the ER and in cell membranes. In mammals, the family of palmitoyl transferases is composed by 23 members (Korycka et al., 2012; Lemonidis et al., 2014; Mitchell et al., 2006; Ohno et al., 2006).

PATs typically have four transmembrane domains, containing the conserved catalytic DHHC (aspartate-histidine-histidine-cysteine) motif, where proteins become auto-palmitoylated. DHHC indicates the presence of a cysteine rich domain (CRD). DHHC proteins also contain other motifs, which are localized at the cytosol: a conserved DPG (aspartate-proline-glycine) motif, a C-terminal threonine-threonine-x-glutamate (TTxE; where x stands for any amino acid residue) motif and Palmitoyltransferase

Conserved C-terminus (PaCCT) motif (Tabaczar et al., 2017). In the Figure 1.13, it is shown a schematic representation of the dynamic S-palmitoylation process, including the typical structure of a DHHC palmitoyl transferase.
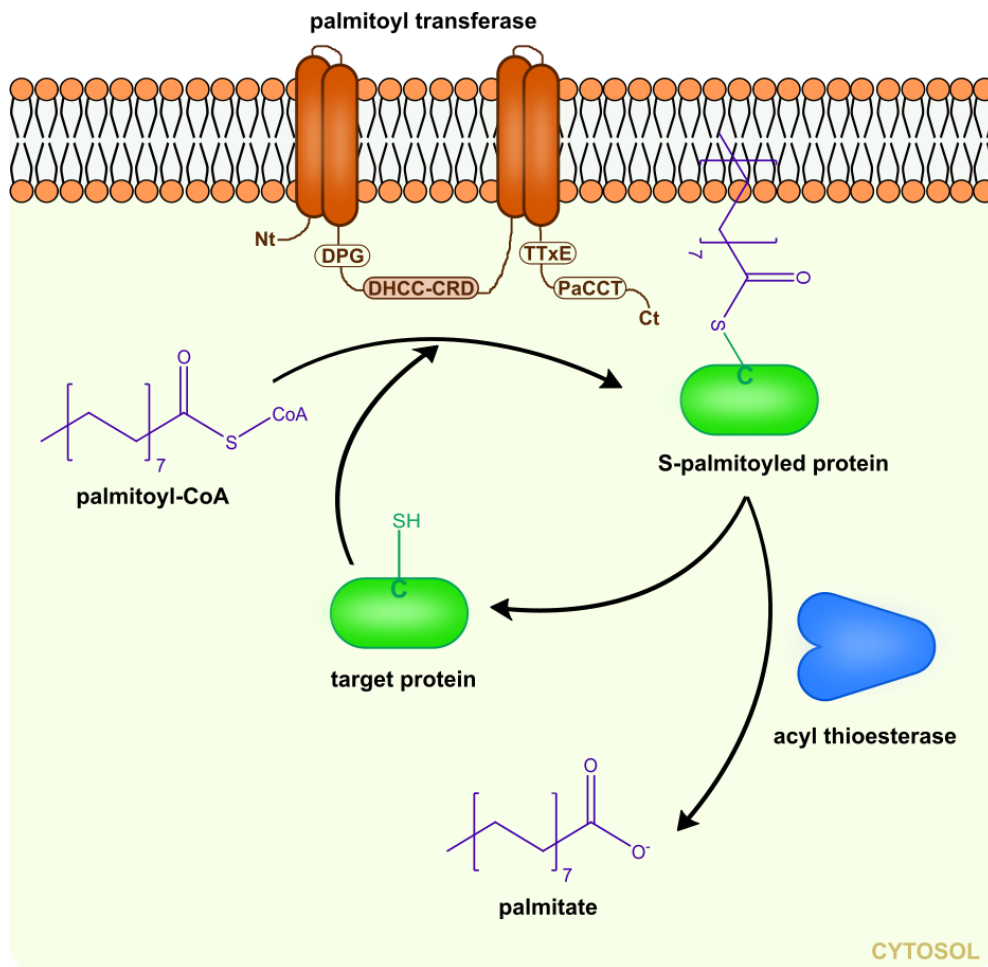
Figure 1.13. S-palmitoylation process. Palmitate is transferred to the thiol group of a cysteine of the target protein from palmitoyl-CoA through DHCC domain of palmitoyl transferases. Hence, upon S-palmitoylation, cytosolic proteins gain a hydrophobic moiety allowing their anchoring to the membrane. Proteins are depalmitoylated by acyl thioesterases and translocate to the cytosol.

Even though there is no strict consensus sequence for palmitoylation, the cysteines that suffered the process share some common characteristics: they are often adjacent to myristoylation and prenylation sites, their surrounding amino acids tend to be basic or hydrophobic and they are frequently located in the cytoplasmic regions flanking transmembrane domains or within transmembrane domains (Salaun et al., 2010).

The major function of palmitoylation is to mediate stable membrane attachment of soluble proteins. It has many distinct effects on modified proteins: regulating protein trafficking and sorting, protein stability, membrane microlocalization, regulating ubiquitination and protein–protein interactions. Although these effects of palmitoylation appear diverse, they are likely determined by two properties of palmitate: hydrophobicity or membrane affinity and preference for liquid-ordered domains or lipid rafts (Brown, 2006; Levental et al., 2010; Melkonian et al., 1999; Resh, 1999; Salaun et al., 2010).

1.3.1. Viral palmitoylated proteins: HIV-1 Env is palmitoylated in several cysteines

Viral RNA does not encode for PATs, thus, viruses need to exploit host cell palmitoylation machinery to modify their own proteins essential for infection of host cells and their own replication (Sobocinska et al., 2018).

Based on their membrane topology, palmitoylated proteins of viruses can be classified into three groups (Sobocinska et al., 2018; Veit, 2012): viral spike glycoproteins, viroporins and peripherial membrane proteins (Figure 1.14).
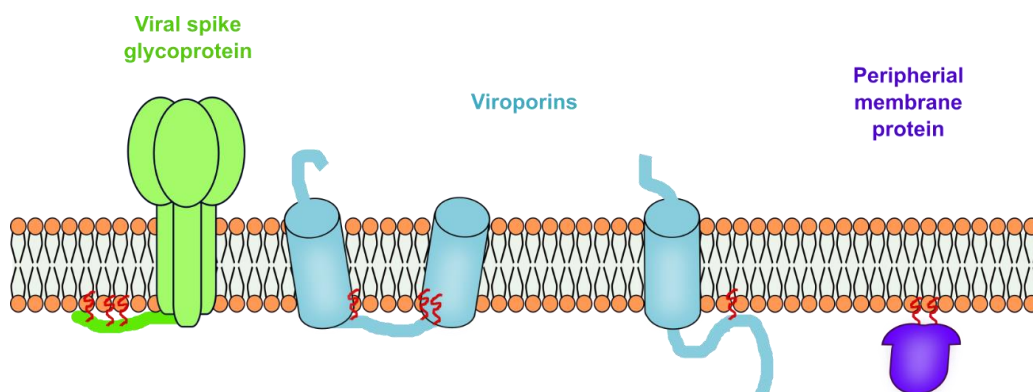
Figure 1.14. Membrane topology of viral palmitoylated proteins. Fatty acids linked to cysteine residues are shown as a zigzag red line.

The best described group is formed by viral spike glycoproteins, mainly with a type I membrane topology. Their structure is based on a N-terminal signalling peptide, a long ectodomain, at least one membrane-spanning region and a cytoplasmic tail. These palmitoylated spikes are in charge of viral entry by catalysing receptor binding and/or membrane fusion. Their palmitoylated cysteines are mostly located in the border region between the transmembrane domain and the cytoplasmic tail, usually within 20 residues from the transmembrane boundary. Typical examples present in human pathogens are the hemagglutinin of influenza virus, the fusion protein of measles virus, the glycoproteins of filoviruses and retroviruses including HIV and the S-protein of sudden acute respiratory syndrome (SARS)-coronavirus (CoV) and of other CoVs.

HIV-1 Env is a viral palmitoylated protein, which belongs to the group formed by viral spike glycoproteins. In this protein, there are four cysteine residues in the gp41 subunit, which are highly conserved in different HIV-1 isolates. They are designated as Cys-598, Cys-604, Cys-764 and Cys-837.

Cys-764 and Cys-837 are located downstream from the hydrophobic membrane anchor region of gp41 and presumed to be in the intracellular domain of gp41, corresponding to the LLPs of the cytoplasmic tail. The Cys-764 is located immediately upstream of LLP2, while Cys-837 is in LLP1. Palmitate groups covalently attached to these cysteines might insert into the lipid bilayer and anchor the LLPs to the cell membrane. In contrast, both Cys-598 and Cys-604 are located upstream from the membrane anchoring region and are believed to be in the extracellular domain of gp41, forming part of the loop of the ectodomain (Bhattacharya et al., 2004; Syu et al., 1991; C. Yang et al., 1995) (Figure 1.15).
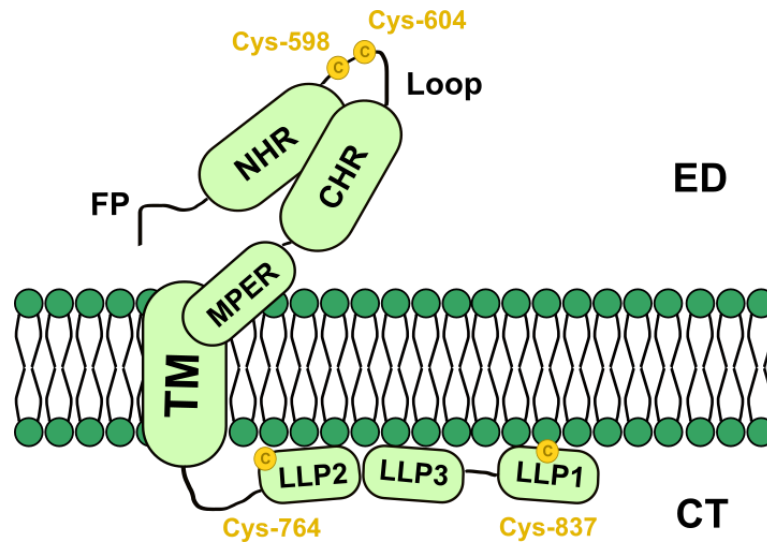
Figure 1.15. Localization of palmitoylated cysteines in the gp41 subunit of HIV-1 Env. Approximate disposition of the regions of gp41 in the viral membrane with the four highly conserved cysteines highlighted in yellow. Ectodomain (ED); Cytoplasmic tail (CT); Fusion Peptide (FP); N-terminal Heptad Repeat (NHR); C-terminal Heptad Repeat (CHR); Membrane Proximal External Region (MPER); Transmembrane Domain (TM); Lentiviral Lytic Peptides (LLP1-3).

Cys-764 is highly conserved in different HIV clades and groups, and even exists in the cytoplasmic tails of the HIV-2 and SIV envelope complexes (C. Yang et al., 1995). Mutation in Cys-764 causes a complete loss of palmitoylation, a decrease in the association with host cell membrane lipid rafts and, therefore, a decrease in the incorporation of Env into virions and a reduction of infectivity that could be severe when associated with a mutation in Tyr-837 in pNL4-3 HIV-1 molecular clone (Bhattacharya et al., 2004; Rousso et al., 2000; C. Yang et al., 1995). Furthermore, a triple mutation in Cys-598, Cys-604, and Cys-764 resulted in the loss of viral infectivity, which could be attributed to severe impairment in the processing of gp160 precursor to gpl20 (Syu et al., 1991).

1.3.2. The relationship between palmitoylation and lipid rafts

As aforesaid mentioned, palmitoylation is one of the best characterised signals for partitioning of proteins into lipid rafts, even though it is neither sufficient nor absolutely required in some cases (Levental et al., 2010; Melkonian et al., 1999; Resh, 1999). Insertion of the palmitoyl chain into the lipid bilayer is energetically favourable and may provide

the driving force for the association of the protein into the raft environment (Schroeder et al., 1994).

Detergent-resistant membranes are composed of specific lipids and proteins that presumably resemble lipid rafts (Brown & Rose, 1992). The presence of a protein in DRMs could indicate an interaction of this protein with lipid species commonly associated with them, such as SM and chol (Simons & Ikonen, 1997). Using this approach, several authors have described an association of HIV-1 Env with DRMs and, consequently, with lipid rafts (Bhattacharya et al., 2006; Rousso et al., 2000; C. Yang et al., 1995; P. Yang et al., 2010).

It is believed that lipid rafts constitute minor domains in most membranes, thus, these domains are thought to concentrate the viral components, facilitating protein-protein interactions. Enrichment of viral spike glycoproteins, like HIV-1 Env, in rafts is thought to provide a platform for viral assembly (Suomalainen, 2002; Veit, 2012).

HIV-1 Env glycoprotein was observed to associate to DRMs through its terminal palmitoylated cysteines. Fusion of HIV-1 virions requires the interaction of viral gp120 with its cellular receptor $CD4^+$ and co-receptors CXCR or CCR5 to form clusters of gp120-CD4-CCR5. This process has been proposed to be mediated by rafts (Crisesg & Rosesii, 1992; Levental et al., 2010; C. Luo et al., 2008; Waheed & Freed, 2009). Removal of palmitoylation sites in Env abolished incorporation of these proteins into DRMs (Bhattacharya et al., 2004; Rousso et al., 2000). However, others have reported that Env does not require palmitoylation for association with DRMs (Chan et al., 2005).

Conflicting results are common when partition into DRMs is used to determine the association of a protein to lipid rafts (Munro, 2003), and, therefore, this tool does not constitute an absolute probe for the partitioning of a protein into lipid rafts *in vivo* (Thiele et al., 2000). Indeed, DRMs have been suggested to be generated after detergent-induced bilayer partial solubilization and reassembly, thus, not necessarily corresponding with structures existing in the membrane *in vivo* (Sot et al., 2002). Despite of all, the HIV-1 Env has been suggested to be associated with rafts in both producer cells and budded virions in a cholesterol-dependent manner (Bhattacharya et al., 2006; Nieto-Garai et al., 2021; Schwarzer et al., 2014; P. Yang et al., 2010) even when non-palmitoylated mutant of Env

protein is present. The use of photoactivatable lipids has revealed that this mutant is capable of binding cholesterol at least in steady-state, which would mean that palmitoylation does not affect their interaction in rafts-like membranes (Nieto-Garai et al., 2021).

Moreover, lipidomic analysis of viral particles indicated that budding of HIV-1 occurs primarily through lipid rafts (Brügger et al., 2006). HIV-1 virions bud incorporating multiple cell-derived proteins associated to lipid rafts. More than 20 different host cell-derived proteins have been identified in the HIV-1 viral membrane, including MHC-I and MHC-II, the adhesion molecules CD44, LFA-1, LFA-2 and LFA-3, and ICAM-1 and ICAM-3 (C. Luo et al., 2008). Among those proteins, it is plausible that some of them could be also palmitoylated like HIV-1 Env.

1.4. The importance of interactions at the cell membrane

As previously stated, typical cell membranes are composed of hundreds of different lipids and proteins that are asymmetrically distributed between the two leaflets of the bilayer. This variety of membrane components gives rise to a complex interplay. Lipids do not simply provide the matrix where proteins are embedded but can actively participate in the regulation of protein activity, trafficking, and localization. Proteins can either bind lipids and other proteins specifically or non-specifically, where lipids act as a medium, and physical properties like thickness, fluidity, or curvature regulate protein function. The characterization of membrane interactions is a key factor in the understanding of the organizational principles of cell membranes, thus, this section is focused on the importance of the existence of these different interactions, particularly in protein-lipid and protein-protein interactions.

1.4.1. Protein-lipid interactions

Proteins and lipids interact with each other to fulfil their cellular functions. On the one hand, it has been discovered that lipids may allosterically control protein localization and structure, and even influence protein stability by acting as cofactors that

mediate cellular signalling. On the other hand, membrane-associated proteins can influence lipid shape, composition and transport, therefore, controlling membrane bilayer properties (Palsdottir & Hunte, 2004).

Indeed, the lipid environment of certain proteins has long been known to regulate their function, both in a direct and indirect way. As an example, several cellular receptors have been described to generate or coalesce lipid rafts, after ligand binding, indicative of a link between lipid nanodomains and the active form of the protein (Gahbauer & Böckmann, 2016; Smart et al., 1999). Similarly, due to the physicochemical properties of a protein this can be excluded or included in certain regions of the membrane (Simons & Toomre, 2000).

Furthermore, dysregulation of lipid-mediated pathways is known to contribute to a series of anomalies or diseases such as diabetes, cancer, cardiovascular and neurodegenerative diseases and pathogen-associated infections, among others (Wymann & Schneiter, 2008). Thus, researchers have been focused on mapping protein-lipid interactomes during the last decade to unveil the key role of membrane lipids and proteins in physiological and pathological conditions to complete understand the cell functioning. Moreover, uncovering these interactions could be crucial to develop new therapies for a huge number of human diseases (Escribá, 2006; Peng et al., 2014), however, this carries the difficulty of the lack of existence of proper tools to study lipids.

As mentioned before, HIV-1 viral membrane is mainly formed by chol, constituting almost half of the total lipid molecules. Hence, chol has been shown to play an important role in this virus. MA and Env, the two viral proteins linked to the viral membrane, have been postulated to be associated with chol. Studies have described interactions of MA and Env with detergent resistant membranes (DRMs) (Bhattacharya et al., 2006; W.-E. Chan et al., 2005; Ding et al., 2003; Halwani et al., 2003; Holm et al., 2003; Lindwasser & Resh, 2001; Nguyen & K Hildreth, 2000; Ono & Freed, 2001; Patil et al., 2010; Rousso et al., 2000; C. Yang et al., 1995; P. Yang et al., 2010), and despite these studies are not probe of the existence of an interaction of a protein with chol (Thiele et al., 2000), these membrane structures are commonly associated with this lipid.

In addition, cholesterol has been found to be necessary for the entry process (C. Luo et al., 2008; Percherancier et al., 2003). Cholesterol-depleting agents such as β-cyclodextrin and statins strongly reduce HIV-1 infectivity at the entry level (Campbell et al., 2002; Kalyana Sundaram et al., 2016; Liao et al., 2001, 2004; Mañes et al., 2000), an effect that has also been shown for cholesterol-binding compounds like amphotericin B methyl ester (Waheed et al., 2006). As Env protein is the responsible for the initiation of the viral replication cycle by inducing the fusion between the viral and cell membranes, this cholesterol-dependent infectivity could suggest a relationship between this lipid and the Env protein. Recent results of our research group have demonstrated that the gp41 subunit of the HIV-1 Env protein interacts with chol in a CT-dependent manner in cellular and viral membranes, confirming this previous hypothesis (Nieto-Garai et al., 2021).

It is known that MA protein interacts with DRMs. Moreover, HIV-1 Gag polyprotein is the responsible of morphogenesis, and additionally, it has been suggested to be implicated in Env incorporation to the budding sites based on the interaction between its MA domain and the cytoplasmic domain of Env (Alfadhli et al., 2016, 2019; Brandano & Stevenson, 2012; Checkley et al., 2011; Davis et al., 2006; Dorfman et al., 1994; Eastep et al., 2021; Freed & Martin, 1995; Groves et al., 2020; Murakami & Freed, 2000; Muranyi et al., 2013; Murphy & Saad, 2020; Patil et al., 2010; Pezeshkian et al., 2019; Tedbury et al., 2013, 2015, 2016, 2019; Tedbury & Freed, 2014; Wyma et al., 2004; Yu et al., 1992). Taking all together, it would be plausible that a Gag/MA-cholesterol interaction could be taken place during morphogenesis and maturation of the viral particle. Therefore, the Chapter 3 of this Thesis is focused on unravelling the existence of this protein-lipid interaction using a bifunctional lipid probe: a photoactivatable and radioactively labelled cholesterol (Section 1.4.1.1).

1.4.1.1. Bifunctional lipid probes

Multiple biochemical and biophysical methods have been used to characterize protein-lipid interactions including co-sedimentation and co-flotation assays, fluorescence spectroscopy, X-ray crystallography, nuclear magnetic resonance (NMR)

spectroscopy and atomic force microscopy (AFM), microarrays and affinity purification-mass spectrometry. However, all of these techniques have several drawbacks, and they were carried out *in vitro*, where the native membrane environment was artificially modified or even disrupted (Contreras et al., 2011; Peng et al., 2014; Zhao & Lappalainen, 2012).

In the last decade, bifunctional lipid probes have been developed as a new approach for directly studying the *in vivo* interaction between a protein and certain lipids, and as a tool that could cover the gaps of structural studies, classical proteomics and functional cell assays.

Bifunctional lipid probes contain a photoactivatable group, either at the polar head or within the hydrophobic core, and they can be incorporated into the lipid bilayer due to the fact that they behave and show the same properties as their natural counterparts. Among the most commonly used photoactivatable functionalities are aryl azides, benzophenones and diazirines, that share the features of bio-orthogonality, chemical stability and high reactivity upon photoactivation (Haberkant & Holthuis, 2014; Peng et al., 2014).

When exposed to UV-light irradiation, the photoactivatable group generates a highly reactive carbene that can form covalent bonds with any neighbouring molecule. The use of photoactivatable lipids offers the principal advantage of a light-controlled conversion of transient non-covalent protein-lipid interactions into covalent isolable adducts, enabling a large-scale enrichment of lipid-binding proteins. The resulting stable complexes are then purified and further characterized due to the presence of an affinity-binding group that allows a bio-orthogonal conjugation to a reporter tag. This clickable reporter allows to attach a fluorescent dye to the molecules for robust fluorescence detection and imaging, or a biotin moiety for affinity enrichment and proteomic analysis (Haberkant & van Meer, 2009; Moses & Moorhouse, 2007; Xia & Peng, 2013). Furthermore, a radiolabelled lipid tag could be used for monitoring lipid-protein interactions in living cells. The resulting radioactively labelled proteins can be detected by thin layer chromatography and autoradiography (Haberkant et al., 2008; Thiele et al., 2000).

In the Chapter 3 of this Thesis, the possible Gag/MA-cholesterol interaction during HIV-1 morphogenesis and maturation is studied using the photoactivatable cholesterol analogue, [³H]-photo-cholesterol (Figure 1.16). This lipid contains a diazirine group in the B ring, attached to 6-C, which is generally buried in the hydrophobic region of the lipid bilayer, thus, avoiding non-specific cross-linking with superficial solvent molecules (Farenholz et al., 2000; Haberkant et al., 2008; Nieto-Garai et al., 2021; Thiele et al., 2000). Moreover, this photoactivatable lipid is radioactively labelled with tritium in the A ring to its easily detection and quantification.
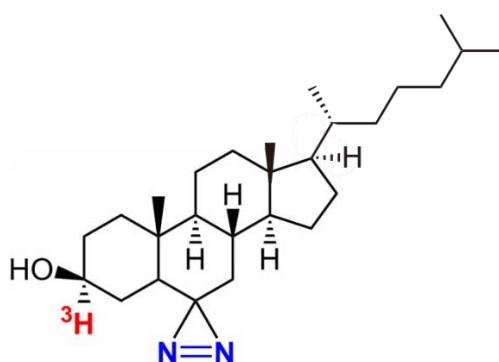
Figure 1.16. Radioactive photoactivatable cholesterol. Structure of tritium-labelled photoactivatable cholesterol analogue, [³H]-photo-cholesterol. The diazirine ring is coloured in blue and the tritium label in red.

1.4.2. Protein-protein interactions

The importance of protein-protein interactions at the cell membrane resides in their involvement in many cellular processes including cell growth, cell differentiation and apoptosis (Nohe & Petersen, 2004); and even in different steps of the HIV-1 replication cycle (Ako-Adjei et al., 2015; Muranyi et al., 2013). Knowing the specific function and behaviour of a protein allows to characterize protein complexes and pathways, however, this is not as easier as it seems.

In the simplest situation, proteins associate with each other directly via specific amino acids that facilitate cognate binding by either covalent bonds, ionic interactions, hydrogen bridges or hydrophobic interactions. However, protein interactions are so complex, being strongly influenced by the local environment, chemical modifications,

the presence of co-factors and lipids. In a more complex setting, protein interaction interfaces can also contain co-factors, such as divalent cations or metals that stabilize the binding, and in the case of the cell membrane, lipids could also play a role in the regulation of protein-protein interactions (Baumgart & Schütz, 2015).

Protein-protein interactions have been studied with many methods and from different perspectives: biochemistry, quantum chemistry, molecular dynamics, signal transduction, among others. Each of the approaches has its own strengths and weaknesses, especially with regard to the sensitivity and specificity of the method. The most conventional and widely used high-throughput methods are yeast two-hybrid screening and affinity purification coupled to mass spectrometry (Herce et al., 2013; Phizicky & Fields, 1995; Titeca et al., 2019).

Taking together all the information about proteins enables the creation of large protein interaction networks that empower the current knowledge on biochemical cascades and molecular etiology of disease (Wang et al., 2012). Mutations or abnormal protein-protein interactions are implicated in the development of several multiple protein aggregation-related pathologies, such as Creutzfeldt–Jakob disease, Alzheimer's disease and cancer. Hence, achieving information on protein-protein interactions is critical for the discovery of putative protein targets of therapeutic interest (Hicks et al., 2012; Ivanov et al., 2013; Rigter et al., 2010).

As explained before, palmitoylation mediate stable membrane attachment of soluble proteins and it is known that trafficking of a protein from the Golgi apparatus to the cell membrane is facilitated by these post-translational modification due to palmitate affinity for lipid rafts (Levental et al., 2010; Melkonian et al., 1999).

HIV-1 virions contain viral palmitoylated proteins and, even, cellular membrane proteins caught during budding (Cantin et al., 2005) that also could be palmitoylated. There are multiple viral palmitoylated proteins, among them, one of the most known is the envelope glycoprotein of HIV-1 virus. Env protein is known to be palmitoylated in four cysteine residues of the transmembrane subunit gp41, designated as Cys-598, Cys-604, Cys-764 and Cys-837. Mutations in Cys-764 showed a complete loss of palmitoylation (C. Yang et al., 1995), a decrease in the association with host cell

membrane lipid rafts and a decrease in the incorporation of Env into virions (Rousso et al., 2000). The aforesaid studies together with lipid analysis of the viral membrane indicating a resemble in structure and composition to raft-like cell nanodomains (Brügger et al., 2006), means that budding of HIV-1 occurs primarily through lipid rafts if Env proteins are properly palmitoylated.

Therefore, these palmitate groups covalently attached to gp41 cysteines insert into the lipid bilayer, potentially interacting with different membrane proteins during HIV-1 budding and assembly and anchor the protein to the cell membrane.

In Chapter 4 of this Thesis, HIV-1 viral-like particles are treated with a clickable palmitoyl analogue (Figure 1.17). This palmitate has an alkyne group attached to its terminal moiety, being accessible to Copper(I)-Catalyzed Azide-Alkyne Cycloaddition (CuAAC) reaction for sensitive fluorescence detection and/or for affinity enrichment and proteomic analysis (Peng et al., 2014). This alkyne-modified palmitoyl analogue is tested to its use in unravelling the HIV-1 Env palmitoylome. Nowadays, HIV-1 proteome is described, however, a detailed HIV-1 palmitoylome remains undiscovered.
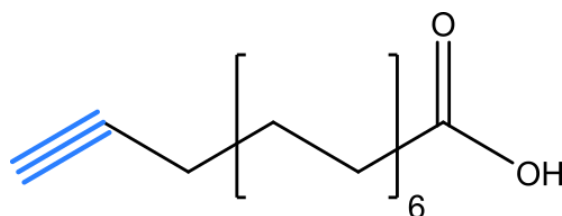
Figure 1.17. Alkyne-modified palmitoyl analogue. Structure of alkyne-modified palmitoyl analogue, 15-octadecynoic acid.

1.5. Objectives

This Thesis focuses primarily on the use of bifunctional lipid probes and clickable lipid probes for the study of relevant protein-lipid and protein-protein interactions in different events taking place at the cell membrane during HIV-1 morphogenesis. This objective was pursued by a multidisciplinary approach, combining different biophysical and biochemical studies.

In order to fulfil the general purpose, the following specific aims were proposed:

4. To study the interaction between HIV-1 Gag/MA proteins and cholesterol in cellular and viral membranes during morphogenesis, using a photoactivatable and radiolabelled cholesterol analogue, [^{3}H]-photo-cholesterol.

5. To test an alkyne-modified palmitoyl analogue to develop a protocol for the extraction of HIV-1 palmitoylated proteins.

6. Try to unveil the HIV-1 palmitoylome by applying the previous stated protocol.

Chapter 2.

Experimental Techniques

Chapter 2: Experimental Techniques

The general experimental techniques, protocols and reagents used during this Thesis are summarized in this chapter, which includes experimental techniques performed in more than one chapter. More specific techniques needed exclusively in a concrete chapter are detailed in the corresponding section of experimental techniques of that chapter.

2.1. Cell lines & Cell culture

Human embryonic kidney cells stably expressing the SV40 large T antigen (HEK 293T or 293T) and Chessie-8 Hybridoma cells were obtained through the NIH AIDS Reagent Program, Division of AIDS, National Institute of Allergy and Infectious Diseases (NIAID), National Institutes of Health (NIH).

HEK 293T cells are a highly transfectable derivative of human embryonic kidney 293 cells, who express a temperature-sensitive allele of the Simian virus 40 (SV40) large T antigen. This enables the amplification of vectors containing the SV40 ori and, thus, considerably increases the expression levels obtained with transient transfection. Therefore, they are commonly used for obtaining huge viral purifications (Lin et al., 2014). HEK 293T cells were maintained at 37 °C and 5% CO_2 in DMEM GlutaMAX™ High glucose culture medium supplemented with 10% Fetal Bovine Serum (FBS), and 100 U/mL Penicillin-Streptomycin. Cells were splitted at a 1:10 ratio every two or three days depending on cell density.

Chessie-8 Hybridoma Balb/c mouse splenocyte cells were used to obtain the α-gp41 antibody Chessie-8. The monoclonal IgG1 antibody Chessie-8 is specific for HIV-1 gp41 recognition and also reacts against HIV-1 gp160 (Abacioglu et al., 1994). Chessie-8 Hybridoma cells were maintained at 37 °C and 5% CO_2 in RPMI 1640 GlutaMAX™

culture medium supplemented with 10% FBS and 100 U/mL Penicillin-Streptomycin. Cells density was always maintained between $0.3 \cdot 10^6$ and $1 \cdot 10^6$ cells/mL.

DMEM GlutaMAX™ High Glucose, RPMI 1640 GlutaMAX™, FBS, Trypsin-EDTA and Penicillin-Streptomycin were purchased from Thermo Fisher Scientific. Cell culture flasks, dishes, plates and Phosphate-Buffered Saline (PBS) (100 mM phosphate buffer, 2.7 mM potassium chloride, 137 mM sodium chloride, pH 7.4) were purchased from Sigma-Aldrich.

2.2. Plasmids

Several non-infectious proviral and Env only expressing plasmids (Table 2.1) have been used. A proviral plasmid could generate complete HIV-1 non-infectious viral-like particles, while an Env only expressing plasmid just codifies for HIV-1 Env protein. All the constructs contain an ampicillin resistance gene for selection of the desired transformed clones.

Table 2.1 – Proviral and Env expressing plasmids.

	Denomination	Description
Proviral plasmids	pCHIV	Non-infectious plasmid expressing all HIV-1$_{NL4-3}$ proteins except Nef. It cannot replicate because of the lack of the viral long-terminal repeat sequences (Müller et al., 2004). The plasmid was kindly provided by Barbara Müller.
	pCHIV PR (-)	pCHIV derivative containing a mutation in the active site of the HIV-1 protease (p.D25N), rendering the enzyme non-functional, and sequestering the viral particle in an immature state.
	C762S	pCHIV variant containing a substitution of palmitoylated cysteine residue in position 762 by a serine.
Env expressing plasmids	pCAGGS.NL4-3	Plasmid expressing the HIV-1$_{NL4-3}$ Env protein. The plasmid was kindly provided by Barbara Müller.

These plasmids were produced in huge quantities by transformation of DH5α *Escherichia coli* competent cells, followed by clone selection, growth in liquid Lysogenic

Broth (LB) medium, plasmid extraction and purification by a commercial NucleoBond®
PC 500 kit (Macherey-Nagel). Finally, plasmid verification was performed by enzymatic
digestion.

2.2.1. Generation of competent bacteria

DH5α *E. coli* competent bacteria for plasmid transformation were generated using
Super Optimal Broth (SOB) medium (20 g/L Tryptone, 5 g/L yeast extract, 0.5 g/L NaCl,
2.5 mM KCl), Transformation Buffer (TFB) I [3 g/L potassium acetate, 10 g/L MnCl$_2$, 16
mM CaCl$_2$, 15% (v/v) glycerol pH 5.8], TFB II [2 g/L MOPS, 76 mM CaCl$_2$, 10 mM KCl,
15% (v/v) glycerol pH 7.0], and LB medium (Laboratorios Conda).

1. 50 µL of the stock of DH5α bacteria was spread in a LB agar petri dish and grown
   overnight at 37 °C.

2. Next day, a colony was picked and grown overnight in 5 mL of liquid LB medium
   (20 g/L lysogeny broth) at 37 °C and constant shaking.

3. Next day, the bacteria-containing medium was diluted 1:200 in liquid SOB medium
   and grown for 3-4 h at 37 °C until its optical density at 600 nm (OD$_{600}$) was $OD_{600} =$
   0,5.

4. The SOB medium containing bacteria was kept in ice for 10 min, splitted in aliquots
   of 50 mL, pelleted by centrifugation at 32,000 rpm for 12 min at 4°C, and each aliquot
   was carefully resuspended in 10 mL cold TFB I buffer.

5. After 10 min incubation at 4°C with TFB I, aliquots were pelleted and carefully
   resuspended in 2.5 mL of cold TFB II.

6. 50 µL aliquots of competent bacteria were then frozen in liquid nitrogen and stored
   at -80 °C until use.

2.2.2. Bacterial transformation and clone selection

Bacterial transformation was performed following the protocol established by
Cohen et al. (1972):

1. 50 µL aliquots of DH5α *E. coli* competent bacteria were defrost on ice and mixed with 0.5 µg of the desired plasmid.

2. The bacteria were maintained on ice for 15 min and then, a heat shock was applied by incubation at 42 °C for 90 s. In this heat shock, the plasmidic DNA enters the bacteria by zone of adhesion channels. The heat shock was followed by incubation on ice for 2 min.

3. After transformation, the bacteria were seeded in LB agar petri dishes supplemented with 100 µg/mL ampicillin to induce a selective growth of the transformed ones. The petri dishes were incubated overnight at 37 °C.

4. Clearly isolated clones from the petri dishes were picked and seeded in 500 mL of liquid LB medium (20 g/L lysogeny broth) supplemented with 100 µg/mL ampicillin. The bacterial culture was grown overnight at 37 °C for no more than 16 h.

5. Once grown, the bacterial culture was used for plasmid extraction and purification.

2.2.3. Plasmid extraction, purification and verification

The plasmid extraction from the bacterial culture and its purification was carried out with NucleoBond® PC 500 kit (Macherey-Nagel) following the manufacturer's instructions with some modifications:

1. The plasmid-containing bacterial culture was centrifuged at 5,000 g for 15 min at 4 °C to pellet the bacterial cells and separate them from the medium.

2. Bacterial culture supernatant was removed, and bacteria were resuspended in 12 mL of resuspension Buffer S1 supplemented with RNase A.

3. 12 mL of lysis Buffer S2 was added to the resuspended cells. The samples were mixed by inverting the tube 6-8 times, and incubated at room temperature (RT) for 3 min. This step induces the lysis of the bacteria under alkaline conditions, letting free the plasmidic and chromosomic DNA.

4. 12 mL of cold (4 °C) neutralization Buffer S3 was added to the samples, mixed by inversion 6-8 times, and incubated on ice for 5 minutes. The neutralization buffer contains acetate which precipitates the proteins bound to the chromosomic DNA, while the protein-free plasmidic DNA remains in solution.

5. In parallel, NucleoBond® AX 500 (Maxi) columns were equilibrated with 6 mL of equilibration Buffer N2.

6. The lysed bacterial samples were cleared through a paper filter to avoid loading the precipitated chromosomic DNA to the column. The plasmidic DNA in solution passes through the filter and enters the column. The cleared lysate passed through the column by gravity flow. The plasmidic DNA sticks to the column.

7. The column was washed with 32 mL of washing Buffer N3 and the plasmidic DNA bound to de column was eluted with 15 mL of elution Buffer N5.

8. 11 mL of room-temperature isopropanol was added to the eluted DNA to induce its precipitation. The samples were mixed and centrifuged at 5,000 g for 30 min at 4 °C.

9. The supernatant was carefully discarded and 1 mL of 70% (v/v) ethanol was added to the precipitated DNA pellet to remove the remaining isopropanol. The pellet was transferred into a microcentrifuge tube and centrifuged at 5,000 g for 10 min at RT.

10. The ethanol supernatant was removed and the plasmidic DNA was allowed to dry for 20 min maximum. The DNA was resuspended in 100 µL of ulttrapure water (Sigma-Aldrich) and its concentration and purity (A_{260}/A_{280} ratio) was measured by a NanoDrop Microvolume Spectrophotometer (Thermo Fisher Scientific). The plasmidic DNA concentration was adjusted to 1 µg/µL.

11. 0.5 µg of the purified plasmidic DNA was digested with 1 µL of Hind III (10 U/ µL) (Thermo Scientific) for 1 h at 37 °C.

12. Digested plasmidic DNA was loaded into a 1% (w/v) agarose in Tris base, acetic acid and EDTA (TAE) gel with 0.01% (v/v) of SYBR™ Safe Gel Stain (Thermo Fisher Scientific) and subjected to electrophoresis.

13. Resulting DNA bands were visualized with an UV transilluminator (Scie-Plas), and the accurate number of bands and their size were checked to be as expected.

2.3. Western blot

Western blot analytical technique is used to detect the proteins of interest during this Thesis. Intercept® Blocking Buffer (LI-COR) is used for membrane blocking and primary and secondary antibody incubations, while Tris-buffered saline and Tween 20

(TBS-T) buffer [150 mM NaCl, 10 mM Tris-HCl, 0.2% (w/v) Tween 20, pH 8] is used for membrane washing. The composition of 6x SDS-PAGE sample buffer used is 125 mM Tris-HCl, pH 6.8, 20% (v/v) glycerol, 4%(w/v) SDS, 10% (v/v) ß-mercaptoethanol and 0.5 mg/ml of Bromophenol Blue (Sigma-Aldrich).

1. The desired samples were dissolved in SDS-PAGE sample buffer and heated at 95 °C for 5 min.

2. Samples were loaded into a 12.5% polyacrylamide gel containing SDS and subjected to electrophoresis in a XCell SureLock™ Mini-Cell Electrophoresis System (Bio-Rad) for 1 h at 120 V.

3. Proteins were transferred to Immobilon®-FL transfer membrane (Merck) using a semi-dry blotting technique with Trans-Blot® SD Semi-Dry Transfer Cell (Bio-Rad) for 1 h at 15 V.

4. The membranes were blocked for 1 hour at RT and constant shaking with 6 mL of Intercept® Blocking Buffer.

5. The blots were probed with the appropriate primary and secondary antibodies diluted in 6 mL of Intercept® Blocking Buffer with 0.1% (w/v) Tween 20, washing three times with TBS-T between antibodies. The primary and secondary antibodies used for Western blot experiments are shown in Table 2.2 and Table 2.3, respectively.

6. Detection of the proteins of interest was carried out by the use of infrared dye-conjugated secondary antibodies using the LI-COR Odyssey imaging system.

Table 2.2 – Primary antibodies used for Western Blot experiments

Antigen	Host	Dilution	Incubation conditions	Manufacturer
gp41 (Chessie-8)	Mouse	1:2,000	Overnight 4 °C	Produced in the lab
CA	Sheep	1:2,000	1 h RT	Kindly donated by Professor Hans-Georg Kräusslich
MA	Rabbit	1:5,000	1 h RT	Kindly donated by Professor Hans-Georg Kräusslich
Caveolin-1	Rabbit	1:1,000	1 h RT	Abcam (# ab2910)
Transferrin receptor	Mouse	1:1,000	1 h RT	Abcam (# ab1086)

Table 2.3 – Secondary antibodies used for Western Blot experiments.

Antigen	Host	Detection	Dilution	Incubation conditions	Manufacturer
Mouse IgG	Donkey	Near infrared fluorescence: IRDye800	1:10,000	45 min RT	LI-COR (#926-32212)
Sheep IgG	Donkey	Near infrared fluorescence: IRDye800	1:10,000	45 min RT	Rockland (#613-732-168)
Rabbit IgG	Donkey	Near infrared fluorescence: IRDye680	1:10,000	45 min RT	LI-COR (#926-68073)

2.4. Chessie-8 antibody

α-gp41 Chessie-8 antibody is a monoclonal antibody of isotype IgG1, which reacts against HIV-1 gp160 and is specific for HIV-1 gp41 (Abacioglu et al., 1994), and it is produced by Chessie-8 α-HIV-1 gp41 Hybridoma cells. This antibody is used for recognition of HIV-1 gp41 in Western blot experiments and for the immunoprecipitation of the same protein. The buffers used for Chessie-8 antibody purification are detailed in Table 2.4.

2.4.1. Chessie-8 IgG1 antibody production and purification

1. Chessie-8 α-HIV-1 gp41 hybridoma cells for antibody production were overgrown until death, generating an approximate yield of 10-20 µg of antibody per mL of culture medium.

2. After cells had died, the culture medium was centrifuged at 500 g for 5 min followed by filtering through 0.45 µm CME filters (Carl-Roth). This clarified culture medium supernatant was stored at -80 °C until antibody purification.

3. For Chessie-8 antibody purification, HiTrap Protein G High Performance 1 mL column (Sigma-Aldrich) were used. The column was equilibrated with 10 mL of equilibration buffer at a 1 mL/min flux at RT.

4. The clarified cell culture supernatant was added to the column in a closed cycle for 3 h, so the total volume of the supernatant (45 mL) could circulate through the column at least three times to ensure a high antibody binding to the column.

5. The column was washed with 10 mL of equilibration buffer.

6. The antibody was eluted with 5 mL of elution buffer. Fractions of 250 µL were collected and, to each fraction, 10 µL of neutralization buffer were added to obtain a final pH value around 7.0.

7. The protein concentration of the fractions was determined by a bicinchoninic acid (BCA) assay with Pierce BCA Protein Assay kit (Thermo Scientific) and the fractions containing a high amount of protein were collected, combined, and dialyzed overnight against 2 L of PBS at 4 °C.

8. The following day, the purified and dialyzed antibody solution was collected and the IgG1 concentration was determined using a BCA assay.

Table 2.4 – Chessie-8 IgG1 antibody purification buffers.

Buffer	Composition	pH
Equilibration buffer	15.6 mM NaH_2PO_4 (Merck) 24.4 mM Na_2HPO_4 (Merck)	7.0
Elution buffer	0.1 M Glycine-HCl (VWR)	2.7
Neutralization buffer	1 M Tris-HCl (Apollo Scientific)	9.0

2.4.2. Chessie-8 antibody coupling to Protein G Sepharose beads

The α-gp41 Chessie-8 antibody is used for both immunoprecipitating the Env protein and performing the Western blot against gp41.

If the immunoprecipitation against the gp41 protein is carried out with an α-gp41 Chessie-8 antibody without coupling with Sepharose Protein G beads, the antibody would also run in the gel along with gp41 when loading the immunoprecipitate in a SDS-PAGE. Being the size of the heavy chain of the antibody (~50 kDa) extremely similar to gp41 size (~41 kDa), the cross-recognition of the heavy chain by the secondary antibody used in the Western blot would interfere with the signal of the immunoprecipitated gp41 protein. Therefore, the α-gp41 Chessie-8 antibody was covalently bound to Protein G Sepharose™ 4 Fast Flow (GE Healthcare) to ensure that the heavy chain remains attached to the beads due to the fact that Protein G is an immunoglobulin binding protein isolated from the surface of group G streptococcal bacteria, which preferentially binds to Fc region of antibody heavy chains (Sjobring et al., 1991). The light chain of the antibody (~25 kDa) does not covalently bind to the beads with this method, so it runs freely in the gel and it is recognized by the secondary

antibody, however, its size is different enough from gp41 size, so it does not interfere in the subsequent analysis.

The buffers needed for Chessie-8 coupling are shown in Table 2.5. The antibody coupled beads were prepared in batches by the following protocol:

1. 50 μL of the Protein G Sepharose beads were aliquoted and washed three times with 500 μL of modified radioimmunoprecipitation assay (RIPA) lysis buffer [20 mM HEPES, 100 mM NaCl, 5 mM EDTA, 0.5% (w/v) sodium deoxycholate, 1% (w/v) Triton X-100, adjusted to a pH of 7.4] by centrifugation at 13,000 rpm for 5 min.

2. 10 μg of the α-gp41 Chessie-8 antibody were then added to the washed beads and incubated overnight at 4 °C with constant stirring.

3. The samples were centrifuged at 13,000 rpm for 1 min to separate the beads bound to the antibody in the pellet from the free antibody in the supernatant.

4. The beads were washed two times with freshly prepared borate buffer, resuspended in 1 mL of DPM borate buffer and incubated for 30 min at RT with continuous stirring.

5. The beads were then washed two times with freshly prepared ethanolamine buffer, resuspended in 1 mL of ethanolamine buffer, and incubated for 2 h at RT with constant stirring.

6. Finally, the beads were washed three times with 500 μL of lysis buffer and stored at 4 °C until use.

7. Two of the aliquots of the batch were used for testing and corroborating that the covalent binding was the adequate. The controls used for this purpose are:

   a. One of the aliquots was used to immunoprecipitate a viral sample containing wild type gp41 following the protocol in Section 2.4.3.

   b. Other aliquot was used as a negative control, which consisted in beads coupled to Chessie-8 mixed only with sample buffer without any viral sample.

   c. Beads mixed with the same amount of Chessie-8 but not coupled to it were also loaded as a control of non-coupled beads.

An adequate binding was considered when a clear gp41 protein band could be observed at ~41 kDa in the Western blot of the immunoprecipitated sample

containing wild type gp41, while no antibody heavy chain band could be observed at ~50 kDa in the negative control. In both samples, a ~25 kDa band can be observed corresponding to the antibody light chain due to the fact that it is not covalently bound to the beads, but it is recognized by the secondary antibody used (Figure 2.1).

Table 2.5 – Buffers used for the covalent coupling of the antibody to the beads.

Buffer	Composition
Borate buffer	0.2M $Na_2B_4O_7$ (Carl Roth) 0.2M H_3BO_3 (Carl Roth)
DPM borate buffer	0.2M $Na_2B_4O_7$ (Carl Roth) 0.2M H_3BO_3 (Carl Roth) 5.184 mg/mL Dymethyl pimelimidate dyhydrochloride or DMP (Fluka Biochemika)
Ethanolamine buffer	0.2 M ethanolamine (Fluka Biochemika) pH 8.0
Modified RIPA lysis buffer	20 mM HEPES 100 mM NaCl 5 mM EDTA 0.5% (w/v) sodium deoxycholate 1% (w/v) Triton X-100 pH 7.4 Supplemented with cOmplete™, EDTA-free Protease Inhibitor Cocktail (Sigma-Aldrich)
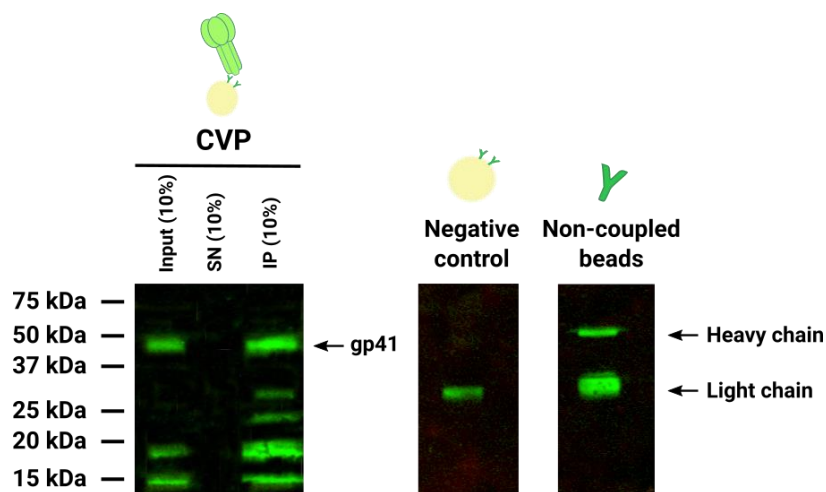
Figure 2.1. Verification of Chessie-8 coupling to beads. To test the adequate coupling of the Chessie-8 antibody to Protein G Sepharose beads, coupled beads were used to immunoprecipitate a sample of concentrated viral particles (CVP), which contains wild type gp41. In parallel, coupled beads not mixed with any sample were used as a negative control and beads mixed with the antibody but not coupled to it were also loaded as a control of non-coupled beads. The Western blot was developed with Chessie-8 α-gp41 primary antibody, and α-mouse IRDye800 secondary antibody.

2.4.3. Immunoprecipitation of HIV-1 gp41 using Chessie-8 coupled beads

For cell and viral particle lysis a modified RIPA buffer was used, composed of 20 mM HEPES, 100 mM NaCl, 5 mM EDTA, 0.5% (w/v) sodium deoxycholate and 1% (w/v) Triton X-100, adjusted to a pH of 7.4. The lysis buffer was supplemented with cOmplete™ EDTA-free Protease Inhibitor Cocktail (Sigma-Aldrich) prior to use to avoid degradation of proteins. Cells and viral samples were resuspended in up to 200 µL of lysis buffer supplemented with protease inhibitor cocktail and incubated for 1 h at 4 °C in constant rotation. The HIV-1 gp41 protein was immunoprecipitated with the following protocol:

1. For viral particles, a viral amount equivalent to 1 µg of CA was mixed with 100 µL of lysis buffer supplemented with protease inhibitor cocktail and lysed for 1 h at 4 °C in constant rotation. For cells, all cells from a 10 cm dish were mixed with 200 µL of lysis buffer supplemented with protease inhibitor cocktail and lysed in the same aforesaid conditions.

2. The lysed samples were centrifuged at 14,000 rpm for 5 min to pellet the non-lysed debris. An aliquot of the supernatant was stored as the input.

3. The rest of the supernatant was mixed with 50 µL of Protein G Sepharose beads covalently coupled to 10 µg of α-gp41 Chessie-8 antibody. The samples were incubated overnight with the beads at 4 °C in constant rotation to ensure a proper recognition between the α-gp41 Chessie-8 antibody and gp41.

4. Next day, the samples were centrifuged at 6,500 rpm for 5 min to pellet the beads with the immunoprecipitated protein, and the supernatant was stored as non-immunoprecipitated sample. The beads were washed three times with 500 µL lysis buffer by centrifugation at 6,500 rpm for 5 min.

The input, non-immunoprecipitated and immunoprecipitated samples were loaded into a SDS-PAGE gel by the following protocol to detect the presence of gp41:

1. An aliquot of the input and the non-immunoprecipitated samples corresponding to 5-10% of the total sample was mixed with 30 µL of SDS-PAGE sample buffer and heated to 95 °C for 5 min.

2. 50 μL of SDS-PAGE sample buffer were also added to the beads and heated in the same manner to induce dissociation between the α-gp41 antibody covalently bound to the beads and the immunoprecipitated gp41 protein.

3. After incubation with SDS-PAGE sample buffer the beads were centrifuged at 6,500 rpm for 10 min, separating the now free gp41 protein (supernatant) from the beads and the bound antibody (pellet).

4. The input and the non-immunoprecipitated samples and the immunoprecipitated gp41 protein were then loaded into a SDS-PAGE gel and the blots were probed with the Chessie-8 mouse α-gp41 primary antibody (1:2,000) overnight at 4 °C and α-mouse IRDye800 secondary antibody (1:10,000) for 45 min at RT, both in Intercept® Blocking Buffer. Final protein bands were visualized using the Odyssey infrared imaging system (LI-COR).

2.5. Viral particle purification

Viral particles have been used in this work for several purposes: gp41-cholesterol interaction and Gag-cholesterol interaction experiments, and protein palmitoylation experiments. The viral particle obtention starts with the transfection of HEK 293T cells with proviral or Env expressing plasmids and purified by sucrose cushion concentration, followed by velocity gradient purification if it is necessary. The general workflow for viral particle purification is shown in Figure 2.2.
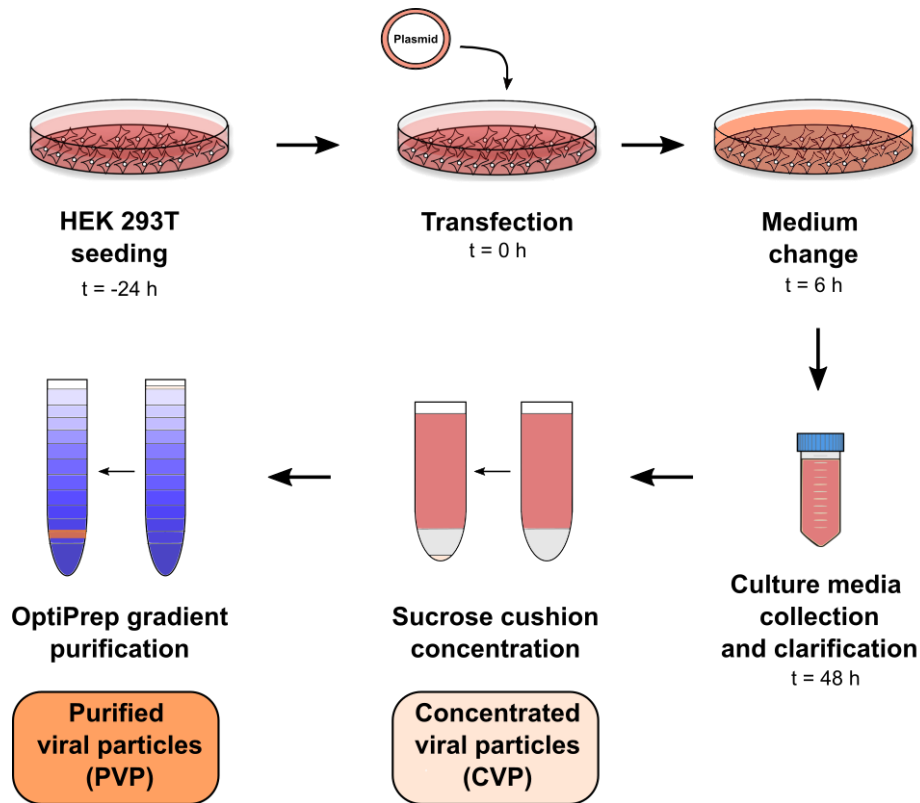
Figure 2.2. Workflow of a general viral particle purification.

2.5.1. Calcium phosphate transfection

Viral particles were produced by transfection with an adapted calcium phosphate method (Guo et al., 2017) to HEK 293T cells with proviral and Env expressing plasmids. The Table 2.6 shows the reagents used to develop the calcium phosphate transfection method. The different reagents for transfection were dissolved in ultrapure water (Sigma-Aldrich).

Table 2.6 – Reagents used for the calcium phosphate transfection method.

Reagent	Composition
Calcium Phosphate method CellPure® Calcium chloride (Carl Roth)	2.5 M $CaCl_2$
2xHBS	280 mM NaCl 50 mM CellPure® HEPES (Carl Roth) 1.5 mM $Na_2HPO_4 \cdot 2H_2O$ (Sigma-Aldrich) pH 7.10

Two types of culture surfaces were used for virus purification: 35 mm and 10 cm dishes. The number of seeded cells and reagents used for transfection in each one of these culture surfaces is detailed in Table 2.7.

Table 2.7 – Seeded cell density and transfection reagents amount used in the different culture surfaces.

	35 mm dish	10 cm dish
Seeded cells	$0.5 \cdot 10^6$	$3,5 \cdot 10^6$
Plasmid	2 µg	10 µg
CaCl$_2$ 0.25 M	25 µL	100 µL
2xHBS	250 µL	1 mL

1. The appropriate amount of HEK 293T cells were seeded in the appropriate dish 24 h prior to transfection.

2. Next day, the cells were transfected with the appropriate plasmidic DNA. The accurate amount of plasmidic DNA was added to a 0.25 M calcium chloride solution and vortexed to ensure a complete mixture.

3. The 2xHBS solution was added to the previous mixture drop wisely while vortexing at low speed, to ensure a homogeneous mixture.

4. This resulting transfection reagent was incubated at RT for 15 min for a complete conjugation of the DNA to the calcium phosphate precipitate.

5. The aggregates were then added drop wisely to the cell culture ensuring a complete spread through the entire culture surface. Cells were incubated in this culture conditions for 6 h.

6. After 6 h, the medium was replaced by fresh culture medium.

2.5.2. Sucrose cushion concentration

1. The culture medium supernatant, where the virions are, was collected after 48 h.

2. Cell debris was eliminated by a clarification process, consisting in a centrifugation at 500 g for 10 minutes followed by a filtration through 0.45 µm CME filters (Carl-Roth).

3. Viral particles were concentrated from this clarified medium by centrifugation through a cushion of 20% (wt/wt) sucrose (Welker et al., 2000). For this, an appropriate amount of 20% Ultrapure Sucrose (Thermo Fisher Scientific) was added to the bottom of an ultracentrifuge tube (Beckman Coultier) and the clarified culture media was carefully added on top. For the different experiments viral purifications of different scales were carried out. Depending on the sample volume to be purified, different ultracentrifuge tubes, 20% sucrose solution volume and centrifugation speeds and time were used (Table 2.8), but always centrifuge at 4 °C. The centrifugation process was developed in TLA-110, SW 28.1 or SW 60Ti rotors and in Optima MAX-TL or Optima L-100 XP ultracentrifuges from Beckman Coultier.

Table 2.8 – Ultracentrifugation conditions for different sample volumes

	Sample volume		
	1-2 mL	4-8 mL	>30 mL
Rotor	TLA-110	SW 60Ti	SW 28.1
Ultracentrifuge	Optima MAX-TL	Optima L-100 XP	Optima L-100 XP
20% sucrose volume/tube (mL)	0.1	0.5	6
Sample volume/tube (mL)	1	4	30
Rotor speed (rpm)	44,000	31,000	25,000
Avg. G-force (g)	80,000	96,000	85,000
k-Factor	81.25	163.7	284
Time (min)	45	90	120

4. After centrifugation, the culture medium and sucrose supernatant were removed, and the pelleted virus was resuspended in HeNa buffer (10 mM HEPES, 150 mM NaCl, pH 7.4), obtaining concentrated viral particles. A schematic representation of the whole viral particle concentration in a sucrose cushion process is shown in Figure 2.3. The samples were stored at -20 °C until their characterization and use.

5. Particles concentrated by sucrose cushion could be further purified using a velocity gradient purification (Section 2.5.3).
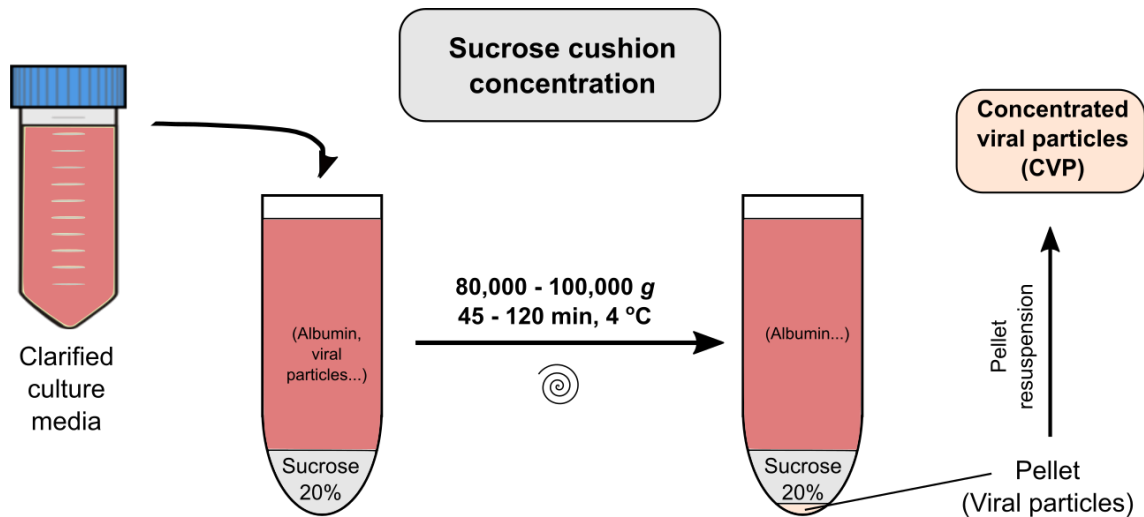
Figure 2.3. Representation of viral particle purification by sucrose cushion concentration.

2.5.3. Velocity gradient purification

Concentrated HIV-1 particles were further purified by a sedimentation velocity gradient using OptiPrep™ from Axis-Shield (Brügger et al., 2006; Dettenhofer & Yu, 1999; Lorizate et al., 2009). OptiPrep is a sterile endotoxin tested solution of 60% iodixanol, which is widely used for viral purification due to the fact that it would not affect viral infectivity. Furthermore, in iodixanol gradients the HIV-1 particles are effectively separated both from extracellular Vif gene and cell-derived microvesicles, avoiding contamination.

A schematic overview of the concentrated virus particle purification by a centrifugation in a discontinuous OptiPrep gradient is shown in Figure 2.4.
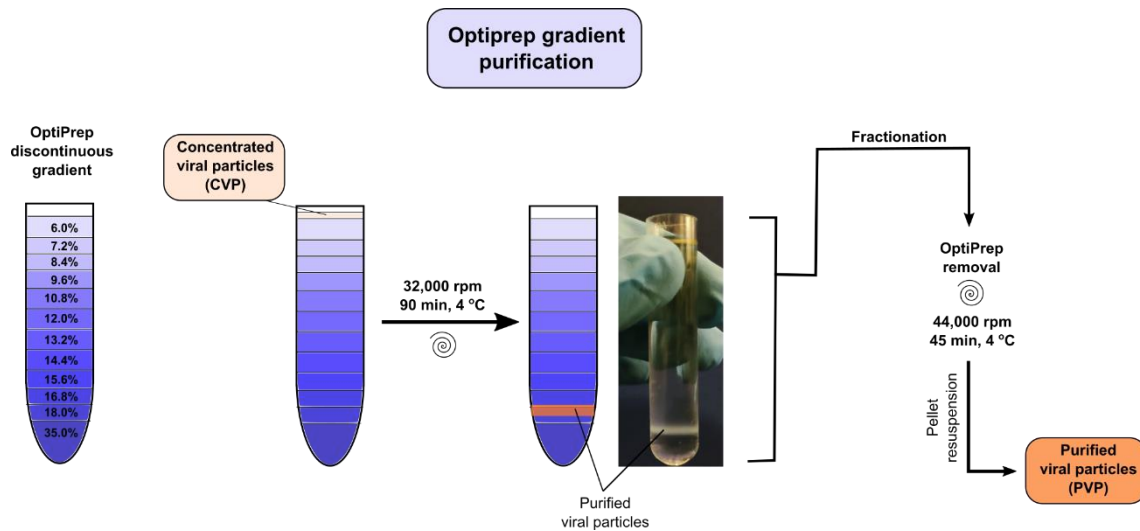
Figure 2.4. Representation of concentrated virus particle purification by sedimentation velocity gradient centrifugation using an OptiPrep gradient.

1. A discontinued gradient was prepared in a SW 60Ti ultracentrifuge tube (Beckman Coultier) with decreasing OptiPrep concentrations shown in Table 2.9. These concentrations were prepared by diluting the commercial OptiPrep in HeNa buffer.

Table 2.9 – Concentration of the different layers of the discontinuous OptiPrep gradient, from bottom to top.

OptiPrep concentration (% wt/wt)	Volume (µL)
35.0	420
18.0	300
16.8	300
15.6	300
14.4	300
13.2	300
12.0	300
10.8	300
9.6	300
8.4	300
7.2	300
6.0	430

2. 150 µL of the resuspended concentrated viral particles were added on top of the 6.0% layer.

3. The samples were centrifuged at 32,000 rpm (100,000 g avg., 153.6 k-Factor) for 90 min at 4 °C in a SW 60Ti rotor.

4. Fractions of 270 μL were collected and those containing the visible viral band (usually fractions 11-13) were combined and diluted 1:8 (v/v) with HeNa buffer.

5. The purified diluted viruses were then pelleted by ultracentrifugation in a SW 60Ti rotor at 44,000 rpm (200,000 g avg., 81.25 k-Factor) for 45 min at 4 °C.

6. The supernatant was removed, and the pelleted purified viruses were resuspended in HeNa buffer, obtaining purified viral particles (PVP). The samples were stored at -20 °C until their characterization and use.

2.6. Characterization of viral particles

2.6.1. Silver Stain

To characterize the concentrated or purified viral particles, an appropriate amount of each sample was loaded into a SDS-PAGE and the gel was then silver-stained. After silver stain, all proteins in the samples are stained. This technique allows to confirm if the samples contain the expected viral protein pattern and, also, to determine if there is contamination from albumin or other proteins from the cell culture or cell debris. Silver stain is carried following the next protocol (Chevallet et al., 2006):

1. 100 mL/gel of different solutions are prepared fresh using MiliQ ultrapure water for the silver stain of the samples. The compositions of the different solutions needed are shown in Table 2.9.

Table 2.9 – Composition of the solutions used for silver stain of SDS-PAGE gels.

Solution	Composition
Fixation	50% methanol (v/v) 12% CH_3COOH (v/v) 0.02% (wt/v) formaldehyde
Solution I	50% ethanol (v/v)
Solution II	0.9 mM Na_2SO_4
Solution III	11.7 mM $AgNO_3$ 0.02% (wt/v) formaldehyde
Solution IV	0.56 M $NaCO_3$ 0.02% (wt/v) formaldehyde 30 μM Na_2SO_4

2. The samples were dissolved in SDS-PAGE sample buffer and heated to 95 °C for 5 min.

3. Samples were loaded into a 12.5% polyacrylamide gel containing SDS and subjected to electrophoresis.

4. The gels were recovered and incubated with 100 mL/gel of Fixation solution for 1 h at RT. The gel could also be incubated in Fixation solution overnight at 4 °C.

5. After fixation, each gel was washed three times for 5 min per wash with Solution I, and then wash with ultrapure water for 20 s.

6. The gels were then incubated with Solution II for 1 min at RT for signal enhancing and washed with ultrapure water.

7. The samples were stained with Solution III for 20 min at RT and a single washing step with ultrapure water was carried out.

8. The gels were developed with Solution IV for the necessary time, 2-5 min should be enough, and the reaction is stopped by a washing step with ultrapure water.

9. The gel could be stored in 100 mL of 1% CH_3COOH (v/v) solution at 4 °C.

A representative image of silver stain of viral particles after purification is shown in Figure 2.5. The different fractions collected after velocity gradient centrifugation using a discontinuous OptiPrep gradient are stained to predict which ones contain the viral particles (Figure 2.5 A). Then, these fractions (9 to 14) are mixed and pelleted in the next centrifugation step. Finally, after viral particle centrifugation, CVP and PVP are stained to corroborate that they present the accurate viral protein pattern (Figure 2.5 B). If enough viral quantity has been loaded into the SDS-PAGE, a visible CA protein band at ~25 kDa and MA protein band at ~15 kDa could be observed after the silver stain. The gp41 band at ~41 kDa is usually to faint to be clearly observed, due to the low copy of Env protein trimers present in each viral particle (Chertova et al., 2002).
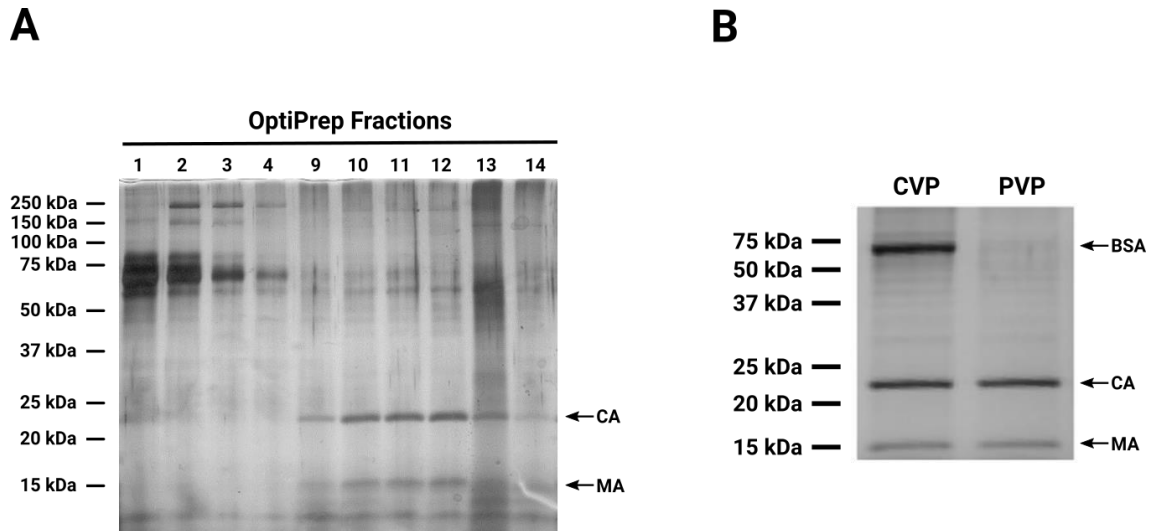
Figure 2.5. Representative image of viral particle purification characterized by silver staining.
A) Silver stain of the different fractions collected after velocity gradient centrifugation using a discontinuous OptiPrep gradient. **B)** Silver stain of concentrated viral particle (CVP) and purified viral particle (PVP) after viral particle purification.

2.6.2. Purification yield quantification by α-CA Western blot

The yield of the viral particle purification was determined by a quantitative Western blot analysis probed against CA (Figure 2.6). A solution of purified CA of known concentration was used as a standard to quantify the viral CA amount. It was kindly donated by Professor Hans-Georg Kräusslich (University Hospital of Heidelberg, Germany).

This purified viral particle method based on the α-CA Western blot has some intrinsic variability. To ensure that the comparison was as fitting as possible, several viral amounts obtained by a serial dilution were loaded for each sample. The protocol used for CA quantification is the following:

1. Several amounts of the CA standard (10, 5, 2.5, 1.25, 0.625, 0.3125 and 0.1563 ng) and a titration of purified viruses were dissolved in SDS-PAGE sample buffer, and a SDS-PAGE was performed following the protocol in Section 2.3.

2. The blots were probed using a sheep α-CA antibody (Table 2.2) as primary antibody and α-sheep IRDye800 (Table 2.3) as a secondary antibody.

3. Protein bands were visualized using the Odyssey infrared imaging system (LI-COR) (Figure 2.6 A). The integrated intensity signal of the bands corresponding to the CA standard were measured using the software of the instrument.

4. A calibration curve was established with the CA standards (Figure 2.6 B) and the CA amount of each viral sample was calculated using the aforesaid calibration curve.

A

B
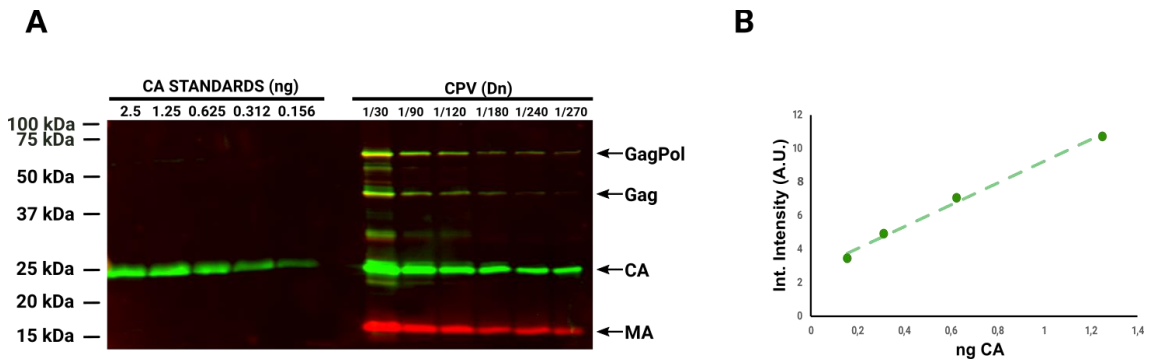
Figure 2.6. Example of CA quantification by Western blot. **A)** A known amount of CA protein is loaded as a standard to generate a calibration curve. In the same Western blot, several dilutions of the viral sample are loaded. The Western blot was developed with rabbit α-MA antibody as control, and α-rabbit IRDye680 antibody (red) and with sheep α-CA and α-sheep IRDye800 antibodies (green). **B)** The integrated intensity of the samples in panel A is measured in the LI-COR Odyssey imaging system. The values of the CA standard are used to build a calibration curve, from which a regression curve is extracted to calculate the amount of CA in the viral sample dilutions.

Chapter 3.

Unravelling HIV-1 Gag/MA – cholesterol interaction using a radioactive photoactivatable cholesterol

Chapter 3: Unravelling HIV-1 Gag/MA – cholesterol interaction using a radioactive photoactivatable cholesterol

3.1. Introduction

Polyprotein Gag leads HIV-1 morphogenesis. It is synthesized as a precursor polyprotein, which, upon viral release, is cleaved into the four main constituents of the mature virion: matrix (MA), capsid (CA), nucleocapsid (NC) and p6. MA is the amino-terminal Gag domain, and it functions to bind to the cell membrane and, although not completely understood, to recruit the viral envelope glycoprotein (Env) to the budding site. The N-terminal domain of the MA protein is modified by the attachment of a myristoyl group (Myr), a 14-carbon fatty acid that can alternate between two conformations: being sequestered in the protein or anchored in the membrane. Gag binds to the cell membrane by electrostatic interactions through a conserved highly basic region (HBR) of MA protein, which induces the switch and anchor to the membrane of the hidden myristoyl group, a process known as myristoyl switch (Freed, 2015; Ghanam et al., 2012; Lorizate & Kräusslich, 2011; Ono et al., 2000; Ono & Freed, 1999; Paillart et al., 1999; Resh, 2004; Spearman et al., 1994, 1997; Sundquist & Kräusslich, 2012; Tanaka et al., 2016; Zhou et al., 1996).

A variety of structural, *in vivo* and *in vitro* studies have shown that Gag trafficking and targeting to the cell membrane are orchestrated events that depend on different cellular proteins, such as AP-1, AP-2, and AP-3 from the endosomal pathway (Klingler et al., 2020); and specific membrane lipids like phosphatidylinositol-4,5-bisphosphate [$PI(4,5)P_2$] (Anraku et al., 2010; Barklis et al., 2018; S. M. Campbell et al., 2001; Shkriabai et al., 2006; Wen et al., 2020). Moreover, the final localization of Gag on punctate sites on the cell membrane is driven by specific interactions between the MA HBR domain plus Myr of Gag, and $PI(4,5)P_2$. Even more, the interaction between Gag

and the membrane is highly dynamic and dependent on specific protein-lipid interactions. Depletion of PI(4,5)P$_2$ results in a loss of already assembled Gag lattices, and its replenishment restores Gag assemblies to the plasma membrane (Chan et al., 2008; Charlier et al., 2014; Chen et al., 2020; Chukkapalli et al., 2008, 2010; Freed & Mouland, 2006; Ghanam et al., 2012; Inlora et al., 2014; Mercredi et al., 2016; Monje-Galvan & Voth, 2020; Mücksch et al., 2017; Ono & Freed, 2004; Saad et al., 2008; Thornhill et al., 2020; Tran et al., 2019).

The fact that Gag can form, by its own, virus-like particles (VLPs) together with the lack of enzymes for lipid biosynthesis on HIV-1 and the different composition of the viral membrane in comparison to the cell membrane (Aloia et al., 1988, 1993; Brugger et al., 2006; Chan et al., 2008; Gheysen et al., 1989; Lorizate et al., 2013; Mariani et al., 2014; Mücksch et al., 2019; Sundquist & Kräusslich, 2012), a possibility exists that lipids such as PI(4,5)P$_2$ and/or proteins could be taking part in the morphogenesis. One perfect candidate could be cholesterol due to its high quantity in the viral membrane, because there are indirect evidences of interaction of Gag with this lipid (Dick & Vogt, 2014; Dick et al., 2012; Doktorova et al., 2017; Favard et al., 2019; Lalonde & Sundquist, 2012; Ono & Freed, 2001; Pérez-Socas & Ambroggio, 2020; Thiele et al., 2000; Yandrapalli et al., 2016), and because Gag is found in detergent resistant membranes (DRMs) (Bhattacharya et al., 2006; Ding et al, 2003; Halwani et al., 2003; Holm et al., 2003; Lindwasser & Resh, 2001; Nguyen & Hildreth, 2000; Ono & Freed, 2001; Patil et al., 2010). Therefore, the aforesaid leads to think that a Gag/MA-cholesterol interaction could be happening during viral morphogenesis, as it is confirmed that cholesterol is required in the HIV-1 entry process (Nieto-Garai et al., 2021; Luo et al., 2008; Percherancier et al., 2003).

On the other hand, the Gag protein has long been suggested to be implicated in Env incorporation to the budding sites based on the proposed interaction between MA and the cytoplasmic tail (CT) of the gp41 subunit of Env (Alfadhli et al., 2016, 2019; Brandano & Stevenson, 2011; Bulgelski et al., 1995; Checkley et al., 2011; Davis et al., 2006; Dorfman et al., 1994; Eastep et al., 2021; Freed & Martin, 1995; Groves et al., 2020; Murakami & Freed, 2000; Muranyi et al., 2013; Murphy & Saad, 2020; Patil et al., 2010; Pezeshkian et al., 2019; Tedbury & Freed, 2014; Tedbury et al., 2013, 2015a, 2015b, 2020;

Wyma et al., 2000; Yu et al., 1992). Moreover, the multimerization of Gag stabilizes, recruits, or reorganizes the cell membrane microdomains by attracting Env polyproteins (Hogue et al., 2012), and Gag is also responsible of the redistribution and targeting of Env upon HIV-1 maturation, since the disappearance of the Gag rigid lattice increases membrane and proteins mobility in the mature virion (Chojnacki et al., 2012, 2017; Groves et al., 2020; Shiraishi et al., 2001). Env incorporation into virions is explained by different models with and without the specific interaction with Gag polyprotein (Buttler et al., 2018; Ghanam et al., 2012; Groppelli et al., 2014; Murphy & Saad, 2020; Pezeshkian et al., 2019; Qu et al., 2021; Tedbury & Freed, 2014), however, the mechanism by which Env is incorporated into viral particles is not completely understood yet.

It is known that Env possess several regions that are proposed as lipid interacting motifs (CRAC, GxxxG, LLPs) (Klug et al., 2017; Schroeder, 2010). In addition, recently it has been seen that Env interacts with cholesterol in an Env-CT dependent manner, and that this interaction has an implication in Env clustering in a single foci during maturation (Nieto-Garai et al., 2021). Thus, Gag/MA could possess other cholesterol-interacting motifs such as Env, and, in addition, through this Gag/MA-cholesterol interaction Gag could influence Env incorporation into HIV-1 virions and may also induce clustering of cholesterol or stablish budding regions through cholesterol platforms.

Bifunctional lipids have emerged as a new specific tool for the study of direct protein-lipid interactions *in vivo*. These probes contain a photoactivatable group, which could be an aryl azide, benzophenone or diazirine among others, that share the features of bio-orthogonality, chemical stability, and high reactivity upon photoactivation (Haberkant & Holthuis, 2014; Peng et al., 2014). After irradiation with UV light, the photoactivatable group generates a highly reactive carbene group. The carbene group covalently binds to any molecule closer than 3 Å, allowing the interaction of the bifunctional lipid with specific molecules. In addition, bifunctional lipids have a radiolabelled tag that could be used for monitoring lipid-protein interactions in living cells. The resulting radioactively labelled proteins can be detected by thin layer chromatography and autoradiography (Haberkant et al., 2008; Thiele et al., 2000).

Photoactivatable and radioactively labelled cholesterol, [3H]-photo-cholesterol ([3H]-photo-chol) (Figure 3.1), is one of the nowadays available bifunctional probe to study direct interactions of proteins with cholesterol. Its properties, metabolism and distribution have been shown to resemble its natural counterpart (Farenholz et al., 2000; Haberkant et al., 2008; Nieto-Garai et al., 2021; Thiele et al., 2000).

Figure 3.1. Radioactive photoactivatable cholesterol. Structure of tritium-labelled photoactivatable cholesterol analogue, [3H]-photocholesterol ([3H]-photo-chol). After irradiation with ultraviolet light (360 nm) the diazirine group (blue) of [3H]-photo-chol generates a highly reactive carbene group in the activated molecule, which covalently binds to any molecule closer than 3 Å of distance. The tritium labelling (red) permits detection and quantification of the lipid by autoradiography.

Similarly, for the study of protein interaction with sphingolipids, lipid analogues are available as precursors of SPLs, such as [3H]-D-erythro-14-azi-sphingosine ([3H]-photo-SP) and [3H]-photo-phosphatidylcholine ([3H]-photo-PC). Together, these cross-linking lipids allow the specific study of the interaction of proteins with chol, SPLs and PC, as well as its association with membrane nanodomains enriched in those lipids.

Taking together all the aforesaid, it is known that Gag polyprotein could interact with DRMs and, indirectly, with cholesterol. Moreover, is the molecule responsible for morphogenesis, and additionally, it has been suggested to be implicated in Env incorporation to the budding sites based on the interaction between its MA domain and Env CT . This information led to think that a plausible Gag/MA-cholesterol interaction could be taking place during HIV-1 morphogenesis. In summary, unravelling the existence of this Gag/MA-cholesterol interaction is the main objective of this chapter, using the bifunctional lipid probe [3H]-photo-cholesterol as a chemical tool.

3.2. Specific experimental techniques

3.2.1. Radioactive photoactivatable cholesterol

Bifunctional lipid probes have been applied to explore specific membrane protein-lipid interactions (Section 1.3.1.1). To study the possible interaction between Gag/MA and cholesterol during HIV-1 morphogenesis, cholesterol was biofunctionalized with a photoactivatable group, a diazirine group, and a radioactive tritium tag in the A ring to easily detect and quantify the cross-linking products (Figure 3.2). The incorporation of an isotope element like tritium has been demonstrated not to alter the structural or functional properties of the natural molecule, and this technique constitutes one of the most sensitive methods for tracking trace amounts of labelled biomolecules (Gevaert et al., 2008).

To obtain a biologically active cholesterol analogue, it is compulsory for the derivative to have an intact alicyclic chain, a free 3β-OH, angular methyl groups, and a branched seven-carbon alkyl chain at the 17β-position (F. Schroeder et al., 1995). Therefore, the bifunctional cholesterol used in this chapter lacks the Δ5(6) double bond and the hydrogen at position C-6 (Figure 3.2 A), being replaced by the photoactivatable diazirine ring (Figure 3.2 B). The position C-6 is generally buried in the hydrophobic region of the lipid bilayer, thus avoiding non-specific cross-linking with superficial solvent molecules.

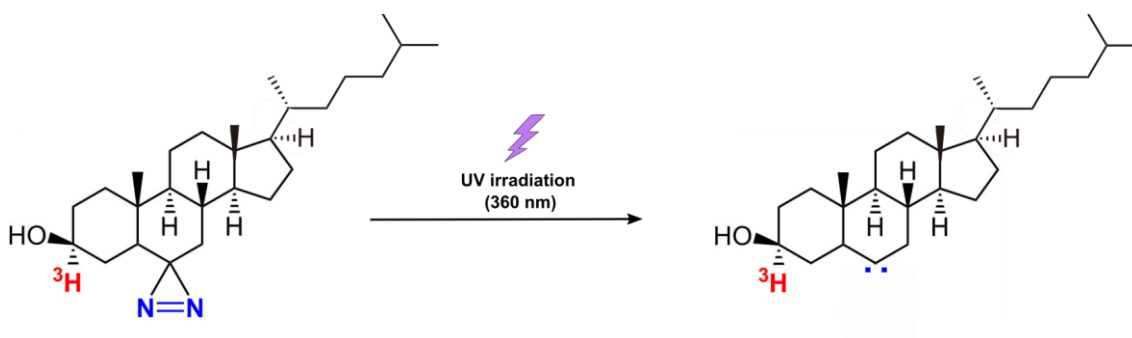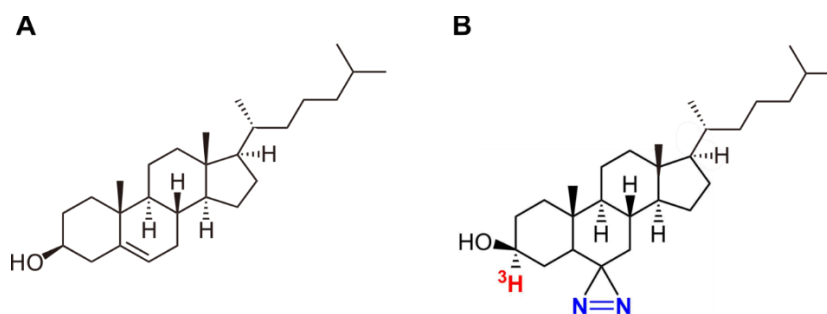**Figure 3.2. Natural vs. bifunctional cholesterol. A)** Structure of natural cholesterol. **B)** Structure of tritium-labelled photoactivatable cholesterol analogue, [³H]-photo-cholesterol ([³H]-photo-chol). Tritium label is coloured in red and the diazirine group in blue.

Diazirines refer to a small, non-perturbing, cyclopropene-like ring with two double-bonded nitrogen atoms, stable under non-activating conditions. This ensures that its incorporation causes minimal steric perturbation, not interfering with the physicochemical properties of the native biomolecule. It exhibits a characteristic photolabile nature, as it undergoes rapid photolysis upon exposure to long-wave UV light (360 nm), which minimizes the incidence of non-specific photo-crosslinking and photodamage to the biological sample.

Subsequent photoactivation of this group results in the formation of highly reactive short-lived carbene intermediates (lifetimes from 10^{-4} to 10^{-9} s), that irreversibly react with its C-H, N-H, and O-H bonds to form stable C-C, C-N, and C-O bonds, respectively, or in the addition to double bonds (Das, 2011; Peng et al., 2014; Xia & Peng, 2013) (Figure 3.3). Furthermore, carbene species could crosslink with any nearby molecule closer than 3Å (Farenholz et al., 2000; Haberkant et al., 2008; Nieto-Garai et al., 2021; Thiele et al., 2000), once embedded in the hydrophobic core of the cell membrane more efficiently than in water. This makes diazirines especially suitable for capturing membrane protein-lipid interactions.
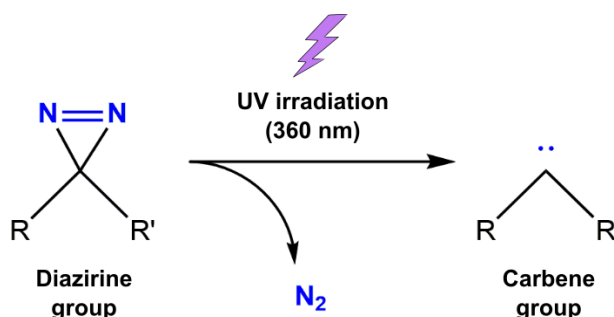
Figure 3.3. Photoactivation of diazirines. UV light irradiation induces the formation of highly reactive carbene intermediates that covalently bind to molecules in close proximity.

3.2.1.1. Radioactive labelling of photoactivable cholesterol

Photoactivatable cholesterol (photo-cholesterol) was chemically synthesized by Dr. F.-Xabier Contreras (Instituto Biofisika, Spain), and labelled with radioactive tritium as described by Thiele et al. (2000). Briefly:

1. 2.5 mg of photo-cholesterol dissolved in 1 mL tetrahydrofuran was added to 25 mCi of tritiated sodium borohydride ($[^3H]$-$NaBH_4$) (Amersham Biosciences) dissolved in 1 mL of 0.1 M NaOH. The mixture was stirred at RT for 16 h to induce photo-cholesterol labelling with radioactive tritium.

2. 300 μL of 1 N HCl was added to the mixture above and stirred for 15 min. The mixture containing tritiated photo-cholesterol was extracted twice with 1 mL ethyl acetate (CH_3–COO–CH_2–CH_3).

3. The combined organic phases from the double extraction were partially evaporated to reduce the volume to 300 μL and subjected to a Thin Layer Chromatography (TLC). The mobile phase was a mixture of hexane/ethyl acetate (2:1 vol:vol).

4. The TLC plate was dried, and radioactive bands were visualized by phosphoimaging. Two products were detected: $[^3H]$-photo-cholesterol and its α-epimer with higher mobility (in a 9:1 ratio).

5. The TLC plate was sprayed with water to prevent dispersion of radioactive dust, and the bands corresponding to $[^3H]$-photo-cholesterol were scraped from the plate and collected.

6. $[^3H]$-photo-cholesterol was purified from the silica dust with four consecutive extractions using 800 μL ethanol. $[^3H]$-photo-cholesterol concentration was determined by a scintillation counter and stored at -20 °C.

3.2.2. Protein-lipid interaction studies

3.2.2.1. $[^3H]$-photo-chol interaction with viral proteins

$[^3H]$-photo-cholesterol addition to the cell culture was performed using delipidated medium to enhance photoactivatable lipid absorption by avoiding competition with other lipids in the medium. The delipidated medium was prepared using DMEM GlutaMAX™ High glucose culture medium supplemented with 10% delipidated FBS, and 100 U/mL Penicillin-Streptomycin.

For protein-lipid interaction studies in cells, HEK 293T cells seeded into a 10 cm dish were transfected with either a proviral or Env expressing plasmid as described in Section 2.5.1. 18 h post-transfection, 100 μCi of $[^3H]$-photo-cholesterol was diluted in 8

mL of culture medium containing delipidated FBS and added to the transfected cells. The photoactivatable lipid was incubated with the cells for 8 h and, after removing the medium, the cells were washed with PBS, and cold PBS supplemented with protease inhibitor cocktail was added. Cells were then irradiated for 5 min at 4 °C with UV light to induce lipid crosslinking. These cells were then scraped, pelleted, and resuspended in 200 μL of lysis buffer (Figure 3.4) for posterior gp41 and/or Gag/MA immunoprecipitation, detailed in Section 2.2.4.3 and Section 3.2.2.3, respectively.
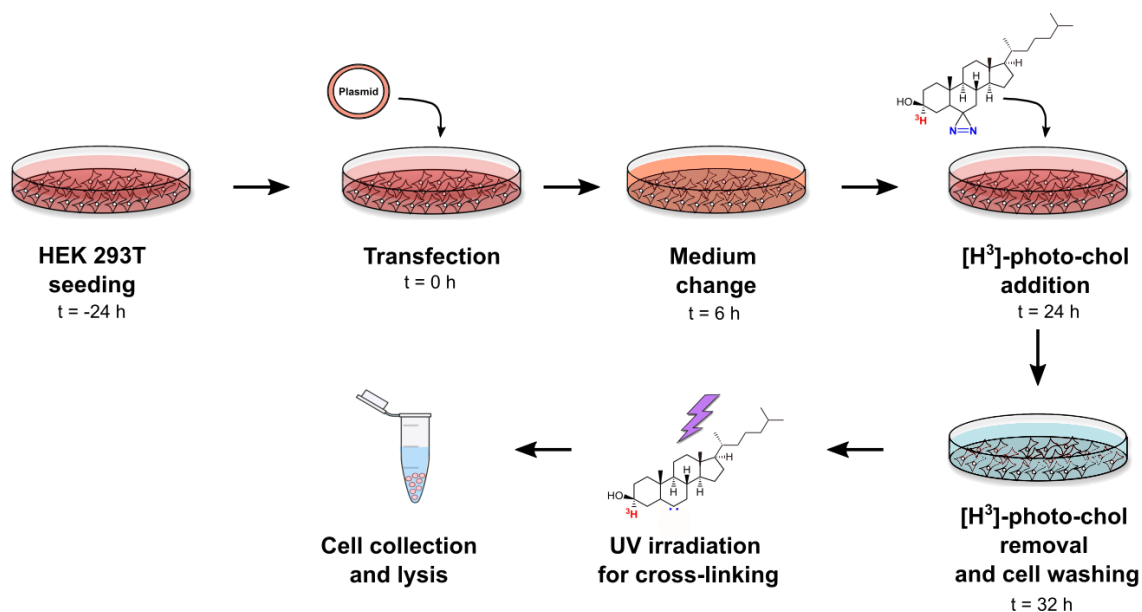
Figure 3.4. Workflow of protein-lipid interaction studies in cells.

For the study of protein interaction with [³H]-photo-cholesterol in cells positive and negative controls were used. As control of positive interaction with cholesterol, the caveolin-1 (Cav-1) protein was selected as it is widely known to bind cholesterol (Brown & London, 1998; S. Li et al., 1996; Smart et al., 1999). On the other hand, the transferrin receptor (TfR) protein was used as a negative control, as it constitutes the archetypal non-lipid raft marker (Magee & Parmryd, 2003).

HEK 293T cells were seeded into a 10 cm dish and transfected with 6 μg of Cav-1-GFP expressing plasmid with the calcium phosphate method. In the case of TfR, endogenous protein was used, so there was no need of transfection. 18 h post-

transfection, 100 μCi of [³H]-photo-chol were added to the cells in delipidated medium and incubated for an additional 6 h. Cells were then washed, irradiated with UV light for 5 min, lysed with lysis buffer, and immunoprecipitated against the GFP tag in the case of Cav-1-GFP and against transferrin receptor following the next protocol:

1. For Cav-1-GFP, 50 μL of Protein A Sepharose 4 Fast Flow beads (GE Healthcare) beads were washed extensively with lysis buffer and mixed with 5 μg of rabbit α-GFP ChIP Grade antibody (Abcam, #ab290). For TfR protein, 50 μL of Protein G Sepharose™ 4 Fast Flow (GE Healthcare) beads were washed extensively with lysis buffer and mixed with 5 μg of rabbit α-transferrin receptor antibody (Santa Cruz Biotechnologies, #sc-32272). In both, cell lysates were then added to the beads and antibody mixture and incubated overnight at 4 °C in constant mixing.

2. The samples were then immunoprecipitated by centrifugation and washed extensively. 50 μL of sample buffer was added to each sample and incubated at 95 °C for 5 min to release the immunoprecipitated protein.

The immunoprecipitated Cav-1 and TfR were then loaded into a 12,5% SDS-PAGE gel and a semi-dry Western blot was carried out developed against the Cav-1 and TfR proteins following the general Western blot protocol detailed in Section 2.3.

1. For Cav-1 detection, the membrane was incubated with a rabbit α-caveolin-1 antibody (Abcam) at a 1:1,000 dilution for 1 h, followed by washing and incubation with α-rabbit IRDye680 (LiCor) secondary antibody at a 1:10,000 dilution for 45 min.

2. For TfR detection, the membrane was incubated with mouse α-transferrin receptor antibody (Abcam) at 1:1,000 dilution for 1 h, followed by washing and incubation with α-mouse IRDye800 (LiCor) secondary antibody at a 1:10,000 dilution for 45 min.

3. Detection of the proteins was carried out using the LI-COR Odyssey imaging system.

The membrane was then dried, and the radioactive lipid signal was visualized by autoradiography of the membrane as explained in Section 3.2.2.4.

3.2.2.2. Production and purification of [³H]-photo-chol containing virus

For protein-lipid interaction studies in virions, HEK 293T cells seeded into 10 cm dishes were transfected with proviral plasmids as described in Section 2.5.1, and 100 μCi of [³H]-photo-cholesterol was added to the cells. The bifunctional lipid was incubated with the cells for 24 h to ensure lipid incorporation into the released virions. Viral particles are generated by budding from the host cells acquiring their viral lipid membrane from the cell membrane, thus, recruiting the [³H]-photo-cholesterol along with other cellular lipids present in the cell membrane. As a result, the cell culture supernatant will contain viral particles with [³H]-photo-cholesterol in their viral membrane. Before viral particle concentration and purification, the clarified cell culture supernatant containing the viral particles was irradiated in a petri dish with UV light for 5 min at 4 °C to induce crosslinking between the diazirine group of the [³H]-photo-cholesterol and any molecule closer than 3 Å. Once irradiated, the viral particles were concentrated and purified following the protocols explained in Sections 2.5.2 & 2.5.3, respectively. The viral particle purification yield was determined by α-CA Western blot and their protein content characterized by silver stain (Section 2.6). A general overview of the workflow for obtaining purified viral particles that contain [³H]-photo-cholesterol is shown in Figure 3.5.
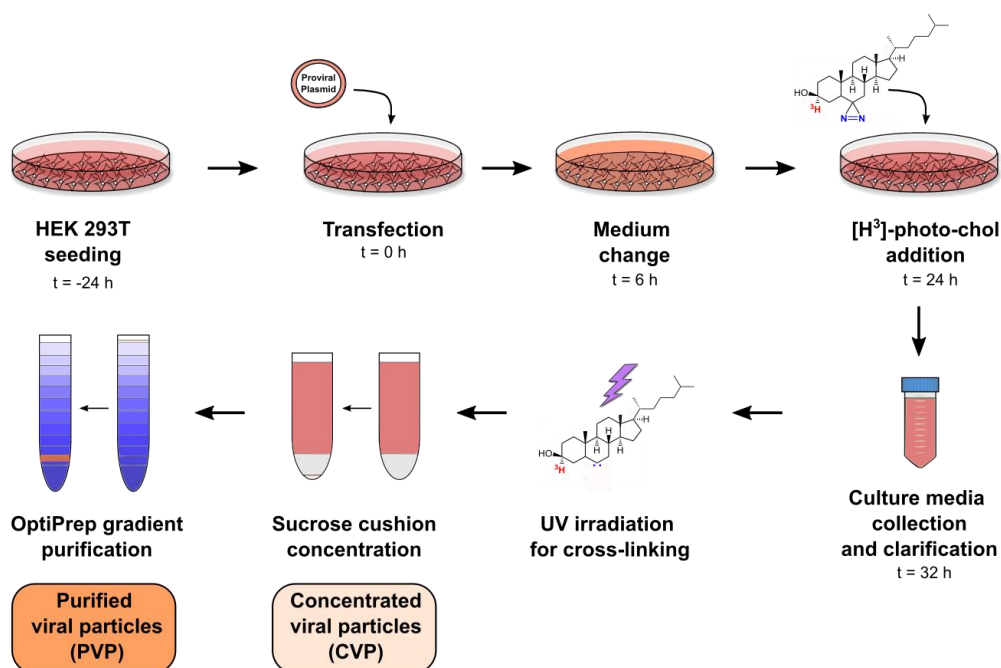
Figure 3.5. Workflow of production and purification of [³H]-photo-chol-containing virus.

After viral particle characterization, the sample was mixed with 100 μL of lysis buffer for gp41 immunoprecipitation as explained in Section 2.2.4.3, and for Gag/MA immunoprecipitation as explained in Section 3.2.2.3 below.

3.2.2.3. Immunoprecipitation of Gag/MA

Cellular and viral samples were resuspended in up to 200 μL of modified RIPA lysis buffer supplemented with protease inhibitors and incubated for 1 h at 4 °C in constant rotation. After the obtention of cellular and viral particles lysates containing crosslinked [^{3}H]-photo-cholesterol, the Gag/MA protein was immunoprecipitated with the following protocol to evaluate the presence of this lipid crosslinked to the protein.

1. For viral particles, a viral amount equivalent to 1 μg of CA was mixed with 100 μL of lysis buffer and lysed for 1 h at 4 °C in constant spinning. For cells, all of them from a 10 cm dish were mixed with 200 μL of lysis buffer and lysed in the same conditions.

2. The lysed samples were centrifuged at 13,000 rpm for 5 min to pellet the non-lysed debris. An aliquot of the supernatant was stored as the input.

3. The rest of the supernatant was mixed with 50 μL of Protein A Sepharose™ 4 Fast Flow (GE Healthcare) beads and 5 μg of rabbit α-MA antibody. The samples were incubated overnight at 4 °C in constant spinning with the beads to ensure a proper recognition between the α-MA antibody and Gag/MA.

4. Next day, the samples were centrifuged at 6,500 rpm for 5 min to pellet the beads and immunoprecipitate the protein, and the supernatant was stored as non-immunoprecipitated sample. The beads were washed three times with 500 μL lysis buffer by centrifugation at 6,500 rpm for 5 min.

The input, non-immunoprecipitated and immunoprecipitated samples were loaded into an 12,5 % SDS-PAGE gel by the following protocol to detect the presence of Gag/MA.

1. An aliquot of the input and non-immunoprecipitated samples corresponding to 5-10% of the total sample was mixed with 30 μL of 6x SDS-PAGE sample buffer and heated to 95 °C for 5 min.

2. 50 μL of 6x SDS-PAGE sample buffer were also added to the beads and heated in the same manner to induce dissociation between the α-MA antibody bound to the beads and the immunoprecipitated Gag/MA protein.

3. After incubation with SDS-PAGE sample buffer the beads were centrifuged at 6,500 rpm for 10 min, separating the proteins in the supernatant from the beads in the pellet.

4. The input and non-immunoprecipitated samples and the immunoprecipitated Gag/MA protein were then loaded into a SDS-PAGE gel and the blots were probed with the rabbit α-MA and sheep α-CA primary antibodies diluted at 1:5,000 and 1:2,000, respectively, in Intercept® Blocking Buffer during 1 h at RT.

5. Gag/MA protein bands were detected using the LI-COR Odyssey imaging system after probing with α-rabbit IRDye680 and α-sheep IRDye800, both at 1:10,000 dilution, for 45 min at RT. Protein bands were visualized using the Odyssey infrared imaging system (LI-COR).

3.2.2.4. Autoradiography and protein-lipid interaction quantification

In order to identify the presence of [^{3}H]-photo-cholesterol crosslinked to the gp41 and Gag/MA proteins in the immunoprecipitated samples, the Western blot membranes used in the previous sections were dried and the radioactive lipid signal was detected by autoradiography of the membrane in a BetaIMAGER™ (Biospace Lab) for up to 18 h.

If a radioactive lipid signal band was present which co-localized with the gp41 or Gag/MA protein bands in the Western blot, its intensity was measured as cpm/mm^2 using the instrument software of the BetaIMAGER™ system.

3.2.3. Statistics

The statistical analysis of the different experimental groups was carried out with SigmaPlot. The significance was determined by analysis of variance and Tukey test, when more than two samples were compared, and by Student's t-test, when only two samples were compared. The final data are represented as means with its correspondent standard deviation (SD).

3.3. Results

3.3.1. Getting ready for protein-lipid interactions

In the last decades, different techniques have used non-natural lipid analogues to study protein-lipid interactions. As result, a non-desired lipid behaviour was obtained where the native membrane environment was artificially modified or even disrupted and whose experimental conditions were *in vitro* (Contreras et al., 2011; Peng et al., 2014; Zhao & Lappalainen, 2012), therefore, in many cases the resulting protein-lipid interactions may not constitute real interactions. Nowadays, specific lipid-protein interaction studies became feasible due to the existence of bifunctional lipids (Haberkant & Holthuis, 2014; Peng et al., 2014), which contain a photoactivatable group and a radiolabelled lipid tag.

3.3.1.1. [3H]-photo-cholesterol experimental conditions

The study of the interaction between Gag/MA and cholesterol relies on the use of radioactively labelled photoactivatable cholesterol, [^{3}H]-photo-cholesterol. First of all, experimental parameters for incorporation time and metabolism of [^{3}H]-photo-chol were performed, and afterwards, since the biggest amount of lipid incorporation is desired, the effect that the use of delipidated serum in the medium could have in its incorporation into cells and virions need to be elucidated.

First, the effect that the presence of other lipids in the medium could have in the incorporation of [^{3}H]-photo-chol was measured by adding this lipid diluted in medium containing either lipidated (normal) or delipidated FBS. The incorporation and metabolism of [^{3}H]-photo-chol was analysed by adding the bifunctional probe to HEK

293T cells and incubated for 5 min, 1 h, 6 h and 24 h in both lipidated and delipidated media (Figure 3.6).

HEK 293T cells seeded into a 35 mm dish were incubated with 2 μCi/mL of [³H]-photo-chol diluted in cell culture medium supplemented with either lipidated or delipidated FBS, and after 5 min, 1 h, 6 h, and 24 h the medium was removed. HEK 293T cells were collected after washing with PBS and an aliquot was used to measure the radioactive signal of each sample by a liquid scintillation counter. The radioactive measurement in the cells at each period of time was compared to the total radioactive signal added at the beginning to calculate the percentage of incorporated [³H]-photo-chol in both culture media. As shown in Figure 3.6 A, when the cell culture is supplemented with delipidated FBS, the maximum incorporation of the bifunctional probe is > 40% and it is reached after 24 h of incubation. In comparison, the uptake observed when the [³H]-photo-chol is incubated in lipidated medium is around 20% at the same period of time, pointing that **the absence of other competing lipids in the medium containing delipidated FBS increases cellular incorporation of [³H]-photo-cholesterol.**
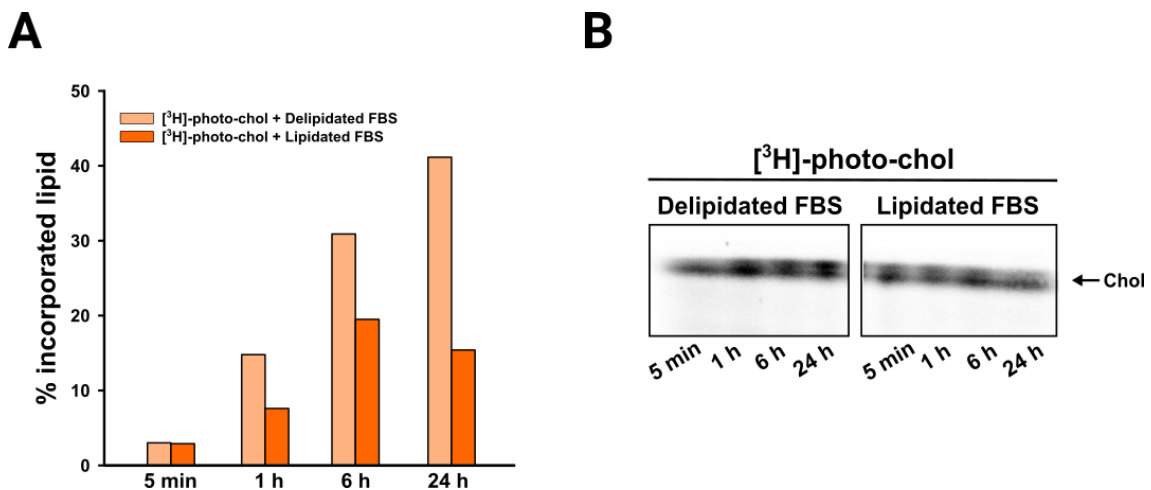
Figure. 3.6. [³H]-photo-cholesterol incorporation and metabolism. A) Percentage of incorporated [³H]-photo-chol into HEK 293T cells after different incubation times. The bifunctional lipid was added in medium containing lipidated or delipidated FBS. **B)** Autoradiography of a thin layer chromatography (TLC) of 0,02 μCi [³H]-photo-chol extracted from HEK 293T cells after different incubation times and added in medium containing lipidated or delipidated FBS.

The lipid metabolism was also studied in the delipidated medium condition to analyse the effect of the delipidated media in [³H]-photo-chol metabolization. Cells were fed for different periods of time, and the lipids from the cells were extracted and loaded into a TLC for each time point. The radioactive signal from the [³H]-photo-chol was observed by autoradiography. Figure 3.6 B shows that **[³H]-photo-cholesterol is preserved in both lipidated and delipidated media, without signals of degradation of metabolization into any derivative**.

Once delipidated FBS usage was proven, the next step was to test if the use of delipidated FBS had an effect in viral processing and production. For this purpose, HEK 293T cells were transfected with a proviral plasmid and, 24 h post-transfection, incubated with lipidated or delipidated medium for an additional 24 h. Then, the culture medium supernatant was collected, and viral particles were first clarified and then purified, and the virus production yield was measured by an α-CA Western blot (Figure 3.7 A). The effect of delipidated FBS media in the viral processing and produced viral amount was examined by silver staining and Western blot (Figure 3.7 B).
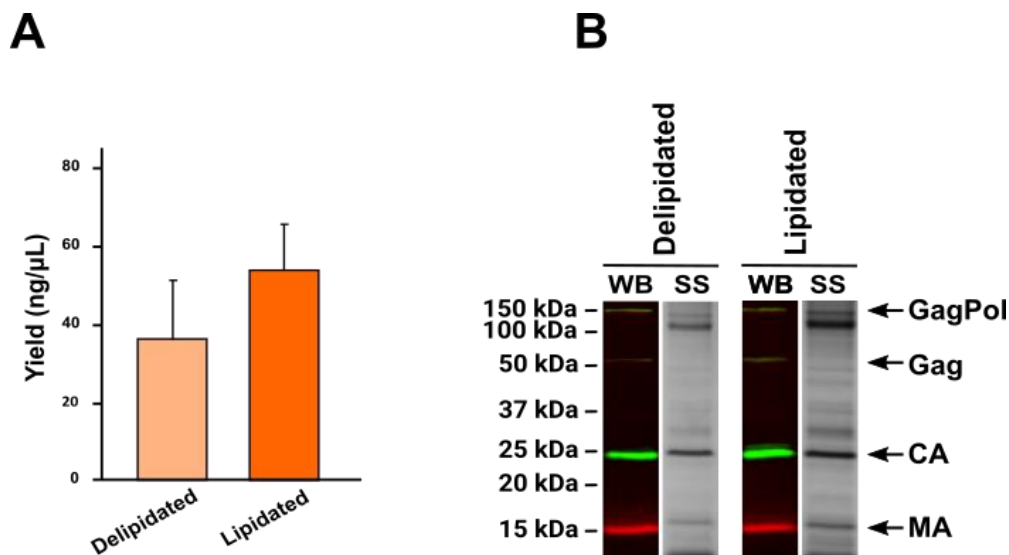
Figure 3.7. Effect of delipidated FBS medium in viral yield and processing. A) The production yield measured with a α-CA Western blot of the resuspended purified viral particles obtained from cells incubated with lipidated or delipidated FBS containing medium. The bars represent the mean ± SD of three independent experiments. **B)** Western blot (WB) and silver stain (SS) of concentrated viral particles obtained from cells incubated with delipidated or delipidated medium. The Western blot was developed with sheep α-CA and α-sheep IRDye800 antibodies (green) and rabbit α-MA and α-rabbit IRDye680 antibodies (red).

Figure 3.7 A shows that delipidated FBS containing medium caused an appreciable decrease in viral yield in comparison to lipidated medium, although the differences between both were not statistically significative. Moreover, no effect was observed in the silver stain in the viral processing and protein pattern of concentrated viral particles when using medium supplemented with delipidated FBS compared to the traditional lipidated medium. In addition, both media presented concentrated viral particles with the expected CA and MA signals in the Western blot (Figure 3.7 B). All together these results indicate that **the use of delipidated FBS containing medium, which significantly increases [³H]-photo-cholesterol uptake by the cells, has no significant effects on viral production, and protein processing.**

Therefore, in the posterior interaction experiments [³H]-photo-chol was added to HEK 293T cells in delipidated FBS containing culture media for 24 h due the fact that the maximum viral production and incorporation of the bifunctional lipid was observed at this point.

3.3.1.2. Proof of concept of [³H]-photo-chol-protein interaction

Bifunctional lipids have the inconvenience that they are not commercially available, so they have to be synthetized. Additionally, its detection requires very long exposition times using X-ray films, or a specific machine such as the BetaIMAGER™. However, these lipid analogues are easy to handle, and their experimental use could give outstanding information about tight interactions between specific lipids and proteins.

When [³H]-photo-chol is irradiated with UV light, it covalently binds to any molecule closer than 3 Å (Haberkant et al., 2008; Nieto-Garai et al., 2021; Thiele et al., 2000). If this lipid is interacting with a protein and covalently binds to it, when this protein is immunoprecipitated from a cellular or viral sample, the covalently bound [³H]-photo-chol will precipitate together with this protein. Hence, the study of the interaction between any protein and [³H]-photo-cholesterol would be based in the comparison of the Western blot signal of the immunoprecipitated protein and the

radioactive signal of this bifunctional lipid in the same Western blot membrane obtained by an autoradiography. Co-localization of both lipid and protein signals in the membrane demonstrate the existence of an unequivocal interaction between [³H]-photo-chol and said protein.

Well-known cholesterol-interacting and non-interacting protein markers were used as proof of concept for the study of protein interaction with [³H]-photo-cholesterol. As control of positive interaction with cholesterol, the Caveolin-1 (Cav-1) protein was selected. Cav-1 is commonly found in chol-enriched domains and have been canonically considered as marker of lipid rafts in the membrane, therefore, its interaction with chol has long been accepted (Brown & London, 1998; S. Li et al., 1996; Smart et al., 1999). Accordingly, Cav-1 was later demonstrated to specifically interact with chol using the same crosslinking [³H]-photo-chol of this thesis (Haberkant et al., 2008), so it constitutes an adequate positive control for interaction of proteins with [³H]-photo-cholesterol. As a negative control, the Transferrin Receptor (TfR) protein was chosen, as it constitutes the archetypal non-lipid raft marker (Magee & Parmryd, 2003), and, thus, it is not expected to specifically interact with chol and, however, it would interact with PC.

In the case of Cav-1, HEK 293T cells transfected with Cav-1-GFP were incubated with [³H]-photo-chol for 6 h in delipidated medium. Shorter incubation times than in the experiments with proviral constructs were used, as for viral production long incubation times (24 h) are needed, since viral production peak occurs approximately 17 h after transfection. After lipid incubation, the cells were washed with PBS, irradiated with UV light to induce lipid photo-crosslinking, and cells were scraped and lysed. The sample was immunoprecipitated against GFP to isolate the Cav-1-GFP protein, and subjected to Western blot against Cav-1, and posteriorly an autoradiography of the same membrane was carried out (Figure 3.8 A). The same process was followed using [H³]-photo-sphingosine in order to study the interaction between Cav-1 and sphingolipids. Once [H³]-photo-SP is incorporated in the cell, it is metabolized into different SLPs (Figure 3.8 B). Concerning TfR, interaction with chol and PC was studied following the same protocol, although in this case endogenous TfR was used (Figure 3.8 C). For both, the Cav-1-GFP and the TfR, the Western blot and autoradiography images were compared

to determine if any radioactive lipid band corresponded with the protein bands obtained in the Western blot.
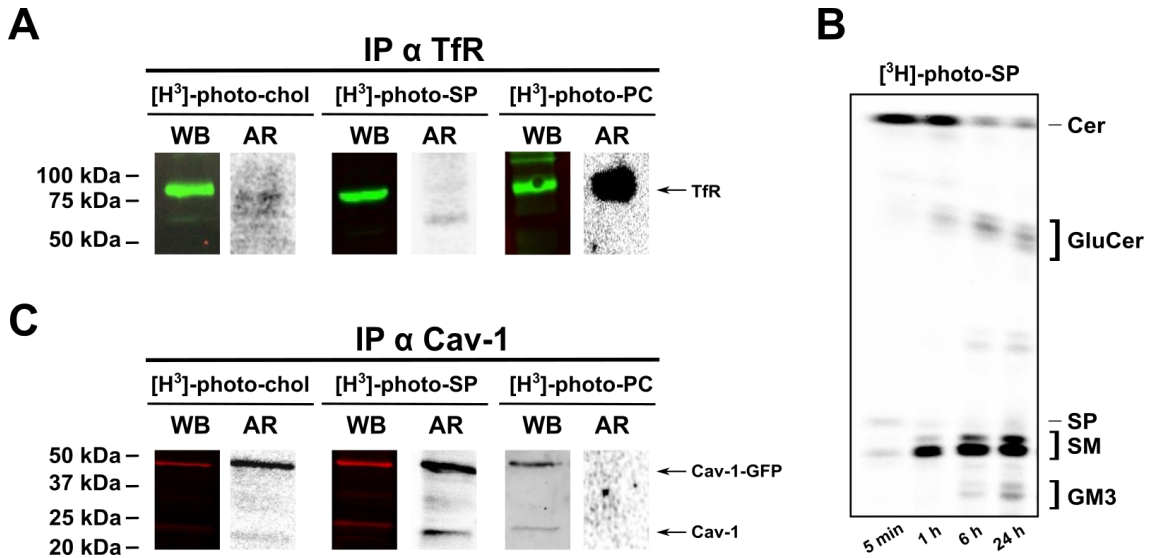
Figure 3.8. Protein-lipid interactions of bifunctional lipid makers. A,C) *In vivo* photoaffinity labelling of TfR and Cav-1 using tritiated and photolabile lipid probes: [H³]-photo-cholesterol ([H³]-photo-chol), [H³]-photo-sphingosine ([H³]-photo-SP), [H³]-photo-phosphatidylcholine ([H³]-photo-PC). HEK 293T cells transiently expressing Cav-1-GFP (**C**) or without transfection (**A**) were treated with 100 mCi (3 mM) [H³]-photo-chol, 60 mCi (2 mM) [H³]-photo-SP or 50 mCi [³H]-photo-SP combined with 10-azi-stearic acid (10-ASA) (100 mM). Then, cells were UV-irradiated, lysed and endogenous TfR protein (**A**) or Cav-1-GFP protein (**C**) were subjected to immunoprecipitation against the TfR protein (**A**) or GFP tag (**C**), respectively. Input and immunoprecipitated (IP) samples were analysed by Western blot (WB) and autoradiography (AR). The Western blot was developed with a mouse α-TfR primary antibody and α-mouse IRDye800 secondary antibody (green) in the case of TfR, and with a rabbit α-Cav-1 primary antibody and α-rabbit IRDye680 secondary antibody (red) in the case of Cav-1. **B)** Representative image of an autoradiography of a thin layer chromatography of the metabolization of 0,02 µCi of [³H]-photo-SP in HEK 293T cells after different incubation times.

As observed in Figure 3.8 A, a clear band corresponding to [³H]-photo-chol and [³H]-photo-sphingolipids can be observed in the autoradiography, co-localizing with the immunoprecipitated Cav-1-GFP protein band observed in the Western blot, and with a lower size band corresponding with Cav-1, which co-immunoprecipitated with Cav-1-GFP in stable formed caveolae. In comparison, in Figure 3.8 C no band corresponding to [³H]-photo-chol is observed in the autoradiography at the position of the TfR band in the Western blot whereas a positive result was obtained for PC.

Therefore, above-mentioned results corroborate that the radioactively labelled lipid can easily be detected by autoradiography and compared with the protein bands observed by Western blot, confirming that **[³H]-photo-cholesterol covalently binds to proteins that are known to interact with cholesterol and proving its use as a powerful tool for the study of specific protein-chol interactions.**

One of the concerns with [³H]-photo-cholesterol is the idea that any protein can interact with chol by chance, due to the high amount of this lipid in the cell membrane. Nevertheless, the results above demonstrate that TfR does not interact with chol, whereas it interacts with PC (Figure 3.8 A), a lipid also present in high quantity within the cell membrane. Additionally, Cav-1 interacts with chol but not with PC (Figure 3.8 C). Even more, previous results of our research group using the photoactivatable and radioactively labelled cholesterol have demonstrated that HIV-1 surface fusion protein Env, specifically interacts with chol through its gp41 cytoplasmic tail (Figure 3.9) (Nieto-Garai et al., 2021). In case of viral particles, [³H]-photo-chol constitutes 0.13% (%mol) of the total lipid molecules, meaning that although viral particles contain up to 50% of cholesterol, **the interaction with [³H]-photo-cholesterol does not occur by chance**.
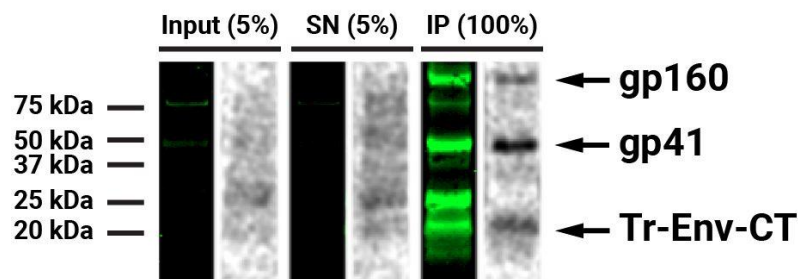
Figure 3.9. Representative image of gp41-chol interaction in purified viral particles. Immunoprecipitated gp41 Western blot (green) and crosslinked [³H]-photo-chol autoradiography (grey). The Western blot was developed with Chessie-8 α-gp41 primary antibody, and α-mouse IRDye800 secondary antibody. The [³H]-photo-chol radioactive signal was detected by autoradiography of the same membrane. SN = non-immunoprecipitated supernatant; IP = immunoprecipitated sample, Tr-Env-CT = truncated cytoplasmic domain of gp41 consisting of the last 139 aminoacidic residues of the protein.

Further, gp41 CT has been described to be palmitoylated on two different cysteines, Cys-764 and Cys-837. The Cys-764 is located immediately upstream of LLP2, while Cys-837 is in LLP1. Palmitoylation of those cysteines has been suggested to drive

Env targeting to DRMs, and consequently, to lipid rafts (Bhattacharya et al., 2004; Rousso et al., 2000; Syu et al., 1991; C. Yang et al., 1995).

The ΔCT_{750} gp41 mutant, which consists in a truncated variant lacking the C-terminal 104 amino-acid residues including all three LLP sequences and 14 residues upstream due to a stop codon at residue 751, has been shown not to interact with cholesterol (Nieto-Garai et al., 2021). This variant lacks the aforementioned C762 cysteine described to be palmitoylated. Hence, to decipher if the loss of interaction derived from the truncation of the $CT_{751-854}$ region is caused by the lack of this palmitoylated C726 cysteine, a new pCHIV variant containing a substitution of the palmitoylated cysteine residue by a serine in position 762 (C762S) was constructed. This mutant was used to study the impact of palmitoylation in the gp41-chol interaction. For this purpose, HEK 293T cells were transfected with C762S mutant, incubated with [^{3}H]-photo-chol during 24 h, irradiated with UV light to induce lipid crosslinking and purified viral particles were obtained as explained in Section 3.2.2.2.
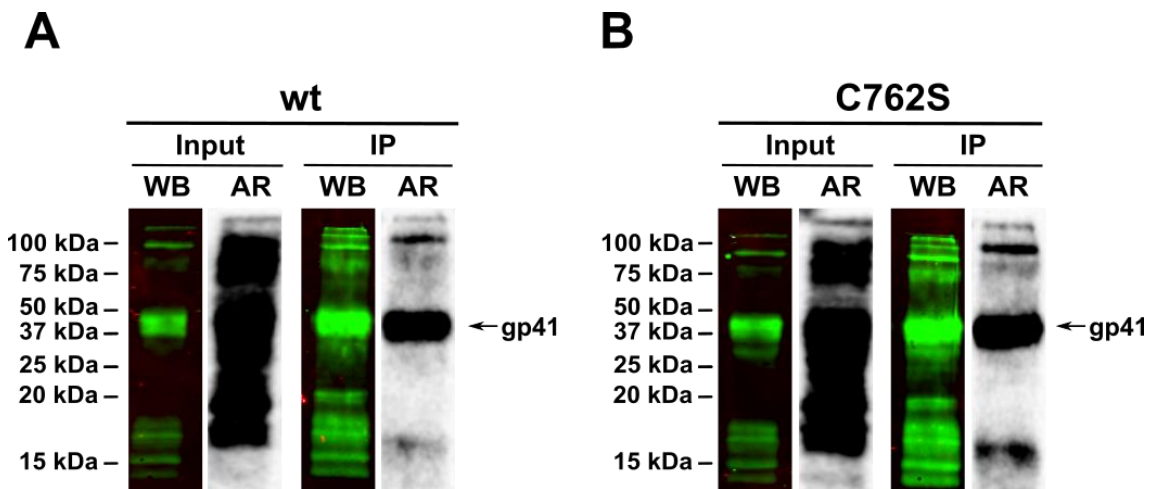
Figure 3.10. Effect of gp41 palmitoylation on gp41–chol interaction in purified viral particles. Input (5% of lysed viral particles) and immunoprecipitated (IP) gp41 from wild type (wt) and mutant (C762S) purified viral particles were detected by Western blot (WB) analysis (green), and its interaction with [^{3}H]-photo-chol by autoradiography (AR) of the same membrane (grey). The Western blot was developed with Chessie-8 α-gp41 primary antibody, and α-mouse IRDye800 secondary antibody.

Representative results in Figure 3.10 show that C762S variant interacted with chol at a level equivalent to that observed for the wild type gp41 protein when comparing both signals of the Western blot and the autoradiography. This demonstrates that **palmitoylation of gp41 at the C762 residue is not required for the interaction with cholesterol**. Therefore, a post-translational modification such as palmitoylation does not interfered with Env-cholesterol interaction.

All in all, **aforesaid interaction experiments between Env and [³H]-photo-cholesterol together with the well-stablished experimental parameters constitute the starting point for the study of the Gag/MA-cholesterol interaction**.

3.3.2. Studying the possible Gag dependency of Env-cholesterol interaction

Considering that Env interacts with cholesterol in HEK 293T cells as it was previously confirmed in Nieto-Garai et al. (2021) and taking into account that MA structure accommodates Env CT so it attracts Env to cell membrane regions where Gag forms a rigid lattice and buds (Hogue et al., 2012; Tedbury & Freed, 2014; Tedbury et al., 2019), the following step was to determine if Env needs the help of other viral proteins to perform its interaction with cholesterol.

Gag protein has long been suggested to be implicated in Env incorporation to the budding sites based on the proposed interaction between MA and the cytoplasmic tail of the gp41 subunit of Env (Alfadhli et al., 2016, 2019; Brandano & Stevenson, 2011; Bulgelski et al., 1995; Checkley et al., 2011; Davis et al., 2006; Dorfman et al., 1994; Eastep et al., 2021; Freed & Martin, 1995; Groves et al., 2020; Murakami & Freed, 2000; Muranyi et al., 2013; Murphy & Saad, 2020; Patil et al., 2010; Pezeshkian et al., 2019; Tedbury & Freed, 2014; Tedbury et al., 2013, 2015, 2016, 2019; Wyma et al., 2000; Yu et al., 1992). Although no definitive mechanism for Env targeting to Gag assembly and viral budding sites have been described, one of the proposed mechanism postulates that Env localization in budding sites and posterior incorporation into the virion depends on Env CT (direct or indirect) interactions with the underlying Gag/MA lattice (Buttler et al., 2018; Checkley et al., 2011; Ghanam et al., 2012; Groppelli et al., 2014; Muranyi et al., 2013; Pezeshkian et al., 2019; Qu et al., 2021; Tedbury & Freed, 2014).

Therefore, according to the literature, protein-protein interactions between gp41 and Gag/MA should be taking place along HIV-1 morphogenesis. This could lead to the hypothesis that a possible co-immunoprecipitation between Gag and Env could be happening. To prove this purpose, HEK 293T cells were transfected with a proviral plasmid and after 48 h, concentrated viral particles were obtained as explained in Section 2.5.2. 1 μg of CA of concentrated viral particles was used to immunoprecipitated Gag/MA following Section 3.2.2.3 (Figure 3.11 A). Then, the supernatant from this IP was used to perform another immunoprecipitation, in this case against gp41 with Chessie-8 coupled to Protein G Sepharose beads as in Section 2.4.3 (Figure 3.11 B).
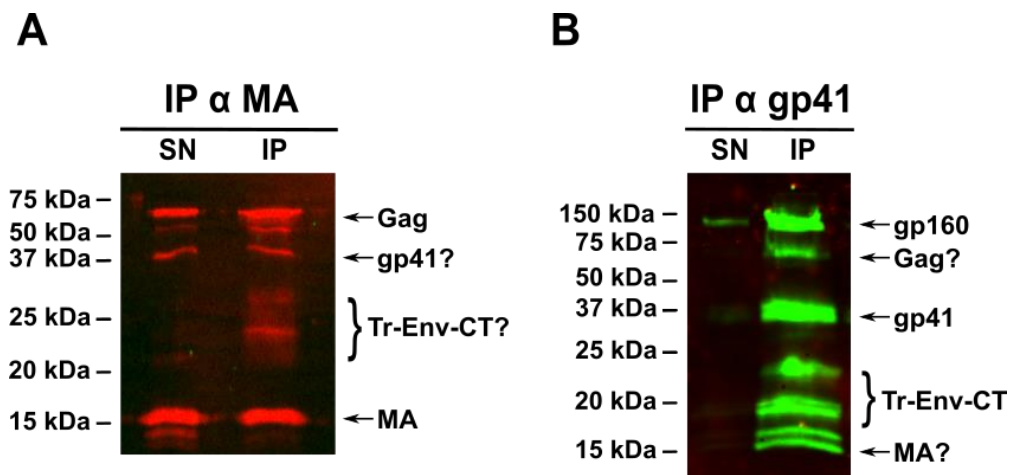
Figure 3.11. Immunoprecipitation assay of Env from the SN of Gag/MA IP. A) 10% of the supernatant (SN) and immunoprecipitate (IP) against MA from concentrated viral particles were detected by Western blot developed with rabbit α-MA primary antibody and α-rabbit IRDye680 secondary antibody (red) to detect Gag/MA. **B**) 10% of the supernatant (SN) of the previous IP α MA in **A** and immunoprecipitate (IP) against gp41 from the SN of IP α MA in **A** were visualized by Western blot with Chessie-8 α-gp41 as primary antibody and α-mouse IRDye800 secondary antibody (green) to detect gp41.

Figure 3.11 A shows the expected bands of Gag and MA of 15 kDa and 50 kDa, respectively. Apart from that, two bands could potentially correspond to MA proteins interacting with Tr-Env-CT and gp41, around 20-25 kDa and ~40 kDa, respectively. After gp41 immunoprecipitation from the SN of previously IP of MA, clear bands corresponding to Tr-Env-CT, gp41 and gp160 could be detected (Figure 3.11 B), moreover, two bands around ~15 kDa and ~50 kDa were obtained, which are the similar

molecular weight of MA and Gag, respectively. Thus, these two bands could potentially correspond to the interaction of CT of gp41 with MA/Gag.

Another manner to assess the hypothesis of co-immunoprecipitation between Gag and Env was the following. On the one hand, the initial amount of 1 μg of CA of concentrated viral particles was utilized to immunoprecipitated gp41 with Chessie-8 coupled to beads (Figure 3.12 A). On the other hand, another 1 μg of CA was used to immunoprecipitated Gag/MA as before (Figure 3.12 B).
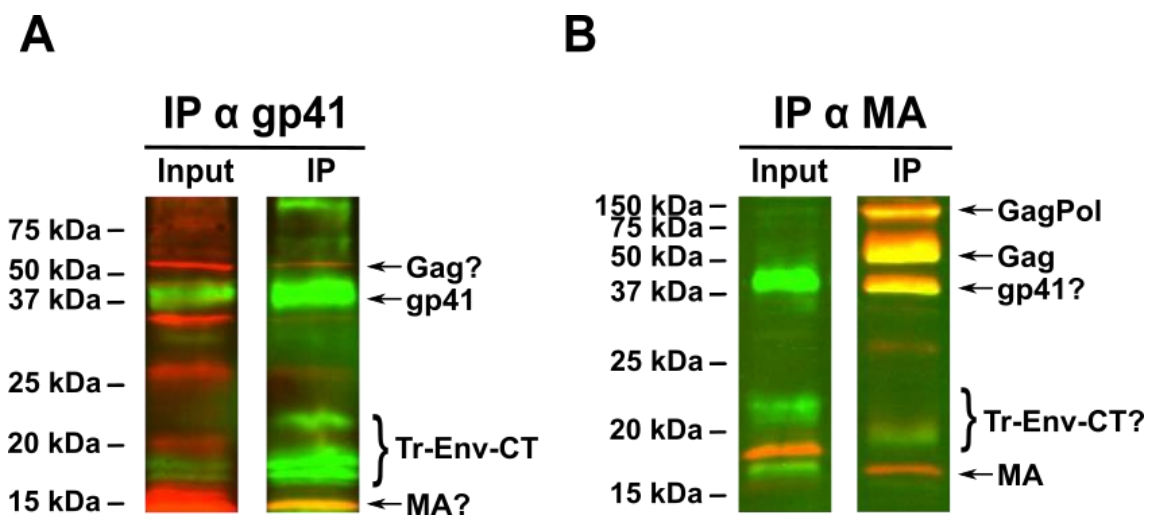
Figure 3.12. Co-immunoprecipitation assays of Env and Gag/MA. Input (10% of lysed viral particles) and immunoprecipitated (IP) gp41 (**A**) or Gag/MA (**B**) from concentrated viral particles were detected by Western blot. Both Western blots were developed with Chessie-8 α-gp41 primary antibody and α-mouse IRDye800 secondary antibody (green) to detect gp41, as well as with rabbit α-MA primary antibody and α-rabbit IRDye680 secondary antibody (red) to detect Gag/MA.

In Figure 3.12 A, apart from the expected bands of gp41 and Tr-Env-CT after gp41 immunoprecipitation, another two bands could be seen around 15 kDa and 50 kDa, respectively, potentially corresponding to MA and Gag proteins. Additionally, it is seemed a co-localization between MA and gp41 signals at the 15 kDa protein band. In Figure 3.12 B, after Gag/MA immunoprecipitation a band of ~40 kDa potentially corresponding with gp41 was detected, which also co-localize with MA signal. Indeed, expected bands for MA, Gag and GagPol also appeared in the Western blot, potentially these Gag and GagPol bands co-localize as well with gp41 signal.

All those results together confirmed a real co-localization of gp41 and Gag/MA in HIV-1 viral particles. This supports the idea of Gag/MA and Env relationship during HIV-1 morphogenesis and could indicate that the presence of Gag/MA plays a role in the interaction of Env with membrane lipids, such as cholesterol.

Therefore, the next step is to study a possible effect of Env-/Gag/MA in cholesterol interaction with Env. To assess this purpose, gp41-cholesterol interaction was performed in two different contexts: cells were transfected with an Env expressing plasmid or with a proviral plasmid. The first one only expresses the Env protein and the second one expresses all the proteins capable of forming non-infectious VLPs. Thus, HEK 293T cells were transfected with either the proviral plasmid pCHIV, or the Env expressing plasmid pCAGGs.NL4-3. Then, cells were incubated with [³H]-photo-cholesterol for 8h, irradiated with UV light to induce lipid crosslinking, washed, lysed, and gp41 was immunoprecipitated.

Figure 3.13. gp41 interaction with cholesterol in HEK 293T cells in a proviral context and in an only Env expressing context. Representative images of the immunoprecipitated gp41 Western blot (green) and cross-linked [³H]-photo-cholesterol derivative autoradiography (grey) signals obtained from HEK 293T cells transfected with a proviral plasmid containing all viral proteins (pCHIV), or an Env only expressing plasmid (pCAGGs), and treated with [³H]-photo-cholesterol for 8 h. The Western blot was developed with Chessie-8 α-gp41 primary antibody, and α-mouse IRDye800 secondary antibody. The [³H]-photo-cholesterol radioactive signal was detected by autoradiography of the same membrane.

The results shown in Figure 3.13 indicate that gp41 interacts with cholesterol at a cellular level, as radioactive signals can be observed in the autoradiography in the

immunoprecipitated sample corresponding to the protein bands observed in the Western blot. Bands corresponding to unprocessed gp160 can also be observed both in the Western blot and autoradiography. The interaction of gp41 with the lipids is observed in a proviral context when all other viral proteins, including Gag, are expressed in the cell. Furthermore, this interaction is also seen when the HIV-1 Env protein is expressed alone, indicating that **the capability of interaction with cholesterol of the gp41 protein does not require the presence of other viral proteins or interactions, and, thus, might have an inherent property for cholesterol interaction.**

3.3.3. Gag-cholesterol interaction in cells

Previous results in cells proved that the interaction of Env with cholesterol is independent of the presence of Gag. However, being Gag the most outstanding protein during morphogenesis of the HIV-1, it could be plausible that an existence of a direct interaction between Gag and cholesterol could be taking place. In the literature, there are multiple results of Gag interacting with DRMs or indirectly interacting with cholesterol (Bhattacharya et al., 2006; Dick & Vogt, 2014; Dick et al., 2012; Ding et al, 2003; Doktorova et al., 2017; Favard et al., 2019; Halwani et al., 2003; Holm et al., 2003; Lindwasser & Resh, 2001; Lalonde & Sundquist, 2012; Nguyen & Hildreth, 2000; Ono & Freed, 2001; Patil et al., 2010; Thiele et al., 2000; Yandrapalli et al., 2016), however the only direct interaction described is with $PI[(4,5)P_2$ (Chukkapalli et al., 2008; Mücksch et al., 2017; Ono et al., 2004), even though both lipids become almost immobile within the viral particle. Here, the interaction between Gag and cholesterol is determined at a cellular level.

HEK 293T cells were transfected with the proviral plasmid pCHIV. Then, they were incubated with $[^3H]$-photo-cholesterol during 24 h, irradiated with UV light to induce lipid crosslinking, washed and lysed. The immunoprecipitation was carried out as explained in Section 3.2.2.3.
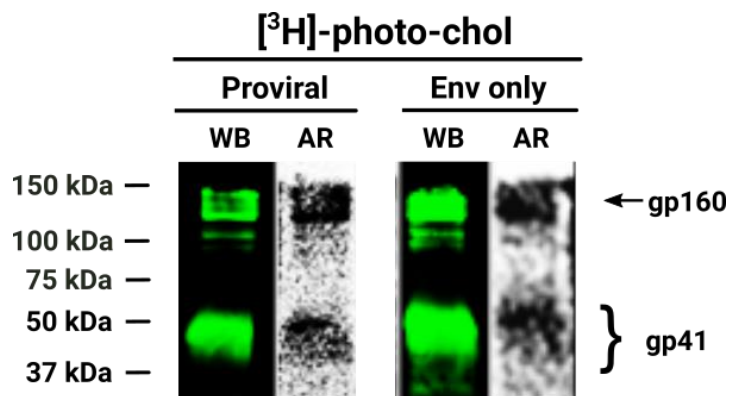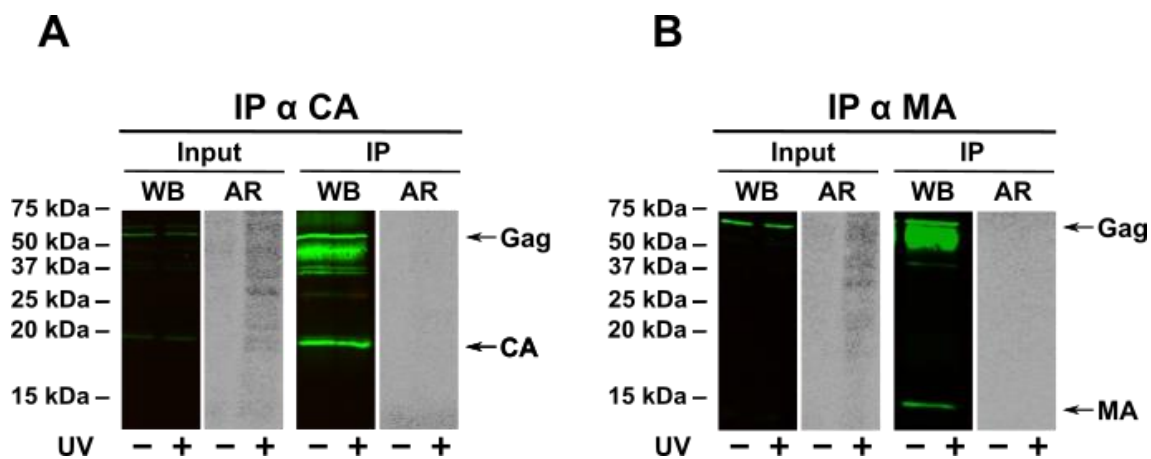
Figure 3.14. Gag/MA interaction with cholesterol in HEK 293T cells. Immunoprecipitated CA (**A**) and MA (**B**) Western blots (green) and cross-linked [^{3}H]-photo-cholesterol derivative autoradiography (grey) signals obtained from HEK 293T cells transfected with a proviral plasmid (pCHIV) and treated with [^{3}H]-photo-cholesterol for 24 h and irradiated with ultraviolet (UV +) to induce the photo-crosslinking. The Western blot was developed with rabbit α-CA (**A**) and α-MA (**B**) primary antibodies, respectively, and α-rabbit IRDye800 secondary antibody for both. The [^{3}H]-photo-cholesterol radioactive signal was detected by autoradiography of the same membrane.

The results shown in Figure 3.14 indicate that neither Gag nor MA seem to interact with cholesterol at a cellular level, as no radioactive signals can be observed in the autoradiography that correspond to the protein bands observed in the Western blot. However, this lack of signal could be explained by the tendency of Gag to form soluble polysomes in the cytosol (Scarlata & Carter, 2003). Gag assembly starts at the cytosol, where Gag is first synthesized on free polysomes binding viral RNA through HBR regions (Alfadhli et al., 2009; Chukkapalli et al., 2010, 2013; Cimarelli & Luban, 1999; Lochrie et al., 1997; Purohit et al., 2001; Shkriabai et al., 2006), therefore, the majority of Gag in the cell could be forming part of free polysomes instead of being anchored to the cell membrane where it could interact with cholesterol during the morphogenesis. Studying Gag/MA-cholesterol interaction at a viral level would avoid the polysome-forming problem. So, the next obvious step would be testing Gag/MA-cholesterol interaction in viral particles.

Another possibility to keep studying Gag/MA-cholesterol interaction at a cellular level would have been labelling Gag protein with a green fluorescent protein tag, however, this procedure introduces a structural modification in the protein, which

affects particle formation. It has been observed that GFP spots did not correspond to membrane associated buds or HIV-1 VLPs visible by electron microscopy (Bednarska et al., 2020), so GFP attached to Gag is affecting viral particle assembly, the main reason why the use of this methodology was totally discarded.

3.3.4. Gag/MA-cholesterol interaction in viral particles

The direct interaction between Gag/MA and cholesterol is studied at viral level to face the problem of Gag polysomes in cells. HIV-1 viral particles contain lower amounts of Gag polyprotein in comparison to producer cells since the protease cleaves it into its major subunits MA, CA, NC and p6. However, the quantity of Gag in the virions could be increased by using a protease defective mutant or by adding protease inhibitors.

3.3.4.1. Gag/MA-cholesterol direct interaction in virions

After each viral purification obtained as explained in Section 3.2.2.2, the resulting virions are characterized by silver stain and quantified by α-CA Western blot (Section 2.2.6). A representative characterization of purified viral particles by silver stain is shown in Figure 3.15.
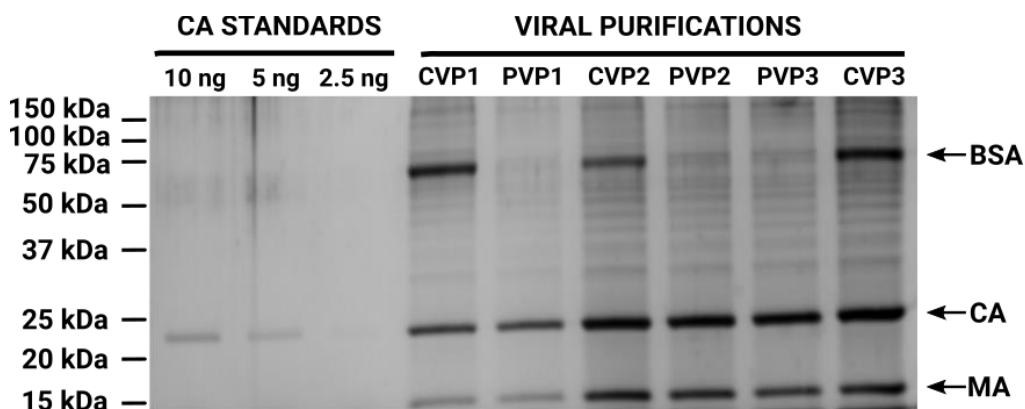
Figure 3.15. Silver stain of concentrated and purified viral particles. CVP = concentrated viral particle; PVP = purified viral particle. CA standards of 10, 5 and 2.5 ng were loaded as pattern control. The silver stain corresponds to three independent viral purifications, showing CVP and PVP for each purification.

As expected, virions obtained from the three independent viral purifications possess a correct viral pattern (Figure 3.15). Each purification shows protein bands around ~15 kDa and ~25 kDa, which correspond to MA and CA proteins, respectively. Concentrated viral particles also show a protein band between 50-75 kDa that corresponds to bovine serum albumin (BSA) (66.5 kDa) from the cell culture medium. After OptiPrep gradient purification, BSA contamination disappears. The gp41 band at ~41 kDa is not present in the silver stain because it is to faint to be clearly observed, due to the low copy of Env protein trimers present in each viral particle (only around 7-10 trimers per virion) (Chertova et al., 2002).

In Figure 3.16, a representative result of the yield of the viral particle purification by a quantitative Western blot analysis probed against CA is shown.
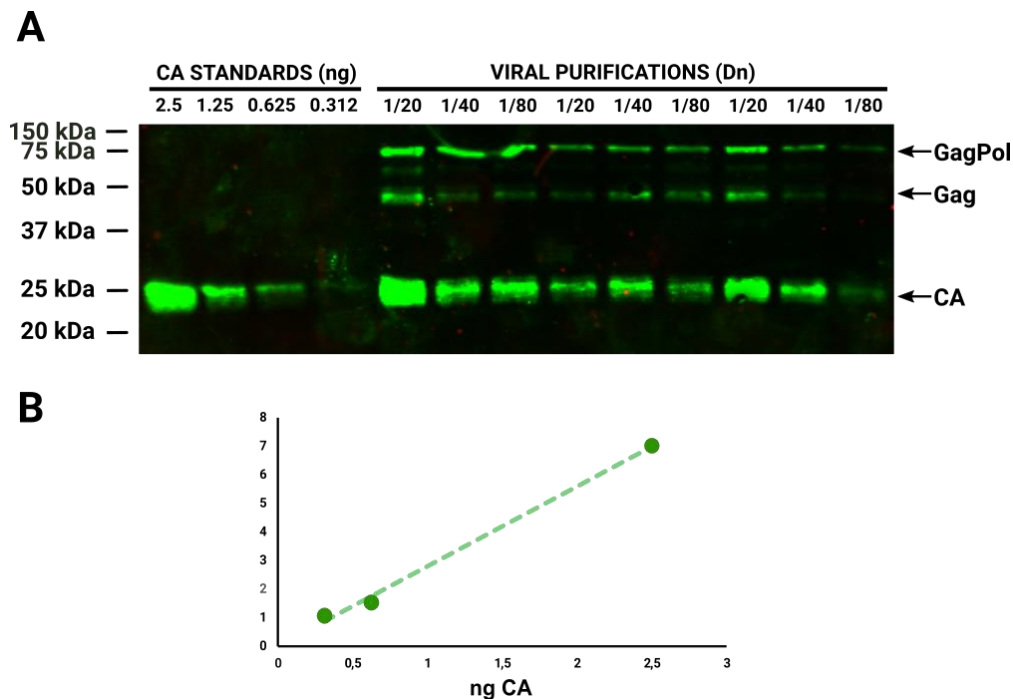
Figure 3.16. CA quantification by Western blot of purified viral samples. A) 2.5, 1.25, 0.625 and 0.312 ng of CA protein is loaded as a standard to generate a calibration curve. In the same Western blot, 1/20, 1/40 and 1/80 dilutions of the viral sample are loaded. The dilutions are made for the three independent viral purifications. The Western blot is developed against CA using sheep α-CA as a primary antibody, and α-sheep IRDye800 as a secondary antibody. **B)** The integrated intensity of the samples in A is measured in the LI-COR Odyssey imaging system. The values of the CA standards are used to build a calibration curve, from which a regression curve is extracted to calculate the amount of CA in the viral sample dilutions.

The amount of CA for each viral purification after Western blot quantification was ~2-5 µg of CA. The possible interaction between Gag/MA was tested using the corresponding volume of viral sample that is equivalent to 1 µg of CA. Non-immunoprecipitated CVP and PVP virions were loaded into a SDS-PAGE and a Western blot against Gag/MA was developed with rabbit α-MA primary antibody, and α-rabbit IRDye800 secondary antibody. The [^{3}H]-photo-cholesterol covalently bound to the protein in the Western blot membrane was then detected by autoradiography.

A representative result of the Gag/MA-cholesterol interaction in viral particles is shown in Figure 3.17.
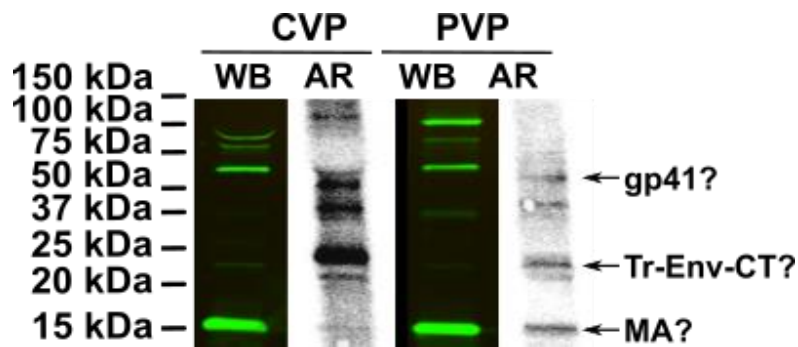
Figure 3.17. Gag/MA-cholesterol interaction in purified viral particles (CVP and PVP). Representative image of the non-immunoprecipitated Gag/MA Western blot (green) and crosslinked [^{3}H]-photo-cholesterol autoradiography (grey) signals. The Western blot was developed with rabbit α-MA primary antibody, and α-rabbit IRDye800 secondary antibody. The [^{3}H]-photo-cholesterol radioactive signal was detected by autoradiography of the same membrane.

Initially, 100 µCi (0.5 µM) of [^{3}]-photo-chol was added to the cell culture, and in the ultrapure particles was detected 0.223 µCi/30 µl (0.26 µM). Since CA quantification yielded a concentration of 60 µg/mL, which corresponds to a 150 µM lipid concentration, the ratio between radioactively labelled cholesterol and its natural counterpart is 1:577, or 0.17% (mol:mol).

Even though there are more than one band present in the autoradiography for both CVP and PVP, there is only a coincidence between a band in the Western blot and in the autoradiography at ~15 kDa in both purified viral samples. This molecular weight corresponds to MA protein; therefore, **an interaction between MA and [^{3}H]-photo-**

cholesterol could be taking place. To verify this interaction, the same experiment is carried with immunoprecipitated viral samples against Gag/MA.
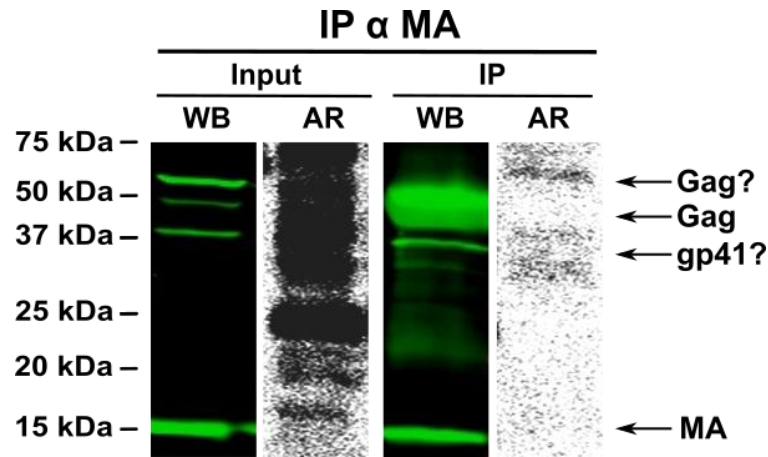
Figure 3.18. Gag/MA-cholesterol interaction in purified viral particles. Representative image of the immunoprecipitated Gag/MA Western blot (green) and cross-linked [3H]-photo-cholesterol autoradiography (grey) signals. The Western blot was developed with rabbit α-MA primary antibody, and α-rabbit IRDye800 secondary antibody. The [3H]-photo-cholesterol radioactive signal was detected by autoradiography of the same membrane.

For this experiment, 9 μg of CA was used, corresponding to 250 μM of the total lipids. In the ultrapure particles, a radioactively labelled lipid concentration of 1.96 μCi/90 μL (0.82 μM) was detected, which represents a 1:330 ratio of [3H]-photo-chol, or 0.33% precisely. In the Western blot (Figure 3.18), a band corresponding to MA with an apparent size of ~15 kDa can be clearly observed in the immunoprecipitated sample, together with a band of ~56 kDa that corresponds to Gag. However, in the autoradiography there is no band at the same size of the aforesaid bands of MA and Gag proteins which means that **there seems not to be a direct interaction between MA and [3H]-photo-cholesterol taking place at a viral level.** Nevertheless, a broad band appears around 40 kDa, which resembles to the signal that is usually obtained for the gp41 subunit of glycosylated Env protein. Even more, the upper radioactive signal around 55 kDa could correspond to Gag binding to cholesterol, which could induce a different migration. Since the BetaIMAGER™ could be able to detect tinny amounts of radioactive lipids, a band in the autoradiography is seen while there is no signal in the Western blot

(Figure 3.18). This leads to argue that Gag interacts with Env and both proteins co-immunoprecipitated, as previously discussed in Section 3.3.2.

Thus, as in the first approach to assess Env-Gag/MA relationship in Section 3.3.2, 1 µg of CA of concentrated viral particles treated with [³H]-photo-chol was used to immunoprecipitated Gag/MA to study the interaction with cholesterol (Figure 3.19 A). Then, the supernatant from this IP was used to perform another immunoprecipitation, in this case against gp41 with Chessie-8 coupled to Protein G Sepharose beads and the interaction with [³H]-photo-chol was also studied (Figure 3.19 B).
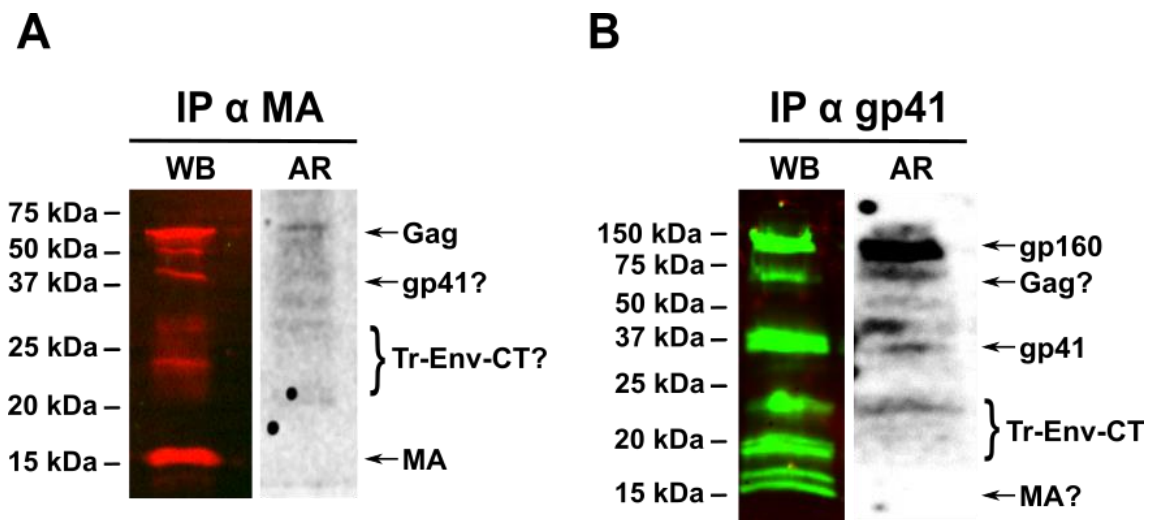
Figure 3.19. Relationship between Env-MA/Gag co-immunoprecipitation and [³H]-photo-chol interaction. A) Immunoprecipitate (IP) against MA from concentrated viral particles were detected by Western blot (WB) and autoradiography developed with rabbit α-MA primary antibody and α-rabbit IRDye680 secondary antibody (red) to detect Gag/MA. **B**) 10% of the supernatant (SN) of the previous IP α MA in **A** and immunoprecipitate (IP) against gp41 from the SN of IP α MA in **A** were visualized by Western blot with Chessie-8 α-gp41 as primary antibody and α-mouse IRDye800 secondary antibody (green) to detect gp41.

In Figure 3.19 A, bands corresponding to MA and Gag with a similar size of ~15 kDa and ~56 kDa could be clearly observed in the Western blot, together with two bands could potentially correspond to MA proteins interacting with Tr-Env-CT and gp41, around 20-25 kDa and ~40 kDa, respectively. However, there is no band in the autoradiography at the same size of the aforesaid bands of MA, gp41 and Tr-Env-CT. A thin band in the autoradiography around ~55 kDa could be detected as in the previous

Figure 3.18, which potentially means that Gag could binding to chol or Gag is interacting with Env, so both co-immunoprecipitate, and Env is interacting with chol at the same time. This final idea is supported by the results obtained in Figures 3.11 & 3.12. In Figure 3.19 B, after gp41 immunoprecipitation from the SN of previously IP of MA, clear bands corresponding to Tr-Env-CT, gp41 and gp160 (Env) could be detected, moreover, two bands around ~15 kDa and ~50 kDa were obtained, which are the similar molecular weight of MA and Gag, respectively. In the autoradiography, expected radioactive signals for gp160, gp41 and Tr-Env-CT appeared, but also a band potentially corresponding to Gag, as in Figure 3.19 A. This leads to the same hypothesis of Gag interacting with Env, which both have co-immunoprecipitated, and Env is interacting with chol as well. So, it seems that Gag/MA is not interacting with [^{3}H]-photo-chol at a viral level, but **according to co-IP results, it could be theorized that Gag is interacting with gp41, while Env is interacting with cholesterol at the same time**.

3.3.4.2. Maturation state effect in Gag-cholesterol relationship

Even though it seems that no direct interaction between MA and cholesterol exists in mature virions, a hypothesis exists that the immature Gag could interact with cholesterol. In other words, the maturation state of the virion could be affecting this interaction. Therefore, the interaction between Gag and cholesterol in immature virions should be assessed.

For this purpose, a proviral pCHIV plasmid containing a mutation in the PR was used [pCHIV PR(-)]. PR(-) mutation constitutes the substitution of an aspartic acid at position 25 for asparagine (D25N), which totally inhibits the proteolytic maturation of Gag, thus, generating viral particles sequestered in an immature state where Gag is not cleaved into its four main constituents: CA, MA, NC and p6 (Figure 3.20).
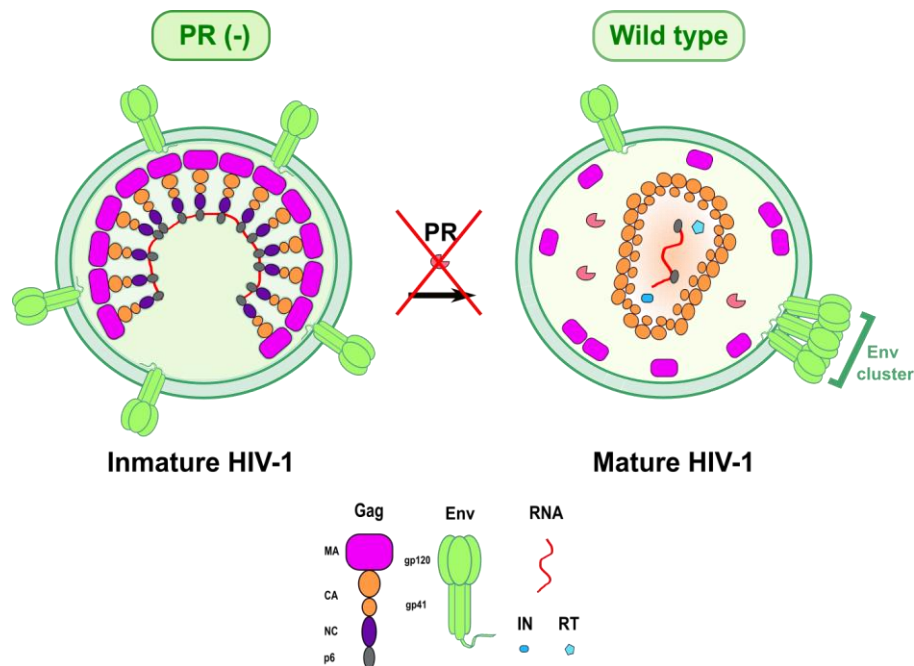
Figure 3.20. HIV-1 wild type particles versus HIV-1 PR(-) mutants. In immature HIV-1 particles obtained from PR(-) mutants, immature Gag lattice is surrounding RNA and reducing Env mobility. HIV-1 wild type particles are formed after protease (PR) cleavage of Gag into its constituents: Matrix (MA), capsid (CA), nucleocapsid (NC) and p6 subunits.

Moreover, to ensure the methodology was running properly, the supernatant of an immunoprecipitation of gp41 treated with [³H]-photo-cholesterol, which resulted positive for gp41-cholesterol interaction, was used to perform an immunoprecipitation of Gag/MA.

Viral particles were purified from HEK 293T cells transfected with a proviral pCHIV plasmid or pCHIV PR(-) plasmid and treated with [³H]-photo-cholesterol. After viral particle purification, gp41 immunoprecipitation, obtention of the Western blot against gp41, and the autoradiographic detection of the lipid were carried out (Figure 3.21 A).

As expected, in Figure 3.21 A a positive interaction between gp41 and cholesterol is shown. The maturation state of the viral particles does not seem to alter gp41 interaction with cholesterol. Immature viral particles containing wild type gp41 do not show a significant difference in interaction with cholesterol when compared to mature particles with the same wild type protein.
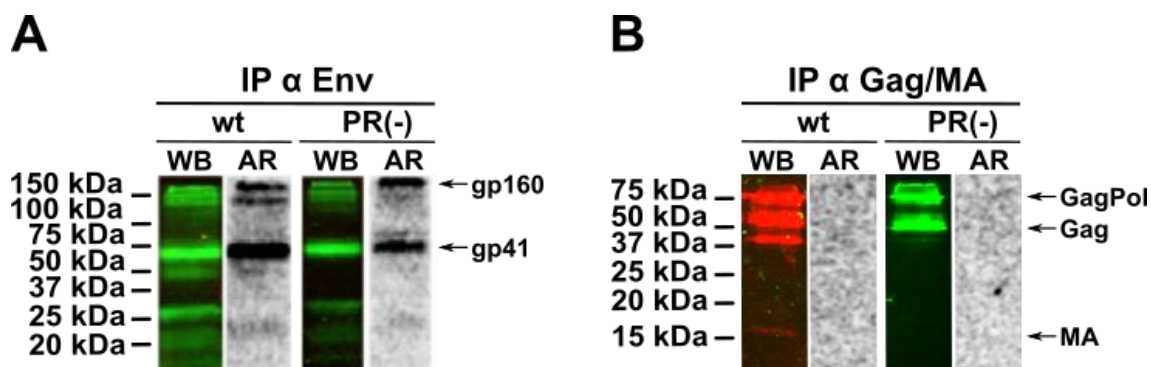
Figure 3.21. HIV-1 Maturation state and [³H]-photo-cholesterol interaction. **A)** Representative images of the immunoprecipitated gp41 Western blot (green) and crosslinked [³H]-photo-cholesterol derivative autoradiography (grey) signals of purified viral particles in mature (wt) and immature virions [PR(-)]. The Western blot was developed with Chessie-8 α-gp41 primary antibody, and α-mouse IRDye800 secondary antibody. **B)** Representative images of the immunoprecipitated Gag/MA Western blot (red and green, respectively) and crosslinked [³H]-photo-cholesterol derivative autoradiography (grey) signals of purified viral particles in mature (wt) and immature virions [PR(-)]. The Western blot was developed with rabbit α-MA and α-rabbit IRDye680 antibodies (red) and with sheep α-CA and α-sheep IRDye800 antibodies (green). The [³H]-photo-cholesterol radioactive signal in both A and B was detected by autoradiography of the same membrane.

The supernatant of the previous gp41 immunoprecipitation was used to perform an immunoprecipitation of Gag/MA (Section 3.2.2.3) in mature and immature virions. Then, following the same procedure as before, the immunoprecipitation was loaded into a SDS-PAGE and a Western blot was developed against MA (Figure 3.21 B).

The Western blot analysis in Figure 3.21 B shows that the PR(-) variant presents a band of medium protein size (~55 kDa), which is recognized by both α-CA and α-MA antibodies, thus, corresponding with Gag. Consequently, the PR(-) variant does not show neither the CA (~24 kDa) nor MA (~15 kDa) protein bands observed in the wild type particles. These results confirm that no free CA nor MA are present in virions obtained from the pCHIV PR(-) proviral plasmid, and that they only contain the Gag polyprotein, as expected. However, in the autoradiography there is no band of the same size as the aforesaid bands of MA and Gag proteins, which means there is no direct interaction between MA or Gag and [³H]-photo-cholesterol, so **the maturation state of the viral particles does not modify the interaction between MA and Gag with cholesterol.** Nevertheless, this experiment was performed using a viral particle amount corresponding to 1 μg of CA, in comparison with the previous experiment (Section

3.3.4.1) where 9 µg of CA were used. Therefore, an immunoprecipation with a higher amount of protein could be performed to ensure that the perceived lack of interaction is not caused by a low amount of immunoprecipitated Gag/MA.

3.4. Discussion

Protein-lipid interactions are key elements in the correct development of multiple cellular functions. It is widely known how proteins and lipids influence each other to regulate this functions. As an example, lipid rafts have been described to be able to exclude or include proteins from concrete regions of the cell membrane, and membrane lipids, such as cholesterol, have been shown to be tightly bound to some specific proteins like caveolins, and even be essential for their function and vice versa (Fielding & Fielding, 2000; Frank et al., 2006; Gahbauer & Böckmann, 2016; Palsdottir & Hunte, 2004; Simons & Toomre, 2000; Smart et al., 1999; Waheed & Freed, 2009).

Indeed, the relevance of protein-lipid interactions is extended to several viral processes, such as viral replication where some membrane lipids are implicated (Lorizate & Kräusslich, 2011). Specifically, the viral membrane of HIV-1 has been shown to be significantly enriched in phosphatidylserine, hexosylceramide, saturated species of phosphatidylcholine, sphingomyelin, PI(4,5)P$_2$ and cholesterol when compared to the host cell membrane. Additionally, this lipidic composition of the HIV-1 membrane has been described to resemble the composition of DRMs, hence, suggesting the existence of raft-like nanodomains in the cell membrane from where mature virions bud (Aloia et al., 1988, 1993; Brügger et al., 2006; R. Chan et al., 2008; Lorizate et al., 2013; Mücksch et al., 2019; Sengupta et al., 2019; Sengupta & Lippincott-Schwartz, 2020).

Cholesterol has been found to constitute almost 50% of the lipid molecules in the viral membrane and it has been described to play an important role in several steps of the HIV-1 replication cycle, such as at the entry and budding processes (Lorizate et al., 2009; Luo et al., 2008; Nieto-Garai et al., 2021; Percherancier et al., 2003). Certainly, cholesterol-depleting agents such as β-cyclodextrin and statins, and cholesterol binding compounds like AME, strongly reduced HIV-1 infectivity (Campbell et al., 2002; Liao et al., 2001, 2003; Mañes et al., 2000; Sundaram et al., 2016; Waheed et al., 2006).

Furthermore, recently it has been seen that HIV-1 Env interacts through its cytoplasmic tail with cholesterol in a way that it is implicated in Env clustering into a single foci (Nieto-Garai et al., 2021).

HIV-1 MA and Env proteins have been postulated to be associated with cholesterol. Several studies have described interactions of MA and Env with DRMs (Bhattacharya et al., 2006; W.-E. Chan et al., 2005; Ding et al., 2003; Halwani et al., 2003; Lindwasser & Resh, 2001; Nguyen & K Hildreth, 2000; Ono & Freed, 2001; Patil et al., 2010; Rousso et al., 2000; C. Yang et al., 1995; P. Yang et al., 2010). Even though DRMs experiments were a starting point to unveil important processes, this technique has the huge drawback of using detergents, which have been described to break certain lipid-protein interactions, therefore, obtaining conflicting results (Munro, 2003). Moreover, they have been described to come from detergent-disrupted membranes that later re-associated at low temperature, so they do not resemble *in vivo* cell membrane domains (Sot et al., 2002). Thus, despite the presence of a protein in DRMs, this would not constitute an absolute probe of the existence of an interaction between this protein and membrane lipids associated to lipid rafts, such as cholesterol or sphingolipids (Nieto-Garai et al., 2021; Thiele et al., 2000).

In this chapter, the interaction of HIV-1 Gag/MA with cell membrane cholesterol during morphogenesis or within the viral membrane has been studied using *in vivo* conditions by applying a bifunctional probe, a radioactive photoactivatable cholesterol, instead of the DRMs approach. [^{3}H]-photo-cholesterol covalently binds to any molecule closer than 3 Å after UV light irradiation (Contreras et al., 2012; Haberkant et al., 2008; Farenholz et al., 2000; Nieto-Garai et al., 2021; Thiele et al., 2000), thus, providing much more concrete information about a specific protein-lipid interaction. In addition, the radioactive tag of [^{3}H]-photo-cholesterol enhances the protein-lipid interaction detection, helping in the quantification of even trace amounts of biomolecules (Gevaert et al., 2008). Bifunctional lipids have the inconveniences of the need to be synthetized, since they are not commercially available, and its detection should be carried out by a specific machine such as the BetaIMAGER™. However, those lipid analogues are easy to handle, and their use could give outstanding information about specific interactions between proteins and lipids.

In this work, [³H]-photo-chol proved to be a potent tool for the study of protein-lipid interactions. With the use of Cav-1 and TfR as controls, the lipid probe demonstrated the accurate behaviour of its natural counterpart. This bifunctional probe interacts with the well-known raft marker Cav-1, and does not bind to non-raftophilic marker TfR, as expected (Figure 3.8). Moreover, [³H]-photo-chol has been used to study the interaction between cholesterol and HIV-1 Env protein (Figure 3.9), synaptophysin (a synaptic-like microvesicle membrane protein), and IFN-γ receptor (Morana et al., 2022; Nieto-Garai et al., 2021; Thiele et al., 2000). Therefore, the above-mentioned results support [³H]-photo-chol as a useful and reliable methodology for studying protein-lipid interactions.

By the use of [³H]-photo-cholesterol, the main conclusion of this chapter is that immature Gag polyprotein and its mature state MA seem not to interact with cell membrane cholesterol during HIV-1 morphogenesis neither in viral producer cells nor in the viral particle. This lack of a direct interaction with cholesterol can be explained as follows. On the one hand, if we compare the results obtained with Gag/MA with the viral Env protein, Env possesses different well-known motifs that could interact with cholesterol (CRAC, GxxxG, LLPs) (Aisenbrey et al., 2020; Epand, 2006; Klug et al., 2017; L. Lu et al., 2008; Murakami & Freed, 2000; Russ & Engelman, 2000; C. Schroeder, 2010; Vincent et al., 2002). However, no evidence of any typical cholesterol-binding domain [CRAC, CARC (the binding domain is similar to the CRAC sequence but exhibits the opposite orientation along the polypeptide chain), StAR-related lipid transfer domain (START), sterol-sensing domain (SDD)] (Epand, 2006; Fantini & Barrantes, 2013) have been found in Gag up to date.

On the other hand, although immunofluorescence microscopy studies have revealed that Gag co-patches with lipid raft markers in cells (Holm et al., 2003; Keller et al., 2009, 2013; Nguyen & K Hildreth, 2000; Ono & Freed, 2001, 2004) and co-fractionates with lipid raft markers in DRMs (Bhattacharya et al., 2006; Ding et al., 2003; Dou et al., 2009; Halwani et al., 2003; Holm et al., 2003; Lindwasser & Resh, 2001, 2002; Nguyen & K Hildreth, 2000; Ono & Freed, 2001, 2005), qualitative differences between canonical DRMs and Gag-containing DRMs have been noted (Ding et al., 2003; Holm et al., 2003; Keller et al., 2009, 2013; Lindwasser & Resh, 2001), and DRMs are not a reliable technique

for the study of *in vivo* protein-lipid interactions. As stated above, DRMs induce the co-patching of proteins due to the low temperatures used. Therefore, these DRMs studies has not shown a real *in vivo* co-localization between cholesterol and Gag in lipid rafts. The only co-localization of Gag with cholesterol known nowadays was shown in Niemann-Pick type 2 (NPC2)-deficient and Niemann-Pick type C-1 (NPC1)-deficient cells after HIV-1 infection, where Gag accumulates in late endosomes and lysosomes. NPC1 and NPC2 proteins are well-known carriers for cholesterol and lipids in vertebrates, therefore, this co-localization suggests that HIV-1 infectivity is profoundly affected by cholesterol trafficking and localization by modulating the cholesterol content of the virions (Coleman et al., 2012; Y. Tang et al., 2009).

Even though this direct interaction does not seem to take place, it has widely been described that an indirect relationship between Gag and cholesterol is highly important for HIV-1 assembly and production. It has been described that Gag could directly detect other lipids than PI(4,5)P$_2$, such as cholesterol (Dick et al., 2012; Lalonde & Sundquist, 2012), and depletion of cellular cholesterol markedly and specifically reduces, permeabilizes and inactivates HIV-1 particle production (Graham et al., 2003; Ono & Freed, 2001), membrane binding, Gag mobility (Gomez & Hope, 2006), higher-order multimerization of Gag (Ono et al., 2007), membrane curvature during budding events (Ivankin et al., 2012) and HIV-1 infectivity (Hawkes et al., 2015; Liao et al., 2001).

Sterol-binding drugs filipin and methyl-β-cyclodextrin induce the redistribution of the cholesterol from the cell membrane to endosomes, causing a re-localization of pre-assemble Gag in the cell membrane to late endosomal/multivesicular bodies (LE/MVBs) (Lindwasser & Resh, 2004), pointing towards a role of cholesterol in Gag targeting to assembly sites.

Gag multimerization is also known to trigger the formation of acidic lipid enriched microdomains (ALEM) at the inner leaflet of the cell membrane, which include cholesterol molecules (Charlier et al., 2014; Kerviel et al., 2013). The generation of ALEM by Gag itself is likely due to lipid sequestering induced by electrostatic interaction as reported before for syntaxin, a protein involved in vesicle fusion during exocytosis, and PI(4,5)P$_2$ (van den Bogaart et al., 2011). This event generates the coalescence of tetraspanin-enriched microdomains (TEMs) and lipid rafts at the viral assembly sites,

forming nanodomains smaller than the size of domains from which HIV-1 buds and different from lipid rafts (Favard et al., 2019; Hogue et al., 2011; Kerviel et al., 2013; Krementsov et al., 2010; Yandrapalli et al., 2016). In a nutshell, Gag recruits $PI(4,5)P_2$ upon its binding to the membrane, then its multimerization induces the formation of ALEM in the inner leaflet of the membrane, which further triggers the coalescence of other nanodomains of the outer leaflet of the membrane, such as lipid rafts and TEMs.

Upon this assembly, HIV-1 is able to specifically trap $PI(4,5)P_2$ and chol, but not PC or SM (Favard et al., 2019). So, HIV-1 assembly sites differentiate from their surroundings, among others, in their lipid composition, becoming enriched in cholesterol and sphingolipids. Multimerization of Gag into a lattice influences the lipid composition of both the inner- and outer-membrane leaflets. Inner-leaflet lipids are impacted because the static Gag lattice has a high affinity for $PI(4,5)P_2$ and Gag acts as the main driving force to restrict the mobility of $PI(4,5)P_2$ and cholesterol at the cell membrane. As $PI(4,5)P_2$ enriches at the assembly site, it could impact outer-leaflet lipids through the process of trans-bilayer coupling. In this mechanism, the long-saturated C-18 acyl chain of $PI(4,5)P_2$ at the assembly site would reach across the bilayer to interact with the long, saturated chains of the outer leaflet lipids including SM and glycosylphosphatidylinositol-anchored proteins (GPI-APs) (Favard et al., 2019; Sengupta et al., 2019).

Furthermore, it is postulated that cholesterol affects Myr(e) accumulation at the membrane surface, which suggests that chol facilitates membrane insertion of the myristate. Neither $PI(4,5)P_2$ nor chol by itself increased HIV-1 MA membrane binding notably, but in combination they boosted both binding affinity, such as free energy gained from binding and protein accumulation at the surface (Barros et al., 2016). In addition, it has been shown that chol affects Rous sarcoma virus MA-membrane association by making the electrostatic potential at the membrane surface more negative, while decreasing the penalty for lipid headgroup desolvation (Doktorova et al., 2017).

Finally, Gag and cholesterol could drive the formation of chol-enriched membrane nanodomains that host-selected proteins, such as Env, and reduce their mobility in the membrane. In there, Env, which interacts directly with this lipid and Gag/MA, could be

stuck forming a sandwich during morphogenesis, where there would not be a direct interaction between Gag/MA and chol, but an indirect interaction could exist via Env glycoprotein (Figure 3.22), due to the fact that it is known that Gag plays a role in the redistribution, targeting and incorporation of Env during viral maturation (Chojnacki et al., 2012, 2017; Chojnacki & Eggeling, 2021; Favard et al., 2019; Groves et al., 2020; Hogue et al., 2012; Javanainen et al., 2017; Nieto-Garai et al., 2021; Urbančič et al., 2018).

Env interacts with MA through the cytoplasmic tail of its gp41 subunit (Alfadhli et al., 2016, 2019; Brandano & Stevenson, 2011; Bulgelski et al., 1995; Checkley et al., 2011; Davis et al., 2006; Dorfman et al., 1994; Eastep et al., 2021; Freed & Martin, 1995; Groves et al., 2020; Murakami & Freed, 2000; Muranyi et al., 2013; Murphy & Saad, 2020; Patil et al., 2010; Pezeshkian et al., 2019; Tedbury & Freed, 2014; Tedbury et al., 2013, 2015a, 2015b, 2020; Wyma et al., 2000; Yu et al., 1992), nevertheless, the implicated domains of both proteins and their mechanism of interaction are still an enigma up to date. In addition, it is known Env-cholesterol interaction is dependent on this CT for clustering, more precisely, in the LLP2 and LLP3 domains, but not the LLP1 (Nieto-Garai et al., 2021). LLP3 and LLP2 have been demonstrated to be inserted into the viral membrane in a parallel orientation with their hydrophobic residues embedded in the membrane (Moreno et al., 2008; Murphy et al., 2017). If this insertion is resembled in the cell membrane, these domains could be directly interacting with cholesterol while the LLP1 is protruding to the cytosol. In this situation, it could be hypothesised that the best candidate to interact with MA is the LLP1 domain, while LLP2 and LLP3 could be interacting with cholesterol at the same time, conforming the sandwich model of interaction mentioned before (Figure 3.22), where Env CT is stuck between MA and cell cholesterol during HIV-1 assembly. Indeed, this disposition would be the adequate to maintain the steric hindrance between the CT and Gag, which has an effect in the final coalescence of Env into a single foci in the mature virions.
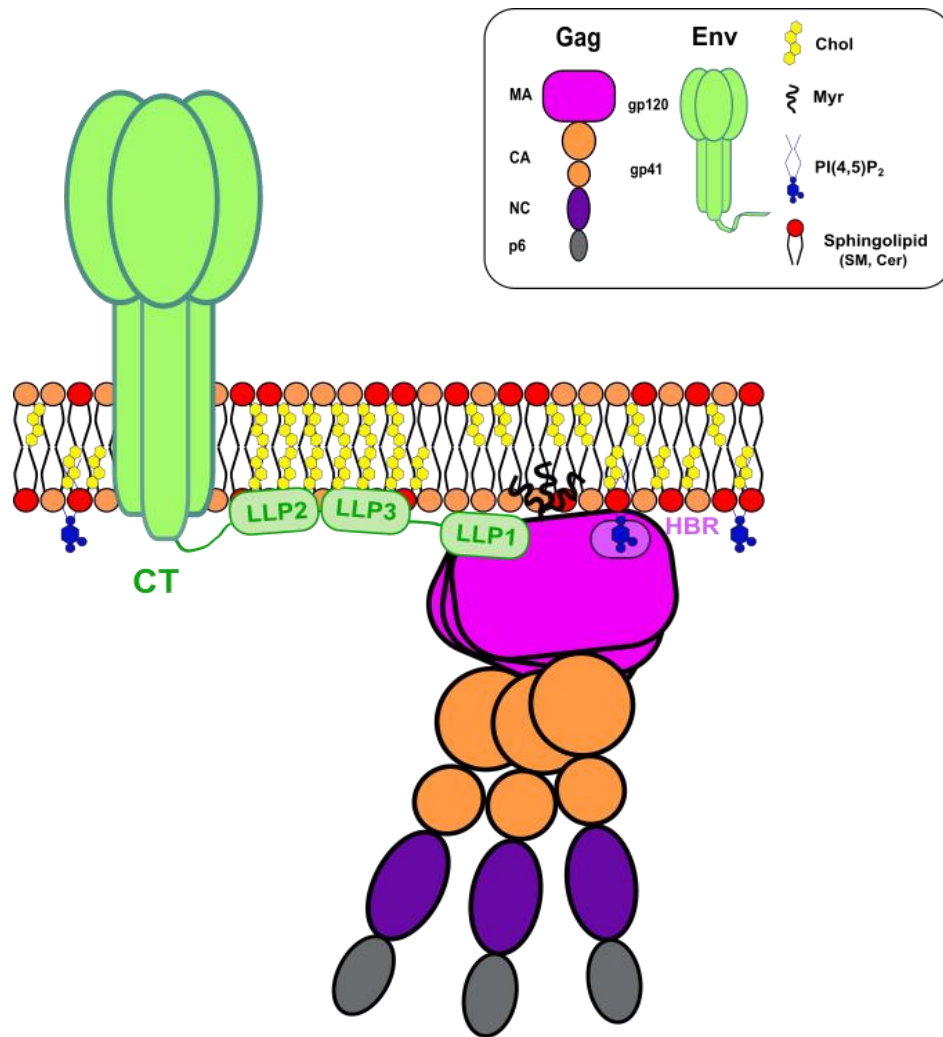
Figure 3.22. Indirect Gag/MA-chol interaction as "the sandwich model". Gag is anchored to the plasma membrane thanks to the interaction between MA (Myr plus HBR) and PI(4,5)P$_2$, causing the myristoyl switch. The presence of Gag and cholesterol in the membrane could drive the formation of chol-enriched nanodomains that could retain some host-selected proteins as Env and reduce their mobility. As it is known that Env could interact with chol through its CT, precisely through LLP2 and LLP3, and could also interact with MA through this same domain, this model hypothesises a interaction between MA and Env LLP1, while at the same time Env could be interacting with chol through the other two LLPs. Thus, Env is stuck between Gag and chol forming a sandwich during morphogenesis, where there is an indirect interaction between Gag/MA and chol, via Env.

This model would be in agreement with the hypothesis arising from Figures 3.18 & 3.19 A. The broad radioactive signal observed around ~55 kDa could correspond to the cholesterol associated with the gp41 protein. Since the immunoprecipitated protein in said experiment was Gag/MA, that would mean that Env would co-immunoprecipitate with MA, which comes in accordance with results seen in Figures

3.11 & 3.12 and, therefore, with the previous sandwich-type distribution proposed, explaining the lack of direct interaction of Gag with [H^3]-photo-chol.

All the aforesaid evidence of the relevance of Gag as a promotor of viral morphogenesis together with the key role of cholesterol during HIV-1 life cycle could led to think of different arguments that could explain the absence of Gag/MA-cholesterol interaction.

First of all, the majority of newly synthesized Gag is forming free polysomes in the cytosol instead of being anchored to the cell membrane. While membrane-targeted Gag was efficiently released, a significant fraction of the remaining cell surface-associated Gag was found to be internalized to late endosomal/multivesicular bodies (LE/MVBs), where it is accumulated. These multivesicular bodies are cholesterol-enriched organelles formed by the endocytic pathway. Gag could bind to these intracellular vesicles entering the endosomal trafficking system, thanks to the possession of an internalization signal that promotes endocytosis. Importantly, this accumulation of Gag in LE/MVB was found to be cholesterol dependent since it was sensitive to the sterol-binding drugs filipin and methyl-β-cyclodextrin. When Gag enters the endosomal trafficking machinery, the MA region becomes bound to endosomal lipids. The final delivery of Gag to the cell membrane seems to involve fusion between endosomal and cell membranes (Finzi et al., 2007; Lindwasser & Resh, 2004; Ono & Freed, 2004; Perlman & Resh, 2006; Scarlata & Carter, 2003). Once it is in the cell membrane, Gag forms high-order multimers by membrane interactions, instead of existing as monomers or low-order multimers in the cytoplasm (Kutluay & Bieniasz, 2010). In addition, even though our experiments were developed on HEK 293T cells is important to keep in mind that in infected macrophages and T cells, it has been observed that Gag accumulated in intracellular compartments that are also positive for LE/MVB markers. Those virus-sequestering compartments are apparently connected to the cell membrane through microchannels, so they could potentially aid HIV-1 to escape host immune responses and their contact with the cell membrane is also well suited for mediating efficient delivery of virions to uninfected T cells via cell-cell contact sites, named as virological synapses (Bennett et al., 2009; Booth et al., 2006; Gousset et al., 2008).

In addition, degradation of defective ribosomal products (DRiPs) constitutes upwards of 30% of newly synthesized proteins as determined in a variety of cell types and, at least, some DRiPs represent ubiquitinated proteins. This is the case of Gag, which can be ubiquitinated on numerous lysine residues. A significant fraction of newly synthesised Gag is degraded before reaching the cell membrane (Gottwein & Kräusslich, 2005; Schubert et al., 2000). Therefore, Gag could mainly be free in polysomes instead of being anchored to the cell membrane where it could interact with cholesterol during morphogenesis, and, moreover, part of Gag is degraded after reaching the membrane. To avoid this problem, the direct interaction between Gag/MA and cholesterol was assessed at a viral level.

Secondly, other issue that could be interfering at a cellular level could be the dissociation of pre-assembled Gag clusters at the cell membrane. Nascent HIV-1 Gag assembly sites are highly dependent on PI(4,5)P$_2$. It has been shown that an average of 8,000 PI(4,5)P$_2$ molecules form part of the viral membrane of each HIV-1 particle, three times more than Gag (Mücksch et al., 2019). The high density of PI(4,5)P$_2$ at the HIV-1 assembly site is mediated by transient interactions with viral Gag polyproteins, facilitating PI(4,5)P$_2$ concentration in this microdomain. Therefore, PI(4,5)P$_2$ is not only required for recruiting, but also for stably maintaining Gag at the cell membrane (Chukkapalli et al., 2008; Mücksch et al., 2017; Ono et al., 2004). Depletion of PI(4,5)P$_2$ completely prevents Gag plasma membrane targeting and assembly site formation. Moreover, PI(4,5)P$_2$ depletion also caused loss of pre-assembled Gag lattices from the cell membrane. Subsequent restoration of PI(4,5)P$_2$ re-induced assembly sites formation even in the absence of new protein synthesis, indicating that the dissociated Gag molecules remained assembly competent. Dissociated pre-assembled Gag clusters transform into numerous intracellular Gag-containing complexes (GCCs) that could comprise more than 20 Gag molecules each. GCCs could act as a reservoir of monomeric Gag that can be incorporated into assembling virions and serve to mitigate non-specific intracellular Gag oligomerization (Deng et al., 2021; Dou et al., 2009; Mücksch et al., 2017, 2019). Thus, the absence of PI(4,5)P$_2$ hampers Gag targeting to the plasma membrane and the formation of GCCs, causing the morphogenesis to revert. Therefore, the constant back and force in the formation of GCCs in the cell membrane due to PI(4,5)P$_2$ effect should

affect the interaction of Gag with [3H]-photo-cholesterol, but do not constitute an impediment for it. Thus, a low radioactive signal should be expected in the autoradiography instead of no signal at all (Figure 3.14).

Thirdly, it must also be considered that, even though the method is in working order, the interaction between [3H]-photo-cholesterol and Gag/MA could not be taking place due to the distance separating both molecules. Membrane interacting regions of Gag/MA are conferred to the amino acids localized in the so called highly basic region (HBR), whose interaction is merely of electrostatic nature and a myristoyl group exposure, which occurs upon membrane adhesion through electrostatic interactions to negatively charged lipids head groups (Barros et al., 2016; Dalton et al., 2007). After UV-irradiation, the diazirine group of the [3H]-photo-cholesterol turns into a carbene that could react with any molecule closer than 3 Å of distance (Contreras et al., 2012; Haberkant et al., 2008; Nieto-Garai et al., 2021; Thiele et al., 2000), however, the myristoyl group of MA could be farther than 3 Å, thus, the [3H]-photo-cholesterol could not reach it in the cell membrane and the Gag/MA-cholesterol interaction could not be detected.

Furthermore, even considering that the myristoyl group of MA was at the appropriate distance for the proper interaction with [3H]-photo-cholesterol after UV-light irradiation, the highly dynamic binding mode of Gag to the cell membrane could be affecting the interaction. Nevertheless, this would not explain the lack of interaction in viral particles.

MA exists in two states of myristoylation, as it was previously explained: myr-exposed [Myr(e)] and myr-sequestered [Myr(s)]. MA exists in equilibrium between monomeric and trimeric states. The monomer is in the Myr(s) state, whereas the trimer is in the Myr(e) state, implying that multimerization promotes exposure of the myristate. Myr(e) binds to membranes 30-fold tighter than does Myr(s) (Elliot Murphy et al., 2019). The equilibrium constant is shifted approximately 20-fold toward the trimeric, myristate-exposed species in a Gag-like construct that includes the capsid domain, indicating that exposure is enhanced by Gag subdomains that promote self-association. Therefore, myristoyl switch is regulated not by mechanically induced conformational changes, but instead by entropic modulation of a pre-existing equilibrium (Saad et al.,

2007; C. Tang et al., 2003). Ten of the 14 methylene groups of the myristate typically penetrate into the lipid bilayer, so Myr–Myr interactions may be altered when Gag is membrane-bound (Peitzsch & McLaughlin, 1993).

Additionally, the myristoyl switch could be modulated by other factors including the pH, protein concentration, binding of calmodulin (Fledderman et al., 2010; Ghanam et al., 2010; C. Tang et al., 2003); and PI(4,5)P$_2$, which is suggested to act as both an allosteric trigger for Myr exposure and as a direct membrane anchor (Saad et al., 2007). The destabilization of oligomeric structures of membrane-bound MA as a result of the proteolytical processing of the HIV-1 Gag polyprotein during viral maturation also could influence the myristoyl switch (Wu et al., 2004).

Nevertheless, the myristoyl switch is equally energetic, so, the myristoyl group is constantly showing and hiding from the MA pocket depending on all the aforesaid factors. These conditions could hamper the detection of the interaction with [^{3}H]-photo-cholesterol, but they do not constitute an impediment for it. If this interaction would be 50:50, it would be expected at least a half of MA proteins interacting with cholesterol, giving a low signal instead of no signal in the autoradiography (Figure 3.14).

To sum up, this chapter of this Thesis it has been mentioned three plausible conditions that could be happening during Gag/MA–chol interaction, which would explain the absence of signal in the previous protein-lipid studies with [^{3}H]-photo-chol. These aforesaid three situations are the following: 1) no interaction between Gag/MA and cholesterol could be real; 2) the interaction could not be assessed because the distance is far from 3 Å; and 3) there could be an indirect Gag/MA–chol interaction via Env based in the previous stated sandwich model. The final hypothesis supported in this work is the last situation, where Gag/MA does not interact directly with cholesterol during HIV-1 morphogenesis, and, however, they maintain an essential and strong relationship during HIV-1 assembly needed for the development of new infectious viral particles.

Chapter 4.

A chemical tool to decipher HIV-1 palmitoylome

Chapter 4: A chemical tool to decipher HIV-1 palmitoylome

4.1. Introduction

S-palmitoylation is a fundamental post-translational protein modification involved in signalling, trafficking, membrane targeting, cellular localization and protein-protein interactions. It consists in the thioesterification of palmitate to cysteine residues, imparting hydrophobicity to the molecule and resulting in the recruitment of these modified proteins to cell membrane-containing compartments. As palmitoylation drives both location and function of proteins, perturbation of this modification could have a profound implication on cellular biology, development, and disease pathogenesis (Duan & Walther, 2015; Grotenbreg & Ploegh, 2007; Smotrys & Linder, 2004).

Palmitoylated proteins are known to preferentially target lipid rafts, specific microdomains existing in the cell membrane *in vivo*, which are composed of tightly packed SPLs, gangliosides, and chol (Brown, 2006; Levental et al., 2010; Melkonian et al., 1999; Resh, 1999; Salaun et al., 2010; Simons & Ikonen, 1997). In the case of HIV-1, it has been thought that viral targeting to lipid rafts is mediated via palmitoylation of Env gp41 (Bhattacharya et al., 2006; Chien et al., 2009; R. A. Dick et al., 2012; Lev & Shai, 2007; Rousso et al., 2000; C. Yang et al., 1995; P. Yang et al., 2010), nevertheless, recently it has been proven that palmitoylation of gp41 Cys-764 and Cys-837 are not involved in lipid raft domain interaction since a non-palmitoylated mutant is able to specifically interact with membrane cholesterol (Nieto-Garai et al., 2021). Even so, lipid rafts constitute minor domains in most membranes, thus, these domains are thought to concentrate palmitoylated proteins together with other viral components, facilitating protein-protein interactions, as well as HIV-1 budding and entry processes (Brügger et al., 2006; Graham et al., 2003; Levental et al., 2010; Liao et al., 2004; Suomalainen, 2002; Veit, 2012).

The HIV-1 palmitoylome corresponds to the complete set of palmitoylated proteins present in the mature virion. These proteins come from the own virion, such as Env glycoprotein (Bhattacharya et al., 2004; Syu et al., 1991; C. Yang et al., 1995), but mainly are host-derived membrane proteins incorporated during HIV-1 budding from presumably raft-like nanodomains (C. Luo et al., 2008). The HIV-1 proteome has been deciphered (Berro et al., 2007; Brégnard et al., 2013; Cantin et al., 2005; Chertova et al., 2006; Denard et al., 2009; Frankel & Young, 1998; Misumi et al., 2002; Ott, 1997, 2002; Ott et al., 1996; Saphire et al., 2006; Segura et al., 2008). However, a detailed HIV-1 palmitoylome remains undiscovered.

Long-term toxicity, inhibitor resistance, and the inability to target persistent reservoirs are problematic issues that current therapies directed against HIV-1 proteins must deal with. Consequently, it is urgent to reach new approaches to selectively target latent reservoirs and discover unique protein targets for the design of new therapeutic drugs (Deeks et al., 2021). Therefore, unravelling the HIV-1 palmitoylome would shed light on different aspects of the HIV-1 viral cycle. It could even be a step forward in developing new antiretroviral therapies that could fight against ongoing difficulties.

Identification of palmitoylated proteins has been challenging because of the lack of antibodies against lipid modifications and the lack of suitable markers or analogues for palmitoyl groups, as well as the inexistence of a consensus sequence for palmitoylation sites prediction (Hang & Linder, 2011; Resh, 2016; Rodenburg et al., 2017). Further, incorporation of labelled palmitoyl groups using radioactivity required long exposure times to measure biologically relevant signals. More recently, mass spectrometry techniques have evolved to monitor the presence of palmitoylated proteins (Ivaldi et al., 2012; Jones et al., 2012; B. R. Martin et al., 2012), however, the low abundance of the modification made quantification difficult, and the lability of the palmitoyl tag also hindered analysis.

To overcome aforementioned issues, bioorthogonal labelling and detection of protein using clickable-analogues of palmitate and myristate have appeared, providing quick and sensitive methods for protein acylations detection (Gao & Hannoush, 2014, 2018; Yap et al., 2010). The copper-catalyzed azide-alkyne cycloaddition (CuAAC)

reaction allows to label cells with alkynyl analogues of fatty acids that can react with azides conjugated to suitable detection tags, such as fluorophores, or affinity tags, like biotin (Ourailidou et al., 2016; Thiele et al., 2012). The strength of click chemistry technique stands in following incorporation the azide-modified proteins can be measured using a host of standard techniques, including electrophoresis, confocal microscopy, flow cytometry, and mass spectrometry.

In this chapter, a chemical tool for the future study of HIV-1 palmitoylome is presented. An alkyne-modified palmitoyl compound was synthetized by Dr. F.-Xabier Contreras, which enables the natural incorporation into the proteins during post-translational modification (Figure. 4.1). This analogue of palmitic acid contains a terminal alkyne group attached to its terminal moiety, which allows the analogue to suffer fluorescence detection or affinity enrichment by CuAAC reaction.
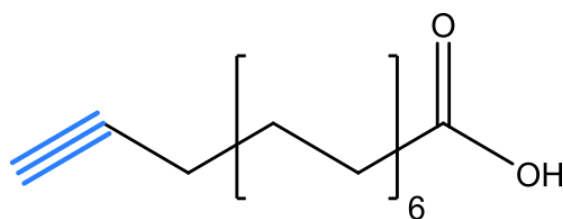
Figure 4.1. Alkyne-modified palmitoyl analogue. Structure of alkyne-modified palmitoyl analogue, 15-octadecynoic acid.

Here, it would have been proven that this alkyne-modified palmitoyl analogue could be properly used for the palmitoylation of HIV-1 proteins, such as Env. Moreover, in order to specifically enrich modified proteins of interest, we developed a strategy for the extraction of HIV-1 palmitoylated proteins based on the mix of this chemical tool, the CuACC reaction, and the biotin-avidin binding strength. The final protocol was applied for the extraction and proteomic analysis of HIV-1 palmitoylated proteins by mass spectrometry.

4.2. Experimental techniques

4.2.1. Alkyne-modified palmitoyl analogue

The alkyne-modified palmitoyl analogue used in this chapter was developed to mimic palmitate moieties added to the proteins during palmitoylation, acting as a substrate for palmitoyltranferases (Charron et al., 2009). This analogue of palmitic acid (C16:0) (Figure 4.2 A) is a clickable 15-hexadecynoic acid or alkynyl palmitate, which has an alkyne group attached to its terminal moiety at position C-15 (Figure 4.2 B). This analogue was chemically synthesized by Dr. F.-Xabier Contreras (Instituto Biofisika, Spain) starting from commercial 16-bromohexadecanoic acid (Sigma-Aldrich, #568708) by pyridinium chlorochromate oxidation, Bestmann-Ohira reaction, and ester cleavage.
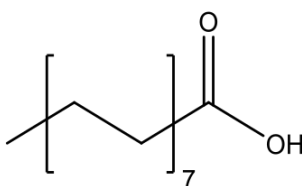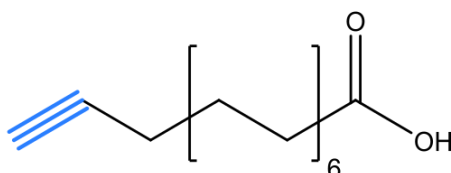
Figure 4.2. Alkyne-modified palmitoyl analogue. A) Structure of natural palmitic acid. **B)** Structure of alkyne-modified palmitoyl analogue, 15-hexadecynoic acid. Alkyne group is coloured in blue.

The palmitoyl analogue is added to the cell culture during growth, so the target proteins after 24 h incubation are labelled with a palmitoyl moiety containing the alkyne group at the end of the fatty acid chain. Palmitoylated proteins can be extracted and subjected to click chemistry to add a detectable chemical probe, such as biotin or a fluorophore (Hang et al., 2007; Ourailidou et al., 2016; Thiele et al., 2012). The presence

of the small terminal alkyne group has a minimal impact on the lipidic structure. It is biologically inert, thus, not perturbing the biophysical and metabolical properties of the molecule (Haberkant & Holthuis, 2014). This group is accessible to react by copper(I)-catalyzed azide-alkyne cycloaddition reaction (Section 4.2.3), the most widely recognized example of click chemistry. In addition, using a clickable probe as the palmitoyl analogue is safer and sensitive than labelling with radiolabelled palmitate (Hang et al., 2007; Martin & Cravatt, 2009).

4.2.2. Viral particle purification and quantification

For palmitoylation of HIV-1 gp41 experiments, $3,5 \cdot 10^6$ HEK 293T cells seeded in 10 cm dishes were transfected with a proviral plasmid as described in Chapter 2, and 500 µM of 15-hexadecynoic acid was added to the cells diluted in 8 mL of culture medium containing delipidated FBS. The alkyne-modified palmitoyl analogue was incubated with the cells for 24 h to ensure proper palmitoylation. Transfected but untreated cells are also cultured to obtain wild type VLPs without palmitoylation with the analogue. Wild type (**wt**) and treated (**pwt**) viral particles are released to the culture media, which is collected and clarified by centrifugation at 500 g for 5 minutes followed by filtration through 0.45 µm filters. Then, the viral particles were concentrated following the protocol shown in Section 2.5.2. The viral particle purification yield was determined by α-CA Western blot, and their protein content was characterized by silver stain. A general overview of the workflow used for obtaining palmitoylated viral particles is shown in Figure 4.3. Afterwards, to confirm the proper palmitoylation of HIV-1 containing proteins, a palmitoylation test based on the copper (I)-catalyzed azide-alkyne cycloaddition reaction (Section 4.2.3.1) was carried out using the Env gp41 as control.
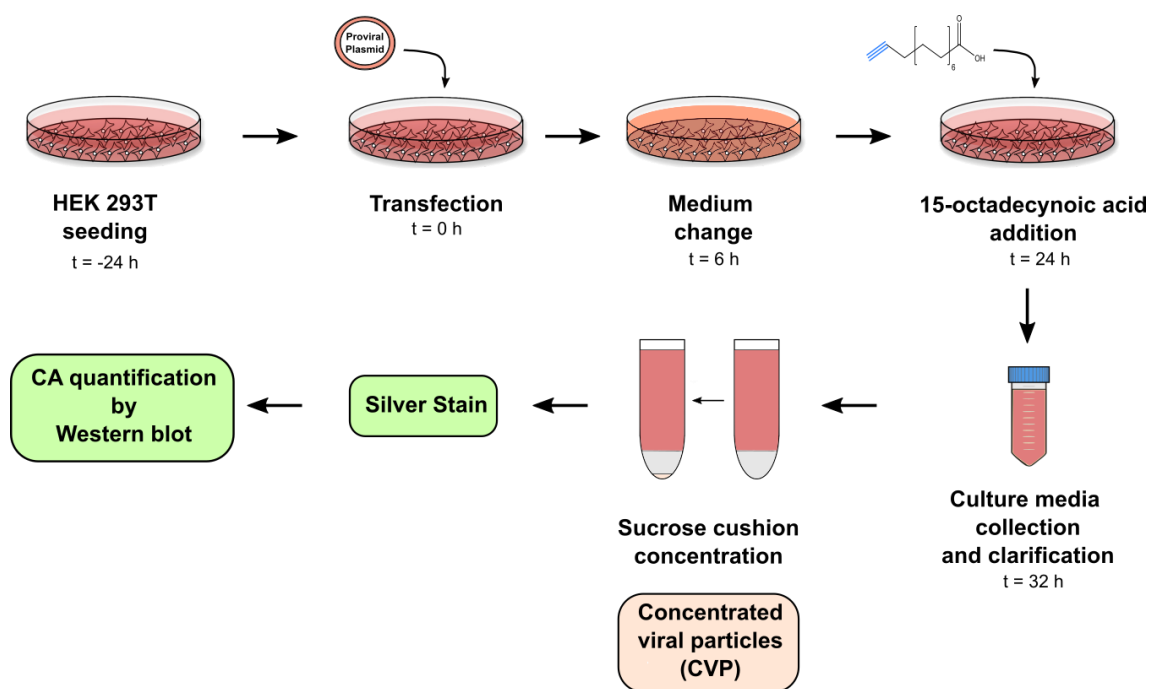
Figure 4.3. Workflow of purification and quantification of palmitoylated viral particles.

4.2.3. Click chemistry: Copper (I)-catalysed azide-alkyne cycloaddition (CuAAC) reaction

Click chemistry comprises a collection of bioorthogonal reactions that allows the selective coupling of two functional groups in biomolecules. Three representative examples of these powerful reactions are Staudinger ligation, the copper (I)-catalyzed azide-alkyne cycloaddition (CuAAC), and the recently developed strain-promoted azide-alkyne cycloaddition (SPAAC) (Haberkant & Holthuis, 2014).

The CuAAC reaction was discovered in 2002, and it is also known as the copper(I)-catalyzed [3+2]-Huisgen 1,3-dipolar cycloaddition of azides and terminal alkynes, which leads to 1,2,3-triazoles (Figure 4.4 B) (Kolb et al., 2001; Tornøe et al., 2002). Azides and terminal alkynes groups used in this reaction are synthetically easier to access and less likely to perturb the biophysical and biochemical properties of the biomolecules in which they are introduced. Therefore, these groups are suitable due to their reliability, specificity, and biocompatibility (Best, 2009; Haberkant & Holthuis, 2014).

A

B
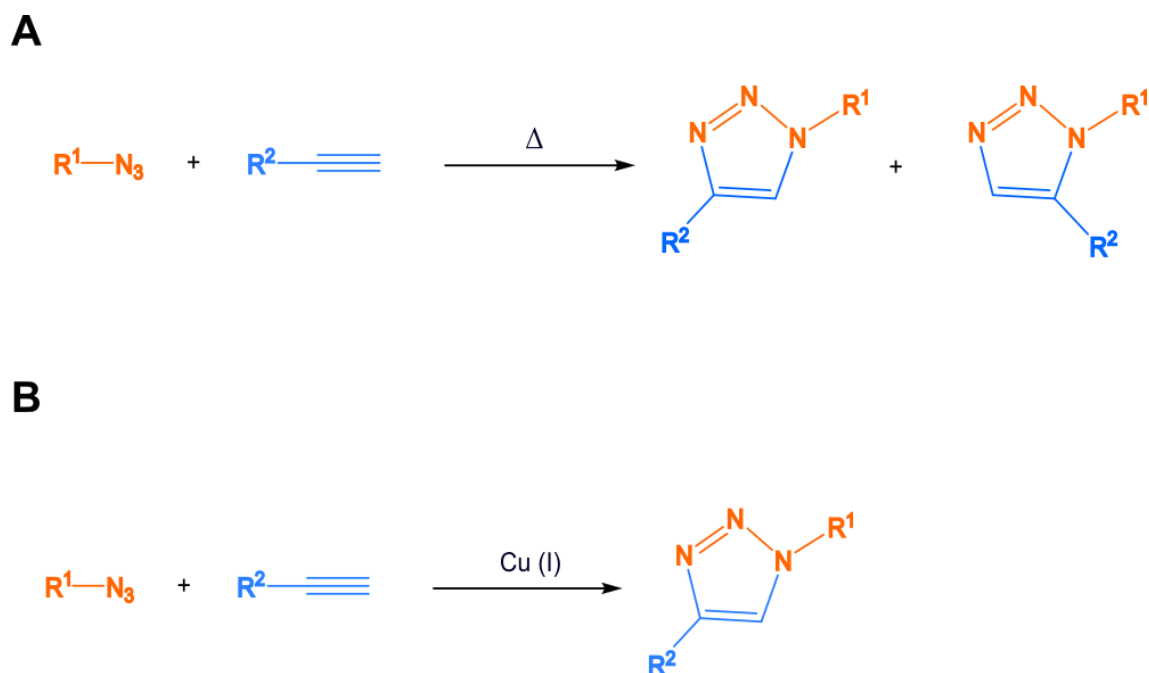
Figure 4.4. Click chemistry reaction. A) [3+2]-Huisgen 1,3-dipolar cycloaddition reaction of azides and terminal alkynes. **B)** Copper (I)-catalyzed Azide-Alkyne Cycloaddition (CuAAC) reaction. Azide is coloured in orange and terminal alkyne in blue.

[3+2]-Huisgen 1,3-dipolar cycloaddition of azides and terminal alkynes is a highly exothermic reaction; hence, it has an elevated activation barrier, which causes low reaction rates for unactivated reactants even at elevated temperatures. The incorporation of copper(I) as a catalyst drastically changes the mechanism and the outcome of the reaction, increasing the rate of CuAAC by a factor of 10^7 compared to the thermal process. In this manner, CuAAC transforms organic azides and terminal alkynes exclusively into the corresponding 1,4-disubstituted 1,2,3-triazoles (Figure 4.4 B), in contrast to the uncatalyzed reaction, which provides a mixture of 1,4- and 1,5-triazole regioisomers (Figure 4.4 A). Consequently, copper(I) makes the reaction fast and below room temperature (Hein & Fokin, 2010).

To maintain the proper oxidation state of copper, sodium ascorbate is the preferred reducing agent used in CuAAC reaction (Hong et al., 2009). In addition, Tris[(1-benzyl-4-triazolyl)methyl]amine (TBTA) or Tris((1-hydroxy-propyl-1H-1,2,3-triazol-4-yl)methyl)amine (THPTA) are added to the reaction due to the fact that is potent stabilizing ligands for copper(I), protecting the catalyst from oxidation and disproportionation, and enhancing its catalytic activity (T. R. Chan et al., 2004).

CuAAC reaction offers the possibility of visualization of clickable lipids. The interaction of an azide/alkyne group in the biomolecule of interest with a commercially available fluorophore/probe containing the corresponding alkyne/azide group allows sensitive fluorescence detection and/or affinity enrichment and proteomic analysis (Peng et al., 2014). The application of CuAAC reaction to the alkyne-modified analogue after viral concentration allows to verify the palmitoylated state of the HIV-1 gp41 in virions (Section 4.2.3.1) and to catch HIV-1 palmitoylated proteins for its subsequent proteomic analysis by an optimized protocol based on a biotin/streptavidin enrichment approach (Section 4.2.3.2).

4.2.3.1. Verification of palmitoylated HIV-1 gp41 by CuAAC reaction

To confirm the adequate palmitoylation of HIV-1 containing proteins, palmitoylation of virus gp41 protein was analysed. The CuAAC reaction is used together with the immunoprecipitation of gp41 by Protein G Sepharose beads covalently coupled to α-gp41 Chessie-8 antibody (Section 2.4.3).

1. After viral quantification by α-CA Western blot, the volume equivalent to 1 µg of CA is used for both wild type (wt) and treated with the palmitoyl analogue (pwt) viral purifications to immunoprecipitate gp41.

2. These volumes were mixed with 100 µL of EDTA-free Lysis Buffer with cOmplete™, EDTA-free Protease Inhibitor Cocktail (Sigma-Aldrich, #COEDTAF-RO), and lysed for 1 h at 4 °C in constant stirring. The composition of the EDTA-free Lysis Buffer is HEPES 20 mM, NaCl 100 mM, sodium deoxycholate 0.5% (w/v) and Triton X-100 0.1% (v/v) adjusted to pH 7.4. The absence of EDTA in the reaction is a key factor because EDTA is a Cu (II)-complexing agent and, as a consequence, a certain amount of the catalyst is retained, negatively influencing the overall reactivity of the CuAAC reaction. Moreover, EDTA is often used to stop the reaction completely (Presolski et al., 2011).

3. The lysed samples were centrifuged at 13,000 rpm for 5 min, and an aliquot of the supernatant was stored as the input. The rest of the samples were mixed with the

beads coupled to α-gp41 Chessie-8 antibody and incubated overnight at 4 °C in constant stirring.

4. The next day, the essential reagents for the CuAAC reaction were prepared prior to collecting the immunoprecipitated samples. They must be prepared fresh and kept stirring in the dark until use. The concentrations required in the assay are detailed in Table 4.1. All the dilutions are prepared using MiliQ H_2O. To ensure proper dissolution of ascorbic acid, it was heated up to 45 °C during stirring.

Table 4.1. Reagents for CuACC reaction.

	[Stock]	[Assay]
Ascorbic acid	1 M	10 mM
CuS0$_4$	100 mM	1 mM
TBTA	10 mM	0.1 mM

5. Once the reagents were ready, the mixture of the coupled beads with the samples was centrifuged at 6,500 rpm for 5 min, and the supernatant was stored as a non-immunoprecipitated sample.

6. The beads were washed three times with 500 µL of PBS Ca^{2+}/Mg^{2+}-free by centrifugation at 6,500 rpm for 3 min.

7. The beads were resuspended in 300 µL of PBS Ca^{2+}/Mg^{2+}-free, and the reagents for CuAAC reaction were added in the following order, vortexing softly after each addition:

   – 0.6 µL of fluorescent probe IRDye® 800CW Azide Infrared Dye (LI-COR, # 929-60000). Stock 8 mM; assay concentration 10 µM.

   – 3 µL of 0.1 mM TBTA.

   – 3 µL of 1 mM CuS0$_4$.

   – 3 µL of 10 mM ascorbic acid.

8. The CuAAC reaction was incubated 1 h at RT in the dark with constant stirring, at least at 800 rpm.

9. After incubation, the beads were centrifuged at 6,500 rpm for 3 min, and the supernatant containing the click reagents was removed.

10. The beads were washed three times with 500 µL of PBS by centrifugation at 6,500 rpm for 3 min to eliminate the unclicked probe.

11. 40 μL of SDS-PAGE sample buffer with low β-mercaptoethanol content (150 mM, half of the usual concentration) were added to the beads. β-Mercaptoethanol is a reducing agent that cleaves the disulfide bonds formed between thiol groups of cysteine residues when is used in excess (Smithies, 1965). Therefore, this would affect the disulfide bond between the modified-palmitoyl analogue and gp41 cysteines. A small amount of β-mercaptoethanol is added to the proper unfolding of proteins and their separation in a SDS-PAGE. 30 μL of normal SDS-PAGE sample buffer were added to 10 μL of the input and supernatant samples.

12. The samples were heated at 60 °C, instead of 95 °C, to avoid breaking the disulfide bonds (B. R. Martin, 2013; Nieto-Garai et al., 2021).

13. After heating, the beads were centrifuged at 6,500 rpm for 10 min, separating the free gp41 protein in the supernatant from the beads and the coupled antibody in the pellet.

14. The input, non-immunoprecipitated and immunoprecipitated samples were then loaded into a SDS-PAGE gel, and a Western blot was carried out as explained in Section 2.3, using α-gp41 Chessie-8 as primary antibody incubated overnight at 4 °C, and as secondary antibody used α-mouse IRDye680 antibody incubated for 45 min at RT.

15. gp41 protein bands were detected using the LI-COR Odyssey imaging system. Immunoprecipitated protein gp41 was visualized in the red channel (700 nm). The palmitoyl-modified analogue bound to gp41 was visualized in the green channel (800 nm), which is expected to be positive in pwt samples with the clickable analogue and negative in wt samples.

4.2.3.2. Definitive protocol for the extraction of palmitoylated proteins

Before proteomic analysis by mass spectrometry, the palmitoylated viral proteins needed to be extracted, and the present palmitoylated proteins must be fished out. Therefore, a specific protocol for extracting of palmitoylated proteins from HIV-1 virions must be designed. After several tests explained in Section 4.3.3, the standard protocol has been established as the following:

1. Lysate viral particles for 1 h at RT and shaking. Lysis buffer: PBS (Mg^{2+}/Ca^{2+}-free) + 1% SDS + protease inhibitor cocktail. Final volume: up to 200 μL.

2. Centrifuge 14,000 rpm 10 min. Save 'input'.

3. Copper-based click chemistry with TAMRA Biotin Azide (Click Chemistry Tools, # 1048-1). Incubate for 1 h at 37 °C and shake in the thermomixer.

4. Concomitantly with the click reaction, blocking with 2% BSA (w/v) of 50 μL of High Capacity Streptavidin Magnetic Beads (Click Chemistry Tools, #1497) previously washed with PBS. 1h at RT.

5. Extract with $CHCl_3$ and MeOH following Haberkant et al. (2016) and resuspend in 100 μL of PBS (Mg^{2+}/Ca^{2+}-free) + 1% SDS in the thermomixer. Adjust the rest of the sample to a final SDS concentration of 0.1% [add 900 μL of PBS (Mg^{2+}/Ca^{2+}-free) to the 100 μL of sample].

6. Wash 50 μL of Protein G Sepharose beads with PBS (Mg^{2+}/Ca^{2+}-free).

7. Mix the 1000 μL of the sample with the washed protein G beads. Incubate 1 h at RT. Centrifuge at 6,500 rpm for 5 min and recover unbound supernatant. In this step all the hydrophobic proteins will bind non-specifically to the beads.

8. Wash beads with 500 μL of PBS (Mg^{2+}/Ca^{2+}-free) by centrifuging at 6,500 rpm for 3 min. Resuspend the beads in 300 μL of PBS (Mg^{2+}/Ca^{2+}-free).

9. Add the washed protein G beads to the blocked magnetic streptavidin beads. Mix several times before incubating 1 h at RT and constant stirring. The idea is to induce the removal of biotinylated palmitoylated proteins from the protein G beads by the magnetic streptavidin beads due to the strong affinity of biotin-streptavidin binding.

10. Before recovering magnetic streptavidin beads, mix several times more. Put the sample in magnetic rack and recover the unbound supernatant and the protein G beads.

11. Wash magnetic beads 5 times with 500 μL of PBS (Mg^{2+}/Ca^{2+}-free) using magnetic rack.

12. To elute magnetic streptavidin beads, use (30+20) μL of sample buffer + 15 min incubation at RT in constant stirring in the thermomixer + 15 min 95 °C + centrifuge 6,500 rpm 10 min RT. Mix volumes and store as 'Eluted.' In this time 95 °C was used since it is not necessary to keep the palmitoyl moiety.

4.2.4. Proteomic studies

Palmitoylated viral proteins extracted after applying the stablished protocol explained in previous Section 4.2.3.2, had to be deciphered by mass spectrometry analysis.

For this purpose, the eluted samples of both wild type VLPs (wt) and VLPs treated with the palmitoyl-modified analogue (pwt) were loaded into four wells (two per sample, in order to load the complete volume of each sample) in a 10% SDS-PAGE gel, and an electrophoresis was carried out at 30-60 V until the bands reached a bit far away for from the stacking part of the gel. Then, the different proteins in the gel were fixed by incubation during 15 min at RT under constant agitation with two different solutions: Solution I [50% (v/v) MeOH, 7% (v/v) AcOH] and Solution II [5% (v/v) MeOH, 7% (v/v) AcOH].

The fixed gel was sent to the Proteomics Service of SGIKER (UPV/EHU), where the observable bands, which corresponded to the mix of all extracted proteins for both wt and pwt, were recovered from the gel, digested with trypsin, and deglycosylated with Peptide-N-Glycosidase F. The deglycosylated tryptic peptides obtained from the protein extracted from the SDS-PAGE were then analysed by a Q Exactive™ Hybrid Quadruple-Orbitrap™ mass spectrometer coupled to an EASY nLC1000 (ThermoFisher Scientific) liquid chromatography.

The SEQUEST™ HT (ThermoFisher Scientific) search engine compared the m/z ratio of the detected peptides by mass spectrometry coupled to liquid chromatography (MS/MS-LC) with a database containing human proteome and HIV-1 isolate BH10 protein sequences, which revealed a number of peptides spanning different regions forming part of potentially palmitoylated proteins. These resulting proteins were confirmed to be palmitoylated by SwissPalm database (Blanc et al., 2015, 2019).

Bioinformatic analyses were carried out by the following software. Cytoscape v.3.9.1 (Cytoscape Consortium) (Shannon et al., 2003) was used to build the interactome of related palmitoylated proteins, where biological networks were free scale due to the fact that it is difficult to guess which protein interacts first with other protein. The analysis was performed with a *p*-value < 0.001. STRING and BioGRID databases (Stark

et al., 2006; Szklarczyk et al., 2021) were used to assess protein-protein interaction networks between the different proteins obtained. Only those experimentally demonstrated are chosen and a *p*-value < 0.001 was used. BiNGO plugin for Cytoscape (Maere et al., 2005) was applied to study the biological and molecular functions in which the resulting palmitoylated proteins are involved in

4.3. Results

4.3.1. Viral particle quantification

42 h after HEK 293T cells transfection with a pCHIV proviral plasmid and 24 h after treatment with the palmitoyl-modified analogue, the culture medium supernatant of wild type and treated cells containing the viral particles was collected, clarified, and concentrated (CVP).

After each non-treated and treated viral purification, the resulting virions were characterized by silver stain and quantified by α-CA Western blot (Sections 2.2.6.1 and 2.2.6.2, respectively). A representative characterization by silver stain of some purifications of wild type and treated viral particles is shown in Figure 4.5.
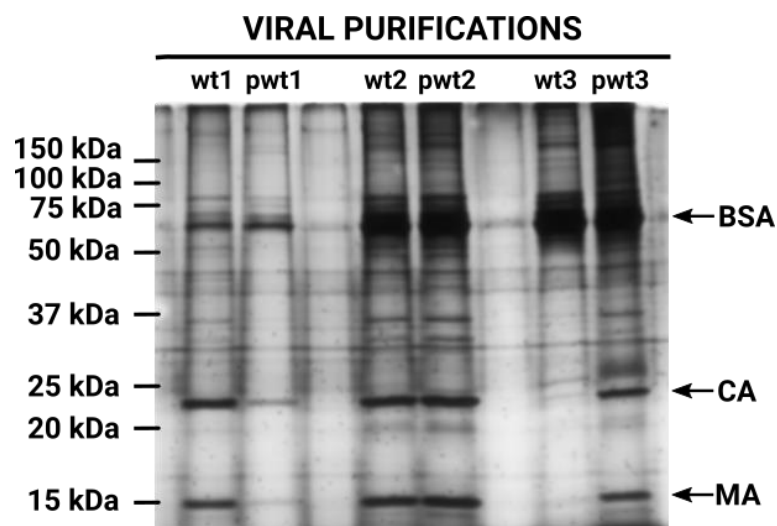
Figure 4.5. Representative silver stain of multiple viral purifications. Several concentrated viral purifications of non-treated wild type VLPs (wt 1-3) and VLPs treated with the palmitoyl-modified analogue (pwt 1-3).

Virions obtained from the six independent viral purifications possessed a correct viral pattern, as expected (Figure 4.5). Each purification showed protein bands around ~15 kDa and ~25 kDa, corresponding to MA and CA proteins, respectively. The intensity of the bands of CA gives a first impression of the concentration of CA that could have each viral purification; thus, the first treated viral purification and the last wild type viral purification seem to be less concentrated than the rest. However, each one of the viral samples is quantified by Western blot to select the most concentrated purifications afterwards to prepare two different pulls: one of the untreated viral particles (wt) and the other of viral particles treated with the palmitoyl analogue (pwt).

In Figure 4.6, a representative result of the yield of a viral particle purification treated with the palmitoyl-modified analogue by a quantitative Western blot analysis probed against CA is shown.
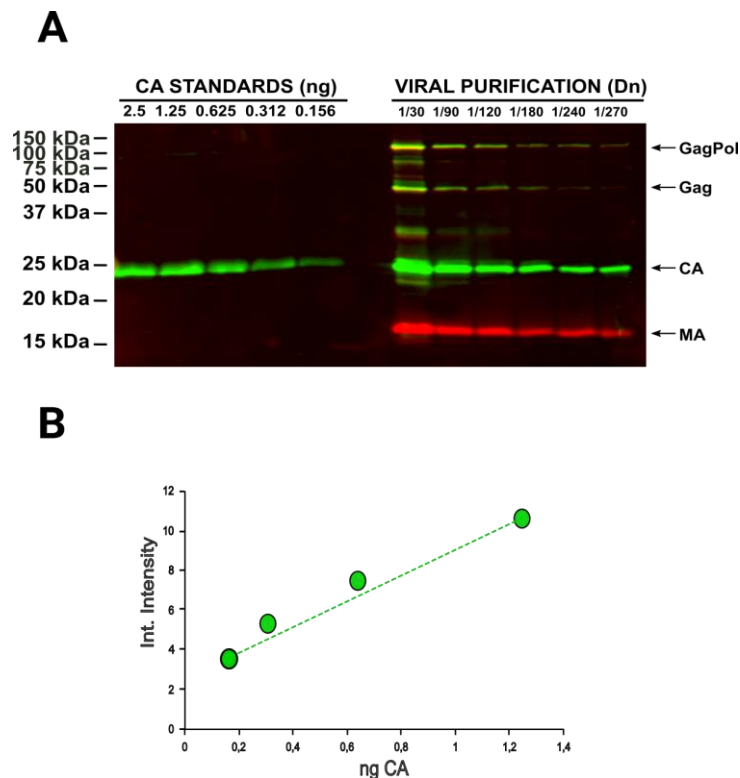
Figure 4.6. Representative CA quantification by Western blot of a purified viral sample treated with the palmitoyl-modified analogue (A). 2.5, 1.25, 0.625, 0.312, and 0.156 ng of CA protein is loaded as a standard to generate a calibration curve (**B**). In the same Western blot, 1/30, 1/90, 1/120, 1/180, 1/240, and 1/270 dilutions of pwt are loaded. The Western blot is developed against CA and MA using sheep α-CA and rabbit α-MA as primary antibodies, and α-sheep IRDye800 and α-rabbit IRDye680 as secondary antibodies.

The amount of CA for the first treated viral and the last wild-type viral purification (Figure 4.6) after Western blot quantification was less than 3 µg of CA. Hence, they were discarded to mix in the viral pull. The rest of viral purifications were put together to form the two viral pulls, one pull for the untreated viral particles that will be used as control and another for the treated viral particles (Figure 4.7). The amount of CA for each pull after Western blot quantification was around 20-25 µg of CA.
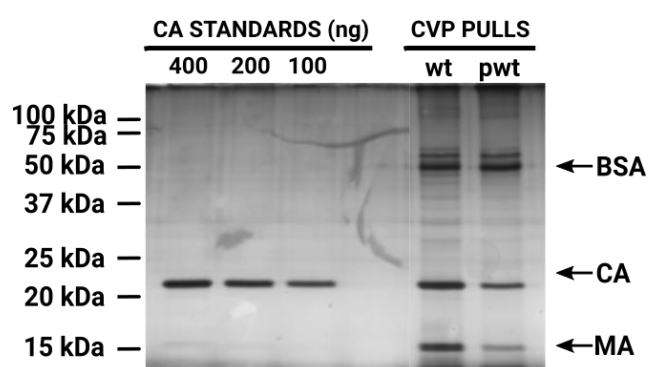
Figure 4.7. Representative silver stain of viral purification pulls. Several concentrated viral purifications of non-treated wild-type VLPs (wt) and VLPs treated with the palmitoyl-modified analogue (pwt) were mixed to form a pull of each other.

4.3.2. Verification of palmitoylated HIV-1 gp41 by CuAAC reaction

The treated pull was tested to verify the positive palmitoylation of gp41 cysteines by CuAAC reaction, using the wild type pull as a negative control. Both samples suffered CuAAC reaction together with the immunoprecipitation of gp41 by Chessie-8 coupled beads, as explained in Section 4.2.3.1.

Figure 4.8 B is a representative schema of final tagged HIV-1 gp41 treated with the palmitoyl analogue, which has been clicked with a fluorophore and after Western blot analysis against gp41. The final results of gp41 palmitoylation test are shown in Figure 4.8 A. The Western blot was developed against Chessie-8 α-gp41 primary antibody and α-mouse IRDye680 antibody as secondary antibody. The palmitoyl-modified analogue was clicked using IRDye 800CW®Azide Infrared Dye. Immunoprecipitated protein gp41 was visualized in the red channel (700 nm), and the palmitoyl-modified analogue bound to gp41 cysteines was visualized in the green channel (800 nm). A corresponding

band to gp41 at ~41-50 kDa can be clearly observed in both channels in the treated viral pull, and it is not present in the green channel in the case of wild type viral pull. Moreover, a band of low protein size (~15-20 kDa) corresponds to a truncated cytoplasmic domain of gp41 that has been described to derive from the full-length protein by proteolytic degradation, named Tr-Env-CT by the authors that first discovered it (Pfeiffer et al., 2013). Tr-Env-CT is also palmitoylated because it includes Cys-764 and Cys-837 residues. Therefore, it could be concluded **that the palmitoyl-modified analogue could palmitoylate cysteines as its natural counterpart and its function could be successfully detected by the palmitoylation test developed based in the CuAAC reaction**.
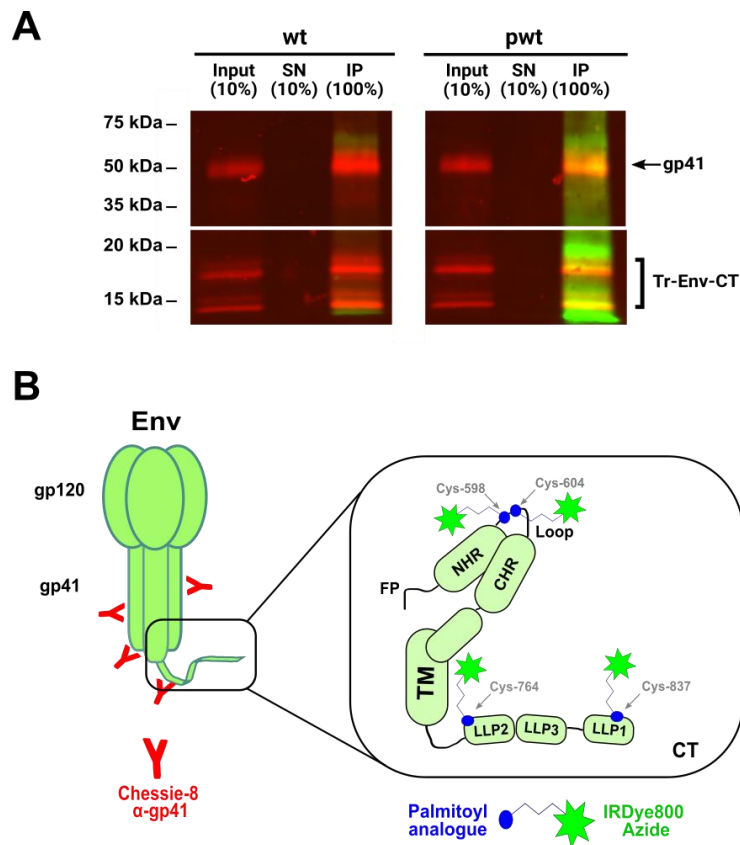
Figure 4.8. Palmitoylated gp41 in treated CPV with the alkyne-modified palmitoyl analogue. A) Western blot images of the input, supernatant (SN) and immunoprecipitate (IP) for Env gp41 protein in wild type VLPs (wt) and VLPs treated with the palmitoyl-modified analogue (pwt). The Western blot was developed with Chessie-8 α-gp41 primary antibody and anti-mouse IRDye680 antibody as a secondary antibody (red). The palmitoyl-modified analogue was clicked using IRDye 800CW Azide Infrared Dye (green). **B)** Representative schema of tagged VLPs treated with the palmitoyl analogue, which has been clicked with a fluorophore (IRDye800), and after Western blot analysis against gp41.

4.3.3. Designing a protocol for HIV-1 palmitoylated proteins extraction

After verifying the correct palmitoylation of HIV-1 gp41, the next step corresponds to set up a protocol for extracting the palmitoylated proteins present in HIV-1 virions before proteomic analysis by mass spectrometry. Subsequent experiments were carried out with the same amounts of CA for wt and pwt samples, normally 1 μg of CA unless a different quantity was specified.

4.3.3.1. Protocol based on Click-&-Go™ approach

The first protocol was developed based on the Click-&-Go™ Dde Protein Enrichment Kit (Click Chemistry Tools, #1152). This kit is a biotin/streptavidin-free tool for capturing azide-modified proteins on a cleavable agarose resin via CuAAC reaction and its subsequent release under mild conditions. The protocol proposed was the following:

1. The wt and pwt viral samples were lysed by incubation for 1 h at 4 °C in constant rotation with modified RIPA lysis buffer supplemented with protease inhibitors.

2. The resulting viral proteins were precipitated using the protocol of Wessel & Flügge (1984) to eliminate undesired lipids that have been competing with the palmitoyl-modified analogue. The pellet was resuspended in 100 μL of PBS Ca^{2+}/Mg^{2+}-free + 1% (w/v) SDS by constant stirring at RT.

3. The total protein content of the samples was measured by Pierce BCA Protein Assay kit (Thermo Fisher Scientific, #23227) using a Synergy™ HT spectrophotometer (BIO-TEK, Aligent Technologies).

4. 50 μL of Dde Azide Agarose resin from the Click-&-Go™ Dde Protein Enrichment Kit, was washed with PBS (Ca^{2+}/Mg^{2+}-free) + 1% (w/v) SDS.

5. The protein samples were added to the beads, and to perform the click reaction, the reagents were incorporated in the following order, vortexing softly after each addition: 1.4 μL of TBTA 0.1 mM, 1.4 μL of $CuSO_4$ 1 mM, and 1.4 μL of ascorbic acid 10 mM. The remaining oxygen is displaced by nitrogen, and the CuAAC reaction was incubated overnight at RT in the dark with constant stirring, at 1,400 rpm.

6. Washing five times with Agarose Wash Buffer with SDS is used for stringent removal of non-specifically bound proteins. After this was, it is critical to remove residual

SDS by washing exhaustively with 8 M urea + 100 mM Tris pH 8,0 and 20% acetonitrile.

7. The cleavage and elution of the resin-bound proteins was done by resuspension of the beads in elution buffer composed of 100 mM sodium phosphate + 2% (v/v) hydrazine. The mixture was incubated 90 min at RT in constant stirring.

8. The final protein content of the samples was measured by NanoDrop™ 2000 (Thermo Fisher Scientific), and a silver stain and a Western blot were performed to confirm the extraction of palmitoylated proteins.

The protocol based on the Click-&-Go™ Dde Protein Enrichment Kit was tested several times starting from different amounts of the viral capsid, being the same amount of CA for both wild type and treated viral samples. The quantities of viral CA varied from 1 to 18 μg.

Although the amounts of initial sample used were increased, the same results were obtained. There was no appreciable signal in the silver stain for the extracted proteins at any of the different CA quantities tested (Figure 4.9 A). This absence of signal in the silver stain could be explained by the continuous loss of sample during the different steps of the protocol (chloroform/methanol extraction and washes), making unappreciable the final amount of pwt by silver stain characterization.
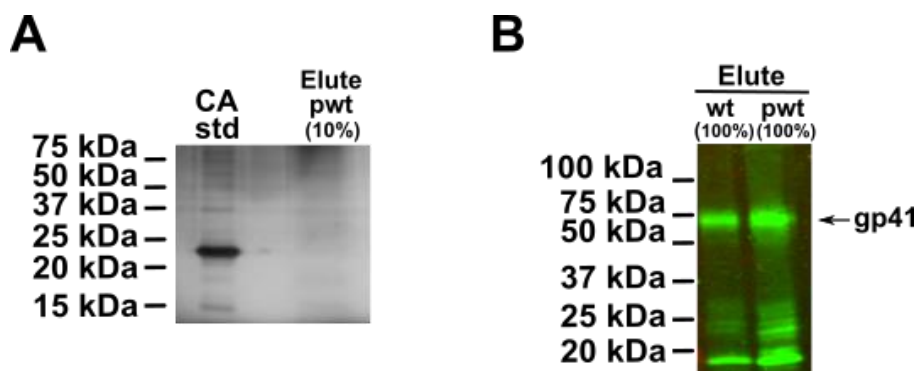
Figure 4.9. Representative results after applying protocol based on Click-&-Go™ strategy. A) Silver stain of the 10% of the eluted VLPs treated with the palmitoyl analogue (pwt). The initial amount of pwt used was 3 μg of CA. 400 ng of CA were loaded as standard (CA std). **B)** Western blot against gp41 of wild type (wt) and treated (pwt) eluted samples after protein extraction with the protocol. The Western blot was developed with Chessie-8 α-gp41 primary antibody and α-mouse IRDye800 secondary antibody. The initial amount of both wt and pwt used were 18 μg of CA.

In addition, the amount of protein expected at the eluted samples should be higher in the palmitoylated ones. However, the difference between wild type and treated samples was slightly inappreciable after quantification by the NanoDrop™ 2000 (Thermo Fisher Scientific), where the concentrations were both around 2-3 µg/µL. A Western blot against gp41 of the eluted samples was performed (Figure 4.9 B) that corroborated previous measurements by showing a similar fluorescence signal in both wt and pwt even though no signal was expected in wild type viral particles. The resulting signals in wt and pwt should be caused by a background coming from the different protocol steps.

Moreover, this protocol was tested in cells, starting from wt and pwt cellular lysates corresponded to one 10 cm dish seeded with $3,5\cdot10^6$ cells each. As explained in Section 4.2.2, HEK 293T cells were seeded, transfected with a proviral plasmid, and treated with the palmitoyl analogue. After 24 h of incubation, the medium was removed and cells were washed with PBS, and cold PBS supplemented with protease inhibitor cocktail was added. These cells were then scraped, pelleted, and resuspended in 200 µL of lysis buffer. Cells were lysed by incubation for 1 h at 4 °C in constant rotation with modified RIPA lysis buffer supplemented with protease inhibitors and 0.125 µL of Benzonase® Nuclease ≥250 U/µL (Sigma-Aldrich, #E1014-5KU). These wt and pwt lysates suffered the same protocol as mentioned at the beginning of this section. No signal was obtained neither in the silver stain nor in the Western blot for pwt sample, supporting the previous results shown in Figure 4.9.

After aforementioned results, **this first protocol-based on the Click-&-Go™ strategy seemed not to be the appropriate for extracting palmitoylated proteins from HIV-1 viral particles**.

4.3.3.2. Protocol based in biotin/avidin approach

The second protocol was developed based on one of the strongest non-covalent interactions: biotin-avidin binding. Its high affinity is robust and stable against

manipulation, proteolytic enzymes, temperature, pH, harsh organic reagents, and other denaturing reagents (Hiller et al., 1987; Jain & Cheng, 2017).

For this purpose, Pierce™ High Capacity NeutrAvidin™ Agarose Resin (ThermoFisher Scientific, #29204) and Disulfide Biotin Azide (Click Chemistry Tools, # 1168-1) probes were used. NeutrAvidin is a chemically modified version of avidin, which is not glycosylated, and it has a near-neutral isoelectric point (pI = 6.3) that confers a minimal non-specific binding. As a result of carbohydrate removal, lectin binding is reduced to undetectable levels, yet biotin-binding affinity is retained because the carbohydrate is not necessary for this activity. The experimental protocol proposed was the following:

1. Wt and pwt viral samples were lysed by incubation for 1 h at 4 °C in constant rotation with modified RIPA lysis buffer supplemented with protease inhibitors.

2. The resulting viral proteins were precipitated using the protocol of Wessel & Flügge (1984). The pellet was resuspended in 100 μL of PBS Ca^{2+}/Mg^{2+}-free + 1% (w/v) SDS by constant stirring at RT.

3. The total protein content of both samples was measured by the Bradford protein assay (Bradford, 1976).

4. The click reaction was performed in the samples, reagents were incorporated in the following order, vortexing softly after each addition: 0.15 μL of fluorescent probe disulfide biotin azide 14.43 mM, 2 μL of TBTA 0.1 mM, 2 μL of Cu(II)S0$_4$ 1 mM and 2 μL of ascorbic acid 10 mM. The CuAAC reaction was incubated 1 h at RT in the dark with constant stirring at 1,400 rpm.

5. Another step of chloroform/methanol extraction was performed to get rid of CuAAC reactives. It is performed as the previous one following the protocol of Wessel & Flügge (1984). The protein content was measured again by Bradford protein assay.

6. NeutrAvidin™ Agarose Resin was washed three times with PBS Ca^{2+}/Mg^{2+}-free buffer, and the samples were added to the beads and incubated overnight at 4 °C in constant stirring.

7. The beads were recovered by centrifugation, 10 min 6,500 rpm, and then they were washed with RIPA lysis buffer three times by centrifugation, 3 min at 6,5000 rpm. The supernatant was stored as 'SN'.

8. The immunoprecipitated samples were recovered by adding SDS-PAGE sample buffer, incubating 5 min at 95 °C, and being centrifuged 10 min at 6,500 rpm. The composition of SDS-PAGE sample buffer is 125 mM Tris-HCl, pH 6.8, 20% (v/v) glycerol, 4%(w/v) SDS, 10% (v/v) β-mercaptoethanol and 0.5 mg/ml of Bromophenol Blue (Sigma-Aldrich).

Starting from 12 µg of CA, it is estimated that after clicking and extractions, about 6 µg of CA are lost, calculated from the total protein after Bradford assay, in the case of the viral samples treated with the palmitoyl analogue. For wild type samples, the loss is less, going from 12.1 µg of CA to 9.6 µg after the process. The intensity obtained in both cases in the eluate is practically identical (Figure 4.10). In addition, the large amount of non-immunoprecipitated sample that remains in the supernatant was detectable. Therefore, **this first attempt in developing a protocol based in the biotin-NeutrAvidin binding strategy is not the accurate for extraction of palmitoylated proteins due to sample loss and shortage of immunoprecipitated proteins in the eluate compared to the supernatant**.
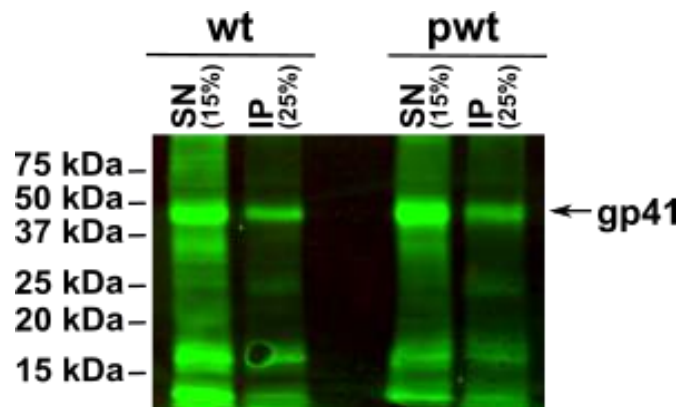
Figure 4.10. Representative results after the biotin-NeutrAvidin approach. Western blot against gp41 of wild type (wt) and treated (pwt) immunoprecipitated samples after protein extraction with the second tested protocol-based on biotin-neutravidin binding. The Western blot was developed with Chessie-8 α-gp41 primary antibody and α-mouse IRDye800 secondary antibody. SN = Supernatant; IP = Immunoprecipitate.

To improve the first trial with this approach, the protocol suffered several modifications based on Haberkant et al. (2016) and the manufacturer's datasheet of the

Pierce™ High Capacity NeutrAvidin™ Agarose Resin (ThermoFisher Scientific, #29204) as shown in Table 4.2.

Table 4.2. First modifications to biotin/NeutrAvidin extraction protocol.

	Initial	**1st Modified**
Cell lysis	1 h 4 °C	1 h RT
CuAAC reaction	1 h RT	3 h 37 °C
CH₃Cl/MeOH extractions after click	1	2
Adjust %(w/v) SDS	No	0.1%
NeutrAvidin agarose beads	Overnight 4 °C	1 h RT
Washes	3 times	10 times
Elution	SDS-PAGE sample buffer, 5 min 95 °C	2% (v/v) β-mercaptoethanol solution, 1 h RT

These new modifications were applied to different amounts of CA, starting from 1 µg to 4 µg. Even so, the difference between wt and pwt was still low (Figure 4.11 A). In addition, there was still a signal in wild type elute that indicates a nonspecific union of the NeutrAvidin agarose beads.
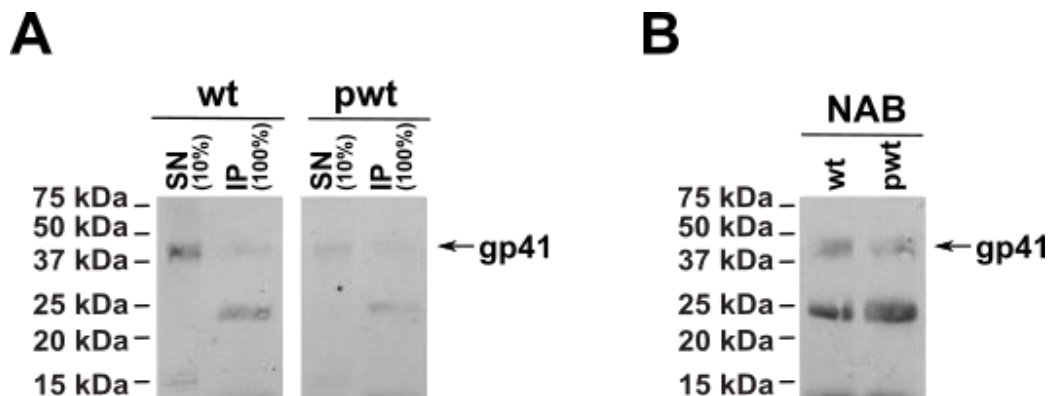
Figure 4.11. Representative results of the modifications to the biotin-NeutrAvidin approach. A) Western blot against gp41 of wild type (wt) and treated (pwt) immunoprecipitated samples after protein extraction with a modified protocol based on biotin-NeutrAvidin binding. SN = Supernatant; IP = Immunoprecipitate. **B)** Western blot of the resting NeutrAvidin agarose beads (NAB) of wild type and treated samples from the applied protocol after the addition of SDS-PAGE sample buffer, incubation for 5 min at 95 °C and 10 min centrifugation at 6,500 rpm. Both Western blots were developed with Chessie-8 α-gp41 primary antibody and α-mouse IRDye800 secondary antibody.

As low antigen yield was observed, it was a suspicion that the proteins were still bound on the beaded support. The best way to confirm this is by boiling a small aliquot of the beads in an extremely harsh buffer such as SDS-PAGE sample buffer. The beads can then be centrifuged, and the supernatant analysed by Western blot to confirm the presence or absence of the antigens. So, to test the elution step, the NeutrAvidin agarose beads used for wt and pwt samples were subjected to incubation for 5 min at 95 °C and 10 min centrifuging at 6,500 rpm (Figure 4.11 B). After this process, it could be seen that **most of the proteins were not eluted with β-mercaptoethanol elution buffer, which indicates that the elution buffer conditions might not be the adequate for the extraction**.

To try to eliminate this non-specificity of the NeutrAvidin agarose beads, the experiment was repeated, but in this case, a sample pre-clearing step was added prior to the incubation with the NeutrAvidin agarose beads. Sample pre-clearing is a step designed to remove proteins and ligands that bind non-specifically to the beaded support (Harlow & Lane, 2006). It is performed on the sample before the binding complex is assembled. Pre-clearing generally involves incubating the sample with plain beads (i.e., the base support to be used for the immunoprecipitation reaction or Protein A/G beads without coupling to an antibody) before performing the experiment. If successful, off-target proteins or other components of the sample that bind non-specifically to the resin will be removed by this pre-clearing step so that they will not co-purify with the target antigen in the subsequent immunoprecipitation. Then, both wt and pwt were incubated 1 h at RT with Protein G Sepharose beads as plain beads to eliminate anything that could non-specifically stick to the NeutrAvidin agarose beads. After incubation, these beads were stored for possible further analysis. Another way to prevent non-specific binding to the leftover spaces in the resin, is to add a blocking step for the beads to the protocol. BSA blocking is a common routine when performing immunoassays to avoid undesired unions (Ahirwar et al., 2015), so NeutrAvidin agarose beads were blocked with 2% (w/v) for 1 h at RT before incubation with each viral sample.

By applying the modifications described above, the signal obtained in the elute of the treated sample was totally reduced (Figure 4.12 A). The most plausible cause was the sample pre-clearing with Protein G Sepharose beads. To further analyse this effect, those

beads were incubated for 5 min at 95 °C in SDS-PAGE sample buffer. As expected, almost all proteins were attached to the beads, leading to the conclusion that the proteins of interest were also stuck there (Figure 4.12 B). Thus, **sample pre-clearing with Protein G Sepharose beads could not be used to eliminate non-specific binding to NeutrAvidin agarose beads in the protocol because their own stickiness was affecting protein extraction by sequestering almost complete the palmitoylated proteins of interest**.
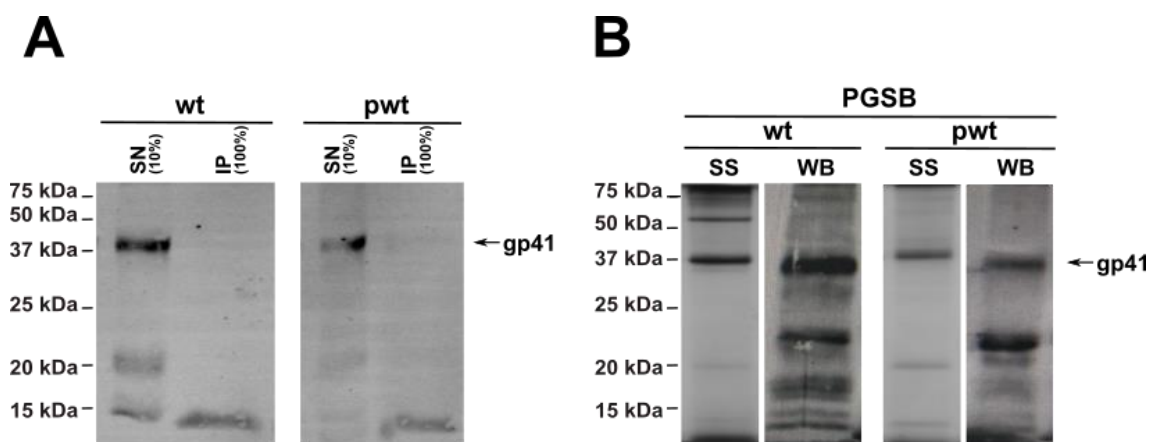
Figure 4.12. Representative results after adding the sample pre-clearing and blocking steps to the protocol. A) Western blot against gp41 of wild type (wt) and treated (pwt) immunoprecipitated samples after protein extraction with a modified protocol based in biotin-NeutrAvidin binding after incorporating a pre-clearing step of the samples by incubation 1h at RT with Protein G Sepharose beads and a blocking step of the NeutrAvidin agarose beads by incubation 1 h at RT with 2% (w/v) BSA. SN = Supernatant; IP = Immunoprecipitate. **B)** Silver staining and Western blot of the Protein G Sepharose beads (PGSB) used for blocking of wild type and treated samples after the addition of sample buffer, incubation for 5 min at 95 °C, and 10 min centrifugation at 6,500 rpm. Both Western blots were developed with Chessie-8 α-gp41 primary antibody and α-mouse IRDye800 secondary antibody.

According to the results above, the sample pre-clearing was discarded. Even though notable differences could be seen in the protein pattern obtained in the silver stain after repeating the protocol only blocking with 2% (w/v) BSA (Figure 4.13), a persistent reduced signal was still obtained in the Western blot against gp41 in the samples treated with the palmitoyl analogue as in previous experiments shown in Figures 4.11 & 4.12. However, **the blocking step with 2% (w/v) BSA would be maintained as a step in the final protocol** due to the fact that it increased the differences

between the control and the treated extracted pattern proteins obtained in the eluate and it also reduced background signal from undesired antigens that could attach to the NeutrAvidin agarose beads.
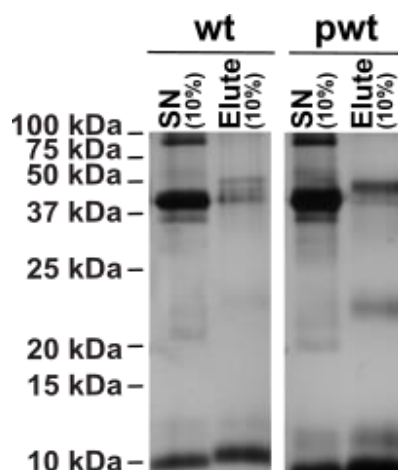
Figure 4.13. Blocking step of NeutrAvidin agarose beads with BSA. Silver staining of wild type (wt) and treated (pwt) samples after the modified protocol by blocking the NeutrAvidin agarose beads with 2% (w/v) BSA during 1 h at RT. SN = Supernatant.

To improve and solve previous issues, the actual protocol suffered again several modifications, as shown in Table 4.3.

Table 4.3. Second modifications to biotin-NeutrAvidin extraction protocol.

	1st Modified	**2nd Modified**
CH_3Cl/MeOH extraction method	Wessel & Flugge (1984)	Haberkant et al. (2015)
CH_3Cl/MeOH extraction before click	Yes	No
CuAAC probe	Disulfide biotin-azide (Click Chemistry Tools, # 1168-1)	TAMRA biotin-azide (Click Chemistry Tools, # 1048-1)
CH_3Cl/MeOH extractions after click	2	1
Blocking NAB with 2%(w/v) BSA	No	1 h RT
Incubation SN with NAB	No	Overnight 4 °C
Elution	β-mercaptoethanol solution, 1 h RT	SDS-PAGE Sample buffer, 15 min 95 °C

NAB = Neutravidin-agarose beads; SN = Supernatant after first incubation with NAB.

143

Among these modifications, it is necessary to highlight the use of 200 µM TAMRA Biotin Azide (Click Chemistry Tools, # 1048-1) instead of disulfide biotin azide due to this probe allows to test fluorescence of both samples with VersaDoc™ MP Imaging System (Bio-Rad) after SDS-PAGE electrophoresis. So, before the Western blot, the fluorescent signal was measured in gel to obtain a first clue of how the modified protocol has been performed. If the CuAAC reaction was properly worked, a fluorescent signal corresponding to the treated viral sample should appear (Figure 4.14 A). However, there was no signal at all. The plausible reason could be that the amount of sample used for the experiment was not enough to detect its signal, or another reason could be that the click chemistry reaction was not well-performed. After the Western blot of this new modified protocol, there was still no signal in the elute and re-elute of the treated sample with the palmitoyl analogue (Figure 4.14 B). The re-elution consisted on an incubation overnight at 4 °C of the supernatant of the first incubation with the NeutrAvidin agarose beads with another aliquot of blocked NeutrAvidin agarose beads, and proceed with the protocol as with the first ones.
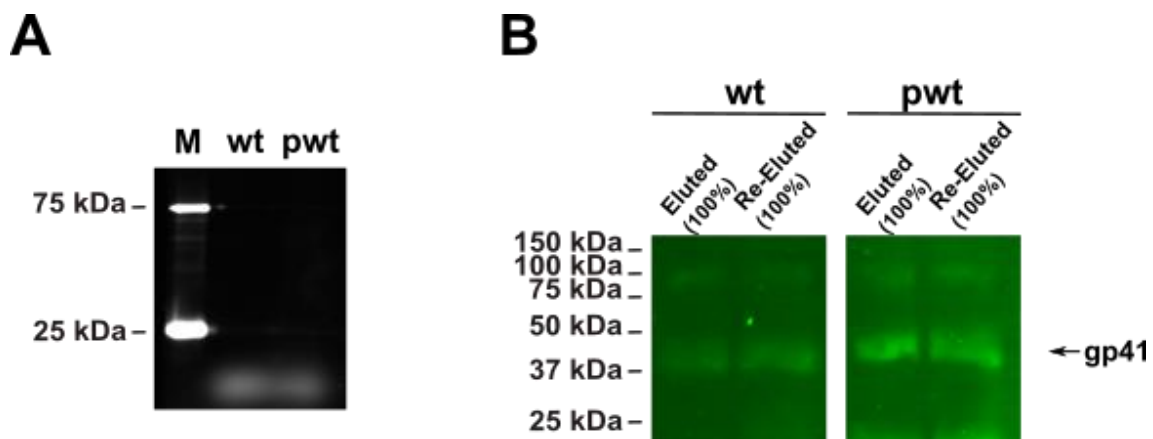
Figure. 4.14. Modified protocol for extracting palmitoylated proteins using TAMRA biotin azide as click chemistry probe. A) Image of fluorescence test of both wild type (wt) and treated (pwt) samples with VersaDoc™ MP Imaging System (Bio-Rad). M = Molecular weight marker, Precision Plus Protein Dual Color Standards (BioRad). **B)** Western blot of both eluted and re-eluted viral particles of wild type (wt) and treated with the palmitoyl analogue (pwt) after the modified extraction protocol including click chemistry with TAMRA biotin azide and a re-elution step of the supernatant of the first incubation with neutravidin-agarose beads. The Western blot was developed with Chessie-8 α-gp41 primary antibody and α-mouse IRDye800 antibody as secondary antibody.

To corroborate that the click chemistry was correctly working in the viral purifications treated with the palmitoyl analogue, a test based on the CuACC reaction with a fluorophore was performed. The development of this fluorophore test was based on (Presolski et al., 2011) and the idea of performing the click chemistry in beads, as in the protocol for the detection of palmitoylated HIV-1 gp41 (Section 4.2.3.1) but in this case, there is no antibody coupled to Protein G Sepharose beads. Here, we are taking advantage of the stickiness of these beads as proved in Figure 4.12 B. Extracted samples were incubated 1 h at RT with Protein G Sepharose beads before CuAAc reaction. In this manner, the vast majority of the proteins in the sample would attach to the beads, including palmitoylated ones. The click chemistry would be performed in the beads with a fluorophore. Thus, palmitoylated proteins would give a fluorescent signal in the Western blot, confirming CuAAC reaction worked perfectly. The complete protocol for the fluorophore test was the following:

1. Lysate viral particles for 1h at RT and shaking. Lysis buffer: 200 μL of PBS (Mg^{2+}/Ca^{2+} free) + 1%(w/v) SDS + protease inhibitors.

2. Extract with $CHCl_3$ and MeOH following Haberkant et al. (2016) and resuspend in 100 μL of PBS (Mg^{2+}/Ca^{2+} free) + 1% SDS in the thermomixer. Store 5% of the sample as 'input'.

3. Adjust the rest of the sample to a final SDS concentration of 0.1% (w/v).

4. Wash 50 μL of Protein G Sepharose beads with PBS (Mg^{2+}/Ca^{2+} free).

5. Mix the adjusted sample with the washed Protein G Sepharose beads. Incubate 1h at RT.

6. Centrifuge at 6,500 rpm for 5 min and recover unbound supernatant. Store the supernatant as 'SN'.

7. Wash beads two times with 500 μL of PBS (Mg^{2+}/Ca^{2+} free) by centrifuging at 6,500 rpm for 3 min each wash.

8. Resuspend the beads in 300 μL of PBS (Mg^{2+}/Ca^{2+} free).

9. Perform click chemistry with IRDye® 800 CW Azide (LI-COR, #929-65000). Incubate for 1h at RT and shake in the thermomixer.

10. Centrifuge at 6,500 rpm for 5 min and recover the supernatant with the click chemistry reactants. Store the supernatant as 'After Click SN'.

11. Wash beads two times with 500 µL of PBS (Mg^{2+}/Ca^{2+} free) by centrifuging at 6,500 rpm for 3 min each wash.

12. To elute samples, 30 µL first and then 20 µL of low β-mercaptoethanol SDS-PAGE sample buffer were incubated for 15 min with constant shaking at RT, were heated for 15 min at 95 °C, and centrifuged at 6,500 rpm for 10 min at RT. Mix volumes and store as 'Eluted.'

13. Develop a Western blot with α-gp41 Chessie-8 and incubate overnight at 4 °C. Use as secondary antibody α-mouse IRDye.

Figure 4.15 B shows representative results of applying protocol for the fluorophore test to 1 µg of CA of concentrated viral particles of wild type and treated viral particles. Only a positive signal in the eluted sample of treated viral particles with the palmitoyl analogue was obtained (Figure 4.15 A), which supports that **the CuAAC reaction is perfectly working and specific for palmitoylated proteins since there is no signal in the eluted sample of wild type viral particles**. In addition, **the developed fluorophore test protocol could be adapted to confirm the adequate functioning of the CuACC reaction for other clickable lipid probes similar to the palmitoyl-modified analogue**.
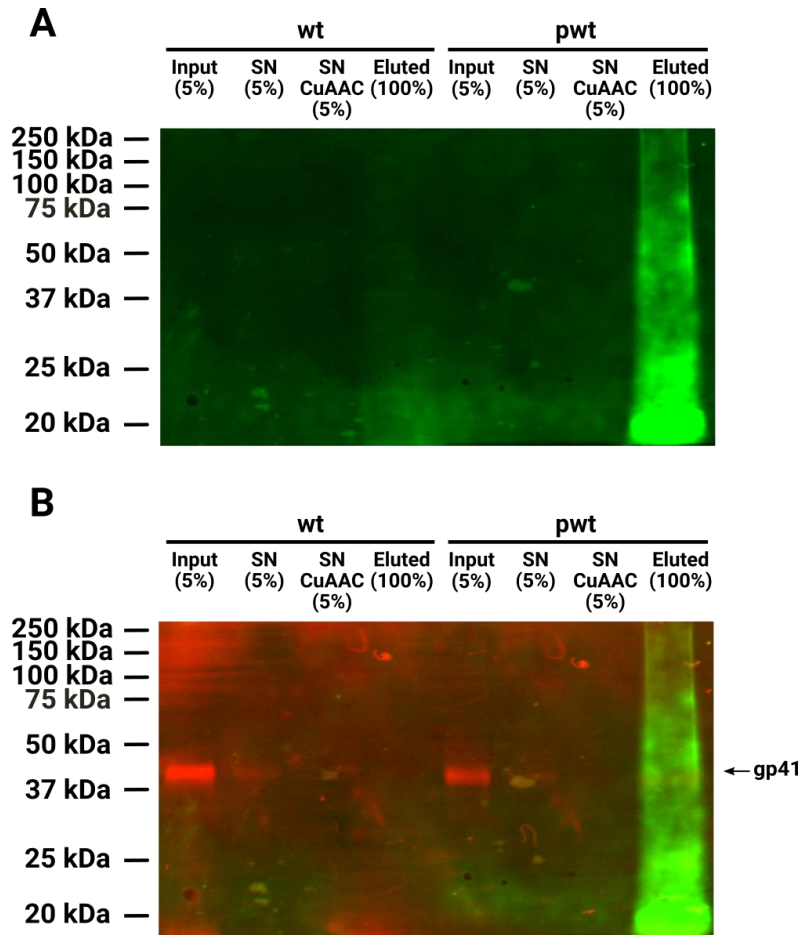
Figure 4.15. Click chemistry test with the palmitoyl analogue and a fluorophore. Western blot image of gp41 (red) and palmitoylated extracted proteins (green) in wild type and treated concentrated viral particles (**B**). Different samples were saved at different steps of the protocol for both wild type and treated samples: initial CVP corresponding to 0.5 µg of CA before lysis (input), supernatant after chloroform/methanol extraction (SN), supernatant after CuAAC reaction with IRDye 800CWAzide Infrared Dye (SN CuAAC) and elution from Protein G Sepharose beads (Eluted). The Western blot was developed with Chessie-8 α-gp41 primary antibody and α-mouse IRDye800 antibody as a secondary antibody. Only positive signal in the elute of CVP treated with the palmitoyl analogue (**A**) supports that the CuAAC is specific for palmitoylated proteins.

As CuAAC reaction was not the bottleneck of the protocol, it let to think of another limiting factor that could be the incubation with the NeutrAvidin agarose beads. As seen before, the incubation with Protein G Sepharose beads seemed adequate to catch the proteins from the sample and perform the click chemistry on them. Therefore, new modifications were done to the protocol for extracting palmitoylated proteins, including incubation with Protein G Sepharose beads after the first extraction with chloroform/methanol. To fish only clicked proteins from the beads, another method of

separation was needed. The competition between the Protein G Sepharose beads and High Capacity Streptavidin Magnetic Beads (Click Chemistry Tools, #1497) was proposed. These magnetic beads have one of the highest biotin-binding capacities in the market, binding at least 12 nmol of free biotin per milligram of beads. In addition, they could be easier captured and separated from the Protein G Sepharose beads due to their excellent magnetic properties. Streptavidin is similar to avidin, but it is isolated from *Streptomyces avidinii* with a mass of 75 kDa and has no carbohydrate, with a mildly acidic pI (5.5) (Green, 1975). The complete modified protocol, including the incubation with Protein G Sepharose beads and with magnetic streptavidin beads, was the following:

1. Lysate viral particles for 1h at RT and shaking. Lysis buffer: 200 μL of PBS (Mg^{2+}/Ca^{2+} free) + 1%(w/v) SDS + protease inhibitors.

2. Extract with $CHCl_3$ and MeOH following Haberkant et al. (2015) and resuspend in 100 μL of PBS (Mg^{2+}/Ca^{2+} free) + 1% SDS in the thermomixer. Store 10% of the sample as 'input'.

3. Adjust the rest of the sample to a final SDS concentration of 0.1% (w/v).

4. Wash 50 μL of Protein G Sepharose beads with PBS (Mg^{2+}/Ca^{2+} free).

5. Mix the adjusted sample with the washed Protein G Sepharose beads. Incubate 1 h at RT.

6. Centrifuge at 6,500 rpm for 5 min and recover unbound supernatant. Store the supernatant as 'SN.'

7. Wash beads two times with 500 μL of PBS (Mg^{2+}/Ca^{2+} free) by centrifuging at 6,500 rpm for 3 min each wash.

8. Resuspend the beads in 300 μL of PBS (Mg^{2+}/Ca^{2+} free).

9. Perform click chemistry with TAMRA biotin azide. Incubate for 3 h at 37 °C and shake in the thermomixer.

10. After the click, centrifuge at 6,500 rpm for 5 min and recover the supernatant with the click chemistry reactants. Store the supernatant as 'After Click SN'.

11. Wash Protein G Sepharose beads three times with 500 μL of PBS by centrifuging at 6,500 rpm for 3 min each wash. Resuspend the beads in 300 μL of PBS (Mg^{2+}/Ca^{2+} free).

12. Blocking with 2% (w/v) BSA of magnetic streptavidin beads previously washed with PBS. 1 h at RT.

13. Add the diluted Protein G Sepharose beads to the dry magnetic streptavidin beads. Mix several times before incubating 1 h at RT and shaking.

14. Before recovering magnetic streptavidin beads, mix several times more. Recover the supernatant and the Protein G Sepharose beads. Store the supernatant as 'beads SN' and the beads as 'prot.G beads'.

15. To elute samples, 30 µL first and then 20 µL of SDS-PAGE sample buffer were incubated for 15 min with constant shaking at RT, were heated for 15 min at 95 °C, and centrifuged at 6,500 rpm for 10 min at RT. Mix volumes and store as 'Eluted'

Figure 4.16 shows a representative Western blot of applying the last modified protocol to 1 µg of CA of concentrated viral particles of wt and pwt. A positive signal for gp41 in the elute of the treated viral sample supports that the optimized protocol has properly worked, and it could be used to extract palmitoylated proteins due to no signal was present in the elute of wild type viral samples. So, **incubation with NeutrAvidin agarose beads was discarded and substituted by the new competing strategy of Protein G Sepharose beads with streptavidin magnetic beads, as it correctly worked for extraction of HIV-1 palmitoylated proteins**.
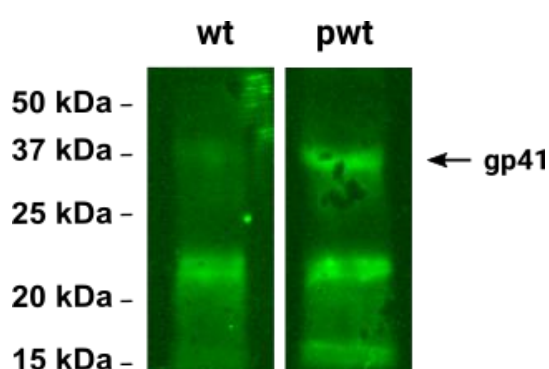
Figure 4.16. Representative results of competing strategy for the extraction of palmitoylated proteins. Western blot of both eluted viral particles of wild type (wt) and treated with the palmitoyl analogue (pwt) after the modified extraction protocol, including the steps of incubation with Protein G Sepharose beads and biotin-streptavidin binding with streptavidin magnetic beads. The Western blot was developed with Chessie-8 α-gp41 primary antibody and α-mouse IRDye800 antibody as secondary antibody.

Even though the last protocol seemed to be the most adequate for the extraction of HIV-1 palmitoylated proteins, other modifications were done to improve the yield.

The CuAAC reaction was developed using TBTA (Click Chemistry Tools) as stabilizing ligand for copper(I) until now. TBTA needs to be diluted in DMSO, so it could not be used in a complete aqueous conjugation reaction. On the other hand, THPTA (Click Chemistry Tools) is soluble in water, and it is used in a 5:1 ratio (ligand to copper) (Presolski et al., 2011), while TBTA is used in a 2:1 ratio, so the quantity of copper needed for the CuAAC reaction is quite less. Therefore, to test the potential of THPTA in the extraction protocol, the copper-based click reaction was performed with TAMRA biotin azide (stock 5 mM, assay 15 µM) and all the reagents diluted in MiliQ H_2O, whose concentrations required in the assay are detailed in Table 4.4. In addition, the incubation time was reduced to 1 h at 37 °C instead of 3 h.

Table 4.4. Reagents for CuACC reaction with THPTA.

	[Stock]	[Assay]
Ascorbic acid	0.5 M	5 mM
$CuSO_4$	10 mM	0.1 mM
THPTA	50 mM	0.5 mM

Figure 4.17 shows the results obtained after applying the last modified protocol to 1 µg of CA of concentrated viral particles of wt and pwt, where the CuAAC reaction was done with THPTA. In the Western blot, <u>**a positive signal for gp41 in the elute of the treated viral particles could be seen**</u> and it was not present in the elute of wild type viral particles, <u>**which means the correct extraction of palmitoylated proteins with the modified protocol**</u> (Figure 4.17 A). So, it confirmed that <u>**this protocol could also be performed with THPTA instead of TBTA**</u>, and the <u>**click chemistry reaction could be reduced to 1 h at 37 °C**</u>. Moreover, a huge difference in the protein pattern between the eluted wt and the eluted pwt could be detected in the silver staining (Figure 4.17 B). Therefore, <u>**treated samples extracted with this optimized protocol seem to be enriched in potentially palmitoylated proteins**</u>.
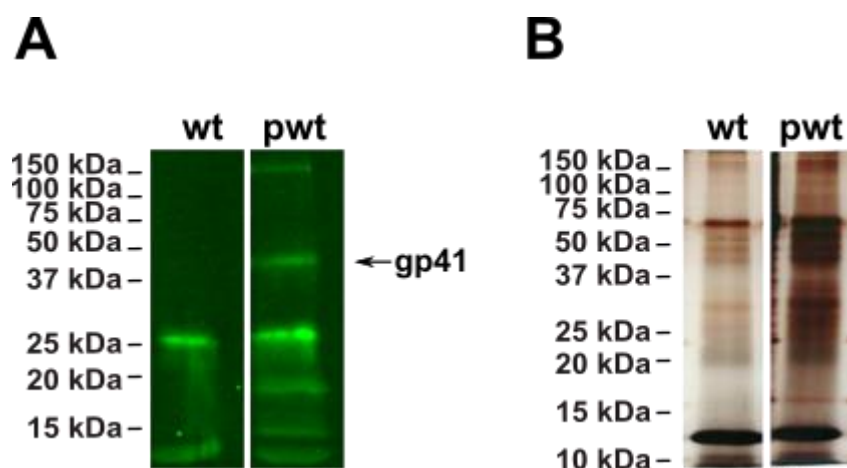
Figure 4.17. Representative results of optimized protocol for extracting palmitoylated proteins using THPTA as a copper ligand in the click reaction. Western blot (**A**) and silver stain (**B**) of both eluted viral particles of wild type (wt) and treated with the palmitoyl analogue (pwt) after the last modified extraction protocol using THPTA instead of TBTA. Western blot was developed with Chessie-8 α-gp41 primary antibody and α-mouse IRDye800 secondary antibody.

Another modification to enhance the protocol consisted in testing the effectiveness of the click chemistry in solution instead of in the Protein G Sepharose beads. Thus, after the lysis of both samples, the CuAAC reaction was carried out with THPTA as before. Then, a chloroform/methanol extraction was performed. To determine if part of the targeted proteins were kept in the supernatant (SN) instead of in the pellet (P), which is the phase of the extraction that was used to proceed with all the rest of the protocols developed until now. Both SN and P were saved and incubated with protein G Sepharose beads. Both SN and P suffered the rest of the steps of the protocol as were aforementioned for streptavidin magnetic beads.

The resulting Western blot is shown in Figure 4.18 A. A positive signal around the size of HIV-1 gp41 in the eluted pellet of the treated viral particles indicates that the click chemistry in the solution could be used in the protocol. As expected, there is no signal in the eluted sample of wild type particles. In addition, comparing these results with the previous obtained for the eluted pwt of Figure 4.17 A, it seems that CuAAC in solution is more effective than in fixed Protein G Sepharose beads. The absence of fluorescent signal in the supernatant of the treated sample indicates that the click chemistry together with the chloroform/methanol extraction is very specific. In the silver staining of Figure 4.18 B, a huge difference in the protein pattern could be seen between

the eluted pellets of wild type and treated with palmitoyl analogue. All together indicate that **performing the click chemistry in solution before incubating with the Protein G Sepharose beads gave better results than the CuAAC reaction on beads, incrementing the quantity of palmitoylated proteins extracted**. So, the click chemistry in solution was incorporated to the final protocol instead of CuAAC reaction on beads.
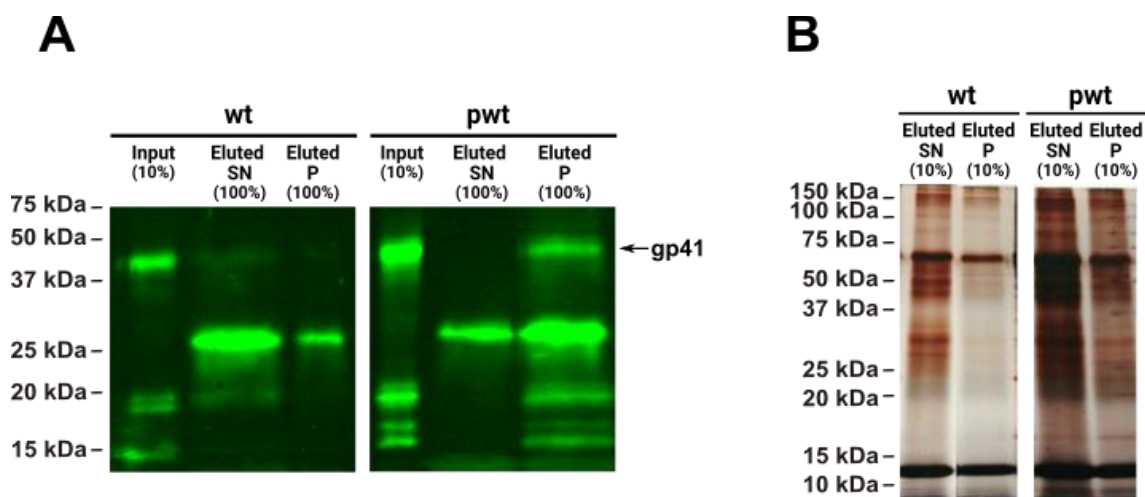
Figure 4.18. Representative results of optimized protocol for extraction of palmitoylated proteins performing CuAAC reaction in solution. Western blot (**A**) and silver stain (**B**) of both eluted viral particles of wild type (wt) and treated with the palmitoyl analogue (pwt) after the last modified extraction protocol performing the click chemistry reaction in solution. P and SN are the pellet and supernatant resulting from the ethanol/chloroform protocol, respectively. Western blot was developed with Chessie-8 α-gp41 primary antibody and α-mouse IRDye800 secondary antibody.

Keeping together all the modifications and improvements performed above, the definitive optimised protocol proposed for the subsequent extraction of HIV-1 palmitoylated proteins is summarized below. The same protocol could be found in Section 4.2.3.2.

1. Lysate viral particles for 1 h at RT and shaking. Lysis buffer: PBS (Mg^{2+}/Ca^{2+}-free) + 1% SDS + protease inhibitor cocktail. Final volume: up to 200 µL.

2. Centrifuge 14,000 rpm 10 min. Save 'input'.

3. Copper-based click chemistry with TAMRA Biotin Azide (Click Chemistry Tools, # 1048-1). Incubate for 1 h at 37 °C and shake in the thermomixer.

4. Concomitantly with the click reaction, blocking with 2% BSA (w/v) of 50 μL of High Capacity Streptavidin Magnetic Beads (Click Chemistry Tools, #1497) previously washed with PBS. 1h at RT.

5. Extract with $CHCl_3$ and MeOH following Haberkant et al. (2016) and resuspend in 100 μL of PBS (Mg^{2+}/Ca^{2+} -free) + 1% SDS in the thermomixer. Adjust the rest of the sample to a final SDS concentration of 0.1% [add 900 μL of PBS (Mg^{2+}/Ca^{2+}-free) to the 100 μL of sample].

6. Wash 50 μL of Protein G Sepharose beads with PBS (Mg^{2+}/Ca^{2+}-free).

7. Mix the 1000 μL of the sample with the washed protein G beads. Incubate 1 h at RT. Centrifuge at 6,500 rpm for 5 min and recover unbound supernatant. In this step all the hydrophobic proteins will bind non-specifically to the beads.

8. Wash beads with 500 μL of PBS (Mg^{2+}/Ca^{2+}-free) by centrifuging at 6,500 rpm for 3 min. Resuspend the beads in 300 μL of PBS (Mg^{2+}/Ca^{2+}-free).

9. Add the washed protein G beads to the blocked magnetic streptavidin beads. Mix several times before incubating 1 h at RT and constant stirring. The idea is to induce the removal of biotinylated palmitoylated proteins from the protein G beads by the magnetic streptavidin beads due to the strong affinity of biotin-streptavidin binding.

10. Before recovering magnetic streptavidin beads, mix several times more. Put the sample in magnetic rack and recover the unbound supernatant and the protein G beads.

11. Wash magnetic beads 5 times with 500 μL of PBS (Mg^{2+}/Ca^{2+}-free) using magnetic rack.

12. To elute magnetic streptavidin beads, use (30+20) μL of sample buffer + 15 min incubation at RT in constant stirring in the thermomixer + 15 min 95 °C + centrifuge 6,500 rpm 10 min RT. Mix volumes and store as 'Eluted.' In this time 95 °C was used since it is not necessary to keep the palmitoyl moiety.

4.3.4. Proteomic analysis

To identify palmitoylated proteins in HIV-1 virions, the wt and pwt pulls after extraction with the previous set-up protocol were run in a 10% SDS-PAGE gel. To analyse the proteins, the gel was fixed, and each band was sectioned and treated as explained in Section 4.2.4. The resulting tryptic peptides for both wt and pwt pulls were subjected to LC-MS/MS.

After curating, MS data confirmed that the digested samples contained high-quality peptides and provided a good estimation of the relative protein concentrations in each sample. The SEQUEST™ HT search engine identified a total of 265 proteins for wt control sample, containing 192 proteins of high confidence (1% False Discovery Rate or FDR) and 73 of medium confidence (5% FDR). In the case of pwt, 414 proteins were detected, containing 368 proteins of high confidence and 46 of medium confidence. Comparison between wt and pwt resulting proteins revealed that only 165 proteins were exclusively detected in the sample treated with the palmitoyl analogue.

After a brief look among these potentially palmitoylated 165 proteins, 12 proteins were completely discarded from being part of the final HIV-1 palmitoylome due to the fact that these proteins were isoforms of heat shock protein 90 (HSP90) or proteins associated to ribosomal subunits 60S or 40S implicated in translation. HSP90 is one of the most abundant proteins in human cells and it has been reported to positively regulate HIV-1 gene expression in acutely infected cells and localize on the viral promoter which might directly control viral transcription (Vozzolo et al., 2010). Also, HSP90 governs HIV-1 reactivation from latent reservoirs present in resting host cells (Timmons et al., 2020). So, these proteins are known to take part in different steps of HIV-1 infective cycle but before assembly and budding of virions. Their presence in the MS data suggested their protein-protein interaction with other palmitoylated proteins in the sample, making them extracted together from the sample after applying the optimized protocol. For example, it is known that HIV-1 Nef interacts with two components of the 40S small ribosomal subunit, the RPS10 protein and the 18S rRNA (Abbas et al., 2012). Thus, those 12 proteins were excluded from the final list of identified palmitoylated proteins.

A definitive list of **153 potentially palmitoylated proteins that were exclusively present in viral particles treated with the palmitoyl-modified analogue** is shown in Table 4.5. This table includes the recommended name and accession number for each protein assigned in the UniProtKB database (Boutet et al., 2007), as well as the estimated total peptides, molecular weight and isoelectric point provided by the MS/MS-LC software. This table only gathers proteins with high confidence and detected from pwt samples. These 153 palmitoylated proteins could possibly be candidates to conform part of the HIV-1 palmitoylome.

Table 4.5. Potentially palmitoylated proteins identified in pwt samples after LC-MS/MS.

Accession[a]	Protein name[b]	Peptides[c]	MW[d] (kDa)	calc. pI[d]
P62258	14-3-3 protein epsilon (14-3-3E)	3	29,2	4,74
P27348	14-3-3 protein theta	2	27,7	4,78
P62333	26S protease regulatory subunit 10B	1	44,1	7,49
P62191	26S protease regulatory subunit 4 (P26s4)	2	49,2	6,21
P17980	26S protease regulatory subunit 6A	2	49,2	5,24
O00232	26S proteasome non-ATPase regulatory subunit 12	2	52,9	7,65
Q13200	26S proteasome non-ATPase regulatory subunit 2	1	100,1	5,2
P48556	26S proteasome non-ATPase regulatory subunit 8	2	39,6	9,7
P05387	60S acidic ribosomal protein P2	1	11,7	4,54
Q96D46	60S ribosomal export protein NMD3 (hNMD3)	1	57,6	7,14
P55263	Adenosine kinase (AK)	1	40,5	6,7
P84085	ADP-ribosylation factor 5	2	20,5	6,79
P06733	Alpha-enolase	2	47,1	7,39
Q13155	Aminoacyl tRNA synthase complex-interacting multifunctional protein 2	1	35,3	8,22
P54136	Arginine--tRNA ligase, cytoplasmic (ArgRS)	2	75,3	6,68
O00148	ATP-dependent RNA helicase DDX39A	5	49,1	5,68
O14965	Aurora kinase A	1	45,8	9,39
P31939	Bifunctional purine biosynthesis protein PURH	3	64,6	6,71
Q9UI42	Carboxypeptidase A4	1	47,3	6,7
O00299	Chloride intracellular channel protein 1	1	26,9	5,17
P53618	Coatomer subunit beta	2	107,1	6,05
P12277	Creatine kinase B-type	1	42,6	5,59
P17812	CTP synthase 1	5	66,6	6,46
Q00526	Cyclin-dependent kinase 3	2	35	8,79
P11802	Cyclin-dependent kinase 4	2	33,7	7,01
Q00535	Cyclin-dependent-like kinase 5	3	33,3	7,66
Q9UHD1	Cysteine and histidine-rich domain-containing protein 1	2	37,5	7,87

Q9BTE7	DCN1-like protein 5 (DCNL5)	2	27,5	5,58
P61962	DDB1- and CUL4-associated factor 7	1	38,9	5,52
P55039	Developmentally-regulated GTP-binding protein 2 (DRG-2)	4	40,7	8,88
P27487	Dipeptidyl peptidase 4	1	88,2	6,04
Q14566	DNA replication licensing factor MCM6	2	92,8	5,41
P31689	DnaJ homolog subfamily A member 1	1	44,8	7,08
P56537	Eukaryotic translation initiation factor 6 (eIF-6)	1	26,6	4,68
O14980	Exportin-1 (Exp1)	1	123,3	6,06
Q92945	Far upstream element-binding protein 2 (FUSE-binding protein 2)	1	73,1	7,3
Q6ZVX7	F-box only protein 50	1	30,8	6,62
P02794	Ferritin heavy chain (Ferritin H subunit)	1	21,2	5,55
Q96QA5	Gasdermin-A	3	49,3	5,29
Q9BQ67	Glutamate-rich WD repeat-containing protein 1	1	49,4	4,92
P47897	Glutamine--tRNA ligase	1	87,7	7,15
Q7RTV2	Glutathione S-transferase A5	1	25,7	8,03
P62873	Guanine nucleotide-binding protein G(I)/G(S)/G(T) subunit beta-1	1	37,4	6
P09651	Heterogeneous nuclear ribonucleoprotein A1 (hnRNP A1)	2	38,7	9,13
Q14103	Heterogeneous nuclear ribonucleoprotein D0 (hnRNP D0)	1	38,4	7,81
P31943	Heterogeneous nuclear ribonucleoprotein H (hnRNP H)	4	49,2	6,3
P14866	Heterogeneous nuclear ribonucleoprotein L (hnRNP L)	1	64,1	8,22
O60506	Heterogeneous nuclear ribonucleoprotein Q (hnRNP Q)	3	69,6	8,59
P07910	Heterogeneous nuclear ribonucleoproteins C1/C2 (hnRNP C1/C2)	5	33,7	5,08
P04908	Histone H2A type 1-B/E	2	14,1	11,05
P0DOX8	Immunoglobulin lambda-1 light chain	2	22,8	6,76
Q9UNM6-2	Isoform 2 of 26S proteasome non-ATPase regulatory subunit 13	2	42,9	6,54
O43390-2	Isoform 2 of Heterogeneous nuclear ribonucleoprotein R (hnRNP R)	3	71,2	8,13
Q9BQG0-2	Isoform 2 of Myb-binding protein 1A	2	149,3	9,28
Q15366-2	Isoform 2 of Poly(rC)-binding protein 2	2	38,6	6,79
Q4G0J3-3	Isoform 3 of La-related protein 7	1	67,6	9,54
P62847-4	Isoform 4 of 40S ribosomal protein S24	1	32,4	10,15
O75534-4	Isoform 4 of Cold shock domain-containing protein E1	1	93,7	6,52
P52434-4	Isoform 4 of DNA-directed RNA polymerases I, II, and III subunit RPABC3 ((RNA polymerases I, II, and III subunit ABC3)	1	19,8	4,67
Q9HA47-4	Isoform 4 of Uridine-cytidine kinase 1	1	32,3	6,86
P35241-5	Isoform 5 of Radixin	1	71	6,71
Q14C86-6	Isoform 6 of GTPase-activating protein and VPS9 domain-containing protein 1	1	166,1	5,21
Q12906-7	Isoform 7 of Interleukin enhancer-binding factor 3	1	95,7	8,81
Q07955-2	Isoform ASF-2 of Serine/arginine-rich splicing factor 1	2	32	5,91
P63000-2	Isoform B of Ras-related C3 botulinum toxin substrate 1	1	23,5	8,63
P36873-2	Isoform Gamma-2 of Serine/threonine-protein phosphatase PP1-gamma catalytic subunit (PP-1G)	3	38,5	6,13
P41252	Isoleucine--tRNA ligase, cytoplasmic	1	144,4	6,15
Q8TBB5	Kelch domain-containing protein 4	1	57,9	5,72
Q9HA64	Ketosamine-3-kinase	1	34,4	7,33

P31025	Lipocalin-1	1	19,2	5,58
O95232	Luc7-like protein 3	1	51,4	9,79
O94776	Metastasis-associated protein MTA2	2	75	9,66
P56192	Methionine--tRNA ligase, cytoplasmic	1	101,1	6,16
Q15785	Mitochondrial import receptor subunit TOM34 (hTom34)	1	34,5	8,98
P27361	Mitogen-activated protein kinase 3 (MAPK 3)	1	43,1	6,74
Q9BYG3	MKI67 FHA domain-interacting nucleolar phosphoprotein	2	34,2	9,88
Q9BXJ9	N-alpha-acetyltransferase 15, NatA auxiliary subunit	3	101,2	7,42
P61081	NEDD8-conjugating enzyme Ubc12	2	20,9	7,69
Q15233	Non-POU domain-containing octamer-binding protein (NonO protein)	2	54,2	8,95
P67809	Nuclease-sensitive element-binding protein 1 (YB-1)	7	35,9	9,88
Q9NR30	Nucleolar RNA helicase 2	8	87,3	9,28
P19338	Nucleolin	1	76,6	4,7
P55209	Nucleosome assembly protein 1-like 1	1	45,3	4,46
Q15645	Pachytene checkpoint protein 2 homolog	1	48,5	6,09
Q9UBV8	Peflin	2	30,4	6,54
Q9NSD9	Phenylalanine--tRNA ligase beta subunit	3	66,1	6,84
P00558	Phosphoglycerate kinase 1	5	44,6	8,1
Q9Y617	Phosphoserine aminotransferase	1	40,4	7,66
Q15149	Plectin (PCN, PLTN)	1	531,5	5,96
Q5JQF8	Polyadenylate-binding protein 1-like 2	2	22,8	9,1
Q6P2Q9	Pre-mRNA-processing-splicing factor 8	5	273,4	8,84
Q9UHI6	Probable ATP-dependent RNA helicase DDX20	1	92,2	6,95
Q9Y6V7	Probable ATP-dependent RNA helicase DDX49	2	54,2	9,06
Q2M2H8	Probable maltase-glucoamylase 2	1	277,8	5,21
P12273	Prolactin-inducible protein	1	16,6	8,05
Q9UQ80	Proliferation-associated protein 2G4	1	43,8	6,55
P25789	Proteasome subunit alpha type-4	2	29,5	7,72
P28070	Proteasome subunit beta type-4	1	29,2	5,97
P28074	Proteasome subunit beta type-5	1	28,5	6,92
O14744	Protein arginine N-methyltransferase 5 (PRMT5)	1	72,6	6,29
O00622	Protein CYR61	1	42	8,21
Q99497	Protein DJ-1	1	19,9	6,79
Q8N9T8	Protein KRI1 homolog	1	82,5	5,14
P00491	Purine nucleoside phosphorylase (PNP)	1	32,1	6,95
P43487	Ran-specific GTPase-activating protein	1	23,3	5,29
P51153	Ras-related protein Rab-13 OS=Homo sapiens GN=RAB13 PE=1 SV=1	2	22,8	9,19
Q9ULC3	Ras-related protein Rab-23	1	26,6	6,6
P40938	Replication factor C subunit 3	1	40,5	8,34
P35249	Replication factor C subunit 4	1	39,7	8,02
P60891	Ribose-phosphate pyrophosphokinase 1	2	34,8	6,98
Q92979	Ribosomal RNA small subunit methyltransferase NEP1	2	26,7	9,17
Q8TDN6	Ribosome biogenesis protein BRX1 homolog	2	41,4	9,92
Q9H0A0	RNA cytidine acetyltransferase	1	115,7	8,27
Q9ULX3	RNA-binding protein NOB1	1	46,6	7,18
Q9UKM9	RNA-binding protein Raly	3	32,4	9,17

Q5JTH9	RRP12-like protein	1	143,6	8,75
Q9Y3B9	RRP15-like protein	1	31,5	5,52
P31153	S-adenosylmethionine synthase isoform type-2 (AdoMet synthase 2)	1	43,6	6,48
P34896	Serine hydroxymethyltransferase, cytosolic (SHMT)	2	53	7,71
O75494	Serine/arginine-rich splicing factor 10	1	31,3	11,27
Q9BRL6	Serine/arginine-rich splicing factor 8	2	32,3	11,72
Q13242	Serine/arginine-rich splicing factor 9	1	25,5	8,65
Q9P0L2	Serine/threonine-protein kinase MARK1	1	88,9	9,36
P62714	Serine/threonine-protein phosphatase 2A catalytic subunit beta isoform (PP2A-beta)	2	35,6	5,43
P49591	Serine--tRNA ligase, cytoplasmic	2	58,7	6,43
P10768	S-formylglutathione hydrolase (FGH)	1	31,4	7,02
Q9NR45	Sialic acid synthase	3	40,3	6,74
P62318	Small nuclear ribonucleoprotein Sm D3 (Sm-D3)	1	13,9	10,32
Q00796	Sorbitol dehydrogenase (SDH)	2	38,3	7,97
P19623	Spermidine synthase (SPDSY)	1	33,8	5,49
P26368	Splicing factor U2AF 65 kDa subunit	1	53,5	9,09
Q16637	Survival motor neuron protein	1	31,8	6,55
Q13148	TAR DNA-binding protein 43 (TDP-43)	3	44,7	6,19
P17987	T-complex protein 1 subunit alpha (TCP-1-alpha)	2	60,3	6,11
P50991	T-complex protein 1 subunit delta (TCP-1-delta)	2	57,9	7,83
P50990	T-complex protein 1 subunit theta (TCP-1-theta)	2	59,6	5,6
P22102	Trifunctional purine biosynthetic protein adenosine-3	1	107,7	6,7
Q9Y3I0	tRNA-splicing ligase RtcB homolog	1	55,2	7,23
Q71U36	Tubulin alpha-1A chain	11	50,1	5,06
Q13509	Tubulin beta-3 chain	7	50,4	4,93
P68371	Tubulin beta-4B chain	12	49,8	4,89
Q14166	Tubulin--tyrosine ligase-like protein 12	2	74,4	5,53
P09661	U2 small nuclear ribonucleoprotein A' (U2 snRNP A')	2	28,4	8,62
Q9Y5J1	U3 small nucleolar RNA-associated protein 18 homolog	1	62	8,76
O75643	U5 small nuclear ribonucleoprotein 200 kDa helicase	1	244,4	6,06
P22314	Ubiquitin-like modifier-activating enzyme 1	1	117,8	5,76
O00159	Unconventional myosin-Ic	2	121,6	9,41
P11172	Uridine 5'-monophosphate synthase (UMP synthase)	3	52,2	7,24
P46459	Vesicle-fusing ATPase	1	82,5	6,95
P08670	Vimentin	2	53,6	5,12
Q2M389	WASH complex subunit 4	1	136,3	7,44
Q9BV38	WD repeat-containing protein 18	1	47,4	6,7
P12956	X-ray repair cross-complementing protein 6	2	69,8	6,64

[a] Accession numbers for UniProtKB (accessible at https://www.uniprot.org/help/uniprotkb).

[b] Recommended protein name and short name (if exists) present in UniProt database. Proteins were listed by alphabetic order.

[c] The total number of distinct peptide sequences identified in the protein group.

[d] Estimated Molecular Weight (MW) and isoelectric point (pI) calculated based on the amino acid sequence in the FASTA database used.

These 153 proteins were submitted to bioinformatic analysis against SwissPalm database (Blanc et al., 2015, 2019). This database agglutinates a large and increasing number of published palmitoyl-proteome datasets, provides useful tools to compare them, and includes curated data from the literature on the identification and analysis of palmitoylated proteins. So, SwissPalm curated and cross-referenced evidence of protein palmitoylation from the literature and palmitoyl-proteome studies with our potentially palmitoylated proteins to confirm if these same proteins were described to be palmitoylated up to date. The comparison was developed against all the protein datasets in the platform corresponding to *Homo sapiens*.

The Figure 4.19 presents the output results from the curated data from Swisspalm database analysis.

General statistics shows that **the 76.47% of the potential palmitoylated proteins obtained from the pwt samples, are described to be palmitoylated** in the literature (Figure 4.19 A). 73.2% corresponds to only-palmitoyl proteome studies and 3.27% are also validated experimentally, and the 23.5% remaining are proteins not known to be palmitoylated. Only a 19.86% of all SwissPalm annotated proteins in *H. sapiens* datasets corresponds to proteins that are described to be palmitoylated by only-palmitoyl proteome studies, palmitoyl proteome and validated studies and only validation studies. This highlights the limited knowledge about protein palmitoylation that still exists nowadays. **The approximate 80% of our detected proteins belongs to this ~20%, so our input list could be considered enriched in SwissPalm annotated proteins**, which means that the optimised extraction protocol for HIV-1 palmitoylated proteins is specific, is working correctly and the majority of proteins obtained are cellular proteins already known to be palmitoylated.

There are different independent techniques used to show direct evidence of palmitoylation (Figure 4.19 B). At least one of the metabolic labelling of palmitate procedures was used to validated 13.7% of the detected proteins. Metabolic labelling techniques comprises click chemistry or radioactive labelling and direct identification by mass spectrometry. A 8.55% of the detected proteins were only validated by chemical modification of cysteines, such as acyl-biotin exchange (ABE) or acyl resin-assisted

capture (Acyl-RAC), together with loss of palmitoylation signal upon hydroxylamine treatment (Figure 4.19 B). **The vast majority of the detected proteins, the 77.8%, were validated by both approaches**.

Concerning to the type of protein (Figure 4.19 C), **49.7% of the total proteins detected are cytoplasmic proteins and 3.27% are transmembrane proteins**. A small part of them, the 5.23% of the total, have cytoplasmic and transmembrane regions, and the rest of the proteins, the 41.8%, has not defined its localization. Among the detected proteins in the membrane, their topology is quite varied (Figure 4.19 D): 3.54% are peripheral membrane proteins, 2.76% have a lipidic anchor and 1.57% are integral membrane proteins with only one transmembrane domain, more concrete, the 0.39% have a single-pass type II transmembrane domain. Comparing with the Dataset 3 of annotated proteins of SwissPalm, very similar values are obtained: 3.37% are peripheral membrane proteins, 3.93% have a lipidic anchor and 1.17% are integral membrane proteins with only one transmembrane domain. This Dataset 3 includes proteins that have been validated as palmitoylated proteins or are found in at least one palmitoyl-proteome of the database.

A huge part of the detected proteins could be localized in the cytoplasm and in the nucleus (> 50%) (Figure 4.19 E), while the rest is distributed among the nucleolus, the cell membrane, the nucleoplasm or associated to the cytoskeleton (< 20%). As assembly and budding process of HIV-1 morphogenesis take place along the cell membrane (Freed, 2015; Sakuragi, 2011; Sundquist & Kräusslich, 2012), it could be predictable that palmitoylated proteins could mainly come from the cell membrane or its boundaries. Thus, these results are quite interesting due to the fact that one of the localization where a remarkable amount of the detected proteins is in the nucleus.

(Next page) – **Figure 4.19. SwissPalm database statistics for potential palmitoylated proteins**. **A)** Percentage of detected proteins that are identified in SwissPalm with evidence of palmitoylation (SwissPalm annotated proteins) versus the overall data for the chosen *H. sapiens.* **B)** Percentage of detected proteins found in palmitoyl-proteomes per experimental techniques used for the validation. **C)** Comparison between the proportion of transmembrane and cytosolic proteins in the detected proteins. **D)** Membrane protein topology of the detected proteins in comparison to the Dataset 3 of SwissPalm database. **E)** Relevant subcellular localization of the input proteins in comparison to the Dataset 3 of SwissPalm database.

A Identified from query / All SwissPalm annotated proteins in H. sapiens

- Palmitoyl-proteomes only
- Not known to be palmitoylated
- Palmitoyl-proteomes and validation experiments
- Validation experiments only
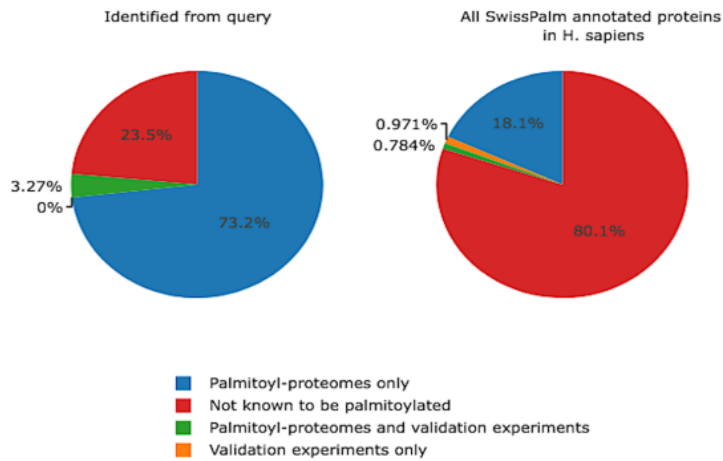
B Percentage of proteins found in palmitoyl-proteomes using independent techniques

- Both
- Metabolic labeling of palmitate
- Chemical modification of S-palmitoylated cysteines
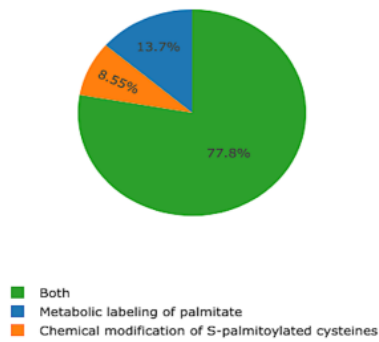
C Transmembrane proteins vs. Cytoplasmic proteins

- Cytoplasmic proteins
- Other proteins
- Cytoplasmic and transmembrane proteins
- Transmembrane proteins

D Membrane protein topology

- SwissPalm annotated proteins (dataset 3)
- Identified proteins

E Subcellular localizations
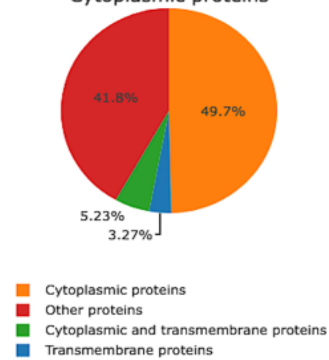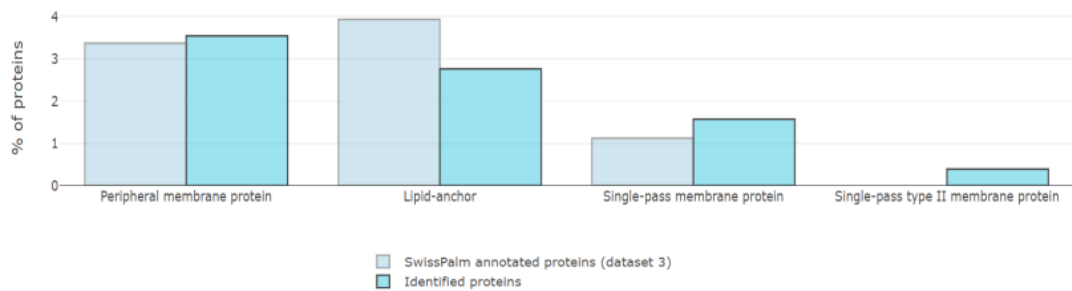
- SwissPalm annotated proteins (dataset 3)
- Identified proteins
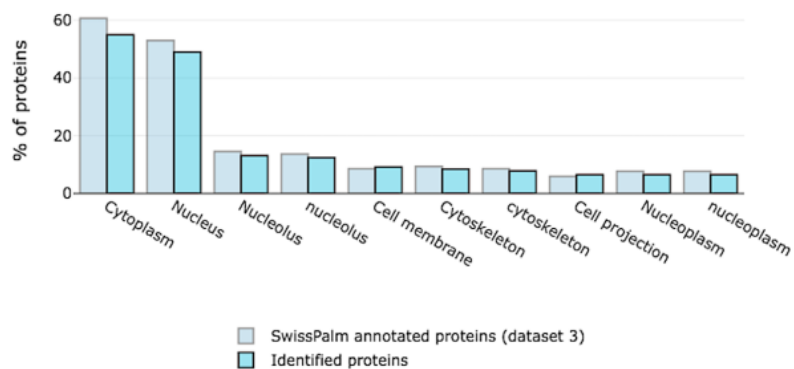
To decipher the biological and molecular functions, together with the cellular localization of the different palmitoylated proteins detected, the Biological Networks Gene Ontology (BiNGO) tool (Maere et al., 2005) was applied to the 153 proteins (Figure 4.20). The analysis was performed with a p-value < 0.001.

The Gene Ontology (GO) project (Ashburner et al., 2000), wants to agglomerate the increasing knowledge on gene function in a controlled vocabulary applicable to all organisms. GO consists of three hierarchically structured vocabularies that describe genes in terms of their associated biological processes, molecular functions and cellular components. BiNGO could inquire among these GO categories to return relevant information about the biological and molecular functions, and the cellular localization of a group of proteins of interest.

The total proteins detected were classified by BiNGO into 10 categories according to their cellular localization (Figure 4.20 A). **These proteins were found to be mainly forming part of three complexes: 35.71% in the spliceosome, 23.81% in the proteasome and 19.05% of spliceosome snRNP**. The other minority localizations where the input proteins were discovered were in the melanosome (4.76%), ribonucleoprotein granule (4.76%), chaperonin-containing T-complex (2.38%), CDR-mediated mRNA stability complex (2.38%), SMN-Sm protein complex (2.38%), preribosome (2.38%) and Cajal body (2.38%).

On the basis of their biological function, the palmitoylated proteins detected were divided into 13 categories (Figure 20 B). **Most of the proteins were involved in the regulation of RNA stability (31.68%) and DNA biosynthetic process (15.27%), and in the mRNA metabolic process (12.21%)**. The other remaining 10 categories correspond to nuclear transport (8.4%), nucleoside monophosphate biosynthetic process (8.02%), nucleocytoplasmic transport (6.87%), posttranscriptional regulation of gene expression (4.96%), RNA processing (4.2%), regulation of mRNA metabolic process (3.44%), cellular amino acid metabolic process (2.29%), ribonucleoprotein complex assembly (1.53%), positive regulation of cellular amide metabolic process (0.76%) and neural nucleus development (0.38%).

A

Cellular localization

% terms per group

- Cajal body 2,38% *
- preribosome 2,38% **
- SMN-Sm protein complex 2,38% **
- CRD-mediated mRNA stability complex 2,38% **
- chaperonin-containing T-complex 2,38% **
- ribonucleoprotein granule 4,76% **
- melanosome 4,76% **
- spliceosomal snRNP complex 19,05% **
- spliceosomal complex 35,71% **
- proteasome complex 23,81% **

B

Biological functions

% terms per group

- neural nucleus development 0,38% *
- positive regulation of cellular amide metabolic process 0,76% **
- ribonucleoprotein complex assembly 1,53% **
- cellular amino acid metabolic process 2,29% **
- regulation of mRNA metabolic process 3,44% **
- RNA processing 4,2% **
- posttranscriptional regulation of gene expression 4,96% **
- nucleocytoplasmic transport 6,87% **
- nucleoside monophosphate biosynthetic process 8,02% **
- nuclear transport 8,4% **
- mRNA metabolic process 12,21% **
- regulation of DNA biosynthetic process 15,27% **
- regulation of RNA stability 31,68% **

C

Molecular functions

% terms per group

- hydroxymethyl-, formyl- and related transferase activity 2,33% **
- mRNA 5'-UTR binding 2,33% *
- snRNA binding 2,33% **
- telomeric DNA binding 2,33% **
- histone deacetylase binding 2,33% *
- ribonucleoprotein complex binding 2,33% *
- tau protein binding 2,33% *
- RNA binding 2,33% **
- unfolded protein binding 2,33% **
- E-box binding 2,33% *
- scaffold protein binding 2,33% *
- double-stranded RNA binding 2,33% *
- transferase activity, transferring alkyl or aryl (other than methyl) groups 2,33% *
- carbon-carbon lyase activity 2,33% *
- miRNA binding 4,65% *
- threonine-type endopeptidase activity 4,65% **
- aminoacyl-tRNA ligase activity 9,3% **
- helicase activity 11,63% **
- mRNA binding 11,63% **
- pre-mRNA binding 11,63% **
- DNA polymerase activity 13,95% **

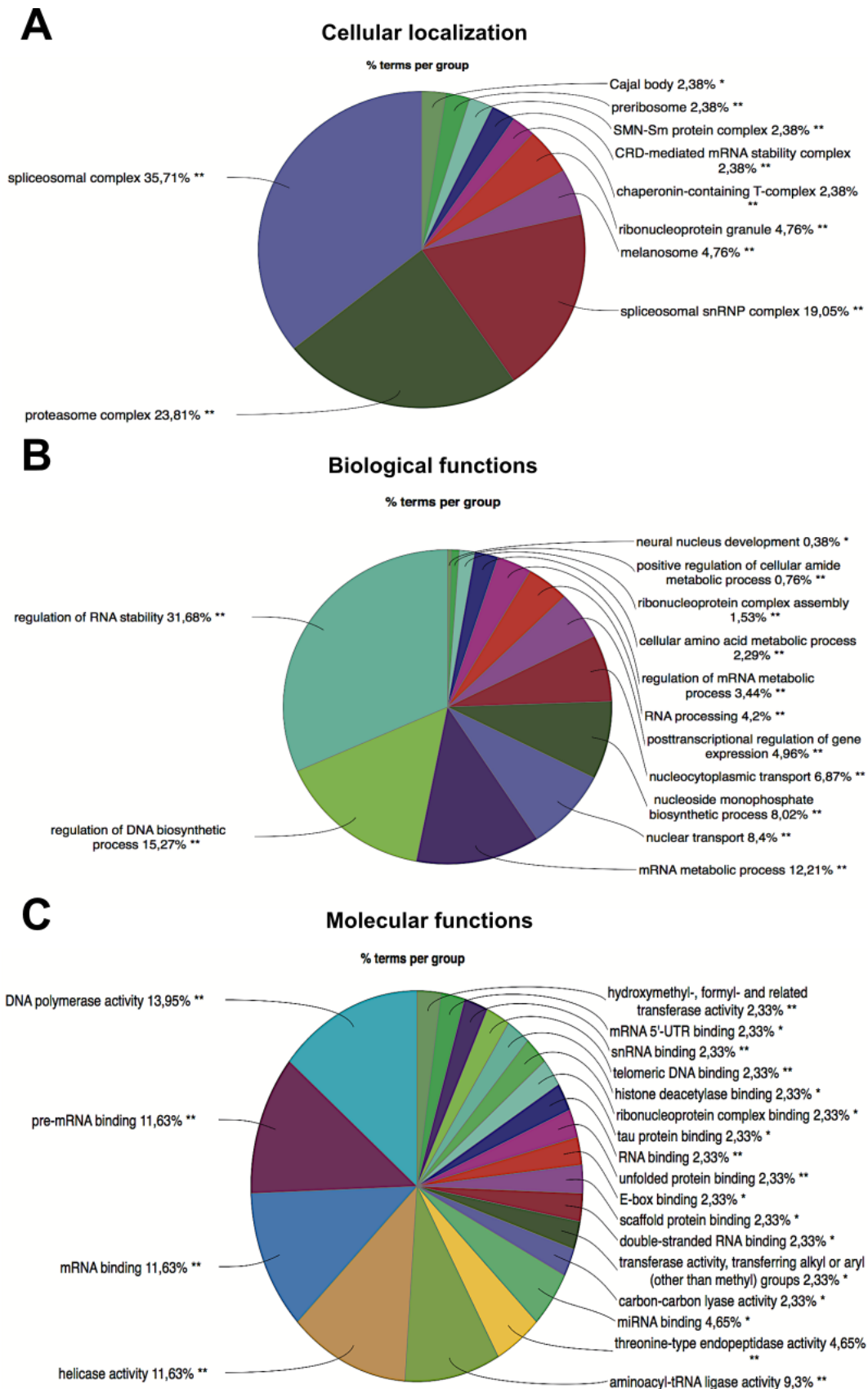**Figure 4.20. Gene Ontology classification of the 153 detected proteins by BiNGO plugin.** This classification is based on their cellular localization **(A)** and their involvement in a biological process **(B)** and in a molecular function **(C)**. A p-value < 0.001 was considered significant.

163

Concerning to their molecular functions, the total palmitoylated proteins were classified into 21 categories (Figure 20 C). **The vast majority of the proteins were noticed to present DNA polymerase activity (13.95%), pre-mRNA binding (11.63%), mRNA binding (11.63%), helicase activity (11.63%) and aminoacyl-tRNA ligase activity (9.3%).** The other molecular functions detected in minor proportion were 4.65% for threonine-type endopeptidase activity, 4.65% for miRNA binding (4.65%) and all the rest with 2.33% were carbon-carbon lyase activity, transferase activity of alkyl or aryl (other than methyl) groups, double-stranded RNA binding, scaffold protein binding, E-box binding, unfolded protein binding, RNA binding, tau protein binding, ribonucleoprotein complex binding, histone deacetylase binding, telomeric DNA binding, snRNA binding, mRNA 5'-UTR binding and transferase activity related to hydroxymethyl and formyl groups.

In accordance with previous mentioned biological and molecular functions (Figure 4.20 B & C), as well as, with their cellular compartment (Figure 4.20 A) and subcellular localization (Figure 4.19 E), it could be estimated that **the detected proteins would be implicated in the control and regulation of the machinery of transcription and secretion during HIV-1 morphogenesis**.

Protein-protein interaction networks play a key role in biological processes. To construct the interactome of the detected palmitoylated proteins, were used two publicly databases: Search Tool for the Retrieval of Interacting Genes/Proteins or STRING (Szklarczyk et al., 2021) and Biological General Repository for Interaction Datasets or BioGRID (Stark et al., 2006). The resulting protein interaction map was visualized in Cytoscape software (Figure 4.21). The protein-protein interaction network of the total palmitoylated proteins detected with the highest confidence scores (>9.0) was constructed. This biological networks were free-scale as it is difficult to guess which protein interacts first with other protein and only those palmitoylated proteins experimentally validated were chosen.

The constructed interactome map in STRING with high-confidence score was constructed by 154 nodes (proteins) and 302 edges (predicted functional associations based in detailed evidence breakdown) with an average node degree of 3.92 and

average of local clustering coefficient of 0.501. The protein-protein interaction (PPI) enrichment *p*-value was < 1.0[-6], which means the input proteins have more interactions among themselves than what would be expected for a random set of proteins of the same size and degree distribution drawn from the genome. This enrichment indicates that the analysed proteins are at least partially biologically connected, as a group. Indeed, in Figure 4.21 could be seen that **the palmitoyl proteins detected are mainly associated into three well-defined interaction clusters**. The implications on these findings in a HIV-1 context will be debated in the discussion section below.
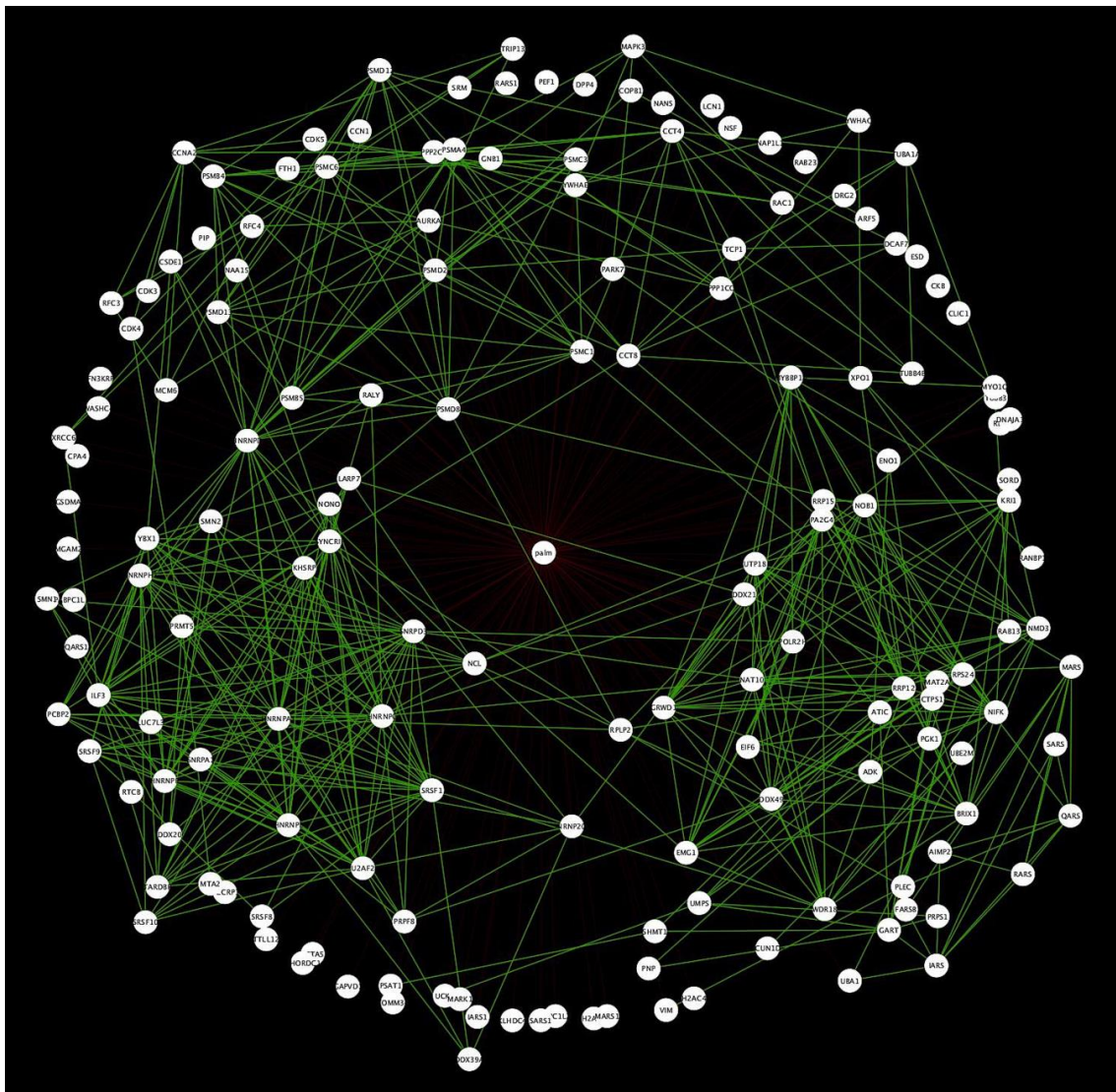

Figure 4.21. Protein-protein interaction network of palmitoylated proteins detected. The network was generated from BioGRID and STRING databases and curated and visualized by Cytoescape software. The nodes are coloured in white and the edges, in green.

4.4. Discussion

S-palmitoylation constitutes a fundamental post-translational modification involved in signalling, trafficking, membrane targeting, and cellular localization (Resh, 1999; Smotrys & Linder, 2004). The addition of palmitate to cysteine residues imparts hydrophobicity to the molecule; it is critical for the correct organization, presentation, and orientation of protein complexes such as MHC II on T-cell surfaces (Komaniwa et al., 2009) and results in the recruitment of these proteins to membrane-containing compartments of the cell. Indeed, palmitoyl residues are known to preferentially target proteins to lipid rafts in the cell membrane (Brown, 2006; Levental et al., 2010; Melkonian et al., 1999; Resh, 1999; Salaun et al., 2010).

As introduced above, S-palmitoylation is involved in several critical steps in the HIV-1 life cycle, potentially playing a key role in viral entry and budding processes. Viral budding to the cell membrane occurs through lipid rafts, and it is thought to be mediated via palmitoylation of gp41 (R. A. Dick et al., 2012; Lev & Shai, 2007; Rousso et al., 2000). It has been shown that lipid rafts are enriched in palmitoylated proteins, and these membrane microdomains are thought to be involved in viral budding and entry (Graham et al., 2003; Liao et al., 2004).

Even though it is a dynamic modification and a regulated process, protein palmitoylation site prediction remains challenging since clear consensus sequences for palmitoyl attachment are not fully characterized yet because of the lack of a consensus sequence; however, algorithms have been developed to predict potential palmitoylation sites (Kumari et al., 2014). A recent compilation drawn from over 5,000 S-palmitoylated proteins suggests that as much as 10% of the human proteome consists of S-palmitoylated proteins (Blanc et al., 2015). Other drawbacks are the lack of antibodies against lipid modifications, inefficiencies of standard mass spectrometry techniques to identify acylated proteins, and the lack of suitable markers or analogues for palmitoyl groups (Hang & Linder, 2011; Resh, 2016; Rodenburg et al., 2017).

The classical method to detect protein palmitoylation consists of using labelled palmitic acid with radioactive isotopes like ^3H, ^{14}C, and ^{125}I to tag proteins metabolically, followed by visualization of the purified proteins autoradiography. Radioactive

labelling was effective; however, this technique has few disadvantages low detection sensitivity, inability to enrich acylated proteins selectively, general complications associated with radioisotope work and long exposure times to measure biologically relevant signals. In addition, the reagents needed are hazardous, cumbersome, and not readily available (Draper & Smith, 2009).

Since then, different approaches have emerged for tracking protein palmitoylation, but they are quite limited, presenting a barrier to its study in biological systems (H. Lu & Fang, 2020). Over the last decade, bioorthogonal reactions coupled to clickable and compatible palmitate analogues have provided quick and sensitive methods for the detection of protein palmitoylation (Gao & Hannoush, 2014, 2018; Yap et al., 2010), even in the context of HIV-1 infection (Colquhoun et al., 2015; Karthigeyan et al., 2021).

The most emblematic example of click chemistry reaction is the copper-catalyzed azide-alkyne cycloaddition (CuAAC), which enables labelling of cells with alkynyl analogues of palmitates that can be reacted with azides conjugated to suitable detection tags, such as fluorophores, or affinity tags, including biotin (Ourailidou et al., 2016; Thiele et al., 2012). Therefore, click chemistry not only allows the detection of the protein of interest based on fluorescence or chemiluminescence also allows labelling proteins for affinity pull-down of the cellular pool of tag proteins, usually based on biotin-streptavidin binding, and their global analysis by mass spectrometry-based proteomics (Charron et al., 2009; B. R. Martin & Cravatt, 2009; Yount et al., 2011). These clickable palmitate analogues overcome several inherent disadvantages of radioactive-labelled probes, such as long sample processing, low sensitivity film exposure times, and being dangerous to handle. In addition, the click chemistry-based approach has high specificity because the alkyne group introduced in the palmitate analogue is not normally found in cells (Draper & Smith, 2009; Gao & Hannoush, 2014, 2018).

Here, we presented a clickable palmitoyl-modified analogue, a 15-hexadecynoic acid or alkynyl palmitate synthetized by Dr. F.-Xabier Contreras, as a biochemical tool whose future purpose would be unveiling the HIV-1 palmitoylome. HIV-1 proteome is described (Berro et al., 2007; Cantin et al., 2005; Chertova et al., 2006; Frankel & Young,

1998; Ott, 1997, 2002; Tremblay et al., 1998). However, a detailed HIV-1 palmitoylome remains an enigma even though its discovery has been tried before (Colquhoun et al., 2015).

This analogue of palmitic acid has an alkyne group attached to its terminal moiety, which allows the compound to suffer fluorescence detection or affinity enrichment by CuAAC reaction. The alkyne group would be a powerful chemical reporter due to its small size, stability, and absence from biological systems (Li & Zhang, 2016). When added to the cell culture medium, the palmitoyl analogue should resemble its natural counterpart, tagging potential palmitoylated proteins. This behaviour needed to be proven, so a palmitoylation test was developed. It is known that HIV-1 gp41 is palmitoylated in four cysteines. Cys-764, is located immediately upstream of LLP2 and Cys-837, which is in LLP1; and both Cys-598 and Cys-604 are located in the ectodomain (Bhattacharya et al., 2004; Syu et al., 1991; C. Yang et al., 1995). Therefore, if the palmitoyl analogue is added to the culture media of cells that produce HIV-1 viral-like particles, a positive signal of palmitoylation is expected with the analogue in the gp41 extracted from those cells after the test. As confirmed before in Figure 4.8, a band in the Western blot corresponding to HIV-1 gp41 could be observed only in concentrated viral particles treated with the palmitoyl analogue, meaning as expected, the properly palmitoylation of gp41 cysteines by the designed probe as its natural counterpart, the palmitic acid. Thus, this palmitoyl analogue has become a tool for the palmitoylation of proteins. Property described above, together with its alkyne group allow the palmitoyl analogue to be the perfect candidate for the design of a purification protocol for the extraction of HIV-1 palmitoylated proteins.

Before developing this new protocol, some important assumptions should be considered. First, the future strategy for purifying of the target proteins should be a protocol that delivers the adequate yield and purity. Second, the protocol would be based on a modified immunoprecipitation assay coupled to the use of click chemistry. In general, it is simple, but the key to its success is affected by multiple variables, factors, and specific binding conditions, that need to be optimized to isolate adequate amounts and purity of the desired proteins. A brief list of such factors and associated variables is

detailed in Table 5. From now on, these parameters will be discussed for setting up the final protocol for the extraction of HIV-1 palmitoylated proteins.

Table 5. Factors and variables affecting the different steps of the protocol.

Factor	Variables
Method format	Column vs. batch method
Type of support	Physical characteristics, capacity, non-specific binding, blocking, time of incubation
Lysate pre-clearing	Necessary or not, Non-specific binding
CuAAC reaction	Work correctly, on bead vs. in solution, TBTA vs. THPTA, reaction time
Binding buffer	Components, stringency
Wash buffer	Components, stringency
Elution buffer	Components, elution strength

All the approaches tested for developing the protocol were based on the batch method instead of gravity-flow columns. The batch method simply involves mixing the components of the concrete reaction in a microcentrifuge tube for a specific period to allow them to interact. The beads are separated from the different solutions at each step: non-bound sample, wash buffer, and elution buffer. As the volume during the different steps of the protocol did not exceed a few microliters, centrifugation would be mandatory to recover the beads because these small volumes will not flow through a filter by gravity alone. The only exception was when magnetic beads were present, which required a specific magnetic stand adapted to these small volumes to recover the beads. The batch method is easy to handle and less expensive than performing gravity-flow column methods.

The type of support used along the multiple tests varied until reaching the most adequate for the final purpose. Firstly, agarose resin was used, which is an easy-to-use and versatile support that could be modified with the appropriate ligand: with an azide tag in Dde Azide Agarose resin from the Click-&-Go™ Dde Protein Enrichment Kit (Click Chemistry Tools) or with a NeutrAvidin protein in Pierce™ High Capacity NeutrAvidin™ Agarose Resin (ThermoFisher Scientific). Even though both types of beads could stand harsh washing conditions to reduce non-specificity, protocols proposed with both gave background signal in wild type and treated samples.

Moreover, after adding more SDS-PAGE sample buffer to the beads after elution and heating them, it has shown that desired proteins remained stuck to the resin (Figure 4.11. B). Agarose beads are quite hydrophobic, so they may be non-specifically coated with whatever insoluble present in the solution that could not be removed only by centrifugation.

Therefore, a lysate pre-clearing with Protein G Sepharose™ 4 Fast Flow (GE Healthcare) beads was added to the protocol. Sepharose is a GE Healthcare-Pharmacia trademark for crosslinked agarose commercially available in different concentrations and sizes, which is more resistant to biological degradation (Ahmed, 2017). This pre-clearing step of wt and pwt show the highest non-specific binding capacity of those beads sequestering almost every protein, including our proteins of interest (Figure 4.12.B). Thus, the pre-clearing step was discarded, and alternatively, the NeutrAvidin agarose beads were blocked by incubating them with an irrelevant protein such as BSA. Although a small amount of the blocker protein may co-elute with the antigens, its identity and molecular weight are known, making it less troublesome in downstream analyses. This blocking step was maintained when streptavidin magnetic beads were incorporated into the protocol.

Even though the stickiness of Protein G Sepharose beads seems to be a handicap, this capability could be exploited in the protocol as a new method to catch proteins from the samples. Together with the strong biotin-streptavidin binding between the clicked proteins and the use of High Capacity Streptavidin Magnetic Beads (Click Chemistry Tools), the final extraction protocol could be settled (Figure 4.18). Unlike agarose or Sepharose, these magnetic beads are solid and do not have a porous center, thus limiting the surface area for attachment. Their size is 1.0 μm in diameter, which is significantly smaller than agarose or Sepharose beads, and the greater number of magnetic beads per volume than agarose or Sepharose beads collectively gives streptavidin magnetic beads an effective surface-area-to-volume ratio. This high binding capacity is translated into reduced quantity required to immobilize biotinylated samples compared to previous NeutrAvidin agarose beads used and in lower background noise from non-specific unions. In addition, this support is faster to use and offers an easy bench-top separation

without centrifuging due to its excellent magnetic properties for rapid and efficient capture using magnetic stands (DeCaprio & Kohl, 2020).

Concerning the click chemistry, it is necessary to control the correct functioning of the reaction during the experiments because it is one of the key factors to obtain a successful protocol. Therefore, developing a fluorophore test for the CuAAC reaction was needed based on Presolski et al (2011) and the idea of performing the click chemistry on beads, as in the protocol for the detection of palmitoylated HIV-1 gp41 (Section 4.2.3.1). Results from the fluorophore test showed a positive signal in the eluted sample of treated viral particles with the palmitoyl analogue was obtained, which means that the settled conditions for the click chemistry reaction were adequate and the CuAAC was perfectly working (Figure 4.15 A).

Even though these CuAAC conditions were enough to perform the reaction, some modifications were tested to improve the final protocol. Click chemistry reaction could be performed in solution or on beads, as it was carried out here in the majority of experiments. The first approach consists in adding the CuAAC reactives to the samples in solution and allowing the reaction to occur, followed by the incubation with the support to bind the clicked proteins. This option seems to give the highest yield of clicked antigen. The second approach consists incubating of the proteins with the beads and performing the click chemistry reaction directly to the proteins that remained attached to the support. This usually gives slightly decreased antigen yields and purity compared to the first method and is thought to decrease non-specific background. Comparing both approaches (Figure 4.17 A vs. Figure 4.18 A), it was decided to incorporate click chemistry in solution instead of on beads due to the yield obtained using the protocol with CuAAC in the solution is increased and the background seemed not to be altered.

Another modification of the click chemistry reaction was the substitution of TBTA for THPTA as stabilizing ligand for copper(I). While TBTA needs to be diluted in DMSO, THPTA is soluble in water, increasing biological compatibility. In addition, it is used in a 5:1 ratio (ligand to copper), while TBTA is used in a 2:1 ratio, so the quantity of copper needed for the CuAAC reaction is relatively less. In addition, this compound was

171

effectively used to perform the click reaction in live cells with high efficiency while maintaining cell viability (Hang & Linder, 2011; Presolski et al., 2011). Therefore, the protocol was tested using THPTA instead of TBTA. The CuAAC reaction was carried out without any inconvenience (Figure 4.17 A), so THPTA could be introduced in the final protocol for extraction of palmitoylated proteins. In addition, this result set the bases to perform click chemistry with the palmitoyl-modified analogue *in vivo*.

The time of CuAAC reaction also varied along with the different experiments. The conditions were 1 h or overnight at 4 °C and 1 or 3 h at 37 °C. As Figure 4.17 confirmed, the click chemistry reaction was not altered after the substitution of 3 h of incubation by 1 h at the same temperature of 37 °C. This result allowed to reduce the extension of the CuAAC step.

As previously seen, this kind of experiment is plagued with troublesome amounts of background, so empirical testing is necessary to discover effective wash conditions. The Click-&-Go™ strategy, uses a specific Agarose Wash Buffer with SDS provided in the kit for stringent removal of non-specifically bound proteins. After this wash, it is critical to remove residual SDS by washing exhaustively with handmade 8 M urea and 20% (v/v) acetonitrile buffers. Even though the manufacturer's protocol stands for efficient elimination of background with this washing buffer, Figure 4.9 B shows high contamination in both the wild type and treated samples. Slightly signal corresponding to HIV-1 gp41 or no signal in the silver stain corresponding to the protein pattern could be detected in the palmitoylated sample (Figure 4.9 A), which could be a consequence of harsh washing methodology to erase the remaining SDS. Thus, those drawbacks were one of the reasons why the Click-&-Go™ strategy was discarded.

According to typical immunoprecipitation protocols, the default starting point for wash buffer optimization in protein affinity methods is either PBS or Tris-buffered saline (TBS), which have physiological levels of salt and pH. If the desired interaction is observed, low levels (typically 0.5-1.0%) of SDS, Triton®-X-100, 3-((3-cholamidopropyl)dimethylammonio)-1-propanesulfonate (CHAPS) or other mild detergents should be included to reduce background. If non-specific interactions still persist and the desired interaction is still strong, the stringency could be further

increased by incrementing the NaCl concentration to 0.5 M or even 1 M to reduce ionic and electrostatic attractions. However, salts and detergents are not compatible with downstream mass spectrometry analysis, therefore, strong conditions were discarded in the modified extraction protocol, which future objective is being applied to viral particles to analyse potential palmitoylated proteins by MS/MS-LC.

In the subsequent experiments, 1% (w/v) SDS+PBS (Ca^{2+}, Mg^{2+}-free) was used as lysis and wash buffer. SDS as detergent was added to keep proteins in an unfolded state that helps extraction, to avoid the formation of protein aggregates during the different steps of the protocol, and to reduce the amount of non-desired proteins that stick to the beads through hydrophobic interactions (Helenius & Simons, 1975; Turro et al., 1995; Winogradoff et al., 2020). The percentage of SDS in the samples is diluted from 1% to 0.1% before incubating with the beads as the manufacture datasheet recommends not adding more than 0.1 % (w/v) SDS. Only PBS (Ca^{2+}/Mg^{2+}-free) was selected to perform CuACC reaction, and the incubation with the different types of beads is selected, due to eliminate chelators and because, in most cases, interactions are fairly robust and will occur in any standard buffer of near-neutral pH, such as PBS or TBS.

Low levels of reducing agents such as 1-2 mM DTT or β-mercaptoethanol are usually added to the wash buffer because they can help disrupt non-specific interactions mediated by disulfide bridges or nucleophilic attractions (Smithies, 1965). However, the palmitoyl analogue presents the alkyne group attached to its terminal moiety through a disulfide bond, which could be broken by the presence of these compounds; thus, reducing agents could not be incorporated into the wash buffer.

The most effective type of elution condition (pH, ionic strength, chaotropic, or denaturant) depends on the specific composition of ionic, hydrophobic, and hydrogen bonds involved in the samples. The ideal elution buffer effectively releases the antigens without irreversibly denaturing or inactivating them. In the practice, all elution buffers cause some loss of antigen function, limiting the number of times the affinity support could be reused. Any of the supports tested during these experiments (Dde Azide Agarose resin, NeutrAvidin agarose beads, Protein G Sepharose beads, magnetic streptavidin beads) could be recovered and reuse for other assays.

173

In the Click-&-Go™ approach, the elution buffer was composed of 100 mM sodium phosphate and 2%(v/v) hydrazine. As the manufacturer's datasheet stated, the treatment with this hydrazine solution would yield a highly enriched population of nascent proteins. If the protocol were adequate, a huge difference would have been expected between the gp41 signal in the wild type and the treated samples. However, as Figure 4.9 A showed, approximately the same signal was obtained from both samples, containing a remarkable background. The potent wash conditions and the strident elution buffer seemed too strong for the extraction, causing damage to the samples. Together with the fact that hydrazine has hazardous properties even in solution (Niemeier & Kjell, 2013), it has made the Click-&-Go™ strategy insufficient for the final purpose of developing an extraction protocol.

In the biotin-avidin binding approach, the β-mercaptoethanol elution buffer was used as was the preferred election for NeutrAvidin agarose beads according to the manufacturer's datasheet. However, no differences were seen between wild type, and treated samples after elution in Figure 4.11 A, and part of the proteins remained stuck on the beads after performed the test showed in Figure 4.11 B; thus, β-mercaptoethanol dilution was not working well as elution buffer.

Traditional immunoprecipitations for downstream analysis by reducing SDS-PAGE and Western blot detection involve elution directly in reducing SDS-PAGE sample buffer (Grabski & Novagen, 2001). This buffer is designed to denature and reduce proteins for electrophoresis. These harsh conditions will cause multiple non-specific proteins to co-elute with the antigen, such as fragments of the immobilized affinity ligand (e.g., subunits of Protein G, NeutrAvidin or streptavidin) may be stripped from the beads but their pattern size should be known, not interfering with the final Western blot analysis of the proteins of interest. Therefore, SDS-PAGE sample buffer was chosen as the final elution agent for the protocol after obtaining positive results after the different extraction attempts (Figures 4.17 & 4.18).

Apart from the variables mentioned above that influence the total process of developing the final protocol, in general terms, one of the most limiting issue to reach a protocol for the extraction of HIV-1 palmitoylated proteins was the quantity of protein

used at the beginning of the extraction experiments. Multiple viral particle purifications to form a decent pull for both wt and pwt were needed, which has implied quite a long time due to working with non-infective viral-like particles. Normally, the initial amounts of total protein after extraction protocols for final proteomic analysis are from 100 μg to 1 mg of total protein from a cell lysate (Feist & Hummon, 2015), which do not necessitate as much care and precision as microscale samples as in this case. During the different steps of the protocol, part of the sample was lost due to the multiple washes and incubations, limiting the final amount of sample obtained in the elute for the future Western blot detection and proteomic analyses. However, After overcoming all the aforesaid variables, the palmitoyl-modified analogue presented in this chapter could be used to stablish an extraction protocol for the extraction of HIV-1 palmitoylated proteins, finally based in the CuAAC reaction and the biotin-avidin strong binding. This final optimized protocol is detailed in Section 4.2.3.2.

This set-up protocol could have successfully applied to pwt pulls to extract potentially HIV-1 palmitoylated proteins, which were subsequently analysed by MS/MS-LC, as it is show in Table 4.5. After curating, 153 potentially palmitoylated proteins were detected exclusively in viral particles treated with the palmitoyl-modified analogue. The first issue that could catch the attention is that HIV-1 gp41 is not listed even it is documented that it is palmitoylated (Rousso et al., 2000; Syu et al., 1991; C. Yang et al., 1995) and proven in this Thesis with the palmitoyl-modified analogue (Figure 4.8). It could be justified by the restrictiveness of the method used during the proteomic analysis. The use of stringent filtering resulted in a decrease in the number of identifications. In the same manner as Env glycoprotein was not present in the final list, other important hits could have been lost. There are two possible explanations for this aspect: the enrichment might be nonspecific, which is unlikely given that proteins were identified far in excess of untreated pulls, or the prediction tools might not properly capture all the potential sites of palmitoylation. Nevertheless, the fact that almost the 80% of the detected proteins have already been deciphered to be palmitoylated according to SwissPalm database, means that our proteomic results are reliable, robust, and very restrictive.

Colquhoun et al. (2015) tried to detect acylated host-proteins during HIV-1 infection by performing a similar strategy to the approach presented in this Thesis, but with some differences. They used bioorthogonal mimetics of palmitoyl-CoA and myristoyl-CoA, thus, they also studied myristoylated proteins not only palmitoylated proteins. Their extraction protocol was based on a system where the modified proteins with the clickable probe are covalently bound to agarose beads, so on-bead tryptic digestion was necessary for the identification of the proteins using mass spectrometry. They detected 185 proteins retained on the resins from cells labelled with palmitic acid azide. They eliminated those proteins which did not contain the proper palmitoylation motif and they obtained that the 65–70% of the identified proteins were considered palmitoylated according to CSS-Palm software (Ren et al., 2008). As 76.47% of the extracted proteins with our protocol are described to be palmitoylated in accordance with the SwissPalm database (Blanc et al., 2015, 2019), it seemed that our extraction protocol and subsequent proteomic analysis were more precise than in Colquhoun et al. (2015). This could be related to inherent limitations of their experimental design: the modified peptide remains conjugated to the beads and undetectable and they attempted to cleave the modifications using a number of methods, but they were unable to achieve satisfactory results; and palmitoylation was subjected to loss during sample preparation. Our experimental design overcomes the limitation of on-bead digestion by the competition between two different types of beads (Protein G Sepharose beads and streptavidin magnetic beads) and the subsequent elution in SDS-PAGE sample buffer, making our extraction protocol more efficient and reproducible.

While further studies with suitable cellular localization markers and their appropriate controls must be undertaken before claims could be made of cellular localization, qualitatively the vast majority of the detected proteins were situated mainly forming part of the spliceosome and the proteasome (Figure 4.20 A) as indicated the BiNGO tool (Maere et al., 2005). In accordance with BiNGO results for their biological and molecular functions, and their cellular compartment (Figure 4.20) and subcellular localization estimated by SwissPalm (Figure 4.19 E), it could be hypothesized that the detected proteins would be implicated in the control and regulation of the machinery of transcription and secretion during HIV-1 morphogenesis.

STRING and BioGRID analyses (Stark et al., 2006; Szklarczyk et al., 2021) suggested that those detected proteins are at least partially biologically connected (Figure 4.21), mainly associated into three well-defined interaction clusters. The importance of the different detected palmitoylated proteins in HIV-1 infection is discussed above.

One of these clusters contains some heterogeneous nuclear ribonucleoproteins (hnRNPs): hnRNP A1, hnRNP R, hnRNP E2 (PCBP2), hnRNP C, hnRNP H1, hnRNP D and hnRNP L. These hnRNPs include RNA-binding proteins that are involved in processing heterogeneous nuclear RNAs into mature mRNAs, and trans-factors which regulate gene expression (Chaudhury et al., 2010). It is known that HIV-1 splicing is regulated in part by some of these hnRNPs (Ostermann et al., 2021).

hnRNP C is found predominately in the nucleus and acts as a key player in nuclear retention of HIV-1 unspliced and intron-containing RNA (Nakielny & Dreyfuss, 1996; Piñol-Roma, 1997). Both hnRNP C and hnRNP A1 bind to adenine-uracil-containing sequences (Hamilton et al., 1997). hnRNP A1 is a shuttling protein that contains a nuclear localization signal as well as an export signal and participates in RNA processing in both the nucleus and cytoplasm (Monette et al., 2009; Nakielny & Dreyfuss, 1996). In accordance with its shuttling nature, hnRNP A1 has been shown to facilitate the nuclear export of mRNAs, but it is also involved in the nuclear retention of transcripts (Black et al., 1995; Izaurralde et al., 1997). The mechanism by which hnRNP A1 decides to retain or export transcripts is still undeciphered. In addition, hnRNP A1 binding stimulates HIV-1 Rev mediated nuclear export of reporter RNA (Mikaélian et al., 1996; Najera et al., 1999). hnRNPD, also known as ARE RNA-binding protein 1 (AUF1), influences RNA stability via ARE binding. During HIV-1 infection, it is relocalized to the cytoplasm and associates with Gag protein, influencing its expression (Lund et al., 2012). hnRNP H1 bound to discrete sites on HIV-1 RNA, and its depletion is deleterious for the infectious virion yield, so it has a splicing enhancer role (Kutluay et al., 2019). The hnRNPs R and E2 are shown to interact with HIV-1 Rev protein by different mechanisms while viral replication as other ribonucleoproteins like A1, E1, Q, K, and U (Hadian et al., 2009; Woolaway et al., 2007). Other hnRNPs such as F, K, P2 (FUS), Q and R have previously been shown to bind to select segments of viral RNA and to have roles in HIV replication

(Knoener et al., 2017). No information is available up to date about the relationship between hnRNP L and HIV-1, but according to Figure 4.20, this protein seems to be mainly forming part of the spliceosome, playing a determinant role during HIV-1 infection.

In the same cluster could be found some members of the serine/arginine (SR)-rich protein family: SRSF1, SRSF8, SRSF9 and SRSF10. These proteins are critical components of the machineries carrying out and maintaining an efficient gene expression. SR proteins are characterized by their ability to interact simultaneously with RNA and other protein components via an RNA recognition motif (RRM) and through a domain rich in arginine and serine residues, the RS domain. Their functional roles in gene expression are quite diverse, from their classical involvement in constitutive and alternative pre-mRNA splicing to various post-splicing activities (mRNA nuclear export, nonsense-mediated decay, and mRNA translation) (Shepard & Hertel, 2009). In HIV-1 replication cycle, it is known that SRSF1 activates transcription of HIV-1 genome in the early stages of viral infection. SRSF1 is substituted by Tat protein in the later stages to promote release of the stalled polymerase and for more efficient transcriptional elongation (Paz et al., 2014). SRSF10 is also important for the proper expression and processing of HIV-1 and other viral transcripts. Its overexpression has functional consequences in a growing list of cancers, and it has also been implicated in the metabolism of glucose, fat, and cholesterol, in the development of the embryonic heart, and in neurological processes. Thus, this factor has become a potentially therapeutic target to fight against cancer and viral infections (Shkreta et al., 2021). There is no information about SRSF8 and SRSF9 proteins in HIV-1 infection but taking into account that other members of the SR family, such as SRSF2 and SRSF6, are common HIV-1 dependency factors (HDF) associated with spliceosome and mRNA splicing related proteins, could lead to think that SRSF8 and SRSF9 are potential HDF. These HDF are essential components for HIV-1 replication, but not lethal to the host cell when their expression is silenced, that interact with pre-mRNA cis-regulatory elements and direct the fate of the nascent transcripts and in turn of viral factors essential for replication (Sertznig et al., 2018).

Other highlighted proteins of this cluster in HIV-1 infection are the following: NONO, LARP7, NCL, YBX1 and ILF3.

- NONO protein is stablished as essential for cyclic GMP-AMP synthase (cGAS) activation by the virus and cGAS association with HIV-1 DNA in the nucleus, an innate strategy to achieve distinction of viruses from self in the nucleus (Lahaye et al., 2018).

- La-related protein 7 (LARP7) has a role in 7SK-mediated regulation of transcription and HIV-1 gene expression, where the 7SK small nuclear ribonucleoprotein plays a central role in RNA polymerase II elongation control (Brogie & Price, 2017; H. Lu et al., 2013; Mizutani et al., 2014).

- Cell-surface Nucleolin (NCL) has been recognised as a low-affinity co-receptor for HIV-1, whose nuclear levels are increased during infection, and could be used as an potential antiviral target (DeBoer et al., 2014; Perrone et al., 2016).

- Y-box binding protein 1 (YBX1) enhanced the gene expression and viral production of HIV-1 by stabilizing HIV-1 RNAs and stimulating transcription (Jung et al., 2018; Mu et al., 2013).

- Interleukin enhancer binding factor 3 (ILF3) is a binding protein that complexes with other proteins, dsRNAs, small noncoding RNAs, and mRNAs to regulate gene expression and stabilize mRNAs. This protein forms a heterodimer with transcription factor ILF2 required for T-cell expression of interleukin 2 and it has been found interacting with HIV-1 Rev and Vpr (Barrero et al., 2013; Naji et al., 2012).

In the second cluster, there is a mixed of proteins with multiple different activities. On the one hand, appeared different members of the tRNA synthetase complex: MARS, SARS, QARS, RARS, IARS, FARSB. It is described that MARS, IARS and RARS could interact with HIV-1 Gag polyprotein (Engeland et al., 2014b). On the other hand, appeared some cellular DEAD-box (DDX) helicases as working partners of Rev during the transport of unspliced and partially spliced viral transcripts to the cytoplasm, such as DDX21 and DDX49 (Awasthi et al., 2018; Hammond et al., 2018; Jeang & Yedavalli, 2006). During this nuclear export process, other proteins are also implicated such as NMD3 and eIF6 (Behrens et al., 2017; Trotta et al., 2003).

Also, other outstanding proteins of this cluster in HIV-1 infection are presented above: Rab13, PGK1, UBE2M, ADK and NAT10.

- small GTP-binding protein Rab13, which is supposed to regulate together with Rab18 the ER-Golgi traffic or lipogenesis while organelle stress and liver injuries are present during HIV-1 pathogenesis (Khalatbari et al., 2020).

- Phosphoglycerate kinase 1 (PGK1) involved in glycolytic and metabolic events, has been seen to bind to HIV-1 Tat Specific Factor 1 (HTATSF1) and exerts functional control during cancer metastasis (Chang et al., 2021).

- Ubiquitin-conjugating enzyme E2 M (UBE2M) is a NEDD8-conjugating enzyme of the neddylation pathway that take part in posttranslational modification and change the activity of target proteins. It is known that HIV relies on neddylation for ubiquitin ligase-mediated functions and interacts with ubiquitin-ligases through Vpr and Vif proteins (Zheng et al., 2021).

- The adenosine kinase (ADK) has been found as a cellular host factor involved in the maintenance of HIV-1 latency (Röling et al., 2021).

- N-acetyltransferase 10 (NAT10), the enzyme that is in charge of acetylation of the N4 position of cytidine to RNAs, it is shown to be subverted by HIV-1 to increase its viral gene expression (Tsai et al., 2020).

The last cluster of detected palmitoylated proteins encompasses multiple components that are forming part of the cellular proteasome, encoded by the next genes: *PSMC1, PSMD2, PSMC3, PSMA4, PSMB4, PSMB5, PSMC6, PSMD8, PSMD12* and *PSMD13*. Generally, HIV-1 manipulate the proteasomal ubiquitination machinery to overcome the host cell defences (apoptosis, type 1 interferon response, and major histocompatibility complex class 1 antigen presentation), where the regulatory functions of HIV-1 Tat factor are essential. This manipulation of host proteasomal machinery by HIV-1 proteins are well-characterized and review in Lata et al. (2018).

In addition, in this cluster could be found different cyclin-dependent kinases (CKs), such as CK3, CK4, CK5 and CK8. Vpr and Tat proteins could perturb the cell cycle to optimize HIV-1 replication. Vpr arrests the cell cycle at G2 by inactivating the cyclin B/CK1 complex. Tat regulates the cell cycle by altering factors involved in proliferation and differentiation and associating with multiple cyclin/CK complexes. Therefore, CKs have become therapeutic targets for developing HIV-1 cure strategies (Fuente et al., 2003; Rice, 2016).

Finally, some other important detected proteins that present a relationship with HIV-1 pathogenesis are forming part of this last cluster: MCM6, CSDE1, AURKA, RFC3, FTH1, COBP1, MAPK3, CCT4 and DPP4.

- The protein encoded by *MCM* gene is one of the highly conserved mini-chromosome maintenance proteins (MCMs) that are essential for the initiation of eukaryotic genome replication. The hexameric protein complex formed by the MCMs (MCM6) is a key component of the pre-replication complex and could be involved in the formation of replication forks and in the recruitment of other DNA replication related proteins. It is shown that different HIV-1 viral proteins need MCM6. Pol and IN have a physical interaction with this protein and Tat upregulates the abundance of MCM6 in the nucleoli and Vpr downregulates it (Gautier et al., 2009; Jäger et al., 2011; Jarboui et al., 2012; Lahouassa et al., 2016).

- Cold shock domain containing E1 (CSDE1) forms part of CRD-mediated mRNA stability complex, a protein complex that binds and promotes stabilization of mRNA molecules containing the coding region instability determinant (CRD). It is seen incorporated into HIV-1 Gag virus-like particles and to have a physical interaction with NC during replication (Jäger et al., 2011; Ritchie et al., 2015).

- Activation of aurora kinase A (AURKA) is a cell cycle-regulated kinase that appears to be involved in microtubule formation and/or stabilization at the spindle pole during chromosome segregation. Vpr upregulates AURKA activity, and this enzyme also could interact with Vpu protein. This two accessory proteins, Vpr and Vpu share a common ability to target cellular proteins such as AURKA for degradation (Lahouassa et al., 2016; Miyakawa et al., 2012; Simon et al., 2015; Sugden et al., 2016).

- The elongation of primed DNA templates by DNA polymerase delta and DNA polymerase epsilon requires the accessory proteins proliferating cell nuclear antigen (PCNA) and replication factor C (RFC), such as the replication factor C subunit 3 (RFC3). It is known that HIV-1 Tat interacts with the RNA polymerase II holoenzyme, which includes some RFCs like RFC3, during gene expression of Tat-mediated transactivation of the HIV-1 long terminal repeat (LTR) (Cujec et al., 1997).

- The coatomer complex or coat protein complex 1 (COBP1) present in the Golgi apparatus, participates in the sorting and retrograde trafficking of proteins and

lipids from the Golgi to the ER. This protein has been implicated in the downregulation of HLA-A2, CD4, CD28 and CD8 by HIV-1 Nef .

- The ferritin heavy chain 1 (FTH1), the major intracellular iron storage protein in prokaryotes and eukaryotes. HIV-1 gp120 and Vpr upregulates the expression of this protein (Barrero et al., 2013; Shah et al., 2013).

- Mitogen-activated protein kinase 3 (MAPK3) is a member of the MAP kinase family, which acts in a signalling cascade that regulates various cellular processes such as proliferation, differentiation, and cell cycle progression in response to a variety of extracellular signals such as viral infection. This kinase is activated by upstream kinases, resulting in its translocation to the nucleus where it phosphorylates nuclear targets. Efficient disengagement of the reverse transcription cellular complex and subsequent nuclear translocation require phosphorylation of reverse transcription complex components by virion-associated kinases, such as these MAPKs. MAPK signal pathway is well-described to positively regulate the replication of HIV-1 (Gong et al., 2011; Jacqué et al., 1998; X. Yang & Gabuzda, 1999).

- Chaperonin containing TCP1 subunit 4 (CCT4) is one of the eight homologous subunits that conform the chaperonin containing TCP1 complex (CCT), also called the TCP1 ring complex. The CCT assists in the folding of newly translated polypeptides. This complex has been shown to interact with multiple HIV-1 viral proteins: Gag, GagPol, gp120, Nef, Tat, Vif and IN (Y. Luo et al., 2016; Milev et al., 2012; Parissi et al., 2001; Wu-Baer et al., 1996).

- Dipeptidyl peptidase 4 (DPP4) or the T cell activation marker CD26 plays an important role in immune regulation, signal transduction, apoptosis and in tumor progression (Morimoto et al., 1994; Pro & Dang, 2004). This protein was shown to be a functional receptor for Middle East respiratory syndrome coronavirus (MERS-CoV), it is suggested that it may play a similar role with SARS-CoV-2, responsible for COVID-19 (Govender et al., 2021). It is shown that HIV-1 Tat inhibits the enzymatic activity of DPP4 triggering the suppression of DNA synthesis and IL-1β production, stimulating secretion of IL-1 receptor antagonist and TNF-α, and causing in part the immunosuppressive effects of Tat (Morimoto et al., 1994; Tansi et

al., 2010; Weihofen et al., 2005; Wrenger et al., 1997). Also, it is known to act as a cofactor for HIV-1 entry in CD4+ cells (Callebaut et al., 1993).

The exhaustive analysis performed above of the HIV-1 palmitoylated proteins detected from the pwt samples lead to think that the vast majority of these proteins are well-described to be implicated in the control and regulation of the machinery of transcription and secretion, as well as, in the gene expression during HIV-1 morphogenesis according to Figure 4.20. These cellular proteins are kept in the mature virions during the budding process due to their multiple interactions with HIV-1 accessory proteins such as Tat, Vpr, Vpu and Nef, or even attached to the viral genome. That it is why these proteins are mainly cytoplasmic and come from the nucleus or its surroundings (Figure 4.19 C & E).

All in all, in this chapter of this doctoral Thesis, a protocol for the extraction of the HIV-1 palmitoylated proteins could have been developed based in the combination of a clickable palmitoyl-modified analogue and the strong union between biotin and avidin derivates. The aforementioned palmitoylated proteins were obtained after applying this set-up protocol to HIV-1 particles treated with the palmitoyl analogue and their analysis by mass spectrometry. These results give a shred of light in deciphering the HIV-1 palmitoylome.

Chapter 5.

General Conclusions

Chapter 5: General Conclusions

In accordance with all the above mentioned results obtained in the different chapters of this doctoral Thesis, the following general conclusions are proposed:

Proving the direct relationship between Gag and Env glycoprotein.

- A real co-localization of gp41 and Gag/MA in HIV-1 viral particles has been shown. This supports the idea of Gag/MA and Env relationship during HIV-1 morphogenesis previously stated in the literature.
- The capability of interaction with cholesterol of the gp41 protein does not require the presence of other viral proteins such as Gag proteins.

An indirect Gag-cholesterol interaction seems to take place during morphogenesis.

- Neither Gag nor MA seem to directly interact with membrane cholesterol at a viral and cellular level.
- The maturation state of the viral particles does not modify the interaction between MA and Gag with cholesterol.
- This Thesis is proposed a model sandwich of indirect interaction between Gag and cholesterol. This model supports that Gag is interacting with gp41, while Env is interacting with cholesterol at the same time. Gag and cholesterol could be driving the formation of chol-enriched membrane nanodomains that host-selected proteins such as Env and reduce their mobility in the membrane. In there, Env, which interacts directly with this lipid and Gag/MA, could be stuck forming a sandwich during morphogenesis, where there would not be a direct interaction between Gag/MA and chol, but an indirect interaction could exist via Env glycoprotein.

The palmitoyl-modified analogue acts as its natural counterpart.

- The palmitoyl analogue could palmitoylate HIV-1 gp41 cysteines as its natural counterpart after incubation in HEK 293T cells.

- The correct function of this clickable probe could be successfully verified by a palmitoylation test developed based in the copper (I)-catalyzed azide-alkyne cycloaddition (CuAAC) reaction together with the immunoprecipitation of gp41 by Chessie-8 coupled to Protein G Sepharose beads.

A definitive protocol for the extraction of HIV-1 palmitoylated proteins could have been developed.

- After multiple assays and tests to control all the variables, factors and specific binding conditions that affect the immunoprecipitation process, a definitive protocol for the extraction of the HIV-1 palmitoylated proteins could have been developed. The final protocol is based in based in the CuAAC reaction, the palmitoyl-modified analogue and the strong biotin-avidin binding.

- A fluorophore test designed during this Thesis could be adapted to confirm the adequate functioning of the CuACC reaction for other clickable lipid probes similar to the palmitoyl-modified analogue.

The final optimised protocol could be successfully applied to extract HIV-1 palmitoylated proteins.

- The develop protocol was used to extract HIV-1 palmitoylated proteins for their subsequent proteomic analysis by MS/MS-LC.

- 153 proteins were exclusively detected in the sample treated with the palmitoyl-modified analogue. The 76.47% of the potential palmitoylated proteins, are described to be palmitoylated in accordance with the SwissPalm database.

- The vast majority of these proteins were cytoplasmic proteins localized in the nucleus or its surroundings, mainly forming part of the spliceosome and the proteasome.

- After analysing their biological and molecular functions, it could be suggested that the detected palmitoylated proteins would be implicated in gene expression and in the control and regulation of the machinery of transcription and secretion during HIV-1 morphogenesis.

Chapter 6.

References

Chapter 6: References

Abacioglu, Y. H., Fouts, T. R., Laman, J. D., Claassen, E., Pincus, S. H., Moore, J. P., Roby, C. A., Kamin-Lewis, R., & Lewis, G. K. (1994). Epitope mapping and topology of baculovirus-expressed HIV-1 gp160 determined with a panel of murine monoclonal antibodies. *AIDS Research and Human Retroviruses*, *10*(4), 371–381. https://doi.org/10.1089/AID.1994.10.371

Abbas, W., Dichamp, I., & Herbein, G. (2012). The HIV-1 Nef Protein Interacts with two components of the 40S small ribosomal subunit, the RPS10 protein and the 18S rRNA. *Virology Journal*, *9*(1), 1–9. https://doi.org/10.1186/1743-422X-9-103/FIGURES/5

Ahirwar, R., Bariar, S., Balakrishnan, A., & Nahar, P. (2015). BSA blocking in enzyme-linked immunosorbent assays is a non-mandatory step: a perspective study on mechanism of BSA blocking in common ELISA protocols. *RSC Advances*, *5*(121), 100077–100083. https://doi.org/10.1039/C5RA20750A

Ahmed, H., & Ahmed PhD, H. (2017). Principles and Reactions of Protein Extraction, Purification, and Characterization. *Principles and Reactions of Protein Extraction, Purification, and Characterization*. https://doi.org/10.1201/9780203507438

Aisenbrey, C., Rifi, O., & Bechinger, B. (2020). Structure, membrane topology and influence of cholesterol of the membrane proximal region: transmembrane helical anchor sequence of gp41 from HIV. *Scientific Reports 2020 10:1*, *10*(1), 1–14. https://doi.org/10.1038/s41598-020-79327-6

Ako-Adjei, D., Fu, W., Wallin, C., Katz, K. S., Song, G., Darji, D., Brister, J. R., Ptak, R. G., & Pruitt, K. D. (2015). HIV-1, human interaction database: current status and new features. *Nucleic Acids Research*, *43*(Database issue), D566–D570. https://doi.org/10.1093/NAR/GKU1126

Alfadhli, A., & Barklis, E. (2014). The roles of lipids and nucleic acids in HIV-1 assembly. In *Frontiers in Microbiology* (Vol. 5, Issue MAY). Frontiers Research Foundation. https://doi.org/10.3389/fmicb.2014.00253

Alfadhli, A., Mack, A., Ritchie, C., Cylinder, I., Harper, L., Tedbury, P. R., Freed, E. O., & Barklis, E. (2016). Trimer Enhancement Mutation Effects on HIV-1 Matrix Protein Binding Activities. *Journal of Virology*, *90*(12), 5657–5664. https://doi.org/10.1128/jvi.00509-16

Alfadhli, A., Staubus, A. O., Tedbury, P. R., Novikova, M., Freed, E. O., & Barklis, E. (2019). Analysis of HIV-1 Matrix-Envelope Cytoplasmic Tail Interactions. *Journal of Virology*, *93*(21). https://doi.org/10.1128/jvi.01079-19

Alfadhli, A., Still, A., & Barklis, E. (2009). Analysis of Human Immunodeficiency Virus Type 1 Matrix Binding to Membranes and Nucleic Acids. *Journal of Virology*, *83*(23), 12196–12203. https://doi.org/10.1128/jvi.01197-09

Aloia, R. C., Jensen, F. C., Curtain, C. C., Mobley, P. W., & Gordon, L. M. (1988). Lipid composition and fluidity of the human immunodeficiency virus. *Proceedings of the National Academy of Sciences of the United States of America*, *85*(3), 900. https://doi.org/10.1073/PNAS.85.3.900

Aloia, R. C., Tian, H., & Jensen, F. C. (1993). Lipid composition and fluidity of the human immunodeficiency virus envelope and host cell plasma membranes. *Proceedings of the National Academy of Sciences of the United States of America*, *90*(11), 5181–5185. https://doi.org/10.1073/PNAS.90.11.5181

Anraku, K., Fukuda, R., Takamune, N., Misumi, S., Okamoto, Y., Otsuka, M., & Fujita, M. (2010). Highly sensitive analysis of the interaction between HIV-1 gag and phosphoinositide derivatives based on surface plasmon resonance. *Biochemistry*, *49*(25), 5109–5116. https://doi.org/10.1021/bi9019274

Ashburner, M., Ball, C. A., Blake, J. A., Botstein, D., Butler, H., Cherry, J. M., Davis, A. P., Dolinski, K., Dwight, S. S., Eppig, J. T., Harris, M. A., Hill, D. P., Issel-Tarver, L., Kasarskis, A., Lewis, S., Matese, J. C., Richardson, J. E., Ringwald, M., Rubin, G. M., & Sherlock, G. (2000). Gene Ontology: tool for the unification of biology. *Nature Genetics 2000 25:1*, *25*(1), 25–29. https://doi.org/10.1038/75556

Awasthi, S., Verma, M., Mahesh, A., Khan, M. I. K., Govindaraju, G., Rajavelu, A., Chavali, P. L., Chavali, S., & Dhayalan, A. (2018). DDX49 is an RNA helicase that affects translation by regulating mRNA export and the levels of pre-ribosomal RNA. *Nucleic Acids Research*, *46*(12), 6304. https://doi.org/10.1093/NAR/GKY231

Barklis, E., Staubus, A. O., Mack, A., Harper, L., Barklis, R. L., & Alfadhli, A. (2018). Lipid biosensor interactions with wild type and matrix deletion HIV-1 Gag proteins. *Virology*, *518*, 264–271. https://doi.org/10.1016/j.virol.2018.03.004

Barrero, C. A., Datta, P. K., Sen, S., Deshmane, S., Amini, S., Khalili, K., & Merali, S. (2013). HIV-1 Vpr modulates macrophage metabolic pathways: a SILAC-based quantitative analysis. *PloS One*, *8*(7). https://doi.org/10.1371/JOURNAL.PONE.0068376

Barros, M., Heinrich, F., Datta, S. A. K., Rein, A., Karageorgos, I., Nanda, H., & Lösche, M. (2016). Membrane Binding of HIV-1 Matrix Protein: Dependence on Bilayer Composition and Protein Lipidation. *Journal of Virology*, *90*(9), 4544–4555. https://doi.org/10.1128/jvi.02820-15

Baumgart, F., & Schütz, G. J. (2015). Detecting protein association at the T cell plasma membrane. *Biochimica et Biophysica Acta (BBA) - Molecular Cell Research*, *1853*(4), 791–801. https://doi.org/10.1016/J.BBAMCR.2014.09.026

Bednarska, J., Pelchen-Matthews, A., Novak, P., Burden, J. J., Summers, P. A., Kuimova, M. K., Korchev, Y., Marsh, M., & Shevchuk, A. (2020). Rapid formation of human immunodeficiency virus-like particles. *Proceedings of the National Academy of Sciences of the United States of America*, *117*(35), 21637–21646. https://doi.org/10.1073/PNAS.2008156117/SUPPL_FILE/PNAS.2008156117.SAPP.P DF

Behrens, R. T., Aligeti, M., Pocock, G. M., Higgins, C. A., & Sherer, N. M. (2017). Nuclear Export Signal Masking Regulates HIV-1 Rev Trafficking and Viral RNA Nuclear Export. *Journal of Virology*, *91*(3), 2107–2123. https://doi.org/10.1128/JVI.02107-16

Bell, S. M., & Bedford, T. (2017). Modern-day SIV viral diversity generated by extensive recombination and cross-species transmission. *PLoS Pathogens*, *13*(7). https://doi.org/10.1371/JOURNAL.PPAT.1006466

Bennett, A. E., Narayan, K., Shi, D., Hartnell, L. M., Gousset, K., He, H., Lowekamp, B. C., Yoo, T. S., Bliss, D., Freed, E. O., & Subramaniam, S. (2009). Ion-abrasion scanning electron microscopy reveals surface-connected tubular conduits in HIV-infected macrophages. *PLoS Pathogens*, *5*(9). https://doi.org/10.1371/journal.ppat.1000591

Berro, R., de La Fuente, C., Klase, Z., Kehn, K., Parvin, L., Pumfery, A., Agbottah, E., Vertes, A., Nekhai, S., & Kashanchi, F. (2007). Identifying the membrane proteome of HIV-1 latently infected cells. *Journal of Biological Chemistry*, *282*(11), 8207–8218. https://doi.org/10.1074/jbc.M606324200

Best, M. D. (2009). Click chemistry and bioorthogonal reactions: Unprecedented selectivity in the labeling of biological molecules. In *Biochemistry* (Vol. 48, Issue 28, pp. 6571–6584). American Chemical Society. https://doi.org/10.1021/bi9007726

Bhattacharya, J., Peters, P. J., & Clapham, P. R. (2004). Human Immunodeficiency Virus Type 1 Envelope Glycoproteins That Lack Cytoplasmic Domain Cysteines: Impact on Association with Membrane Lipid Rafts and Incorporation onto Budding Virus Particles. *JOURNAL OF VIROLOGY*, *78*(10), 5500–5506. https://doi.org/10.1128/.78.10.5500-5506.2004

Bhattacharya, J., Repik, A., & Clapham, P. R. (2006). Gag Regulates Association of Human Immunodeficiency Virus Type 1 Envelope with Detergent-Resistant Membranes. *Journal of Virology*, *80*(11), 5292–5300. https://doi.org/10.1128/jvi.01469-05

Björkbom, A., Róg, T., Kaszuba, K., Kurita, M., Yamaguchi, S., Lönnfors, M., Nyholm, T. K. M., Vattulainen, I., Katsumura, S., & Slotte, J. P. (2010). Effect of Sphingomyelin

Headgroup Size on Molecular Properties and Interactions with Cholesterol. *Biophysical Journal*, *99*(10), 3300–3308. https://doi.org/10.1016/J.BPJ.2010.09.049

Black, A. C., Luo, J., Watanabe, C., Chun, S., Bakker, A., Fraser, J. K., Morgan, J. P., Rosenblatt, J. D., Black, C., Ruland, C. T., Luo, J., Bakker, A., Fraser, J. K., & Rosenblatt, J. D. (1995). Polypyrimidine tract-binding protein and heterogeneous nuclear ribonucleoprotein A1 bind to human T-cell leukemia virus type 2 RNA regulatory elements. *Journal of Virology*, *69*(11), 6852. https://doi.org/10.1128/JVI.69.11.6852-6858.1995

Blanc, M., David, F., Abrami, L., Migliozzi, D., Armand, F., Bürgi, J., & van der Goot, F. G. (2015). SwissPalm: Protein Palmitoylation database. *F1000Research*, *4*. https://doi.org/10.12688/f1000research.6464.1

Blanc, M., David, F. P. A., & van der Goot, F. G. (2019). SwissPalm 2: Protein S-Palmitoylation Database. *Methods in Molecular Biology (Clifton, N.J.)*, *2009*, 203–214. https://doi.org/10.1007/978-1-4939-9532-5_16

Booth, A. M., Fang, Y., Fallon, J. K., Yang, J. M., Hildreth, J. E. K., Gould, S. J., Sandefur, S., & Varthakavi, V. (2006). Exosomes and HIV Gag bud from endosome-like domains of the T cell plasma membrane. *Journal of Cell Biology*, *172*(6), 923–935. https://doi.org/10.1083/jcb.200508014

Bou-Nader, C., Muecksch, F., Brown, J. B., Gordon, J. M., York, A., Peng, C., Ghirlando, R., Summers, M. F., Bieniasz, P. D., & Zhang, J. (2021). HIV-1 matrix-tRNA complex structure reveals basis for host control of Gag localization. *Cell Host & Microbe*, *29*(9), 1421-1436.e7. https://doi.org/10.1016/J.CHOM.2021.07.006

Boutet, E., Lieberherr, D., Tognolli, M., Schneider, M., & Bairoch, A. (2007). UniProtKB/Swiss-Prot. *Methods in Molecular Biology (Clifton, N.J.)*, *406*, 89–112. https://doi.org/10.1007/978-1-59745-535-0_4

Bradford, M. M. (1976). A Rapid and Sensitive Method for the Quantitation of Microgram Quantities of Protein Utilizing the Principle of Protein-Dye Binding. In *ANALYTICAL BIOCHEMISTRY* (Vol. 72).

Brandano, L., & Stevenson, M. (2012). A Highly Conserved Residue in the C-Terminal Helix of HIV-1 Matrix Is Required for Envelope Incorporation into Virus Particles. *Journal of Virology*, *86*(4), 2347–2359. https://doi.org/10.1128/jvi.06047-11

Brégnard, C., Zamborlini, A., Leduc, M., Chafey, P., Camoin, L., Saïb, A., Benichou, S., Danos, O., & Basmaciogullari, S. (2013). Comparative proteomic analysis of HIV-1 particles reveals a role for Ezrin and EHD4 in the Nef-dependent increase of virus infectivity. *Journal of Virology*, *87*(7), 3729–3740. https://doi.org/10.1128/JVI.02477-12

Briggs, J. A. G., Wilk, T., & Fuller, S. D. (2003). Do lipid rafts mediate virus assembly and pseudotyping? In *Journal of General Virology* (Vol. 84, Issue 4, pp. 757–768). https://doi.org/10.1099/vir.0.18779-0

Brogie, J. E., & Price, D. H. (2017). Reconstitution of a functional 7SK snRNP. *Nucleic Acids Research*, *45*(11), 6864–6880. https://doi.org/10.1093/NAR/GKX262

Brown, D. A. (2006). Lipid rafts, detergent-resistant membranes, and raft targeting signals. *Physiology (Bethesda, Md.)*, *21*(6), 430–439. https://doi.org/10.1152/PHYSIOL.00032.2006

Brown, D. A., & London, E. (1998). Functions of lipid rafts in biological membranes. *Annual Review of Cell and Developmental Biology*, *14*, 111–136. https://doi.org/10.1146/ANNUREV.CELLBIO.14.1.111

Brown, D. A., & Rose, J. K. (1992). Sorting of GPI-anchored proteins to glycolipid-enriched membrane subdomains during transport to the apical cell surface. *Cell*, *68*(3), 533–544. https://doi.org/10.1016/0092-8674(92)90189-J

Brügger, B., Glass, B., Haberkant, P., Leibrecht, I., Wieland, F. T., & Kräusslich, H. G. (2006). The HIV lipidome: A raft with an unusual composition. *Proceedings of the National Academy of Sciences of the United States of America*, *103*(8), 2641–2646. https://doi.org/10.1073/PNAS.0511136103/SUPPL_FILE/11136FIG12.PDF

Buttler, C. A., Pezeshkian, N., Fernandez, M. v., Aaron, J., Norman, S., Freed, E. O., & van Engelenburg, S. B. (2018). Single molecule fate of HIV-1 envelope reveals late-stage viral lattice incorporation. *Nature Communications 2018 9:1*, *9*(1), 1–15. https://doi.org/10.1038/s41467-018-04220-w

Callebaut, C., Krust, B., Jacotot, E., & Hovanessian, A. G. (1993). T cell activation antigen, CD26, as a cofactor for entry of HIV in CD4+ cells. *Science (New York, N.Y.)*, *262*(5142), 2045–2050. https://doi.org/10.1126/SCIENCE.7903479

Campbell, S., Gaus, K., Bittman, R., Jessup, W., Crowe, S., & Mak, J. (2004). The raft-promoting property of virion-associated cholesterol, but not the presence of virion-associated Brij 98 rafts, is a determinant of human immunodeficiency virus type 1 infectivity. *Journal of Virology*, *78*(19), 10556–10565. https://doi.org/10.1128/JVI.78.19.10556-10565.2004

Campbell, S. M., Crowe, S. M., & Mak, J. (2001). Lipid rafts and HIV-1: from viral entry to assembly of progeny virions. In *Journal of Clinical Virology* (Vol. 22). www.elsevier.com/locate/jcv

Campbell, S. M., Crowe, S. M., & Mak, J. (2002). Virion-associated cholesterol is critical for the maintenance of HIV-1 structure and infectivity. *AIDS (London, England)*, *16*(17), 2253–2261. https://doi.org/10.1097/00002030-200211220-00004

Cantin, R., Méthot, S., & Tremblay, M. J. (2005). Plunder and Stowaways: Incorporation of Cellular Proteins by Enveloped Viruses. *Journal of Virology*, *79*(11), 6577–6587. https://doi.org/10.1128/jvi.79.11.6577-6587.2005

Casares, D., Escribá, P. v., & Rosselló, C. A. (2019). Membrane Lipid Composition: Effect on Membrane and Organelle Structure, Function and Compartmentalization and

Therapeutic Avenues. *International Journal of Molecular Sciences*, *20*(9). https://doi.org/10.3390/IJMS20092167

Chan, R., Uchil, P. D., Jin, J., Shui, G., Ott, D. E., Mothes, W., & Wenk, M. R. (2008). Retroviruses Human Immunodeficiency Virus and Murine Leukemia Virus Are Enriched in Phosphoinositides. *Journal of Virology*, *82*(22), 11228–11238. https://doi.org/10.1128/JVI.00981-08/SUPPL_FILE/SUPPLFIGURELEGENDS.ZIP

Chan, T. R., Hilgraf, R., Sharpless, K. B., & Fokin, V. v. (2004). Polytriazoles as copper(I)-stabilizing ligands in catalysis. *Organic Letters*, *6*(17), 2853–2855. https://doi.org/10.1021/ol0493094

Chan, W.-E., Lin, H.-H., & Chen, S. S.-L. (2005). Wild-Type-Like Viral Replication Potential of Human Immunodeficiency Virus Type 1 Envelope Mutants Lacking Palmitoylation Signals. *Journal of Virology*, *79*(13), 8374–8387. https://doi.org/10.1128/jvi.79.13.8374-8387.2005

Chang, Y. C., Chan, M. H., Li, C. H., Yang, C. J., Tseng, Y. W., Tsai, H. F., Chiou, J., & Hsiao, M. (2021). Metabolic protein phosphoglycerate kinase 1 confers lung cancer migration by directly binding HIV Tat specific factor 1. *Cell Death Discovery*, *7*(1). https://doi.org/10.1038/S41420-021-00520-1

Charlier, L., Louet, M., Chaloin, L., Fuchs, P., Martinez, J., Muriaux, D., Favard, C., & Floquet, N. (2014). Coarse-grained simulations of the HIV-1 matrix protein anchoring: Revisiting its assembly on membrane domains. *Biophysical Journal*, *106*(3), 577–585. https://doi.org/10.1016/j.bpj.2013.12.019

Charron, G., Zhang, M. M., Yount, J. S., Wilson, J., Raghavan, A. S., Shamir, E., & Hang, H. C. (2009). Robust fluorescent detection of protein fatty-acylation with chemical reporters. *Journal of the American Chemical Society*, *131*(13), 4967–4975. https://doi.org/10.1021/ja810122f

Chaudhury, A., Chander, P., & Howe, P. H. (2010). Heterogeneous nuclear ribonucleoproteins (hnRNPs) in cellular processes: Focus on hnRNP E1's multifunctional regulatory roles. *RNA*, *16*(8), 1449. https://doi.org/10.1261/RNA.2254110

Checkley, M. A., Luttge, B. G., & Freed, E. O. (2011). HIV-1 envelope glycoprotein biosynthesis, trafficking, and incorporation. In *Journal of Molecular Biology* (Vol. 410, Issue 4, pp. 582–608). Academic Press. https://doi.org/10.1016/j.jmb.2011.04.042

Chen, S., Xu, J., Liu, M., Rao, A. L. N., Zandi, R., Gill, S. S., & Mohideen, U. (2020). Investigation of HIV-1 Gag binding with RNAs and lipids using Atomic Force Microscopy. *PLoS ONE*, *15*(2). https://doi.org/10.1371/JOURNAL.PONE.0228036

Chertova, E., Bess, J. W., Crise, B. J., Sowder, R. C., Schaden, T. M., Hilburn, J. M., Hoxie, J. A., Benveniste, R. E., Lifson, J. D., Henderson, L. E., & Arthur, L. O. (2002). Envelope glycoprotein incorporation, not shedding of surface envelope

glycoprotein (gp120/SU), Is the primary determinant of SU content of purified human immunodeficiency virus type 1 and simian immunodeficiency virus. *Journal of Virology*, *76*(11), 5315–5325. https://doi.org/10.1128/JVI.76.11.5315-5325.2002

Chertova, E., Chertov, O., Coren, L. v., Roser, J. D., Trubey, C. M., Bess, J. W., Sowder, R. C., Barsov, E., Hood, B. L., Fisher, R. J., Nagashima, K., Conrads, T. P., Veenstra, T. D., Lifson, J. D., & Ott, D. E. (2006). Proteomic and Biochemical Analysis of Purified Human Immunodeficiency Virus Type 1 Produced from Infected Monocyte-Derived Macrophages. *Journal of Virology*, *80*(18), 9039–9052. https://doi.org/10.1128/jvi.01013-06

Chevallet, M., Luche, S., & Rabilloud, T. (2006). Silver staining of proteins in polyacrylamide gels. *Nature Protocols*, *1*(4), 1852–1858. https://doi.org/10.1038/NPROT.2006.288

Chien, M. P., Lin, C. H., & Chang, D. K. (2009). Recruitment of HIV-1 envelope occurs subsequent to lipid mixing: A fluorescence microscopic evidence. *Retrovirology*, *6*. https://doi.org/10.1186/1742-4690-6-20

Chojnacki, J., & Eggeling, C. (2021). Super-resolution sted microscopy-based mobility studies of the viral env protein at hiv-1 assembly sites of fully infected t-cells. *Viruses*, *13*(4). https://doi.org/10.3390/v13040608

Chojnacki, J., Staudt, T., Glass, B., Bingen, P., Engelhardt, J., Anders, M., Schneider, J., Müller, B., Hell, S. W., & Kräusslich, H. G. (2012). Maturation-dependent HIV-1 surface protein redistribution revealed by fluorescence nanoscopy. *Science*, *338*(6106), 524–528. https://doi.org/10.1126/science.1226359

Chojnacki, J., Waithe, D., Carravilla, P., Huarte, N., Galiani, S., Enderlein, J., & Eggeling, C. (2017). Envelope glycoprotein mobility on HIV-1 particles depends on the virus maturation state. *Nature Communications*, *8*(1). https://doi.org/10.1038/s41467-017-00515-6

Chukkapalli, V., Hogue, I. B., Boyko, V., Hu, W.-S., & Ono, A. (2008). Interaction between the Human Immunodeficiency Virus Type 1 Gag Matrix Domain and Phosphatidylinositol-(4,5)-Bisphosphate Is Essential for Efficient Gag Membrane Binding. *Journal of Virology*, *82*(5), 2405–2417. https://doi.org/10.1128/jvi.01614-07

Chukkapalli, V., Inlora, J., Todd, G. C., & Ono, A. (2013). Evidence in support of RNA-mediated inhibition of phosphatidylserine-dependent HIV-1 Gag membrane binding in cells. *Journal of Virology*, *87*(12), 7155–7159. https://doi.org/10.1128/JVI.00075-13

Chukkapalli, V., Oh, S. J., & Ono, A. (2010). Opposing mechanisms involving RNA and lipids regulate HIV-1 Gag membrane binding through the highly basic region of the matrix domain. *Proceedings of the National Academy of Sciences of the United States of America*, *107*(4), 1600–1605. https://doi.org/10.1073/pnas.0908661107

Ciftci, H., Tateishi, H., Koiwai, K., Koga, R., Anraku, K., Monde, K., Dağ, Ç., Destan, E., Yuksel, B., Ayan, E., Yildirim, G., Yigin, M., Ertem, F. B., Shafiei, A., Guven, O., Besler, S. O., Sierra, R. G., Yoon, C. H., Su, Z., … DeMirci, H. (2021). Structural insight into host plasma membrane association and assembly of HIV-1 matrix protein. *Scientific Reports*, *11*(1). https://doi.org/10.1038/s41598-021-95236-8

Cimarelli, A., & Luban, J. (1999). Translation elongation factor 1-alpha interacts specifically with the human immunodeficiency virus type 1 Gag polyprotein. *Journal of Virology*, *73*(7), 5388–5401. https://doi.org/10.1128/JVI.73.7.5388-5401.1999

Cohen, S. N., Chang, A. C., & Hsu, L. (1972). Nonchromosomal Antibiotic Resistance in Bacteria: Genetic Transformation of Escherichia coli by R-Factor DNA. *Proceedings of the National Academy of Sciences of the United States of America*, *69*(8), 2110. https://doi.org/10.1073/PNAS.69.8.2110

Coleman, E. M., Walker, T. N., & Hildreth, J. E. K. (2012). Loss of Niemann Pick type C proteins 1 and 2 greatly enhances HIV infectivity and is associated with accumulation of HIV Gag and cholesterol in late endosomes/lysosomes. *Virology Journal*, *9*. https://doi.org/10.1186/1743-422X-9-31

Colquhoun, D. R., Lyashkov, A. E., Mohien, C. U., Aquino, V. N., Bullock, B. T., Dinglasan, R. R., Agnew, B. J., & Graham, D. R. M. (2015). Bioorthogonal mimetics of palmitoyl-CoA and myristoyl-CoA and their subsequent isolation by click chemistry and characterization by mass spectrometry reveal novel acylated host-proteins modified by HIV-1 infection. *Proteomics*, *15*(12), 2066–2077. https://doi.org/10.1002/pmic.201500063

Contreras, F. X., Ernst, A. M., Wieland, F., & Brügger, B. (2011). Specificity of intramembrane protein-lipid interactions. *Cold Spring Harbor Perspectives in Biology*, *3*(6), 1–18. https://doi.org/10.1101/cshperspect.a004705

Cooper, G. M., & Hausman, R. E. (2013). *The Cell: A Molecular Approach* (6th ed.). Sinauer Associates.

Crisesg, B., & Rosesii, J. K. (1992). Identification of Palmitoylation Sites on CD4, the Human Immunodeficiency Virus Receptor*. *THE JOURNAL OF BIOLOGICAL CHEMISTRY*, *267*(19), 13593–13597.

Crowell, D. N., & Huizinga, D. H. (2009). Protein isoprenylation: the fat of the matter. In *Trends in Plant Science* (Vol. 14, Issue 3, pp. 163–170). Elsevier Ltd. https://doi.org/10.1016/j.tplants.2008.12.001

Cujec, T. P., Cho, H., Maldonado, E., Meyer, J., Reinberg, D., & Peterlin, B. M. (1997). The human immunodeficiency virus transactivator Tat interacts with the RNA polymerase II holoenzyme. *Molecular and Cellular Biology*, *17*(4), 1817–1823. https://doi.org/10.1128/MCB.17.4.1817

Dalton, A. K., Ako-Adjei, D., Murray, P. S., Murray, D., & Vogt, V. M. (2007). Electrostatic Interactions Drive Membrane Association of the Human Immunodeficiency Virus Type 1 Gag MA Domain. *Journal of Virology*, *81*(12), 6434–6445. https://doi.org/10.1128/jvi.02757-06

Das, J. (2011). Aliphatic diazirines as photoaffinity probes for proteins: Recent developments. *Chemical Reviews*, *111*(8), 4405–4417. https://doi.org/10.1021/CR1002722/ASSET/CR1002722.FP.PNG_V03

Datta, S. A. K., Heinrich, F., Raghunandan, S., Krueger, S., Curtis, J. E., Rein, A., & Nanda, H. (2011). HIV-1 Gag extension: Conformational changes require simultaneous interaction with membrane and nucleic acid. *Journal of Molecular Biology*, *406*(2), 205–214. https://doi.org/10.1016/j.jmb.2010.11.051

Datta, S. A. K., Zhao, Z., Clark, P. K., Tarasov, S., Alexandratos, J. N., Campbell, S. J., Kvaratskhelia, M., Lebowitz, J., Rein, A., Campbell, S. J., & Baker, J. A. (2007). Interactions between HIV-1 Gag Molecules in Solution: An Inositol Phosphate-mediated Switch NIH Public Access. In *J Mol Biol* (Vol. 365, Issue 3).

Davis, M. R., Jiang, J., Zhou, J., Freed, E. O., & Aiken, C. (2006). A Mutation in the Human Immunodeficiency Virus Type 1 Gag Protein Destabilizes the Interaction of the Envelope Protein Subunits gp120 and gp41. *Journal of Virology*, *80*(5), 2405–2417. https://doi.org/10.1128/jvi.80.5.2405-2417.2006

DeBoer, J., Jagadish, T., Haverland, N. A., Madson, C. J., Ciborowski, P., & Belshan, M. (2014). Alterations in the nuclear proteome of HIV-1 infected T-cells. *Virology*, *468–470*, 409–420. https://doi.org/10.1016/J.VIROL.2014.08.029

DeCaprio, J., & Kohl, T. O. (2020). Immunoprecipitation. In *Cold Spring Harbor Protocols* (Vol. 2020, Issue 11, pp. 449–461). Cold Spring Harbor Laboratory Press. https://doi.org/10.1101/pdb.top098509

Deeks, S. G., Archin, N., Cannon, P., Collins, S., Jones, R. B., de Jong, M. A. W. P., Lambotte, O., Lamplough, R., Ndung'u, T., Sugarman, J., Tiemessen, C. T., Vandekerckhove, L., Lewin, S. R., Deeks, S., Lewin, S., de Jong, M., Ndhlovu, Z., Chomont, N., Brumme, Z., … Kankaka, E. N. (2021). Research priorities for an HIV cure: International AIDS Society Global Scientific Strategy 2021. *Nature Medicine*, *27*(12), 2085–2098. https://doi.org/10.1038/s41591-021-01590-5

Denard, J., Rundwasser, S., Laroudie, N., Gonnet, F., Naldini, L., Radrizzani, M., Galy, A., Merten, O. W., Danos, O., & Svinartchouk, F. (2009). Quantitative proteomic analysis of lentiviral vectors using 2-DE. *Proteomics*, *9*(14), 3666–3676. https://doi.org/10.1002/PMIC.200800747

Deng, Y., Hammond, J. A., Pauszek, R., Ozog, S., Chai, I., Rabuck-Gibbons, J., Lamichhane, R., Henderson, S. C., Millar, D. P., Torbett, B. E., & Williamson, J. R. (2021). Discrimination between Functional and Non-functional Cellular Gag Complexes involved in HIV-1 Assembly: Characterizing Intracellular HIV-1 Gag

Complexes. *Journal of Molecular Biology*, *433*(8). https://doi.org/10.1016/j.jmb.2021.166842

Dettenhofer, M., & Yu, X.-F. (1999). Highly purified human immunodeficiency virus type 1 reveals a virtual absence of Vif in virions. *Journal of Virology*, *73*(2), 1460–1467. https://doi.org/10.1128/JVI.73.2.1460-1467.1999

Dick, A., & Cocklin, S. (2021). Subtype differences in the interaction of hiv-1 matrix with calmodulin: Implications for biological functions. *Biomolecules*, *11*(9). https://doi.org/10.3390/biom11091294

Dick, R. A., Goh, S. L., Feigenson, G. W., & Vogt, V. M. (2012). HIV-1 gag protein can sense the cholesterol and acyl chain environment in model membranes. *Proceedings of the National Academy of Sciences of the United States of America*, *109*(46), 18761–18766. https://doi.org/10.1073/pnas.1209408109

Dick, R. A., & Vogt, V. M. (2014). Membrane interaction of retroviral Gag proteins. In *Frontiers in Microbiology* (Vol. 5, Issue APR). Frontiers Research Foundation. https://doi.org/10.3389/fmicb.2014.00187

Dick, R. A., Zadrozny, K. K., Xu, C., Schur, F. K. M., Lyddon, T. D., Ricana, C. L., Wagner, J. M., Perilla, J. R., Ganser-Pornillos, B. K., Johnson, M. C., Pornillos, O., & Vogt, V. M. (2018). Inositol phosphates are assembly co-factors for HIV-1. *Nature*, *560*(7719), 509–512. https://doi.org/10.1038/s41586-018-0396-4

Ding, L., Derdowski, A., Wang, J.-J., & Spearman, P. (2003). Independent Segregation of Human Immunodeficiency Virus Type 1 Gag Protein Complexes and Lipid Rafts. *Journal of Virology*, *77*(3), 1916–1926. https://doi.org/10.1128/jvi.77.3.1916-1926.2003

Doktorova, M., Heberle, F. A., Kingston, R. L., Khelashvili, G., Cuendet, M. A., Wen, Y., Katsaras, J., Feigenson, G. W., Vogt, V. M., & Dick, R. A. (2017). Cholesterol Promotes Protein Binding by Affecting Membrane Electrostatics and Solvation Properties. *Biophysical Journal*, *113*(9), 2004–2015. https://doi.org/10.1016/j.bpj.2017.08.055

Dorfman, T., Mammano, F., Haseltine, W. A., & Gottlinger, H. G. (1994). Role of the Matrix Protein in the Virion Association of the Human Immunodeficiency Virus Type 1 Envelope Glycoprotein. In *JOURNAL OF VIROLOGY*.

Dostálková, A., Kaufman, F., Křížová, I., Vokatá, B., Ruml, T., & Rumlová, M. (2020). In Vitro Quantification of the Effects of IP6 and Other Small Polyanions on Immature HIV-1 Particle Assembly and Core Stability . *Journal of Virology*, *94*(20). https://doi.org/10.1128/jvi.00991-20

Dou, J., Wang, J. J., Chen, X., Li, H., Ding, L., & Spearman, P. (2009). Characterization of a myristoylated, monomeric HIV Gag protein. *Virology*, *387*(2), 341–352. https://doi.org/10.1016/j.virol.2009.02.037

Draper, J. M., & Smith, C. D. (2009). Palmitoyl acyltransferase assays and inhibitors (Review). In *Molecular Membrane Biology* (Vol. 26, Issues 1–2, pp. 5–13). https://doi.org/10.1080/09687680802683839

Duan, G., & Walther, D. (2015). The Roles of Post-translational Modifications in the Context of Protein Interaction Networks. *PLoS Computational Biology*, *11*(2). https://doi.org/10.1371/journal.pcbi.1004049

Dupuy, A. D., & Engelman, D. M. (2008). Protein area occupancy at the center of the red blood cell membrane. *Proceedings of the National Academy of Sciences of the United States of America*, *105*(8), 2848–2852. https://doi.org/10.1073/PNAS.0712379105

Durand, S., Seigneuret, F., Burlaud-Gaillard, J., Lemoine, R., Tassi, M.-F., Moreau, A., Mougel, M., Roingeard, P., Tauber, C., & de Rocquigny, H. (2022). Quantitative analysis of the formation of nucleoprotein complexes between HIV-1 Gag protein and genomic RNA using transmission electron microscopy. *Journal of Biological Chemistry*, *298*(1), 101500. https://doi.org/10.1016/j.jbc.2021.101500

Eastep, G. N., Ghanam, R. H., Green, T. J., & Saad, J. S. (2021). Structural characterization of HIV-1 matrix mutants implicated in envelope incorporation. *Journal of Biological Chemistry*, *296*. https://doi.org/10.1016/j.jbc.2021.100321

Eells, R., Barros, M., Scott, K. M., Karageorgos, I., Heinrich, F., & Lösche, M. (2017). Structural characterization of membrane-bound human immunodeficiency virus-1 Gag matrix with neutron reflectometry. *Biointerphases*, *12*(2), 02D408. https://doi.org/10.1116/1.4983155

Elliot Murphy, R., Samal, A. B., Vlach, J., Mas, V., Prevelige, P. E., & Saad, J. S. (2019). Structural and biophysical characterizations of HIV-1 matrix trimer binding to lipid nanodiscs shed light on virus assembly. *Journal of Biological Chemistry*, *294*(49), 18600–18612. https://doi.org/10.1074/jbc.RA119.010997

Engeland, C. E., Brown, N. P., Börner, K., Schümann, M., Krause, E., Kaderali, L., Müller, G. A., & Kräusslich, H. G. (2014a). Proteome analysis of the HIV-1 Gag interactome. *Virology*, *460–461*(1), 194–206. https://doi.org/10.1016/j.virol.2014.04.038

Engeland, C. E., Brown, N. P., Börner, K., Schümann, M., Krause, E., Kaderali, L., Müller, G. A., & Kräusslich, H. G. (2014b). Proteome analysis of the HIV-1 Gag interactome. *Virology*, *460–461*(1), 194–206. https://doi.org/10.1016/J.VIROL.2014.04.038

Engelman, D. M. (2005). Membranes are more mosaic than fluid. *Nature*, *438*(7068), 578–580. https://doi.org/10.1038/NATURE04394

Epand, R. M. (2006). Cholesterol and the interaction of proteins with membrane domains. In *Progress in Lipid Research* (Vol. 45, Issue 4, pp. 279–294). https://doi.org/10.1016/j.plipres.2006.02.001

Escribá, P. v. (2006). Membrane-lipid therapy: a new approach in molecular medicine. *Trends in Molecular Medicine*, *12*(1), 34–43. https://doi.org/10.1016/J.MOLMED.2005.11.004

Fadeel, B., & Xue, D. (2009). The ins and outs of phospholipid asymmetry in the plasma membrane: roles in health and disease. *Critical Reviews in Biochemistry and Molecular Biology*, *44*(5), 264. https://doi.org/10.1080/10409230903193307

Fantini, J., & Barrantes, F. J. (2013). How cholesterol interacts with membrane proteins: an exploration of cholesterol-binding sites including CRAC, CARC, and tilted domains. *Frontiers in Physiology*, *4*. https://doi.org/10.3389/FPHYS.2013.00031

Farenholz, J., Huttner, F., Matyash, W. B., Geier, V., Henske, C., Mukherjee, A., Hirsh, S., Thiele, D., Grant, C., Maxfield, B., Kurzchalia, F. R., Simons, T. v, Kramer, M., Thiele, E. M., Stoffel, C., & Trotter, W. (2000). Behavior of a photoactivatable analog of cholesterol, 6-photocholesterol, in model membranes. In *Nat. Cell Biol* (Vol. 2).

Faria, N. R., Rambaut, A., Suchard, M. A., Baele, G., Bedford, T., Ward, M. J., Tatem, A. J., Sousa, J. D., Arinaminpathy, N., Pépin, J., Posada, D., Peeters, M., Pybus, O. G., & Lemey, P. (2014). The early spread and epidemic ignition of HIV-1 in human populations. *Science*, *346*(6205), 56–61. https://doi.org/10.1126/science.1256739

Favard, C., Chojnacki, J., Merida, P., Yandrapalli, N., Mak, J., Eggeling, C., & Muriaux, D. (2019). HIV-1 Gag specifically restricts PI(4,5)P2 and cholesterol mobility in living cells creating a nanodomain platform for virus assembly. *Science Advances*, *5*(10). https://doi.org/10.1126/sciadv.aaw8651

Feist, P., & Hummon, A. B. (2015). Proteomic challenges: sample preparation techniques for microgram-quantity protein analysis from biological samples. *International Journal of Molecular Sciences*, *16*(2), 3537–3563. https://doi.org/10.3390/IJMS16023537

Fielding, C. J., & Fielding, P. E. (2000). Cholesterol and caveolae: structural and functional relationships. *Biochimica et Biophysica Acta*, *1529*(1–3), 210–222. https://doi.org/10.1016/S1388-1981(00)00150-5

Finzi, A., Orthwein, A., Mercier, J., & Cohen, É. A. (2007). Productive Human Immunodeficiency Virus Type 1 Assembly Takes Place at the Plasma Membrane. *Journal of Virology*, *81*(14), 7476. https://doi.org/10.1128/JVI.00308-07

Fledderman, E. L., Fujii, K., Ghanam, R. H., Waki, K., Prevelige, P. E., Freed, E. O., & Saad, J. S. (2010). Myristate exposure in the human immunodeficiency virus type 1 matrix protein is modulated by pH. *Biochemistry*, *49*(44), 9551–9562. https://doi.org/10.1021/bi101245j

Frank, P. G., Cheung, M. W. C., Pavlides, S., Llaverias, G., Park, D. S., & Lisanti, M. P. (2006). Caveolin-1 and regulation of cellular cholesterol homeostasis. *American Journal of Physiology. Heart and Circulatory Physiology*, *291*(2). https://doi.org/10.1152/AJPHEART.01092.2005

Frankel, A. D., & Young, J. A. T. (1998). HIV-1: Fifteen Proteins and an RNA. In *Annu. Rev. Biochem* (Vol. 67). www.annualreviews.org

Freed, E. O. (2015). HIV-1 assembly, release and maturation. In *Nature Reviews Microbiology* (Vol. 13, Issue 8, pp. 484–496). Nature Publishing Group. https://doi.org/10.1038/nrmicro3490

Freed, E. O., & Martin, M. A. (1995). Virion Incorporation of Envelope Glycoproteins with Long but Not Short Cytoplasmic Tails Is Blocked by Specific, Single Amino Acid Substitutions in the Human Immunodeficiency Virus Type 1 Matrix. In *JOURNAL OF VIROLOGY* (Vol. 69, Issue 3).

Freed, E. O., & Mouland, A. J. (2006). The cell biology of HIV-1 and other retroviruses. In *Retrovirology* (Vol. 3). https://doi.org/10.1186/1742-4690-3-77

Fuente, C., Maddukuri, A., Kehn, K., Baylor, S., Deng, L., Pumfery, A., & Kashanchi, F. (2003). Pharmacological cyclin-dependent kinase inhibitors as HIV-1 antiviral therapeutics. *Current HIV Research*, *1*(2), 131–152. https://doi.org/10.2174/1570162033485339

Füllekrug, J., & Simons, K. (2004). Lipid rafts and apical membrane traffic. In *Annals of the New York Academy of Sciences* (Vol. 1014, pp. 164–169). New York Academy of Sciences. https://doi.org/10.1196/annals.1294.017

Gahbauer, S., & Böckmann, R. A. (2016). Membrane-mediated oligomerization of G protein coupled receptors and its implications for GPCR function. *Frontiers in Physiology*, *7*(OCT), 494. https://doi.org/10.3389/FPHYS.2016.00494/BIBTEX

Gaines, C. R., Tkacik, E., Rivera-Oven, A., Somani, P., Achimovich, A., Alabi, T., Zhu, A., Getachew, N., Yang, A. L., McDonough, M., Hawkins, T., Spadaro, Z., & Summers, M. F. (2018). HIV-1 Matrix Protein Interactions with tRNA: Implications for Membrane Targeting. *Journal of Molecular Biology*, *430*(14), 2113–2127. https://doi.org/10.1016/j.jmb.2018.04.042

Gao, X., & Hannoush, R. N. (2014). Single-cell in situ imaging of palmitoylation in fatty-acylated proteins. *Nature Protocols*, *9*(11), 2607–2623. https://doi.org/10.1038/NPROT.2014.179

Gao, X., & Hannoush, R. N. (2018). A Decade of Click Chemistry in Protein Palmitoylation: Impact on Discovery and New Biology. *Cell Chemical Biology*, *25*(3), 236–246. https://doi.org/10.1016/J.CHEMBIOL.2017.12.002

Garmy, N., Taïeb, N., Yahi, N., & Fantini, J. (2005). Interaction of cholesterol with sphingosine: physicochemical characterization and impact on intestinal absorption. *Journal of Lipid Research*, *46*(1), 36–45. https://doi.org/10.1194/JLR.M400199-JLR200

Gautier, V. W., Gu, L., O'Donoghue, N., Pennington, S., Sheehy, N., & Hall, W. W. (2009). In vitro nuclear interactome of the HIV-1 Tat protein. *Retrovirology*, *6*. https://doi.org/10.1186/1742-4690-6-47

Gevaert, K., Impens, F., Ghesquière, B., van Damme, P., Lambrechts, A., & Vandekerckhove, J. (2008). Stable isotopic labeling in proteomics. *Proteomics*, *8*(23–24), 4873–4885. https://doi.org/10.1002/PMIC.200800421

Ghanam, R. H., Fernandez, T. F., Fledderman, E. L., & Saad, J. S. (2010). Binding of calmodulin to the HIV-1 matrix protein triggers myristate exposure. *Journal of Biological Chemistry*, *285*(53), 41911–41920. https://doi.org/10.1074/jbc.M110.179093

Ghanam, R. H., Samal, A. B., Fernandez, T. F., & Saad, J. S. (2012). Role of the HIV-1 matrix protein in Gag intracellular trafficking and targeting to the plasma membrane for virus assembly. *Frontiers in Microbiology*, *3*(FEB). https://doi.org/10.3389/fmicb.2012.00055

Gheysen, D., Jacobs,' Franqoise De Foresta,', E., Thiriart, C., Francotte, M., Thines, D., & de Wilde', M. (1969). Assembly and Release of HIV-1 Precursor Pr5Wg Virus-like Particles from Recombinant Baculovirus-Infected Insect Cells. In *Cell* (Vol. 59).

Goldstein, J. L., Anderson, R. G. W., & Brown, M. S. (1979). Coated pits, coated vesicles, and receptor-mediated endocytosis. *Nature 1979 279:5715*, *279*(5715), 679–685. https://doi.org/10.1038/279679a0

Gomez, C. Y., & Hope, T. J. (2006). Mobility of Human Immunodeficiency Virus Type 1 Pr55 Gag in Living Cells . *Journal of Virology*, *80*(17), 8796–8806. https://doi.org/10.1128/jvi.02159-05

Gong, J., Shen, X., Chen, C., Qiu, H., Yang, R., Gong, J., Shen, X., Chen, C., Qiu, H., & Yang, R. (2011). Down-regulation of HIV-1 Infection by Inhibition of the MAPK Signaling Pathway. *Virologica Sinica, 2011, Vol. 26, Issue 2, Pages: 114-122*, *26*(2), 114–122. https://doi.org/10.1007/S12250-011-3184-Y

Goñi, F. M. (2014). The basic structure and dynamics of cell membranes: an update of the Singer-Nicolson model. *Biochimica et Biophysica Acta*, *1838*(6), 1467–1476. https://doi.org/10.1016/J.BBAMEM.2014.01.006

Gottwein, E., & Kräusslich, H.-G. (2005). Analysis of Human Immunodeficiency Virus Type 1 Gag Ubiquitination. *Journal of Virology*, *79*(14), 9134. https://doi.org/10.1128/JVI.79.14.9134-9144.2005

Gousset, K., Ablan, S. D., Coren, L. v., Ono, A., Soheilian, F., Nagashima, K., Ott, D. E., & Freed, E. O. (2008). Real-time visualization of HIV-1 GAG trafficking in infected macrophages. *PLoS Pathogens*, *4*(3). https://doi.org/10.1371/journal.ppat.1000015

Govender, Y., Shalekoff, S., Ebrahim, O., Waja, Z., Chaisson, R. E., Martinson, N., & Tiemessen, C. T. (2021). Systemic DPP4/CD26 is associated with natural HIV-1 control: Implications for COVID-19 susceptibility. *Clinical Immunology (Orlando, Fla.)*, *230*. https://doi.org/10.1016/J.CLIM.2021.108824

Grabski, A., & Novagen, R. (2001). *Preparation of protein samples for SDS-polyacrylamide gel electrophoresis: procedures and tips.* http://citeseerx.ist.psu.edu/viewdoc/summary?doi=10.1.1.378.613

Graham, D. R. M., Chertova, E., Hilburn, J. M., Arthur, L. O., & Hildreth, J. E. K. (2003). Cholesterol Depletion of Human Immunodeficiency Virus Type 1 and Simian Immunodeficiency Virus with β-Cyclodextrin Inactivates and Permeabilizes the Virions: Evidence for Virion-Associated Lipid Rafts. *Journal of Virology*, *77*(15), 8237. https://doi.org/10.1128/JVI.77.15.8237-8248.2003

Green, N. M. (1975). Avidin. *Advances in Protein Chemistry*, *29*(C), 85–133. https://doi.org/10.1016/S0065-3233(08)60411-8

Groppelli, E., Len, A. C., Granger, L. A., & Jolly, C. (2014). Retromer regulates HIV-1 envelope glycoprotein trafficking and incorporation into virions. *PLoS Pathogens*, *10*(10). https://doi.org/10.1371/JOURNAL.PPAT.1004518

Grotenbreg, G., & Ploegh, H. (2007). Dressed-up proteins. *Nature*, *446*(7139), 994–995.

Groves, N. S., Bruns, M. M., & van Engelenburg, S. B. (2020). A quantitative live-cell superresolution imaging framework for measuring the mobility of single molecules at sites of virus assembly. *Pathogens*, *9*(11), 1–14. https://doi.org/10.3390/pathogens9110972

Guo, L., Wang, L., Yang, R., Feng, R., Li, Z., Zhou, X., Dong, Z., Ghartey-Kwansah, G., Xu, M. M., Nishi, M., Zhang, Q., Isaacs, W., Ma, J., & Xu, X. (2017). Optimizing conditions for calcium phosphate mediated transient transfection. *Saudi Journal of Biological Sciences*, *24*(3), 622–629. https://doi.org/10.1016/J.SJBS.2017.01.034

Haberkant, P., & Holthuis, J. C. M. (2014). Fat & fabulous: Bifunctional lipids in the spotlight. In *Biochimica et Biophysica Acta - Molecular and Cell Biology of Lipids* (Vol. 1841, Issue 8, pp. 1022–1030). Elsevier. https://doi.org/10.1016/j.bbalip.2014.01.003

Haberkant, P., Schmitt, O., Contreras, F. X., Thiele, C., Hanada, K., Sprong, H., Reinhard, C., Wieland, F. T., & Brügger, B. (2008). Protein-sphingolipid interactions within cellular membranes. *Journal of Lipid Research*, *49*(1), 251–262. https://doi.org/10.1194/JLR.D700023-JLR200

Haberkant, P., Stein, F., Höglinger, D., Gerl, M. J., Brügger, B., van Veldhoven, P. P., Krijgsveld, J., Gavin, A. C., & Schultz, C. (2016). Bifunctional Sphingosine for Cell-Based Analysis of Protein-Sphingolipid Interactions. *ACS Chemical Biology*, *11*(1), 222–230. https://doi.org/10.1021/ACSCHEMBIO.5B00810/SUPPL_FILE/CB5B00810_SI_002.XLSX

Haberkant, P., & van Meer, G. (2009). Protein-lipid interactions: Paparazzi hunting for snap-shots. In *Biological Chemistry* (Vol. 390, Issue 8, pp. 795–803). https://doi.org/10.1515/BC.2009.074

Hadian, K., Vincendeau, M., Mäusbacher, N., Nagel, D., Hauck, S. M., Ueffing, M., Loyter, A., Werner, T., Wolff, H., & Brack-Werner, R. (2009). Identification of a Heterogeneous Nuclear Ribonucleoprotein-recognition Region in the HIV Rev Protein. *Journal of Biological Chemistry*, *284*(48), 33384–33391. https://doi.org/10.1074/JBC.M109.021659

Halwani, R., Khorchid, A., Cen, S., & Kleiman, L. (2003). Rapid Localization of Gag/GagPol Complexes to Detergent-Resistant Membrane during the Assembly of Human Immunodeficiency Virus Type 1. *Journal of Virology*, *77*(7), 3973–3984. https://doi.org/10.1128/jvi.77.7.3973-3984.2003

Hamilton, B. J. N., Burns, C. M., Nichols, R. C., & Rigby, W. F. C. (1997). Modulation of AUUUA response element binding by heterogeneous nuclear ribonucleoprotein A1 in human T lymphocytes: The roles of cytoplasmic location, transcription, and phosphorylation. *Journal of Biological Chemistry*, *272*(45), 28732–28741. https://doi.org/10.1074/jbc.272.45.28732

Hammond, J. A., Zhou, L., Lamichhane, R., Chu, H. Y., Millar, D. P., Gerace, L., & Williamson, J. R. (2018). A Survey of DDX21 Activity During Rev/RRE Complex Formation. *Journal of Molecular Biology*, *430*(4), 537–553. https://doi.org/10.1016/J.JMB.2017.06.023

Hang, H. C., Geutjes, E. J., Grotenbreg, G., Pollington, A. M., Bijlmakers, M. J., & Ploegh, H. L. (2007). Chemical probes for the rapid detection of fatty-acylated proteins in mammalian cells. *Journal of the American Chemical Society*, *129*(10), 2744–2745. https://doi.org/10.1021/ja0685001

Hang, H. C., & Linder, M. E. (2011). Exploring protein lipidation with chemical biology. In *Chemical Reviews* (Vol. 111, Issue 10, pp. 6341–6358). https://doi.org/10.1021/cr2001977

Harayama, T., & Riezman, H. (2018). Understanding the diversity of membrane lipid composition. *Nature Reviews. Molecular Cell Biology*, *19*(5), 281–296. https://doi.org/10.1038/NRM.2017.138

Harder, T., Scheiffele, P., Verkade, P., & Simons, K. (1998). Lipid Domain Structure of the Plasma Membrane Revealed by Patching of Membrane Components. In *The Journal of Cell Biology* (Vol. 141, Issue 4). http://www.jcb.org

Harlow, E., & Lane, D. (2006). Immunoprecipitation: Preclearing the Lysate. *Cold Spring Harbor Protocols*, *2006*(4), pdb.prot4535. https://doi.org/10.1101/PDB.PROT4535

Harrison, R., & Lunt, G. G. (1980). *Biological membranes, their structure and function*. 288. https://books.google.com/books/about/Biological_Membranes_Their_Structure_an d.html?hl=es&id=KX7wAAAAMAAJ

Hawkes, D., Jones, K. L., Smyth, R. P., Pereira, C. F., Bittman, R., Jaworowski, A., & Mak, J. (2015). Properties of HIV-1 associated cholesterol in addition to raft formation are

important for virus infection. *Virus Research*, *210*, 18–21. https://doi.org/10.1016/j.virusres.2015.06.023

Hein, J. E., & Fokin, V. v. (2010). Copper-catalyzed azide-alkyne cycloaddition (CuAAC) and beyond: new reactivity of copper(i) acetylides. *Chemical Society Reviews*, *39*(4), 1302–1315. https://doi.org/10.1039/b904091a

Helenius, A., & Simons, K. (1975). Solubilization of membranes by detergents. *Biochimica et Biophysica Acta*, *415*(1), 29–79. https://doi.org/10.1016/0304-4157(75)90016-7

Herce, H. D., Deng, W., Helma, J., Leonhardt, H., & Cardoso, M. C. (2013). Visualization and targeted disruption of protein interactions in living cells. *Nature Communications*, *4*. https://doi.org/10.1038/NCOMMS3660

Hicks, D. A., Nalivaeva, N. N., & Turner, A. J. (2012). Lipid rafts and Alzheimer's disease: Protein-lipid interactions and perturbation of signaling. *Frontiers in Physiology*, *3 JUN*, 189. https://doi.org/10.3389/FPHYS.2012.00189/BIBTEX

Hiller, Y., Gershoni, J. M., Bayer, E. A., & Wilchek, M. (1987). Biotin binding to avidin Oligosaccharide side chain not required for ligand association. In *Biochem. J* (Vol. 248).

Hogue, I. B., Grover, J. R., Soheilian, F., Nagashima, K., & Ono, A. (2011). Gag Induces the Coalescence of Clustered Lipid Rafts and Tetraspanin-Enriched Microdomains at HIV-1 Assembly Sites on the Plasma Membrane. *Journal of Virology*, *85*(19), 9749–9766. https://doi.org/10.1128/jvi.00743-11

Hogue, I. B., Llewellyn, G. N., & Ono, A. (2012). Dynamic Association between HIV-1 Gag and Membrane Domains. *Molecular Biology International*, *2012*, 1–13. https://doi.org/10.1155/2012/979765

Holm, K., Weclewicz, K., Hewson, R., & Suomalainen, M. (2003). Human Immunodeficiency Virus Type 1 Assembly and Lipid Rafts: Pr55 gag Associates with Membrane Domains That Are Largely Resistant to Brij98 but Sensitive to Triton X-100 . *Journal of Virology*, *77*(8), 4805–4817. https://doi.org/10.1128/jvi.77.8.4805-4817.2003

Hong, V., Presolski, S. I., Ma, C., & Finn, M. G. (2009). Analysis and optimization of copper-catalyzed azide-alkyne cycloaddition for bioconjugation. *Angewandte Chemie - International Edition*, *48*(52), 9879–9883. https://doi.org/10.1002/anie.200905087

Huang, J., & Feigenson, G. W. (1999). A microscopic interaction model of maximum solubility of cholesterol in lipid bilayers. *Biophysical Journal*, *76*(4), 2142. https://doi.org/10.1016/S0006-3495(99)77369-8

Inlora, J., Collins, D. R., Trubin, M. E., Chung, J. Y. J., & Ono, A. (2014). Membrane binding and subcellular localization of retroviral gag proteins are differentially

regulated by MA interactions with phosphatidylinositol-(4,5)-bisphosphate and RNA. *MBio*, *5*(6). https://doi.org/10.1128/mBio.02202-14

Ivaldi, C., Martin, B. R., Kieffer-Jaquinod, S., Chapel, A., Levade, T., Garin, J., & Journet, A. (2012). Proteomic analysis of S-acylated proteins in human B cells reveals palmitoylation of the immune regulators CD20 and CD23. *PloS One*, *7*(5). https://doi.org/10.1371/JOURNAL.PONE.0037187

Ivankin, A., Kuzmenko, I., & Gidalevitz, D. (2012). Cholesterol mediates membrane curvature during fusion events. *Physical Review Letters*, *108*(23). https://doi.org/10.1103/PhysRevLett.108.238103

Ivanov, A. A., Khuri, F. R., & Fu, H. (2013). Targeting protein-protein interactions as an anticancer strategy. *Trends in Pharmacological Sciences*, *34*(7), 393–400. https://doi.org/10.1016/J.TIPS.2013.04.007

Izaurralde, E., Jarmolowski, A., Beisel, C., Mattaj, I. W., Dreyfuss, G., & Fischer, U. (1997). A Role for the M9 Transport Signal of hnRNP A1 in mRNA Nuclear Export. *The Journal of Cell Biology*, *137*(1), 27. https://doi.org/10.1083/JCB.137.1.27

Jacobson, K., Sheets, E. D., & Simson, R. (1995). Revisiting the fluid mosaic model of membranes. *Science (New York, N.Y.)*, *268*(5216), 1441–1442. https://doi.org/10.1126/SCIENCE.7770769

Jacqué, J. M., Mann, A., Enslen, H., Sharova, N., Brichacek, B., Davis, R. J., & Stevenson, M. (1998). Modulation of HIV-1 infectivity by MAPK, a virion–associated kinase. *The EMBO Journal*, *17*(9), 2607–2618. https://doi.org/10.1093/EMBOJ/17.9.2607

Jäger, S., Cimermancic, P., Gulbahce, N., Johnson, J. R., McGovern, K. E., Clarke, S. C., Shales, M., Mercenne, G., Pache, L., Li, K., Hernandez, H., Jang, G. M., Roth, S. L., Akiva, E., Marlett, J., Stephens, M., D'Orso, I., Fernandes, J., Fahey, M., … Krogan, N. J. (2011). Global landscape of HIV-human protein complexes. *Nature*, *481*(7381), 365–370. https://doi.org/10.1038/NATURE10719

Jain, A., & Cheng, K. (2017). The principles and applications of avidin-based nanoparticles in drug delivery and diagnosis. In *Journal of Controlled Release* (Vol. 245, pp. 27–40). Elsevier B.V. https://doi.org/10.1016/j.jconrel.2016.11.016

Jarboui, M. A., Bidoia, C., Woods, E., Roe, B., Wynne, K., Elia, G., Hall, W. W., & Gautier, V. W. (2012). Nucleolar protein trafficking in response to HIV-1 Tat: rewiring the nucleolus. *PloS One*, *7*(11). https://doi.org/10.1371/JOURNAL.PONE.0048702

Javanainen, M., Martinez-Seara, H., & Vattulainen, I. (2017). Nanoscale Membrane Domain Formation Driven by Cholesterol. *Scientific Reports*, *7*(1). https://doi.org/10.1038/s41598-017-01247-9

Jeang, K. T., & Yedavalli, V. (2006). Role of RNA helicases in HIV-1 replication. *Nucleic Acids Research*, *34*(15), 4198–4205. https://doi.org/10.1093/NAR/GKL398

Jones, B. R., Schultz, G. A., Eckstein, J. A., & Ackermann, B. L. (2012). Surrogate matrix and surrogate analyte approaches for definitive quantitation of endogenous biomolecules. *Bioanalysis*, *4*(19), 2343–2356. https://doi.org/10.4155/BIO.12.200

Jouvenet, N., Neil, S. J. D., Bess, C., Johnson, M. C., Virgen, C. A., Simon, S. M., & Bieniasz, P. D. (2006). Plasma membrane is the site of productive HIV-1 particle assembly. *PLoS Biology*, *4*(12), 2296–2310. https://doi.org/10.1371/journal.pbio.0040435

Jung, Y. M., Yu, K. L., Park, S. H., Lee, S. D., Kim, M. J., & You, J. C. (2018). Investigation of function and regulation of the YB-1 cellular factor in HIV replication. *BMB Reports*, *51*(6), 290–295. https://doi.org/10.5483/BMBREP.2018.51.6.231

Kalyana Sundaram, R. V., Li, H., Bailey, L., Rashad, A. A., Aneja, R., Weiss, K., Huynh, J., Bastian, A. R., Papazoglou, E., Abrams, C., Wrenn, S., & Chaiken, I. (2016). Impact of HIV-1 Membrane Cholesterol on Cell-Independent Lytic Inactivation and Cellular Infectivity. *Biochemistry*, *55*(3), 447–458. https://doi.org/10.1021/ACS.BIOCHEM.5B00936

Karthigeyan, K. P., Zhang, L., Loiselle, D. R., Haystead, T. A. J., Bhat, M., Yount, J. S., & Kwiek, J. J. (2021). A bioorthogonal chemical reporter for fatty acid synthase–dependent protein acylation. *Journal of Biological Chemistry*, *297*(5). https://doi.org/10.1016/j.jbc.2021.101272

Keele, B. F., van Heuverswyn, F., Li, Y., Bailes, E., Takehisa, J., Santiago, M. L., Bibollet-Ruche, F., Chen, Y., Wain, L. v, Liegeois, F., Loul, S., Ngole, E. M., Bienvenue, Y., Delaporte, E., Brookfield, J. F. Y., Sharp, P. M., Shaw, G. M., Peeters, M., & Hahn, B. H. (2006). Chimpanzee Reservoirs of Pandemic and Nonpandemic HIV-1. In *Science* (Vol. 313, Issue 5786).

Keller, H., Kräusslich, H. G., & Schwille, P. (2013). Multimerizable HIV Gag derivative binds to the liquid-disordered phase in model membranes. *Cellular Microbiology*, *15*(2), 237–247. https://doi.org/10.1111/CMI.12064

Keller, H., Lorizate, M., & Schwille, P. (2009). PI(4,5)P2 degradation promotes the formation of cytoskeleton-free model membrane systems. *Chemphyschem: A European Journal of Chemical Physics and Physical Chemistry*, *10*(16), 2805–2812. https://doi.org/10.1002/CPHC.200900598

Kerviel, A., Thomas, A., Chaloin, L., Favard, C., & Muriaux, D. (2013). Virus assembly and plasma membrane domains: which came first? In *Virus research* (Vol. 171, Issue 2, pp. 332–340). https://doi.org/10.1016/j.virusres.2012.08.014

Khalatbari, A., Mishra, P., Han, H., He, Y., MacVeigh-Aloni, M., & Ji, C. (2020). Ritonavir and Lopinavir Suppress RCE1 and CAAX Rab Proteins Sensitizing the Liver to Organelle Stress and Injury. *Hepatology Communications*, *4*(6), 932–944. https://doi.org/10.1002/HEP4.1515

Klingler, J., Anton, H., Réal, E., Zeiger, M., Moog, C., Mély, Y., & Boutant, E. (2020). How HIV-1 Gag Manipulates Its Host Cell Proteins: A Focus on Interactors of the Nucleocapsid Domain. *Viruses*, *12*(8). https://doi.org/10.3390/V12080888

Klug, Y. A., Rotem, E., Schwarzer, R., & Shai, Y. (2017). Mapping out the intricate relationship of the HIV envelope protein and the membrane environment. *Biochimica et Biophysica Acta - Biomembranes*, *1859*(4), 550–560. https://doi.org/10.1016/j.bbamem.2016.10.012

Knoener, R. A., Becker, J. T., Scalf, M., Sherer, N. M., & Smith, L. M. (2017). Elucidating the in vivo interactome of HIV-1 RNA by hybridization capture and mass spectrometry. *Scientific Reports 2017 7:1*, *7*(1), 1–16. https://doi.org/10.1038/s41598-017-16793-5

Kolb, H., Finn, M., & Sharpless, K. (2001). Click Chemistry : Diverse Chemical Function from a Few Good Reactions. *Angewandte Chemie International Edition*, *40*(11), 2004–2021.

Komaniwa, S., Hayashi, H., Kawamoto, H., Sato, S. B., Ikawa, T., Katsura, Y., & Udaka, K. (2009). Lipid-mediated presentation of MHC class II molecules guides thymocytes to the CD4 lineage. *European Journal of Immunology*, *39*(1), 96–112. https://doi.org/10.1002/eji.200838796

Korycka, J., Łach, A., Heger, E., Bogusławska, D. M., Wolny, M., Toporkiewicz, M., Augoff, K., Korzeniewski, J., & Sikorski, A. F. (2012). Human DHHC proteins: A spotlight on the hidden player of palmitoylation. In *European Journal of Cell Biology* (Vol. 91, Issue 2, pp. 107–117). https://doi.org/10.1016/j.ejcb.2011.09.013

Krementsov, D. N., Rassam, P., Margeat, E., Roy, N. H., Schneider-Schaulies, J., Milhiet, P. E., & Thali, M. (2010). HIV-1 assembly differentially alters dynamics and partitioning of tetraspanins and raft components. *Traffic*, *11*(11), 1401–1414. https://doi.org/10.1111/j.1600-0854.2010.01111.x

Krogh, A., Larsson, B., von Heijne, G., & Sonnhammer, E. L. L. (2001). Predicting transmembrane protein topology with a hidden markov model: application to complete genomes. *Journal of Molecular Biology*, *305*(3), 567–580. https://doi.org/10.1006/JMBI.2000.4315

Kumar, G. A., Jafurulla, M., & Chattopadhyay, A. (2016). The membrane as the gatekeeper of infection: Cholesterol in host-pathogen interaction. *Chemistry and Physics of Lipids*, *199*, 179–185. https://doi.org/10.1016/J.CHEMPHYSLIP.2016.02.007

Kumari, B., Kumar, R., & Kumar, M. (2014). PalmPred: An SVM based palmitoylation prediction method using sequence profile information. *PLoS ONE*, *9*(2). https://doi.org/10.1371/journal.pone.0089246

Kutluay, S. B., & Bieniasz, P. D. (2010). Analysis of the initiating events in HIV-1 particle assembly and genome packaging. *PLoS Pathogens*, *6*(11). https://doi.org/10.1371/journal.ppat.1001200

Kutluay, S. B., Emery, A., Penumutchu, S. R., Townsend, D., Tenneti, K., Madison, M. K., Stukenbroeker, A. M., Powell, C., Jannain, D., Tolbert, B. S., Swanstrom, R. I., & Bieniasz, P. D. (2019). Genome-Wide Analysis of Heterogeneous Nuclear Ribonucleoprotein (hnRNP) Binding to HIV-1 RNA Reveals a Key Role for hnRNP H1 in Alternative Viral mRNA Splicing. *Journal of Virology*, *93*(21). https://doi.org/10.1128/JVI.01048-19/ASSET/84CA6E22-79B3-4C94-AE2E-2008BAEE0243/ASSETS/GRAPHIC/JVI.01048-19-F0012.JPEG

Kuzu, O. F., Noory, M. A., & Robertson, G. P. (2016). The role of cholesterol in cancer. *Cancer Research*, *76*(8), 2063. https://doi.org/10.1158/0008-5472.CAN-15-2613

Lahaye, X., Gentili, M., Silvin, A., Conrad, C., Picard, L., Jouve, M., Zueva, E., Maurin, M., Nadalin, F., Knott, G. J., Zhao, B., Du, F., Rio, M., Amiel, J., Fox, A. H., Li, P., Etienne, L., Bond, C. S., Colleaux, L., & Manel, N. (2018). NONO Detects the Nuclear HIV Capsid to Promote cGAS-Mediated Innate Immune Activation. *Cell*, *175*(2), 488-501.e22. https://doi.org/10.1016/J.CELL.2018.08.062

Lahouassa, H., Blondot, M. L., Chauveau, L., Chougui, G., Morel, M., Leduc, M., Guillonneau, F., Ramirez, B. C., Schwartz, O., & Margottin-Goguet, F. (2016). HIV-1 Vpr degrades the HLTF DNA translocase in T cells and macrophages. *Proceedings of the National Academy of Sciences of the United States of America*, *113*(19), 5311–5316. https://doi.org/10.1073/PNAS.1600485113

Lalonde, M. S., & Sundquist, W. I. (2012). How HIV finds the door. In *Proceedings of the National Academy of Sciences of the United States of America* (Vol. 109, Issue 46, pp. 18631–18632). https://doi.org/10.1073/pnas.1215940109

Lata, S., Mishra, R., & Banerjea, A. C. (2018). Proteasomal Degradation Machinery: Favorite Target of HIV-1 Proteins. *Frontiers in Microbiology*, *9*(NOV). https://doi.org/10.3389/FMICB.2018.02738

Lemonidis, K., Gorleku, O. A., Sanchez-Perez, M. C., Grefen, C., & Chamberlain, L. H. (2014). The Golgi S-acylation machinery comprises zDHHC enzymes with major differences in substrate affinity and S-acylation activity. *Molecular Biology of the Cell*, *25*(24), 3870–3883. https://doi.org/10.1091/mbc.E14-06-1169

Lev, N., & Shai, Y. (2007). Fatty Acids can Substitute the HIV Fusion Peptide in Lipid Merging and Fusion: An Analogy between Viral and Palmitoylated Eukaryotic Fusion Proteins. *Journal of Molecular Biology*, *374*(1), 220–230. https://doi.org/10.1016/j.jmb.2007.09.008

Leventhal, I., Grzybek, M., & Simons, K. (2010). Greasing their way: Lipid modifications determine protein association with membrane rafts. In *Biochemistry* (Vol. 49, Issue 30, pp. 6305–6316). https://doi.org/10.1021/bi100882y

Levy, J. A. (1993). HIV pathogenesis and long-term survival. *AIDS (London, England)*, *7*(11), 1401–1410. https://doi.org/10.1097/00002030-199311000-00001

Li, C., Burdick, R. C., Nagashima, K., Hu, W.-S., Pathak, V. K., & Goff, S. P. (n.d.). *HIV-1 cores retain their integrity until minutes before uncoating in the nucleus*. https://doi.org/10.1073/pnas.2019467118/-/DCSupplemental

Li, L., & Zhang, Z. (2016). Development and Applications of Copper-Catalyzed Azide-Alkyne Cycloaddition (CuACC) as a Bioorthogonal Reaction. *Molecules*, *21*(10), 1393.

Li, S., Song, K. S., & Lisanti, M. P. (1996). Expression and Characterization of Recombinant Caveolin. *Journal of Biological Chemistry*, *271*(1), 568–573. https://doi.org/10.1074/JBC.271.1.568

Liao, Z., Cimakasky, L. M., Hampton, R., Nguyen, D. H., & Hildreth, J. E. K. (2001). Lipid Rafts and HIV Pathogenesis: Host Membrane Cholesterol Is Required for Infection by HIV Type 1. In *AIDS RESEARCH AND HUMAN RETROVIRUSES* (Vol. 17, Issue 11). Mary Ann Liebert, Inc.

Liao, Z., Graham, D. R., & Hildreth, J. E. K. (2004). Lipid Rafts and HIV Pathogenesis: Virion-Associated Cholesterol Is Required for Fusion and Infection of Susceptible Cells. *Https://Home.Liebertpub.Com/Aid*, *19*(8), 675–687. https://doi.org/10.1089/088922203322280900

Lin, Y. C., Boone, M., Meuris, L., Lemmens, I., van Roy, N., Soete, A., Reumers, J., Moisse, M., Plaisance, S., Drmanac, R., Chen, J., Speleman, F., Lambrechts, D., van de Peer, Y., Tavernier, J., & Callewaert, N. (2014). Genome dynamics of the human embryonic kidney 293 lineage in response to cell biology manipulations. *Nature Communications 2014 5:1*, *5*(1), 1–12. https://doi.org/10.1038/ncomms5767

Lindwasser, O. W., & Resh, M. D. (2001). Multimerization of Human Immunodeficiency Virus Type 1 Gag Promotes Its Localization to Barges, Raft-Like Membrane Microdomains. *Journal of Virology*, *75*(17), 7913–7924. https://doi.org/10.1128/jvi.75.17.7913-7924.2001

Lindwasser, O. W., & Resh, M. D. (2002). Myristoylation as a target for inhibiting HIV assembly: Unsaturated fatty acids block viral budding. *Proceedings of the National Academy of Sciences of the United States of America*, *99*(20), 13037. https://doi.org/10.1073/PNAS.212409999

Lindwasser, O. W., & Resh, M. D. (2004). Human Immunodeficiency Virus Type 1 Gag Contains a Dileucine-Like Motif That Regulates Association with Multivesicular Bodies. *Journal of Virology*, *78*(11), 6013–6023. https://doi.org/10.1128/jvi.78.11.6013-6023.2004

Lochrie, M. A., Waugh, S., Pratt, D. G., Clever, J., Parslow, T. G., & Polisky, B. (1997). In vitro selection of RNAs that bind to the human immunodeficiency virus type-1 gag

polyprotein. *Nucleic Acids Research*, *25*(14), 2902–2910. https://doi.org/10.1093/NAR/25.14.2902

Lodish, H., Berk, A., Kaiser, C. A., Krieger, M., Scott, M. P., Bretscher, A., Ploegh, H., & Matsudaira, P. (2007). *Molecular Cell Biology (Lodish, Molecular Cell Biology)*. 973. https://books.google.com/books/about/Molecular_Cell_Biology.html?hl=es&id=K3 JbjG1JiUMC

Lombard, J. (2014). Once upon a time the cell membranes: 175 years of cell boundary research. *Biology Direct*, *9*(1), 1–35. https://doi.org/10.1186/S13062-014-0032-7/FIGURES/11

Lorizate, M., Brügger, B., Akiyama, H., Glass, B., Müller, B., Anderluh, G., Wieland, F. T., & Kräusslich, H. G. (2009). Probing HIV-1 membrane liquid order by Laurdan staining reveals producer cell-dependent differences. *Journal of Biological Chemistry*, *284*(33), 22238–22247. https://doi.org/10.1074/jbc.M109.029256

Lorizate, M., & Kräusslich, H. G. (2011). Role of lipids in virus replication. In *Cold Spring Harbor Perspectives in Biology* (Vol. 3, Issue 10, pp. 1–20). Cold Spring Harbor Laboratory Press. https://doi.org/10.1101/cshperspect.a004820

Lorizate, M., Sachsenheimer, T., Glass, B., Habermann, A., Gerl, M. J., Kräusslich, H. G., & Brügger, B. (2013). Comparative lipidomics analysis of HIV-1 particles and their producer cell membrane in different cell lines. *Cellular Microbiology*, *15*(2), 292–304. https://doi.org/10.1111/cmi.12101

Lorizate, M., Terrones, O., Nieto-Garai, J. A., Rojo-Bartolomé, I., Ciceri, D., Morana, O., Olazar-Intxausti, J., Arboleya, A., Martin, A., Szynkiewicz, M., Calleja-Felipe, M., Bernardino de la Serna, J., & Contreras, F. X. (2021). Super-Resolution Microscopy Using a Bioorthogonal-Based Cholesterol Probe Provides Unprecedented Capabilities for Imaging Nanoscale Lipid Heterogeneity in Living Cells. *Small Methods*, *5*(9). https://doi.org/10.1002/SMTD.202100430

Lu, H., & Fang, C. (2020). Methodology for Detecting Protein Palmitoylation. In *Advances in Experimental Medicine and Biology* (Vol. 1248, pp. 425–430). Springer. https://doi.org/10.1007/978-981-15-3266-5_17

Lu, H., Li, Z., Xue, Y., & Zhou, Q. (2013). Viral-host interactions that control HIV-1 transcriptional elongation. *Chemical Reviews*, *113*(11), 8567. https://doi.org/10.1021/CR400120Z

Lu, L., Zhu, Y., Huang, J., Chen, X., Yang, H., Jiang, S., & Chen, Y. H. (2008). Surface Exposure of the HIV-1 Env Cytoplasmic Tail LLP2 Domain during the Membrane Fusion Process: INTERACTION WITH gp41 FUSION CORE. *Journal of Biological Chemistry*, *283*(24), 16723–16731. https://doi.org/10.1074/JBC.M801083200

Lucero, H. A., & Robbins, P. W. (2004). Lipid rafts-protein association and the regulation of protein activity. In *Archives of Biochemistry and Biophysics* (Vol. 426, Issue 2, pp. 208–224). https://doi.org/10.1016/j.abb.2004.03.020

Lund, N., Milev, M. P., Wong, R., Sanmuganantham, T., Woolaway, K., Chabot, B., Abou Elela, S., Mouland, A. J., & Cochrane, A. (2012). Differential effects of hnRNP D/AUF1 isoforms on HIV-1 gene expression. *Nucleic Acids Research*, *40*(8), 3663–3675. https://doi.org/10.1093/NAR/GKR1238

Luo, C., Wang, K., Liu, D., Li, Y., & Zhao, Q. (2008). *The Functional Roles of Lipid Rafts in T Cell Activation, Immune Diseases and HIV Infection and Prevention* (Vol. 5).

Luo, Y., Jacobs, E. Y., Greco, T. M., Mohammed, K. D., Tong, T., Keegan, S., Binley, J. M., Cristea, I. M., Fenyö, D., Rout, M. P., Chait, B. T., & Muesing, M. A. (2016). HIV-host interactome revealed directly from infected cells. *Nature Microbiology*, *1*(7). https://doi.org/10.1038/NMICROBIOL.2016.68

Maere, S., Heymans, K., & Kuiper, M. (2005). BiNGO: a Cytoscape plugin to assess overrepresentation of gene ontology categories in biological networks. *Bioinformatics (Oxford, England)*, *21*(16), 3448–3449. https://doi.org/10.1093/BIOINFORMATICS/BTI551

Magee, A. I., & Parmryd, I. (2003). Detergent-resistant membranes and the protein composition of lipid rafts. *Genome Biology*, *4*(11), 1–4. https://doi.org/10.1186/GB-2003-4-11-234/FIGURES/1

Malikov, V., da Silva, E. S., Jovasevic, V., Bennett, G., de Souza Aranha Vieira, D. A., Schulte, B., Diaz-Griffero, F., Walsh, D., & Naghavi, M. H. (2015). HIV-1 capsids bind and exploit the kinesin-1 adaptor FEZ1 for inward movement to the nucleus. *Nature Communications*, *6*. https://doi.org/10.1038/NCOMMS7660

Mañes, S., del Real, G., Lacalle, R. A., Lucas, P., Gómez-Moutón, C., Sánchez-Palomino, S., Delgado, R., Alcamí, J., Mira, E., & Martínez-A, C. (2000). Membrane raft microdomains mediate lateral assemblies required for HIV-1 infection. *EMBO Reports*, *1*(2), 190. https://doi.org/10.1093/EMBO-REPORTS/KVD025

Mariani, C., Desdouits, M., Favard, C., Benaroch, P., & Muriaux, D. M. (2014). Role of Gag and lipids during HIV-1 assembly in CD4+ T cells and macrophages. *Frontiers in Microbiology*, *5*(JUN), 312. https://doi.org/10.3389/FMICB.2014.00312/BIBTEX

Martin, B. R. (2013). Nonradioactive analysis of dynamic protein palmitoylation. *Current Protocols in Protein Science*, *SUPPL.73*. https://doi.org/10.1002/0471140864.ps1415s73

Martin, B. R., & Cravatt, B. F. (2009). Large-scale profiling of protein palmitoylation in mammalian cells. *Nature Methods*, *6*(2), 135–138. https://doi.org/10.1038/nmeth.1293

Martin, B. R., Wang, C., Adibekian, A., Tully, S. E., & Cravatt, B. F. (2012). Global profiling of dynamic protein palmitoylation. *Nature Methods*, *9*(1), 84–89. https://doi.org/10.1038/nmeth.1769

Martin, D. D. O., Beauchamp, E., & Berthiaume, L. G. (2011). Post-translational myristoylation: Fat matters in cellular life and death. In *Biochimie* (Vol. 93, Issue 1, pp. 18–31). https://doi.org/10.1016/j.biochi.2010.10.018

Maxfield, F. R., & Tabas, I. (2005). Role of cholesterol and lipid organization in disease. *Nature 2005 438:7068*, *438*(7068), 612–621. https://doi.org/10.1038/nature04399

Maxfield, F. R., & van Meer, G. (2010). Cholesterol, the central lipid of mammalian cells. *Current Opinion in Cell Biology*, *22*(4), 422–429. https://doi.org/10.1016/J.CEB.2010.05.004

Melkonian, K. A., Ostermeyer, A. G., Chen, J. Z., Roth, M. G., & Brown, D. A. (1999). *Role of Lipid Modifications in Targeting Proteins to Detergent-resistant Membrane Rafts MANY RAFT PROTEINS ARE ACYLATED, WHILE FEW ARE PRENYLATED**. http://www.jbc.org/

Mercredi, P. Y., Bucca, N., Loeliger, B., Gaines, C. R., Mehta, M., Bhargava, P., Tedbury, P. R., Charlier, L., Floquet, N., Muriaux, D., Favard, C., Sanders, C. R., Freed, E. O., Marchant, J., & Summers, M. F. (2016). Structural and Molecular Determinants of Membrane Binding by the HIV-1 Matrix Protein. *Journal of Molecular Biology*, *428*(8), 1637–1655. https://doi.org/10.1016/j.jmb.2016.03.005

Meusser, B., Purfuerst, B., & Luft, F. C. (2020). HIV-1 gag release from yeast reveals ESCRT interaction with the gag N-terminal protein region. *Journal of Biological Chemistry*, *295*(52), 17950–17972. https://doi.org/10.1074/jbc.RA120.014710

Mikaélian, I., Krieg, M., Gait, M. J., & Karn, J. (1996). Interactions of INS (CRS) elements and the splicing machinery regulate the production of Rev-responsive mRNAs. *Journal of Molecular Biology*, *257*(2), 246–264. https://doi.org/10.1006/JMBI.1996.0160

Milev, M. P., Ravichandran, M., Khan, M. F., Schriemer, D. C., & Mouland, A. J. (2012). Characterization of staufen1 ribonucleoproteins by mass spectrometry and biochemical analyses reveal the presence of diverse host proteins associated with human immunodeficiency virus type 1. *Frontiers in Microbiology*, *3*(OCT). https://doi.org/10.3389/FMICB.2012.00367

Misumi, S., Fuchigami, T., Takamune, N., Takahashi, I., Takama, M., & Shoji, S. (2002). Three isoforms of cyclophilin A associated with human immunodeficiency virus type 1 were found by proteomics by using two-dimensional gel electrophoresis and matrix-assisted laser desorption ionization-time of flight mass spectrometry. *Journal of Virology*, *76*(19), 10000–10008. https://doi.org/10.1128/JVI.76.19.10000-10008.2002

Mitchell, D. A., Vasudevan, A., Linder, M. E., & Deschenes, R. J. (2006). Protein palmitoylation by a family of DHHC protein S-acyltransferases. In *Journal of Lipid Research* (Vol. 47, Issue 6, pp. 1118–1127). https://doi.org/10.1194/jlr.R600007-JLR200

Miyakawa, K., Sawasaki, T., Matsunaga, S., Tokarev, A., Quinn, G., Kimura, H., Nomaguchi, M., Adachi, A., Yamamoto, N., Guatelli, J., & Ryo, A. (2012).

Interferon-induced SCYL2 limits release of HIV-1 by triggering PP2A-mediated dephosphorylation of the viral protein Vpu. *Science Signaling*, *5*(245). https://doi.org/10.1126/SCISIGNAL.2003212

Mizutani, T., Ishizaka, A., Suzuki, Y., & Iba, H. (2014). 7SK small nuclear ribonucleoprotein complex is recruited to the HIV-1 promoter via short viral transcripts. *FEBS Letters*, *588*(9), 1630–1636. https://doi.org/10.1016/J.FEBSLET.2014.01.067

Monette, A., Ajamian, L., López-Lastra, M., & Mouland, A. J. (2009). Human Immunodeficiency Virus Type 1 (HIV-1) Induces the Cytoplasmic Retention of Heterogeneous Nuclear Ribonucleoprotein A1 by Disrupting Nuclear Import: IMPLICATIONS FOR HIV-1 GENE EXPRESSION*. *The Journal of Biological Chemistry*, *284*(45), 31350. https://doi.org/10.1074/JBC.M109.048736

Monje-Galvan, V., & Voth, G. A. (2020). Binding mechanism of the matrix domain of HIV-1 gag on lipid membranes. *ELife*, *9*, 1–23. https://doi.org/10.7554/ELIFE.58621

Moore, M. D., & Hu, W. S. (2009). HIV-1 RNA Dimerization: It Takes Two to Tango. *AIDS Reviews*, *11*(2), 91. /pmc/articles/PMC3056336/

Morana, O., Nieto-Garai, J. A., Björkholm, P., Bernardino de la Serna, J., Terrones, O., Arboleya, A., Ciceri, D., Rojo-Bartolomé, I., Blouin, C. M., Lamaze, C., Lorizate, M., & Contreras, F. X. (2022). Identification of a New Cholesterol-Binding Site within the IFN-γ Receptor that is Required for Signal Transduction. *Advanced Science*, *9*(11), 2105170. https://doi.org/10.1002/ADVS.202105170

Moreno, M. R., Pérez-Berná, A. J., Guillén, J., & Villalaín, J. (2008). Biophysical characterization and membrane interaction of the most membranotropic region of the HIV-1 gp41 endodomain. *Biochimica et Biophysica Acta - Biomembranes*, *1778*(5), 1298–1307. https://doi.org/10.1016/j.bbamem.2007.12.023

Morimoto, C., Lord, C. I., Zhang, C., Duke-Cohan, J. S., Letvin, N. L., & Schlossman, S. F. (1994). Role of CD26/dipeptidyl peptidase IV in human immunodeficiency virus type 1 infection and apoptosis. *Proceedings of the National Academy of Sciences of the United States of America*, *91*(21), 9960–9964. https://doi.org/10.1073/PNAS.91.21.9960

Moses, J. E., & Moorhouse, A. D. (2007). The growing applications of click chemistry. *Chemical Society Reviews*, *36*(8), 1249–1262. https://doi.org/10.1039/B613014N

Mouritsen, O. G., & Zuckermann, M. J. (2004). What's so special about cholesterol? *Lipids*, *39*(11), 1101–1113. https://doi.org/10.1007/S11745-004-1336-X

Mu, X., Li, W., Wang, X., & Gao, G. (2013). YB-1 stabilizes HIV-1 genomic RNA and enhances viral production. *Protein & Cell*, *4*(8), 591–597. https://doi.org/10.1007/S13238-013-3011-3

Mücksch, F., Citir, M., Lüchtenborg, C., Glass, B., Traynor-Kaplan, A., Schultz, C., Brügger, B., & Kräusslich, H. G. (2019). Quantification of phosphoinositides reveals

strong enrichment of PIP2 in HIV-1 compared to producer cell membranes. *Scientific Reports 2019 9:1*, *9*(1), 1–13. https://doi.org/10.1038/s41598-019-53939-z

Mücksch, F., Laketa, V., Müller, B., Schultz, C., & Kräusslich, H. G. (2017). Synchronized HIV assembly by tunable PIP2 changes reveals PIP2 requirement for stable gag anchoring. *ELife*, *6*. https://doi.org/10.7554/ELIFE.25287

Müller, B., Daecke, J., Fackler, O. T., Dittmar, M. T., Zentgraf, H., & Kräusslich, H.-G. (2004). Construction and characterization of a fluorescently labeled infectious human immunodeficiency virus type 1 derivative. *Journal of Virology*, *78*(19), 10803–10813. https://doi.org/10.1128/JVI.78.19.10803-10813.2004

Munro, S. (2003). Review Lipid Rafts: Elusive or Illusive? detection, resistance to solubilization by the nonionic. In *Cell* (Vol. 115).

Murakami, T., & Freed, E. O. (2000). Genetic Evidence for an Interaction between Human Immunodeficiency Virus Type 1 Matrix and-Helix 2 of the gp41 Cytoplasmic Tail. In *JOURNAL OF VIROLOGY* (Vol. 74, Issue 8).

Muranyi, W., Malkusch, S., Müller, B., Heilemann, M., & Kräusslich, H. G. (2013). Super-resolution microscopy reveals specific recruitment of HIV-1 envelope proteins to viral assembly sites dependent on the envelope C-terminal tail. *PLoS Pathogens*, *9*(2). https://doi.org/10.1371/JOURNAL.PPAT.1003198

Murphy, R. E., & Saad, J. S. (2020). The interplay between HIV-1 gag binding to the plasma membrane and env incorporation. In *Viruses* (Vol. 12, Issue 5). MDPI AG. https://doi.org/10.3390/v12050548

Murphy, R. E., Samal, A. B., Vlach, J., & Saad, J. S. (2017). Solution Structure and Membrane Interaction of the Cytoplasmic Tail of HIV-1 gp41 Protein. *Structure*, *25*(11), 1708-1718.e5. https://doi.org/10.1016/j.str.2017.09.010

Najera, I., Krieg, M., & Karn, J. (1999). Synergistic stimulation of HIV-1 rev-dependent export of unspliced mRNA to the cytoplasm by hnRNP A1. *Journal of Molecular Biology*, *285*(5), 1951–1964. https://doi.org/10.1006/JMBI.1998.2473

Naji, S., Ambrus, G., Cimermančič, P., Reyes, J. R., Johnson, J. R., Filbrandt, R., Huber, M. D., Vesely, P., Krogan, N. J., Yates, J. R., Saphire, A. C., & Gerace, L. (2012). Host cell interactome of HIV-1 Rev includes RNA helicases involved in multiple facets of virus production. *Molecular & Cellular Proteomics : MCP*, *11*(4). https://doi.org/10.1074/MCP.M111.015313

Nakielny, S., & Dreyfuss, G. (1996). The hnRNP C proteins contain a nuclear retention sequence that can override nuclear export signals. *The Journal of Cell Biology*, *134*(6), 1365. https://doi.org/10.1083/JCB.134.6.1365

Nguyen, D. H., & K Hildreth, J. E. (2000). Evidence for Budding of Human Immunodeficiency Virus Type 1 Selectively from Glycolipid-Enriched Membrane Lipid Rafts. In *JOURNAL OF VIROLOGY* (Vol. 74, Issue 7).

Niemeier, J. K., & Kjell, D. P. (2013). Hydrazine and Aqueous Hydrazine Solutions: Evaluating Safety in Chemical Processes. *Organic Process Research and Development*, *17*(12), 1580–1590. https://doi.org/10.1021/OP400120G/SUPPL_FILE/OP400120G_SI_001.PDF

Nieto-Garai, J. A., Arboleya, A., Otaegi, S., Chojnacki, J., Casas, J., Fabriàs, G., Contreras, F. X., Kräusslich, H. G., & Lorizate, M. (2021). Cholesterol in the Viral Membrane is a Molecular Switch Governing HIV-1 Env Clustering. *Advanced Science*, *8*(3). https://doi.org/10.1002/advs.202003468

Nieto-Garai, J. A., Glass, B., Bunn, C., Giese, M., Jennings, G., Brankatschk, B., Agarwal, S., Börner, K., Xabier Contreras, F., Knölker, H. J., Zankl, C., Simons, K., Schroeder, C., Lorizate, M., & Kräusslich, H. G. (2018). Lipidomimetic compounds act as HIV-1 entry inhibitors by altering viral membrane structure. *Frontiers in Immunology*, *9*(SEP). https://doi.org/10.3389/fimmu.2018.01983

Nohe, A., & Petersen, N. O. (2004). Analyzing protein-protein interactions in cell membranes. *BioEssays : News and Reviews in Molecular, Cellular and Developmental Biology*, *26*(2), 196–203. https://doi.org/10.1002/BIES.10380

Ohno, Y., Kihara, A., Sano, T., & Igarashi, Y. (2006). Intracellular localization and tissue-specific distribution of human and yeast DHHC cysteine-rich domain-containing proteins. *Biochimica et Biophysica Acta - Molecular and Cell Biology of Lipids*, *1761*(4), 474–483. https://doi.org/10.1016/j.bbalip.2006.03.010

Ono, A., & Freed, E. O. (1999). Binding of Human Immunodeficiency Virus Type 1 Gag to Membrane: Role of the Matrix Amino Terminus. In *JOURNAL OF VIROLOGY* (Vol. 73, Issue 5).

Ono, A., & Freed, E. O. (2001). Plasma membrane rafts play a critical role in HIV-1 assembly and release. *Proceedings of the National Academy of Sciences of the United States of America*, *98*(24), 13925–13930. https://doi.org/10.1073/PNAS.241320298/SUPPL_FILE/INDEX.HTML

Ono, A., & Freed, E. O. (2004). Cell-Type-Dependent Targeting of Human Immunodeficiency Virus Type 1 Assembly to the Plasma Membrane and the Multivesicular Body. *Journal of Virology*, *78*(3), 1552–1563. https://doi.org/10.1128/jvi.78.3.1552-1563.2004

Ono, A., & Freed, E. O. (2005). Role of Lipid Rafts in Virus Replication**This chapter was written by Akira Ono and Eric O. Freed in their personal capacity. The views expressed in this chapter do not necessarily reflect the views of the NIH, DHHS, or the United States. In *Advances in Virus Research* (Vol. 64, pp. 311–358). https://doi.org/10.1016/S0065-3527(05)64010-9

Ono, A., Orenstein, J. M., & Freed, E. O. (2000). Role of the Gag Matrix Domain in Targeting Human Immunodeficiency Virus Type 1 Assembly. In *JOURNAL OF VIROLOGY* (Vol. 74, Issue 6).

Ono, A., Waheed, A. A., & Freed, E. O. (2007). Depletion of cellular cholesterol inhibits membrane binding and higher-order multimerization of human immunodeficiency virus type 1 Gag. *Virology*, *360*(1), 27–35. https://doi.org/10.1016/J.VIROL.2006.10.011

Ostermann, P. N., Ritchie, A., Ptok, J., & Schaal, H. (2021). Let It Go: HIV-1 cis-Acting Repressive Sequences. *Journal of Virology*, *95*(15). https://doi.org/10.1128/JVI.00342-21

Ott, D. E. (1997). Cellular Proteins in HIV Virions. In *Rev. Med. Virol* (Vol. 7).

Ott, D. E. (2002). Potential roles of cellular proteins in HIV-1. In *Reviews in Medical Virology* (Vol. 12, Issue 6, pp. 359–374). https://doi.org/10.1002/rmv.367

Ott, D. E., Coren, L. v, Kane, B. P., Busch, L. K., Johnson, D. G., Sowder Ii, R. C., Chertova, E. N., Arthur, L. O., & Henderson, L. E. (1996). Cytoskeletal proteins inside human immunodeficiency virus type 1 virions. *Journal of Virology*, *70*(11), 7734. https://doi.org/10.1128/JVI.70.11.7734-7743.1996

Ourailidou, M. E., Zwinderman, M. R. H., & Dekker, F. J. (2016). Bioorthogonal metabolic labelling with acyl-CoA reporters: Targeting protein acylation. In *MedChemComm* (Vol. 7, Issue 3, pp. 399–408). Royal Society of Chemistry. https://doi.org/10.1039/c5md00446b

Paillart, J.-C., Go¨ttlinger, H. G., & Go¨ttlinger, G. (1999). Opposing Effects of Human Immunodeficiency Virus Type 1 Matrix Mutations Support a Myristyl Switch Model of Gag Membrane Targeting. In *JOURNAL OF VIROLOGY* (Vol. 73, Issue 4).

Palsdottir, H., & Hunte, C. (2004). Lipids in membrane protein structures. In *Biochimica et Biophysica Acta - Biomembranes* (Vol. 1666, Issues 1–2, pp. 2–18). https://doi.org/10.1016/j.bbamem.2004.06.012

Parissi, V., Calmels, C., de Soultrait, V. R., Caumont, A., Fournier, M., Chaignepain, S., & Litvak, S. (2001). Functional interactions of human immunodeficiency virus type 1 integrase with human and yeast HSP60. *Journal of Virology*, *75*(23), 11344–11353. https://doi.org/10.1128/JVI.75.23.11344-11353.2001

Patil, A., Gautam, A., & Bhattacharya, J. (2010). Evidence that Gag facilitates HIV-1 envelope association both in GPI-enriched plasma membrane and detergent resistant membranes and facilitates envelope incorporation onto virions in primary CD4+ T cells. *Virology Journal*, *7*. https://doi.org/10.1186/1743-422X-7-3

Paz, S., Krainer, A. R., & Caputi, M. (2014). HIV-1 transcription is regulated by splicing factor SRSF1. *Nucleic Acids Research*, *42*(22), 13812–13823. https://doi.org/10.1093/NAR/GKU1170

Peitzsch, R. M., & McLaughlin, S. (1993). Binding of acylated peptides and fatty acids to phospholipid vesicles: pertinence to myristoylated proteins. *Biochemistry*, *32*(39), 10436–10443. https://doi.org/10.1021/BI00090A020

Peng, T., Yuan, X., & Hang, H. C. (2014). Turning the spotlight on protein-lipid interactions in cells. In *Current Opinion in Chemical Biology* (Vol. 21, pp. 144–153). Elsevier Ltd. https://doi.org/10.1016/j.cbpa.2014.07.015

Percherancier, Y., Lagane, B., Planchenault, T., Staropoli, I., Altmeyer, R., Virelizier, J. L., Arenzana-Seisdedos, F., Hoessli, D. C., & Bachelerie, F. (2003). HIV-1 entry into T-cells is not dependent on CD4 and CCR5 localization to sphingolipid-enriched, detergent-resistant, raft membrane domains. *Journal of Biological Chemistry*, *278*(5), 3153–3161. https://doi.org/10.1074/jbc.M207371200

Pérez Socas, L. B., & Ambroggio, E. E. (2020). The influence of myristoylation, liposome surface charge and nucleic acid interaction in the partition properties of HIV-1 Gag-N-terminal peptides to membranes. *Biochimica et Biophysica Acta - Biomembranes*, *1862*(11). https://doi.org/10.1016/j.bbamem.2020.183421

Perlman, M., & Resh, M. D. (2006). Identification of an intracellular trafficking and assembly pathway for HIV-1 gag. *Traffic (Copenhagen, Denmark)*, *7*(6), 731–745. https://doi.org/10.1111/J.1398-9219.2006.00428.X

Perrone, R., Butovskaya, E., Lago, S., Garzino-Demo, A., Pannecouque, C., Palù, G., & Richter, S. N. (2016). The G-quadruplex-forming aptamer AS1411 potently inhibits HIV-1 attachment to the host cell. *International Journal of Antimicrobial Agents*, *47*(4), 311–316. https://doi.org/10.1016/J.IJANTIMICAG.2016.01.016

Pezeshkian, N., Groves, N. S., & van Engelenburg, S. B. (2019). *Single-molecule imaging of HIV-1 envelope glycoprotein dynamics and Gag lattice association exposes determinants responsible for virus incorporation*. *10*. https://doi.org/10.1073/pnas.1910008116/-/DCSupplemental

Pfeiffer, T., Erkelenz, S., Widera, M., Schaal, H., & Bosch, V. (2013). Mutational analysis of the internal membrane proximal domain of the HIV glycoprotein C-terminus. *Virology*, *440*(1), 31–40. https://doi.org/10.1016/j.virol.2013.01.025

Phizicky, E. M., & Fields, S. (1995). Protein-protein interactions: methods for detection and analysis. *Microbiological Reviews*, *59*(1), 94–123. https://doi.org/10.1128/MR.59.1.94-123.1995

Piñol-Roma, S. (1997). HnRNP proteins and the nuclear export of mRNA. *Seminars in Cell & Developmental Biology*, *8*(1), 57–63. https://doi.org/10.1006/SCDB.1996.0122

Presolski, S. I., Hong, V. P., & Finn, M. G. (2011). Copper-Catalyzed Azide–Alkyne Click Chemistry for Bioconjugation. *Current Protocols in Chemical Biology*, *3*(4), 153–162. https://doi.org/10.1002/9780470559277.ch110148

Pro, B., & Dang, N. H. (2004). CD26/dipeptidyl peptidase IV and its role in cancer. *Histology and Histopathology*, *19*(4), 1345–1351. https://doi.org/10.14670/HH-19.1345

Purohit, P., Dupont, S., Stevenson, M., & Green, M. R. (2001). Sequence-specific interaction between HIV-1 matrix protein and viral genomic RNA revealed by in

vitro genetic selection. *RNA (New York, N.Y.)*, *7*(4), 576–584. https://doi.org/10.1017/S1355838201002023

Qu, K., Ke, Z., Zila, V., Anders-Össwein, M., Glass, B., Mücksch, F., Müller, R., Schultz, C., Müller, B., Kräusslich, H.-G., & Briggs, J. A. G. (2021). Maturation of the matrix and viral membrane of HIV-1. *Science*, *373*(6555), 700–704.

Ren, J., Wen, L., Gao, X., Jin, C., Xue, Y., & Yao, X. (2008). CSS-Palm 2.0: an updated software for palmitoylation sites prediction. *Protein Engineering, Design & Selection : PEDS*, *21*(11), 639–644. https://doi.org/10.1093/PROTEIN/GZN039

Resh, M. D. (1999). Fatty acylation of proteins: new insights into membrane targeting of myristoylated and palmitoylated proteins. *Biochimica et Biophysica Acta*, *1451*(1), 1–16. https://doi.org/10.1016/S0167-4889(99)00075-0

Resh, M. D. (2004). *A myristoyl switch regulates membrane binding of HIV-1 Gag*. www.pnas.orgcgidoi10.1073pnas.0308043101

Resh, M. D. (2016). Fatty acylation of proteins: The long and the short of it. *Progress in Lipid Research*, *63*, 120–131. https://doi.org/10.1016/J.PLIPRES.2016.05.002

Rice, A. P. (2016). Cyclin-Dependent Kinases as Therapeutic Targets for HIV-1 Infection. *Expert Opinion on Therapeutic Targets*, *20*(12), 1453. https://doi.org/10.1080/14728222.2016.1254619

Rigter, A., Langeveld, J. P. M., van Zijderveld, F. G., & Bossers, A. (2010). Prion protein self-interactions: a gateway to novel therapeutic strategies? *Vaccine*, *28*(49), 7810–7823. https://doi.org/10.1016/J.VACCINE.2010.09.012

Ritchie, C., Cylinder, I., Platt, E. J., & Barklis, E. (2015). Analysis of HIV-1 Gag protein interactions via biotin ligase tagging. *Journal of Virology*, *89*(7), 3988–4001. https://doi.org/10.1128/JVI.03584-14

Roberts, J. D., Bebenek, K., & Kunkel, T. A. (1988). The Accuracy of Reverse Transcriptase from HIV-1. *Science*, *242*(4882), 1171–1173.

Rodenburg, R. N. P., Snijder, J., van de Waterbeemd, M., Schouten, A., Granneman, J., Heck, A. J. R., & Gros, P. (2017). Stochastic palmitoylation of accessible cysteines in membrane proteins revealed by native mass spectrometry. *Nature Communications*, *8*(1). https://doi.org/10.1038/s41467-017-01461-z

Röling, M., Sisakht, M. M., Ne, E., Moulos, P., Crespo, R., Stoszko, M., de Crignis, E., Bodmer, H., Kan, T. W., Akbarzadeh, M., Harokopos, V., Hatzis, P., Palstra, R. J., & Mahmoudi, T. (2021). A Two-Color Haploid Genetic Screen Identifies Novel Host Factors Involved in HIV-1 Latency. *MBio*, *12*(6). https://doi.org/10.1128/MBIO.02980-21

Rose, K. M., Hirsch, V. M., & Bouamr, F. (2020). Budding of a retrovirus: Some assemblies required. In *Viruses* (Vol. 12, Issue 10). MDPI AG. https://doi.org/10.3390/v12101188

Rossi, E., Meuser, M. E., Cunanan, C. J., & Cocklin, S. (2021). Structure, function, and interactions of the hiv-1 capsid protein. In *Life* (Vol. 11, Issue 2, pp. 1–25). MDPI AG. https://doi.org/10.3390/life11020100

Rousso, I., Mixon, M. B., Chen, B. K., & Kim, P. S. (2000). *Palmitoylation of the HIV-1 envelope glycoprotein is critical for viral infectivity.* www.pnas.orgcgidoi10.1073pnas.240459697

Russ, W. P., & Engelman, D. M. (2000). The GxxxG motif: A framework for transmembrane helix-helix association. *Journal of Molecular Biology*, *296*(3), 911–919. https://doi.org/10.1006/jmbi.1999.3489

Saad, J. S., Ablan, S. D., Ghanam, R. H., Kim, A., Andrews, K., Nagashima, K., Soheilian, F., Freed, E. O., & Summers, M. F. (2008). Structure of the Myristylated Human Immunodeficiency Virus Type 2 Matrix Protein and the Role of Phosphatidylinositol-(4,5)-Bisphosphate in Membrane Targeting. *Journal of Molecular Biology*, *382*(2), 434–447. https://doi.org/10.1016/j.jmb.2008.07.027

Saad, J. S., Kim, A., Ghanam, R. H., Dalton, A. K., Vogt, V. M., Wu, Z., Lu, W., & Summers, M. F. (2007). Mutations that mimic phosphorylation of the HIV-1 matrix protein do not perturb the myristyl switch. *Protein Science : A Publication of the Protein Society*, *16*(8), 1793–1797. https://doi.org/10.1110/PS.072987607

Saad, J. S., Miller, J., Tai, J., Kim, A., Ghanam, R. H., & Summers, M. F. (2006). Structural basis for targeting HIV-1 Gag proteins to the plasma membrane for virus assembly. *Proceedings of the National Academy of Sciences of the United States of America*, *103*(30), 11364–11369. https://doi.org/10.1073/PNAS.0602818103

Sadava, D. E., Hillis, D. M., & Heller, H. C. (2009). *Life: the science of biology* (Vol. 2). Macmillan.

Sakuragi, J. I. (2011). Morphogenesis of the infectious HIV-1 virion. *Frontiers in Microbiology*, *2*(DEC). https://doi.org/10.3389/fmicb.2011.00242

Salaun, C., Greaves, J., & Chamberlain, L. H. (2010). The intracellular dynamic of protein palmitoylation. In *Journal of Cell Biology* (Vol. 191, Issue 7, pp. 1229–1238). https://doi.org/10.1083/jcb.201008160

Saphire, A. C. S., Gallay, P. A., & Bark, S. J. (2006). Proteomic analysis of human immunodeficiency virus using liquid chromatography/tandem mass spectrometry effectively distinguishes specific incorporated host proteins. *Journal of Proteome Research*, *5*(3), 530–538. https://doi.org/10.1021/pr050276b

Scarlata, S., & Carter, C. (2003). Role of HIV-1 Gag domains in viral assembly. *Biochimica et Biophysica Acta (BBA) - Biomembranes*, *1614*(1), 62–72. https://doi.org/10.1016/S0005-2736(03)00163-9

Scarlata, S., Ehrlich, L. S., & Carter, C. A. (1998). *Communication: Membrane-Induced Alterations in HIV-1 Gag and Matrix Protein-Protein Interactions*.

Schroeder, C. (2010). Cholesterol-binding viral proteins in virus entry and morphogenesis. *Sub-Cellular Biochemistry*, *51*, 77–108. https://doi.org/10.1007/978-90-481-8622-8_3

Schroeder, F., Woodford, J. K., Kavecansky, J., Wood, W. G., & Joiner, C. (1995). Cholesterol domains in biological membranes. *Molecular Membrane Biology*, *12*(1), 113–119. https://doi.org/10.3109/09687689509038505

Schroeder, R., London, E., & Brown, D. (1994). Interactions between saturated acyl chains confer detergent resistance on lipids and glycosylphosphatidylinositol (GPI)-anchored proteins: GPI-anchored proteins in liposomes and cells show similar behavior (membrane domain/model membrane/liquid-ordered phase/glycosphingolipid/cholesterol). In *Proc. Nati. Acad. Sci. USA* (Vol. 91).

Schubert, U., Antón, L. C., Gibbs, J., Norbury, C. C., Yewdell, J. W., & Bennink, J. R. (2000). Rapid degradation of alarge fraction of newly synthesizedproteins by proteasomes. *Nature*, *404*(6779), 770–774.

Schwarzer, R., Levental, I., Gramatica, A., Scolari, S., Buschmann, V., Veit, M., & Herrmann, A. (2014). The cholesterol-binding motif of the HIV-1 glycoprotein gp41 regulates lateral sorting and oligomerization. *Cellular Microbiology*, *16*(10), 1565–1581. https://doi.org/10.1111/cmi.12314

Segura, M. M., Garnier, A., di Falco, M. R., Whissell, G., Meneses-Acosta, A., Arcand, N., & Kamen, A. (2008). Identification of Host Proteins Associated with Retroviral Vector Particles by Proteomic Analysis of Highly Purified Vector Preparations. *Journal of Virology*, *82*(3), 1107–1117. https://doi.org/10.1128/JVI.01909-07/ASSET/90EB525D-E8CA-47BE-BA75-E2B7395C6BEC/ASSETS/GRAPHIC/ZJV0030801600003.JPEG

Sengupta, P., & Lippincott-Schwartz, J. (2020). Revisiting Membrane Microdomains and Phase Separation: A Viral Perspective. *Viruses*, *12*(7). https://doi.org/10.3390/V12070745

Sengupta, P., Seo, A. Y., Pasolli, H. A., Song, Y. E., Johnson, M. C., & Lippincott-Schwartz, J. (2019). A lipid-based partitioning mechanism for selective incorporation of proteins into membranes of HIV particles. *Nature Cell Biology 2019 21:4*, *21*(4), 452–461. https://doi.org/10.1038/s41556-019-0300-y

Sertznig, H., Hillebrand, F., Erkelenz, S., Schaal, H., & Widera, M. (2018). Behind the scenes of HIV-1 replication: Alternative splicing as the dependency factor on the quiet. *Virology*, *516*, 176–188. https://doi.org/10.1016/J.VIROL.2018.01.011

Shah, A., Kumar, S., Simon, S. D., Singh, D. P., & Kumar, A. (2013). HIV gp120- and methamphetamine-mediated oxidative stress induces astrocyte apoptosis via cytochrome P450 2E1. *Cell Death & Disease*, *4*(10). https://doi.org/10.1038/CDDIS.2013.374

Shannon, P., Markiel, A., Ozier, O., Baliga, N. S., Wang, J. T., Ramage, D., Amin, N., Schwikowski, B., & Ideker, T. (2003). Cytoscape: a software environment for integrated models of biomolecular interaction networks. *Genome Research*, *13*(11), 2498–2504. https://doi.org/10.1101/GR.1239303

Sharp, P. M., & Hahn, B. H. (2010). The evolution of HIV-1 and the origin of AIDS. *Philosophical Transactions of the Royal Society B: Biological Sciences*, *365*(1552), 2487. https://doi.org/10.1098/RSTB.2010.0031

Shepard, P. J., & Hertel, K. J. (2009). The SR protein family. *Genome Biology*, *10*(10), 242. https://doi.org/10.1186/GB-2009-10-10-242

Shevchenko, A., & Simons, K. (2010). Lipidomics: coming to grips with lipid diversity. *Nature Reviews Molecular Cell Biology 2010 11:8*, *11*(8), 593–598. https://doi.org/10.1038/nrm2934

Shiraishi, T., Misumi, S., Takama, M., Takahashi, I., & Shoji, S. (2001). Myristoylation of human immunodeficiency virus type 1 gag protein is required for efficient env protein transportation to the surface of cells. *Biochemical and Biophysical Research Communications*, *282*(5), 1201–1205. https://doi.org/10.1006/bbrc.2001.4696

SHKRETA, L., DELANNOY, A., SALVETTI, A., & CHABOT, B. (2021). SRSF10: an atypical splicing regulator with critical roles in stress response, organ development, and viral replication. *RNA (New York, N.Y.)*, *27*(11), 1302–1317. https://doi.org/10.1261/RNA.078879.121

Shkriabai, N., Datta, S. A. K., Zhao, Z., Hess, S., Rein, A., & Kvaratskhelia, M. (2006). Interactions of HIV-1 Gag with assembly cofactors. *Biochemistry*, *45*(13), 4077–4083. https://doi.org/10.1021/bi052308e

Siliciano, J. D., Kajdas, J., Finzi, D., Quinn, T. C., Chadwick, K., Margolick, J. B., Kovacs, C., Gange, S. J., & Siliciano, R. F. (2003). Long-term follow-up studies confirm the stability of the latent reservoir for HIV-1 in resting CD4+ T cells. *Nature Medicine*, *9*(6), 727–728. https://doi.org/10.1038/NM880

Silvius, J. R. (2003). Role of cholesterol in lipid raft formation: lessons from lipid model systems. *Biochimica et Biophysica Acta*, *1610*(2), 174–183. https://doi.org/10.1016/S0005-2736(03)00016-6

Simon, V., Bloch, N., & Landau, N. R. (2015). Intrinsic host restrictions to HIV-1 and mechanisms of viral escape. *Nature Immunology*, *16*(6), 546–553. https://doi.org/10.1038/NI.3156

Simons, K., & Ikonen, E. (1997). Functional rafts in cell membranes. In *Nature © Macmillan Publishers Ltd* (Vol. 387).

Simons, K., & Toomre, D. (2000). Lipid rafts and signal transduction. *Nature Reviews Molecular Cell Biology 2000 1:1*, *1*(1), 31–39. https://doi.org/10.1038/35036052

Singer, S. J., & Nicolson, G. L. (1972). The fluid mosaic model of the structure of cell membranes. *Science (New York, N.Y.)*, *175*(4023), 720–731. https://doi.org/10.1126/SCIENCE.175.4023.720

Sjobring, U., Bjorck, L., & Kastern, W. (1991). Streptococcal protein G. Gene structure and protein binding properties. *Journal of Biological Chemistry*, *266*(1), 399–405. https://doi.org/10.1016/S0021-9258(18)52448-0

Smart, E. J., Graf, G. A., McNiven, M. A., Sessa, W. C., Engelman, J. A., Scherer, P. E., Okamoto, T., & Lisanti, M. P. (1999). Caveolins, Liquid-Ordered Domains, and Signal Transduction. *Molecular and Cellular Biology*, *19*(11), 7289. https://doi.org/10.1128/MCB.19.11.7289

Smith, J. A., & Daniel, R. (2006). Following the path of the virus: the exploitation of host DNA repair mechanisms by retroviruses. *ACS Chemical Biology*, *1*(4), 217–226. https://doi.org/10.1021/CB600131Q/ASSET/IMAGES/CB600131Q.SOCIAL.JPEG_V 03

Smithies, O. (1965). Disulfide-Bond Cleavage and Formation in Proteins. *Science*, *150*(3703), 1595–1598. https://doi.org/10.1126/SCIENCE.150.3703.1595

Smotrys, J. E., & Linder, M. E. (2004). Palmitoylation of Intracellular Signaling Proteins: Regulation and function. In *Annual Review of Biochemistry* (Vol. 73, pp. 559–587). https://doi.org/10.1146/annurev.biochem.73.011303.073954

Sobocinska, J., Roszczenko-Jasinska, P., Ciesielska, A., & Kwiatkowska, K. (2018). Protein palmitoylation and its role in bacterial and viral infections. In *Frontiers in Immunology* (Vol. 8, Issue JAN). Frontiers Media S.A. https://doi.org/10.3389/fimmu.2017.02003

Socas, L. B. P., & Ambroggio, E. E. (2018). Myristoylation and Oligonucleotide Interaction Modulate Peptide and Protein Surface Properties: The Case of the HIV-1 Matrix Domain. *Langmuir*, *34*(21), 6051–6062. https://doi.org/10.1021/acs.langmuir.8b01005

Song, Y., Liu, J., Zhao, K., Gao, L., & Zhao, J. (2021). Cholesterol-induced toxicity: An integrated view of the role of cholesterol in multiple diseases. *Cell Metabolism*, *33*(10), 1911–1925. https://doi.org/10.1016/J.CMET.2021.09.001

Sot, J., Collado, M. I., Arrondo, J. L. R., Alonso, A., & Goñ, F. M. (2002). Triton X-100-Resistant Bilayers: Effect of Lipid Composition and Relevance to the Raft Phenomenon. *Langmuir*, *18*(7), 2828–2835. https://doi.org/10.1021/LA011381C

Sowd, G. A., & Aiken, C. (2021). Inositol phosphates promote HIV-1 assembly and maturation to facilitate viral spread in human CD4+ T cells. *PLoS Pathogens*, *17*(1). https://doi.org/10.1371/journal.ppat.1009190

Spearman, P., Horton, R., Ratner, L., & Kuli-Zade, I. (1997). Membrane Binding of Human Immunodeficiency Virus Type 1 Matrix Protein In Vivo Supports a

Conformational Myristyl Switch Mechanism. In *JOURNAL OF VIROLOGY* (Vol. 71, Issue 9).

Spearman, P., Wang, J., vander Heyden, N., Ratner, L., & Louis, S. (1994). Identification of Human Immunodeficiency Virus Type 1 Gag Protein Domains Essential to Membrane Binding and Particle Assembly. In *JOURNAL OF VIROLOGY* (Vol. 68, Issue 5).

Stark, C., Breitkreutz, B. J., Reguly, T., Boucher, L., Breitkreutz, A., & Tyers, M. (2006). BioGRID: a general repository for interaction datasets. *Nucleic Acids Research*, *34*(Database issue), D535. https://doi.org/10.1093/NAR/GKJ109

Stillwell, W. (2016). An Introduction to Biological Membranes: Composition, Structure and Function: Second Edition. In *An Introduction to Biological Membranes: Composition, Structure and Function: Second Edition*. Elsevier Inc. https://doi.org/10.1016/C2015-0-06226-8

Sugden, S. M., Bego, M. G., Pham, T. N. Q., & Cohen, É. A. (2016). Remodeling of the Host Cell Plasma Membrane by HIV-1 Nef and Vpu: A Strategy to Ensure Viral Fitness and Persistence. *Viruses*, *8*(3). https://doi.org/10.3390/V8030067

Sumner, C., Kotani, O., Liu, S., Musier-Forsyth, K., Sato, H., & Ono, A. (2022). Molecular Determinants in tRNA D-arm Required for Inhibition of HIV-1 Gag Membrane Binding. *Journal of Molecular Biology*, *434*(2), 167390. https://doi.org/10.1016/j.jmb.2021.167390

Sundquist, W. I., & Kräusslich, H. G. (2012). HIV-1 assembly, budding, and maturation. In *Cold Spring Harbor Perspectives in Medicine* (Vol. 2, Issue 7). Cold Spring Harbor Laboratory Press. https://doi.org/10.1101/cshperspect.a006924

Suomalainen, M. (2002). Lipid Rafts and Assembly of Enveloped Viruses. *Traffic*, *3*, 705–709.

Syu, W.-J., Lee, W.-R., Yu, Q.-C., Essex, M., & Lee, T.-H. (1991). *Role of Conserved gp4l Cysteine Residues in the Processing of Human Immunodeficiency Virus Envelope Precursor and Viral Infectivity* (Vol. 65, Issue 11).

Szklarczyk, D., Gable, A. L., Nastou, K. C., Lyon, D., Kirsch, R., Pyysalo, S., Doncheva, N. T., Legeay, M., Fang, T., Bork, P., Jensen, L. J., & von Mering, C. (2021). The STRING database in 2021: customizable protein-protein networks, and functional characterization of user-uploaded gene/measurement sets. *Nucleic Acids Research*, *49*(D1), D605–D612. https://doi.org/10.1093/NAR/GKAA1074

Tabaczar, S., Czogalla, A., Podkalicka, J., Biernatowska, A., & Sikorski, A. F. (2017). Protein palmitoylation: Palmitoyltransferases and their specificity. In *Experimental Biology and Medicine* (Vol. 242, Issue 11, pp. 1150–1157). SAGE Publications Inc. https://doi.org/10.1177/1535370217707732

Tanaka, M., Robinson, B. A., Chutiraka, K., Geary, C. D., Reed, J. C., & Lingappa, J. R. (2016). Mutations of Conserved Residues in the Major Homology Region Arrest Assembling HIV-1 Gag as a Membrane-Targeted Intermediate Containing Genomic RNA and Cellular Proteins. *Journal of Virology*, *90*(4), 1944–1963. https://doi.org/10.1128/jvi.02698-15

Tang, C., Loeliger, E., Luncsford, P., Kinde, I., Beckett, D., & Summers, M. F. (2003). *Entropic switch regulates myristate exposure in the HIV-1 matrix protein.* www.pnas.orgcgidoi10.1073pnas.0305665101

Tang, Y., Leao, I. C., Coleman, E. M., Broughton, R. S., & Hildreth, J. E. K. (2009). Deficiency of Niemann-Pick Type C-1 Protein Impairs Release of Human Immunodeficiency Virus Type 1 and Results in Gag Accumulation in Late Endosomal/Lysosomal Compartments. *Journal of Virology*, *83*(16), 7982–7995. https://doi.org/10.1128/jvi.00259-09

Tansi, F. L., Blanchard, V., Berger, M., Tauber, R., Reutter, W., & Fan, H. (2010). Interaction of human dipeptidyl peptidase IV and human immunodeficiency virus type-1 transcription transactivator in Sf9 cells. *Virology Journal*, *7*(1), 1–12. https://doi.org/10.1186/1743-422X-7-267/FIGURES/4

Tedbury, P. R., Ablan, S. D., & Freed, E. O. (2013). Global Rescue of Defects in HIV-1 Envelope Glycoprotein Incorporation: Implications for Matrix Structure. *PLoS Pathogens*, *9*(11). https://doi.org/10.1371/journal.ppat.1003739

Tedbury, P. R., & Freed, E. O. (2014). The role of matrix in HIV-1 envelope glycoprotein incorporation. In *Trends in Microbiology* (Vol. 22, Issue 7, pp. 372–378). Elsevier Ltd. https://doi.org/10.1016/j.tim.2014.04.012

Tedbury, P. R., & Freed, E. O. (2015). The cytoplasmic tail of retroviral envelope glycoproteins. In *Progress in Molecular Biology and Translational Science* (Vol. 129, pp. 253–284). Elsevier B.V. https://doi.org/10.1016/bs.pmbts.2014.10.009

Tedbury, P. R., Mercredi, P. Y., Gaines, C. R., Summers, M. F., & Freed, E. O. (2015). Elucidating the mechanism by which compensatory mutations rescue an hiv-1 matrix mutant defective for gag membrane targeting and envelope glycoprotein incorporation. *Journal of Molecular Biology*, *427*(6), 1413–1427. https://doi.org/10.1016/j.jmb.2015.01.018

Tedbury, P. R., Novikova, M., Ablan, S. D., & Freed, E. O. (2016). Biochemical evidence of a role for matrix trimerization in HIV-1 envelope glycoprotein incorporation. *Proceedings of the National Academy of Sciences of the United States of America*, *113*(2), E182–E190. https://doi.org/10.1073/pnas.1516618113

Tedbury, P. R., Novikova, M., Alfadhli, A., Hikichi, Y., Kagiampakis, I., KewalRamani, V. N., Barklis, E., & Freed, E. O. (2019). HIV-1 Matrix Trimerization-Impaired Mutants Are Rescued by Matrix Substitutions That Enhance Envelope Glycoprotein Incorporation. *Journal of Virology*, *94*(1). https://doi.org/10.1128/jvi.01526-19

Thiele, C., Hannah, M. J., Fahrenholz, F., & Huttner, W. B. (2000). Cholesterol binds to synaptophysin and is required for biogenesis of synaptic vesicles. In *NATURE CELL BIOLOGY* (Vol. 2).

Thiele, C., Papan, C., Hoelper, D., Kusserow, K., Gaebler, A., Schoene, M., Piotrowitz, K., Lohmann, D., Spandl, J., Stevanovic, A., Shevchenko, A., & Kuerschner, L. (2012). Tracing fatty acid metabolism by click chemistry. *ACS Chemical Biology*, *7*(12), 2004–2011. https://doi.org/10.1021/CB300414V

Thomas, C. M., & Smart, E. J. (2008). Caveolae structure and function. *Journal of Cellular and Molecular Medicine*, *12*(3), 796. https://doi.org/10.1111/J.1582-4934.2008.00295.X

Thornhill, D., Murakami, T., & Ono, A. (2020). Rendezvous at plasma membrane: Cellular lipids and tRNA Set up sites of HIV-1 particle assembly and incorporation of host transmembrane proteins. In *Viruses* (Vol. 12, Issue 8). MDPI AG. https://doi.org/10.3390/v12080842

Timmons, A., Fray, E., Kumar, M., Wu, F., Dai, W., Bullen, C. K., Kim, P., Hetzel, C., Yang, C., Beg, S., Lai, J., Pomerantz, J. L., Yukl, S. A., Siliciano, J. D., & Siliciano, R. F. (2020). HSF1 inhibition attenuates HIV-1 latency reversal mediated by several candidate LRAs In Vitro and Ex Vivo. *Proceedings of the National Academy of Sciences of the United States of America*, *117*(27), 15763–15771. https://doi.org/10.1073/PNAS.1916290117

Titeca, K., Lemmens, I., Tavernier, J., & Eyckerman, S. (2019). Discovering cellular protein-protein interactions: Technological strategies and opportunities. *Mass Spectrometry Reviews*, *38*(1), 79–111. https://doi.org/10.1002/MAS.21574

Todd, G. C., Duchon, A., Inlora, J., Olson, E. D., Musier-Forsyth, K., & Ono, A. (2017). *Inhibition of HIV-1 Gag-membrane interactions by specific RNAs*. https://doi.org/10.1261/rna

Tornøe, C. W., Christensen, C., & Meldal, M. (2002). Peptidotriazoles on solid phase: [1,2,3]-Triazoles by regiospecific copper(I)-catalyzed 1,3-dipolar cycloadditions of terminal alkynes to azides. *Journal of Organic Chemistry*, *67*(9), 3057–3064. https://doi.org/10.1021/jo011148j

Tran, R. J., Lalonde, M. S., Sly, K. L., & Conboy, J. C. (2019). Mechanistic Investigation of HIV-1 Gag Association with Lipid Membranes. *Journal of Physical Chemistry B*, *123*(22), 4673–4687. https://doi.org/10.1021/acs.jpcb.9b02655

Tremblay, M., Fortin, J., & Cantin, R. (1998). The acquisition of host-encoded proteinsby nascent HIV-1. *Immunology Today*, *19*(8), 346–351.

Trotta, C. R., Lund, E., Kahan, L., Johnson, A. W., & Dahlberg, J. E. (2003). Coordinated nuclear export of 60S ribosomal subunits and NMD3 in vertebrates. *The EMBO Journal*, *22*(11), 2841. https://doi.org/10.1093/EMBOJ/CDG249

Tsai, K., Jaguva Vasudevan, A. A., Martinez Campos, C., Emery, A., Swanstrom, R., & Cullen, B. R. (2020). Acetylation of Cytidine Residues Boosts HIV-1 Gene Expression by Increasing Viral RNA Stability. *Cell Host & Microbe, 28*(2), 306-312.e6. https://doi.org/10.1016/J.CHOM.2020.05.011

Turro, N. J., Lei, X. G., Ananthapadmanabhan, K. P., & Aronson, M. (1995). Spectroscopic Probe Analysis of Protein-Surfactant Interaciion: The BSA/SDS System. *Langmuir*, *11*(7), 2525–2533. https://doi.org/10.1021/LA00007A035

Urbančič, I., Brun, J., Shrestha, D., Waithe, D., Eggeling, C., & Chojnacki, J. (2018). Lipid composition but not curvature is the determinant factor for the low molecular mobility observed on the membrane of virus-like vesicles. *Viruses*, *10*(8). https://doi.org/10.3390/v10080415

van den Bogaart, G., Meyenberg, K., Risselada, H. J., Amin, H., Willig, K. I., Hubrich, B. E., Dier, M., Hell, S. W., Grubmüller, H., Diederichsen, U., & Jahn, R. (2011). Membrane protein sequestering by ionic protein-lipid interactions. *Nature*, *479*(7374), 552–555. https://doi.org/10.1038/NATURE10545

van Meer, G., Voelker, D. R., & Feigenson, G. W. (2008). Membrane lipids: where they are and how they behave. *Nature Reviews Molecular Cell Biology 2008 9:2*, *9*(2), 112–124. https://doi.org/10.1038/nrm2330

Vance, J. E. (2012). Dysregulation of cholesterol balance in the brain: contribution to neurodegenerative diseases. *Disease Models & Mechanisms*, *5*(6), 746–755. https://doi.org/10.1242/DMM.010124

Veit, M. (2012). Palmitoylation of virus proteins. *Biology of the Cell*, *104*(9), 493–515. https://doi.org/10.1111/BOC.201200006

Vincent, N., Genin, C., & Malvoisin, E. (2002). Identification of a conserved domain of the HIV-1 transmembrane protein gp41 which interacts with cholesteryl groups. *Biochimica et Biophysica Acta (BBA) - Biomembranes*, *1567*(SUPPL.), 157–164. https://doi.org/10.1016/S0005-2736(02)00611-9

Vlach, J., & Saad, J. S. (2013). Trio engagement via plasma membrane phospholipids and the myristoyl moiety governs HIV-1 matrix binding to bilayers. *Proceedings of the National Academy of Sciences of the United States of America*, *110*(9), 3525–3530. https://doi.org/10.1073/pnas.1216655110

Vozzolo, L., Loh, B., Gane, P. J., Tribak, M., Zhou, L., Anderson, I., Nyakatura, E., Jenner, R. G., Selwood, D., & Fassati, A. (2010). Gyrase B inhibitor impairs HIV-1 replication by targeting Hsp90 and the capsid protein. *The Journal of Biological Chemistry*, *285*(50), 39314–39328. https://doi.org/10.1074/JBC.M110.155275

Waheed, A. A., Ablan, S. D., Mankowski, M. K., Cummins, J. E., Ptak, R. G., Schaffner, C. P., & Freed, E. O. (2006). Inhibition of HIV-1 replication by amphotericin B

methyl ester: selection for resistant variants. *The Journal of Biological Chemistry*, *281*(39), 28699–28711. https://doi.org/10.1074/JBC.M603609200

Waheed, A. A., & Freed, E. O. (2009). Lipids and membrane microdomains in HIV-1 replication. In *Virus Research* (Vol. 143, Issue 2, pp. 162–176). https://doi.org/10.1016/j.virusres.2009.04.007

Wang, X., Wei, X., Thijssen, B., Das, J., Lipkin, S. M., & Yu, H. (2012). Three-dimensional reconstruction of protein networks provides insight into human genetic disease. *Nature Biotechnology*, *30*(2), 159–164. https://doi.org/10.1038/NBT.2106

Weihofen, W. A., Liu, J., Reutter, W., Saenger, W., & Fan, H. (2005). Crystal structures of HIV-1 Tat-derived nonapeptides Tat-(1-9) and Trp2-Tat-(1-9) bound to the active site of dipeptidyl-peptidase IV (CD26). *The Journal of Biological Chemistry*, *280*(15), 14911–14917. https://doi.org/10.1074/JBC.M413400200

Welker, R., Hohenberg, H., Tessmer, U., Huckhagel, C., & Kräusslich, H.-G. (2000). Biochemical and Structural Analysis of Isolated Mature Cores of Human Immunodeficiency Virus Type 1. *Journal of Virology*, *74*(3), 1168. https://doi.org/10.1128/JVI.74.3.1168-1177.2000

Wen, Y., Feigenson, G. W., Vogt, V. M., & Dick, R. A. (2020). Mechanisms of PI(4,5)P2 Enrichment in HIV-1 Viral Membranes. *Journal of Molecular Biology*, *432*(19), 5343–5364. https://doi.org/10.1016/j.jmb.2020.07.018

Wessel, D., & Fl~gge, U. I. (1984). A Method for the Quantitative Recovery of Protein in Dilute Solution in the Presence of Detergents and Lipids. In *ANALYTICAL BIOCHEMISTRY* (Vol. 138).

Whittaker, V. P., Michaelson, I. A., & Kirkland, R. J. (1964). The separation of synaptic vesicles from nerve-ending particles (`synaptosomes'). *Biochemical Journal*, *90*(2), 293. https://doi.org/10.1042/BJ0900293

Wilen, C. B., Tilton, J. C., & Doms, R. W. (2012). HIV: Cell Binding and Entry. *Cold Spring Harbor Perspectives in Medicine*, *2*(8). https://doi.org/10.1101/CSHPERSPECT.A006866

Winogradoff, D., John, S., & Aksimentiev, A. (2020). Protein unfolding by SDS: The microscopic mechanisms and the properties of the SDS-protein assembly. *Nanoscale*, *12*(9), 5422–5434. https://doi.org/10.1039/c9nr09135a

Wiśniewska, A., Draus, J., & Subczynski, W. K. (2003). Is a fluid-mosaic model of biological membranes fully relevant? Studies on lipid organization in model and biological membranes. *Cellular & Molecular Biology Letters*, *8*(1), 147–159. https://pubmed.ncbi.nlm.nih.gov/12655369/

Woolaway, K., Asai, K., Emili, A., & Cochrane, A. (2007). hnRNP E1 and E2 have distinct roles in modulating HIV-1 gene expression. *Retrovirology*, *4*, 28. https://doi.org/10.1186/1742-4690-4-28

Wrenger, S., Hoffmann, T., Faust, J., Mrestani-Klaus, C., Brandt, W., Neubert, K., Kraft, M., Olek, S., Frank, R., Ansorge, S., & Reinhold, D. (1997). The N-terminal structure of HIV-1 Tat is required for suppression of CD26-dependent T cell growth. *The Journal of Biological Chemistry*, *272*(48), 30283–30288. https://doi.org/10.1074/JBC.272.48.30283

Wu, Z., Alexandratos, J., Ericksen, B., Lubkowski, J., Gallo, R. C., & Lu, W. (2004). Total chemical synthesis of N-myristoylated HIV-1 matrix protein p17: Structural and mechanistic implications of p17 myristoylation. *Proceedings of the National Academy of Sciences of the United States of America*, *101*(32), 11587–11592. https://doi.org/10.1073/PNAS.0404649101/ASSET/0EFC76D4-F259-4F60-B0BC-2DCB34CB99B2/ASSETS/GRAPHIC/ZPQ0330457080004.JPEG

Wu-Baer, F., Lane, W. S., & Gaynor, R. B. (1996). Identification of a group of cellular cofactors that stimulate the binding of RNA polymerase II and TRP-185 to human immunodeficiency virus 1 TAR RNA. *The Journal of Biological Chemistry*, *271*(8), 4201–4208. https://doi.org/10.1074/JBC.271.8.4201

Wyma, D. J., Jiang, J., Shi, J., Zhou, J., Lineberger, J. E., Miller, M. D., & Aiken, C. (2004). Coupling of Human Immunodeficiency Virus Type 1 Fusion to Virion Maturation: a Novel Role of the gp41 Cytoplasmic Tail. *Journal of Virology*, *78*(7), 3429–3435. https://doi.org/10.1128/jvi.78.7.3429-3435.2004

Wymann, M. P., & Schneiter, R. (2008). Lipid signalling in disease. *Nature Reviews. Molecular Cell Biology*, *9*(2), 162–176. https://doi.org/10.1038/NRM2335

Xia, Y., & Peng, L. (2013). Photoactivatable lipid probes for studying biomembranes by photoaffinity labeling. In *Chemical Reviews* (Vol. 113, Issue 10, pp. 7880–7929). American Chemical Society. https://doi.org/10.1021/cr300419p

Xu, X., & London, E. (2000). The effect of sterol structure on membrane lipid domains reveals how cholesterol can induce lipid domain formation. *Biochemistry*, *39*(5), 843–849. https://doi.org/10.1021/BI992543V

Yandrapalli, N., Lubart, Q., Tanwar, H. S., Picart, C., Mak, J., Muriaux, D., & Favard, C. (2016). Self assembly of HIV-1 Gag protein on lipid membranes generates PI(4,5)P2/Cholesterol nanoclusters. *Scientific Reports*, *6*. https://doi.org/10.1038/srep39332

Yang, C., Spiest, C. P., & Compans, R. W. (1995). The human and simian immunodeficiency virus envelope glycoprotein transmembrane subunits are palmitoylated. In *Biochemistry* (Vol. 92).

Yang, P., Ai, L.-S., Huang, S.-C., Li, H.-F., Chan, W.-E., Chang, C.-W., Ko, C.-Y., & Chen, S. S.-L. (2010). The Cytoplasmic Domain of Human Immunodeficiency Virus Type 1 Transmembrane Protein gp41 Harbors Lipid Raft Association Determinants. *Journal of Virology*, *84*(1), 59–75. https://doi.org/10.1128/jvi.00899-09

Yang, X., & Gabuzda, D. (1999). Regulation of human immunodeficiency virus type 1 infectivity by the ERK mitogen-activated protein kinase signaling pathway. *Journal of Virology*, *73*(4), 3460–3466. https://doi.org/10.1128/JVI.73.4.3460-3466.1999

Yap, M. C., Kostiuk, M. A., Martin, D. D. O., Perinpanayagam, M. A., Hak, P. G., Siddam, A., Majjigapu, J. R., Rajaiah, G., Keller, B. O., Prescher, J. A., Wu, P., Bertozzi, C. R., Falck, J. R., & Berthiaume, L. G. (2010). Rapid and selective detection of fatty acylated proteins using ω-alkynyl-fatty acids and click chemistry. *Journal of Lipid Research*, *51*(6), 1566–1580. https://doi.org/10.1194/jlr.D002790

Yeagle, Philip. (2012). *The structure of biological membranes*. CRC Press. https://www.routledge.com/The-Structure-of-Biological-Membranes/Yeagle/p/book/9781439809570

Yount, J. S., Zhang, M. M., & Hang, H. C. (2011). Visualization and Identification of Fatty Acylated Proteins Using Chemical Reporters. *Current Protocols in Chemical Biology*, *3*(2), 65–79. https://doi.org/10.1002/9780470559277.ch100225

Yu, X., Yuan, X., Matsuda, Z., Lee, T.-H., & Essex, M. (1992). The Matrix Protein of Human Immunodeficiency Virus Type 1 Is Required for Incorporation of Viral Envelope Protein into Mature Virions. In *JOURNAL OF VIROLOGY*.

Zhao, H., & Lappalainen, P. (2012). A simple guide to biochemical approaches for analyzing protein-lipid interactions. *Molecular Biology of the Cell*, *23*(15), 2823–2830. https://doi.org/10.1091/MBC.E11-07-0645

Zheng, Y. C., Guo, Y. J., Wang, B., Wang, C., Mamun, M. A. A., Gao, Y., & Liu, H. M. (2021). Targeting neddylation E2s: a novel therapeutic strategy in cancer. *Journal of Hematology & Oncology 2021 14:1*, *14*(1), 1–13. https://doi.org/10.1186/S13045-021-01070-W

Zhou, W., Parent, L. J., Wills, J. W., & Reshl2, M. D. (1994). Identification of a Membrane-Binding Domain within the Amino-Terminal Region of Human Immunodeficiency Virus Type 1 Gag Protein Which Interacts with Acidic Phospholipids. In *JOURNAL OF VIROLOGY* (Vol. 68, Issue 4).

Zhou, W., Resh, M. D., Zhou, (W, Parent, L. J., Wills, J. W., Resh, M. D., & Virol, J. (1996). Differential Membrane Binding of the Human Immunodeficiency Virus Type 1 Matrix Protein. In *JOURNAL OF VIROLOGY* (Vol. 70, Issue 12).

Zila, V., Margiotta, E., Turoňová, B., Müller, T. G., Zimmerli, C. E., Mattei, S., Allegretti, M., Börner, K., Rada, J., Müller, B., Lusic, M., Kräusslich, H. G., & Beck, M. (2021). Cone-shaped HIV-1 capsids are transported through intact nuclear pores. *Cell*, *184*(4), 1032-1046.e18. https://doi.org/10.1016/j.cell.2021.01.025